STATUS OF THESIS

Title of thesis | EXPERIMENTAL STUDY ON UPDRAFT GASIFICATION OF OIL PALM FRONDS

I RAMZY ELNEEL KONDA KUKU

hereby allow my thesis to be placed at the Information Resource Center (IRC) of Universiti Teknologi PETRONAS (UTP) with the following conditions:

1. The thesis becomes the property of UTP
2. The IRC of UTP may make copies of the thesis for academic purposes only.
3. This thesis is classified as

☐ Confidential

☑ Non-confidential

If this thesis is confidential, please state the reason:

_____
_____
_____

The contents of the thesis will remain confidential for _____ years.

Remarks on disclosure:

_____
_____
_____

Endorsed by

_____ _____

Signature of Author | Signature of Supervisor

Permanent address:_____
Department of Mechanical Engineering,
Faculty of Engineering, Red Sea
University. Portsudan, Sudan

Name of Supervisor
Assoc. Prof. Ir. Dr. Shaharin Anwar Sulaiman

Date : _____ | Date : _____

UNIVERSITI TEKNOLOGI PETRONAS

EXPERIMENTAL STUDY ON UPDRAFT GASIFICATION OF OIL PALM FRONDS

by

RAMZY ELNEEL KONDA KUKU

The undersigned certify that they have read, and recommend to the Postgraduate Studies Programme for acceptance this thesis for the fulfillment of the requirements for the degree stated.

Signature: _____

Main Supervisor: Assoc. Prof. Ir. Dr. Shaharin Anwar Sulaiman

Signature: _____

Co-Supervisor: Assoc. Prof. Dr. Bambang Ariwhajoedi

Signature: _____

Head of Department: Assoc. Prof. Ir. Dr. Masri Bin Baharom

Date: _____

EXPERIMENTAL STUDY ON UPDRAFT GASIFICATION OF OIL PALM FRONDS

by

RAMZY ELNEEL KONDA KUKU

A Thesis

Submitted to the Postgraduate Studies Programme

as a Requirement for the Degree of

DOCTOR OF PHILOSOPHY

MECHANICAL ENGINEERING DEPARTMENT

UNIVERSITI TEKNOLOGI PETRONAS

BANDAR SERI ISKANDAR,

PERAK

JAN 2014

DECLARATION OF THESIS

Title of thesis | EXPERIMENTAL STUDY ON UPDRAFT GASIFICATION OF OIL PALM FRONS

I RAMZY ELNEEL KONDA KUKU

hereby declare that the thesis is based on my original work except for quotations and citations which have been duly acknowledged. I also declare that it has not been previously or concurrently submitted for any other degree at UTP or other institutions.

Witnessed by

_____	_____
Signature of Author	Signature of Supervisor
Permanent address: Department of Mechanical Engineering, Faculty of Engineering, Red Sea University. Portsudan, Sudan	Name of Supervisor Assoc. Prof. Ir. Dr. Shaharin Anwar Sulaiman
Date : _____	Date : _____

DEDICATION

To My father and Mother

To my lovely wife

For their presence in my life and love

To my brothers and sisters for their support and encouragement

ACKNOWLEDGEMENTS

First, I would like to thank almighty God for all the wonderful blessings that I have received in my life and for helping me to come to the end of this work, which would not be finished without His support.

I am deeply indebted to my advisor Associate Professor Ir. Dr. Shaharin Anwar Sulaiman, for his supervision, guidance and encouragement during the research work and writing the thesis. I would also like to express my heartily thanks to my Co-supervisor Associate Professor Dr. Bambang Ariwahjoedi for his contributions and counseling.

I would like to extend my thanks to mechanical engineering department and center for postgraduate studies at Universiti Teknologi PETRONAS for providing the financial support and research facilities for this work.
I would like to pay my sincere appreciation to parents, brothers, sisters and my wife for their inspiration, encouragement during the difficulties and supporting to achieve my dreams.

Finally special thanks are due to all my friends, especially country mate friends for their friendship, love and support. Without the help of my almighty God, family love, and UTP supports this work wouldn’t have come to an end.

ABSTRACT

As a leader in palm oil production, Malaysia produces tremendous quantities of oil palm frond during harvesting, pruning and replanting activities period. Up to now, most of the generated fronds are left rotting in the plantations mainly for nutrient recycling resulting in several environmental problems. The huge quantities of fronds every year make them a very promising source for energy generation. Many activates were carried out to convert the fronds into valuable products, but there was no report on study of updraft gasification of oil palm fronds. In this work, small scale updraft gasifier was built to investigate experimentally the behavior and performance of the updraft gasification of oil palm fronds with air as the gasification agent. The study was conducted in five stages: (a) characterization of the material, (b) design and construction of an updraft gasifier with data acquisition system, (c) experiments to investigate performance behavior of updraft gasification of oil palm fronds by varying various operation conditions, (d) experiments to investigate the effects of secondary air injection on gasification performance and tar removal and finally (e) using the fronds synthetic gas in domestic cooking stove. Gasification experiments were carried out at various equivalence ratio, oil palm fronds moisture content, biomass size and primary air position. The equivalence ratio of 0.22 to 0.29 and oil palm fronds with a particle size of 13-25 mm appeared to be optimum with respect to gas quality, while oil palm fronds up to 40% moisture content (wet basis) successfully produced high gas quality. However, a gas composition of 26, 7.7, 1.1 and 6% for the CO, CO_2, CH_4 and H_2 respectively have been produced for the above equivalence ratio and biomass size, while a gas with heating value in the range of 4.6-3.2 MJ/Nm^3 has been produced for the moisture content of 0-40%. The implantation of secondary air injection in the reduction zone appeared to increase the gas heating value and gasification efficiency by 19% and 14% respectively. In general, the results proved satisfactory for using the fronds in updraft gasifier to generate energy for thermal applications.

ABSTRAK

Sebagai peneraju dalam penghasil minyak sawit, Malaysia menghasikan pelepah kelapa sawit dalam jumlah yang besar dalam masa, menuai, mencantas, dan penanaman semula. sehingga sekarang, hampir semua pelepah kelapa sawit yang dikasikan dibiarkan reput dalam perkebunan. Kaedah ini telah mengakebatkan masalah alam sekitar. Jumlah pelepah yang besar setiap tahun dapat menjadi sumber tenaga yang menjanjikan. Banyak usaha yang telah dilakukan untuk mengubah pelepah menjadi produk yang lebih bernilai, tetapi tidak ada laporan studi tentang pengegasan pelepah kelapa sawit. Dalam kajian ini, perangkat pengegasan skala kecil telah dibina untuk menyiasat secara eksperimen tingkah laku dan prestasi pengegasan pelepah kelapa sawit dengan ejen pengegasan udara. Kajian ini telah dijalankan lalam lima peringkat: (a) pencirian dari bahan pelepah kelapa sawit, (b) reka bentuk dan pembinaan dari perangkat pengegasan dengan system perolehan data, (c) eksperimen untuk menyisasat prestasi pengegasan pelepah kelapa sawit dengan mengubah pelbagai keadaan operasi, (d) eksperimen untuk menyiasat kesan dari suntikan udara sekunder pada prestasi pengegasan dan penyingkiran tar dan akhirnya (e) penggunaan gas sintetik pelepah pada dapur memasak domestic. Eksperimen pengegasan telah dijalankan pada variasi nisbah kesetaraan, kandungan kelembapan pelepah kelapa sawit, saiz biomass dan kedudukan udara utama. nisbah kesetaraan dari pada 0.22-0.29 dan pelepah kelapa sawit dengan saiz biomass 13-25 mm kelihatan optimum terhadap kualiti gas, sedangkan pelepah kelapa sawit sehinga 40% (asas basah) telah menghasilkan gas kualiti tinggi. Tetapi, gas dengan kandungan 26, 7.7, 1.1 dan 6% untuk CO, CO_2, CH_4 dan H_2 masing-masing telah dihasilkan dari nisbah kesetaraan dan saiz biomass, sedangkan gas dengan nilai kandungan kelembapan 0-40%. Implantasi suntikan udara sekunder dalam zon pengurangan kelihatan meningkatkan nilai pengegasan gas dan kecekapan pengegasan 19% dan 14% masing-masing. Pada umumnya, keputasan terbukti menuaskan untuk penggunaan pelepah pada perngkat pengegasan untuk menjana tenaga pada pemakaian haba.

TABLE OF CONTENT

LIST OF FIGURES

LIST OF TABLES

NOMENCLATURES

a	Cross section air of gasifier nozzle	m^2
A	Frequency factor	-
AF_{stoich}	Air fuel ratio at stoichimetric condition	-
D	Gasifier diameter	m
D_e	Diameter of clean gas outlet of the cyclone separator	m
E	Activation energy	kJ/mol
F_w	Weight fraction of moisture content in combustion gas	-
J_c	Diameter of dust outlet of the cyclone separator	m
h_w	Heat vaporization of water	MJ/kg
H	Height of the gasifier	m
H_c	Height of cyclone inlet duct	m
HHV	Higher heating value of biomass	MJ/kg
LHV	Lower heating value of biomass	MJ/kg
HHV	Higher heating value of producer gas	MJ/Nm^3
LHV	Lower heating value of producer gas	MJ/Nm^3
L_c	Length of cyclone body	m
MC_{wet}	Moisture content on wet basis	%
m_f	Mass flow rate of fuel	kg/h
M_{fuel}	Mass input of fuel	kg
M_i	Total mass input to the gasifier	kg/h
M_o	Total mass output from the gasifier	kg/h
n	Order of reaction	-
Q_{air}	Air flow rate	m^3/h
Q_i	Input power to the gasifier	kw
R	Gas constant	J/mol K
R^2	Regression coefficient	%
S_c	Height of cyclone outlet duct	m
t	Duration time of gasification	Min

T	Temperature	^{o}C
u_e	Ramdom uncertainty	%
u_i	Instrument uncertainty	%
u_s	Systematic uncertainty	%
u_t	Total uncertainty	%
U_{AFR}	Total uncertainty arisen from the measurement air flow meter	%
U_{c-a}	Total uncertainty arisen from the measurement of char-ash	%
U_{CCE}	Total uncertainty in the calculation of CCE	%
U_{CGE}	Total uncertainty in the calculation of CGE	%
U_{CH4}	Total uncertainty arisen from the measurement of CH_4	%
U_{CO}	Total uncertainty arisen from the measurement of CO	%
U_{CO2}	Total uncertainty arisen from the measurement of CO_2	%
U_{ER}	Total uncertainty in the calculation of equivalence ratio	%
U_{HHV}	Total uncertainty in the calculation of gas heating value	%
U_{CH4}	Total uncertainty arisen from the measurement of H_2	%
U_{OPF}	Total uncertainty arisen from the OPF weight	%
U_{N2}	Total uncertainty arisen from the measurement of N_2	%
U_{t-c}	Total uncertainty arisen from the measurement of condensate	%
U_{T1}	The uncertainty arisen from thermocouple at oxidation zone	%
U_{T2}	The uncertainty arisen from thermocouple at reduction zone	%
U_{T3}	The uncertainty arisen from thermocouple at pyrolysis zone	%
U_{T4}	The uncertainty arisen from thermocouple at drying zone	%
U_{T6}	The uncertainty arisen from thermocouple at gas outlet	%
U_{yield}	Total uncertainty in the calculation of gas production yield	%
v	Air velocity	m/sec
w	Actual mass of sample	g
w_o	Initial mass of sample	g
w_f	Final mass of sample	g
W_c	Width of cyclone inlet duct	m
WD	Weight mass of sample after drying	g
W_{OPF}	Fuel consumption rate	kg/h
WW	Weight mass of sample before drying	g

Y_{gas}	Dry gas yield	m^3/kg
η_g	Gasification efficiency	%
η_c	Carbon conversion efficiency	%
ε	Equivalence ratio	-
ρ_{air}	Air density	kg/m^3
β	Heating rate	$^oC/min$
α	Degrees of conversion	%

ABBREVIATION

AAE	Average absolute error
ABE	Average basis error
AF	Air-fuel ratio
ASTR	Air-steam ratio
C	Carbon element
CCE	Carbon conversion efficiency
CGE	Cold gas efficiency
CH_4	Methane
CO	Carbon monoxide
CO_2	Carbon dioxide
DSC	Differential scanning calorimetry
DTG	Derivative thermogravimetric
ER	Equivalence ratio
ER_M	Modified equivalence ratio
FC	Fixed carbon
FCR	Fuel consumption rate
FTIR	Fourier Transform Infrared Spectroscopy
H	Hydrogen element
H_2	Hydrogen gas
H_2O	Water vapor
MC	Moisture content
N	Nitrogen element
O	Oxygen element
S	Sulfur
S/B	Steam to biomass ratio
SA	Stoichiometric air of biomass fuel
SGR	Specific gasification rate
TDR	Thermal degradation rate

THC	Total hydrocarbons
VM	Volatile matter

CHAPTER 1

INTRODUCTION

This chapter provides a general background of energy shortage problems and an overview of biomass fuel as an alternative source of energy. The importance of biomass to protect the environment and its characterization are also reported. Moreover, gasification as a promising technology for the future and its advantages over the other methods of biomass conversion are presented. In addition, the problem statement, objectives and scope of the study are presented as well.

1.1 Background of Study

Nowadays, fossil fuels such as petroleum, coal and natural gas provide more than 80% of the total global energy demand and almost 100% of the energy needed for transportation sector [1]. However, excessive usage of fossil fuels is leading to fast depletion of fossil fuels as well as deterioration of the environment due to increase in greenhouse emissions [2]. Moreover the release of CO_2 pollutants is considered as one of the primary causes of the global warming and acid rain, which have started to affect the earth's climate, weather, vegetation and aquatic ecosystems. The related energy problems (fossil fuel depletion and environmental pollution) demonstrate a need for cheap, non-polluting and renewable source of energy [3]. Among all the renewable energy sources, biomass is considered as an alternative energy source that could provide national energy security, economic growth and environmental benefits. The term biomass represents all organic materials derived from organic matter (wood, crops, *etc.*), food processing, animal manure and municipal solid waste [4]. Biomass has significant features such as it is renewable, cheap and produces low emissions of greenhouse gases [5]. In addition, biomass material is the only renewable energy source that can be converted into convenient solid, liquid and gaseous fuel [6].

.

As a tropical country, Malaysia generates a tremendous amount of biomass waste each year. The biomass energy potential in Malaysia is shown in Table 1.1. The table also shows that oil-palm waste has the second largest energy potential to generate energy, next to forest residues. The types of oil palm waste that are generated from palm oil industries and plantations are empty fruit bunches (EFB), oil palm fronds (OPF), oil palm trunk (OPT), palm kernel cake (PKC), oil palm shell (OPSh), palm press fiber (PPF), palm oil mill effluent (POME) , and oil palm stone (OPS) [7].

Table 1.1: Potential of renewable energy in Malaysia [8]

Renewable Energy Resource	Annual Energy Value (RM Million)
Forest Residue	11984
Palm oil biomass	6379
Solar thermal	3023
Hydro	506
Solar PV	378
Municipal waste	190
Rice husk	77
Landfill gas	4

Although a number of studies have been carried out to investigate the feasibility of the converted oil palm waste such as EFB, shells and fibres into useful energy through different methods of biomass conversion [1, 9-12]. No previous study had been carried out on gasification of OPF for production of syngas via an updraft gasifier. There were some efforts have been made to convert the OPF into valuable products such as production of animal roughage [13], pulp and paper [14], activated carbon [15] and renewable sugar [16], but up to now almost all the generated OPF (26 million tons per year) are still left in the plantations mainly for nutrient recycling, soil conservation and erosion control [17], as all these method are still in the research stage.

As long as OPF has slow degradation rate and thus requiring long time to decompose and remain so long in the plantations causing mobilization problems and

to some extent can threaten the life of the workers. Moreover, the extensive use of the OPFs on the plantations land causes environmental pollution problems in nearby areas [15] and imbalance of nutrients in the soil. As a conclusion, this method of their disposal has serious negative effects on the environment.

On the other side, the fresh OPF contains about 70% of the moisture content, it is about 7–8 meters in length and contains relatively high amount of ash content. Moreover, the chemical structure of OPF shows that it composes of 49.8% cellulose, 83.5% hemicellulose and 20.5% lignin. Moreover, as the OPF drop in the plantations ground, it may mix with the mud or sand. Therefore, it is low-grade biomass in terms of cleanness.

Gasification technology could offer an alternative process for the conversion of low value material into a more valuable product (producer gas). The producer gas contains the gases such as H_2, CO, CO_2, CH_4 and traces of hydrocarbons by the supply of a gasification agent [18]. Gasification technology has many potential benefits when compared to other conventional options such as incineration or disposal by combustion, pyrolysis and liquefaction. Gasification for different biomass materials such as wood; coal; agriculture crops; bagasse from sugar cane; animal dung; chicken litters and marsupial solid waste has been tested in the past, however, gasification has feedstock flexibility [19]. Moreover, the gas produced from gasification technology is more versatile in its use than the original biomass as it can be used for thermal applications, power generation as well as to make synthetic fuels (product flexibility). Furthermore, gasification technology has a high efficiency and near-zero emission.

Gasification process takes place in gasifiers, which can be defined as a device or a reactor for converting the solid fuel into combustible gases; however, all the chemical reactions for gasification processes take place in it. Currently, there are four types of gasifiers available for research and commercial use. Gasifiers can be classified into fixed-bed, fluidized bed, entrained flow and cyclone type. The main difference between all these types of gasifier is concerned with how the biomass fuel and gasifying agent are moved in the gasifier [20].

Among all the gasifier types, fixed bed updraft gasifier is mostly suitable for high-ash (up to 25%) and high moisture content biomass fuel (up to 60%). It is also suitable for biomass with low volatile matter, possible to gasify biomass with large particle size and more suitable for direct combustion, where the producer gas is to be burnt in a furnace or boiler [21]. The major drawback of the updraft gasifier is that the producer gas contains high amount of tar, which requires extensive cleanup when the gas is to be used for internal combustion engine or turbines, but this drawback is of minor importance when the gas is to be used for direct heat applications [22].

1.2 Problem Statement

As a tropical country, Malaysia produces enormous amount of oil palm fronds annually as a by-product of the oil palm trees. Currently the oil palm fronds are unexploited and mostly left at the plantations as fertilizers, but as the OPFs have slow degradation rate and require a long time to decompose, thus remain long enough in the plantations causing mobilization problems and to some extent can threaten the life of the workers as it provides home for dangerous animals. Moreover, the accumulation of OPFs on the plantations land causes environmental problems such as pollution of ground water and imbalance of nutrients in the soil. Currently, it offers limited value to the industry. Therefore, converting OPFs into useful energy through gasification should be a promising disposal solution thus providing a source of green and renewable energy, which is considered as a good opportunity for the palm oil industry by adding value to the waste fronds. In addition, the structure of the OPFs fibers is comparable to those of hardwood, and both H/C and O/C ratios of the OPFs are equal to that of wood-based biomass, therefore, the replacement of expensive woody biomass with low price and high quality non-woody biomass could be achieved by a successful gasification of OPF.

It is well known that biomass varies in its physical, chemical and thermochemical properties due to its diverse origin and species. However, gasification of biomass is strongly affected by these properties. Despite the fact that few studies on OPF properties and its gasification in downdraft gasifier have conducted, no study had

been carried out on the effect of OPF properties on updraft gasification process. Full understanding of these properties on updraft gasification is essential in order to accomplish the process in a better, safe and environmentally acceptable manner. Moreover as the gasification process is highly dependable on biomass type, gasifying agent and the gasifier design, there is a need to investigate the performance of OPF gasification with different operation conditions. In addition, the tar formed during updraft gasification remains the biggest limitation and technical barrier that hinders the application of the product gases, nevertheless, the current methods of cleaning the tar such as filters and gas scrubbing have became unacceptable due to the fact that, these methods require water treatment and tar disposal equipments, which are considered as hazardous and costly. Therefore, there is a need to implement new, cheap and safety method for tar removal. The implementation of secondary air injection in an updraft fixed bed gasifier is totally absent from the literature.

1.3 Research Objectives

From the problem statement and opportunity of the research, the main objective of the research was to study the gasification of oil palm fronds in an updraft fixed bed gasifier with air as a gasifying medium. The specific objectives are listed as follow:

1. Characterization of oil palm fronds in order to develop correlations for the OPF moisture content and heating value based on its properties and to design and build a laboratory scale updraft gasifier and related accessories for gasification OPF material.

2. Investigate the performance and operation of updraft gasification of oil palm fronds with air as the gasification agent by varying various operation conditions.

3. Investigate in details the thermal behavior and gasification performance of updraft gasifier with variation of gasification air position.

4. Test and evaluate the effects of secondary air injection on the OPF gasification performance and tar removal.

1.4 Scope of Study

The scope of the present study is:

a. To characterize the OPF biomass material in terms of moisture content, density, proximate analyses, ultimate analyses, heating value, surface morphology, mineral analyses, fourier transform infrared (FTIR) as well as thermogravimetric analysis (TGA) at both inert gas and oxidant gas.

b. To develop a correlation for the prediction of OPF heating value and OPF moisture content based on the ultimate analyses and density, respectively.

c. To design and build an updraft gasification batch system to facilitate the study of the effects of different parameters on the gasification performance as well as to modify the gasifier in order to study the effect of gasification air configuration as well as the effects of secondary air injection.

d. To determine the performance of the gasifier by varying the operation conditions and fuel characteristics such as equivalence ratio, gasification air position, OPF moisture content and particle size.

e. To investigate the effect of secondary air injection on gasification performance and tar reduction.

1.5 Thesis Outline

This thesis consists of six chapters with references list as the last section. In the first chapter, general background about energy scarcity and problems were reported, and a brief statement of biomass as an alternative energy source and its importance to protect the environment are presented. Gasification as a promising technology for the future and its advantages over the other methods of biomass conversion are reported. In addition, problem statement, objectives and scope of the study are presented.

Chapter 2 present a literature review related to the gasification background, gasification advantages as well as gasification principles and its chemistry. Moreover, the chapter provides insight on updraft gasification and elaborates the factors

affecting gasification behavior in updraft gasifiers. Furthermore, the chapter describes the methods used to reduce the tar content and at the end of the chapter, conclusion remarks and highlights the importance of converting the fronds into useful energy is presented.

Chapter 3 describes the raw material and its characterization methods. It also describes design and construction of updraft gasifier gasifier and gasification system and finally presents the general procedure of the gasification experiments which used in this study. Chapter 4 presents the theoretical framework. However, all the theories employed in this study are described in details. Chapter 5 presents the results and discussions of the experiments, while conclusions derived from this study and suggestions for future work were reported in Chapter 6.

CHAPTER 2

LITERATURE REVIEW

This chapter presents a brief review on biomass properties that relate to thermochemical conversion methods and a brief assessment of oil palm plant wastes in Malaysia and their conversion technology into valuable products. Moreover, the chapter provides a literature review on gasification technology including background, reactions or chemistry of gasification, gasifier classification and updraft gasification as well as tar removal methods.

2.1 Biomass as a Fuel

Biomass fuel refers to organic materials derived from organic matter (wood, crops *etc.*), food processing and animal wastes. It is considered as one of the major potential resources for energy production, it is attractive in certain countries, because of its availability, renewability and neutral CO_2 content. Biomass can be converted into useful products via physical (extraction, briquetting and distillation), chemical, biological and thermochemical conversion processes as illustrated in Figure 2.1 [23]. However, biological and thermochemical processes are considered as the two main routes of producing bio-energy [24]. Biological conversion process consists of two pathways, fermentation or bio-ethanol and anaerobic digestion or bio-methanol. Bio-ethanol is accomplished by fermenting the biomass through a process similar to brewing, whereas there are several methods to convert biomass to bio-methanol. On the other hand, thermochemical route consist four pathways; combustion, liquefaction, pyrolysis and gasification [7, 25, 26]. Among all these conversion methods, biomass gasification is considered as a promising technology for converting solid biomass into fuel gas [27]. The most prominent properties of biomass fuels that

relate to biomass gasification are its moisture content, ash content and volatile matter content, heating value, energy density and bulk density [22].

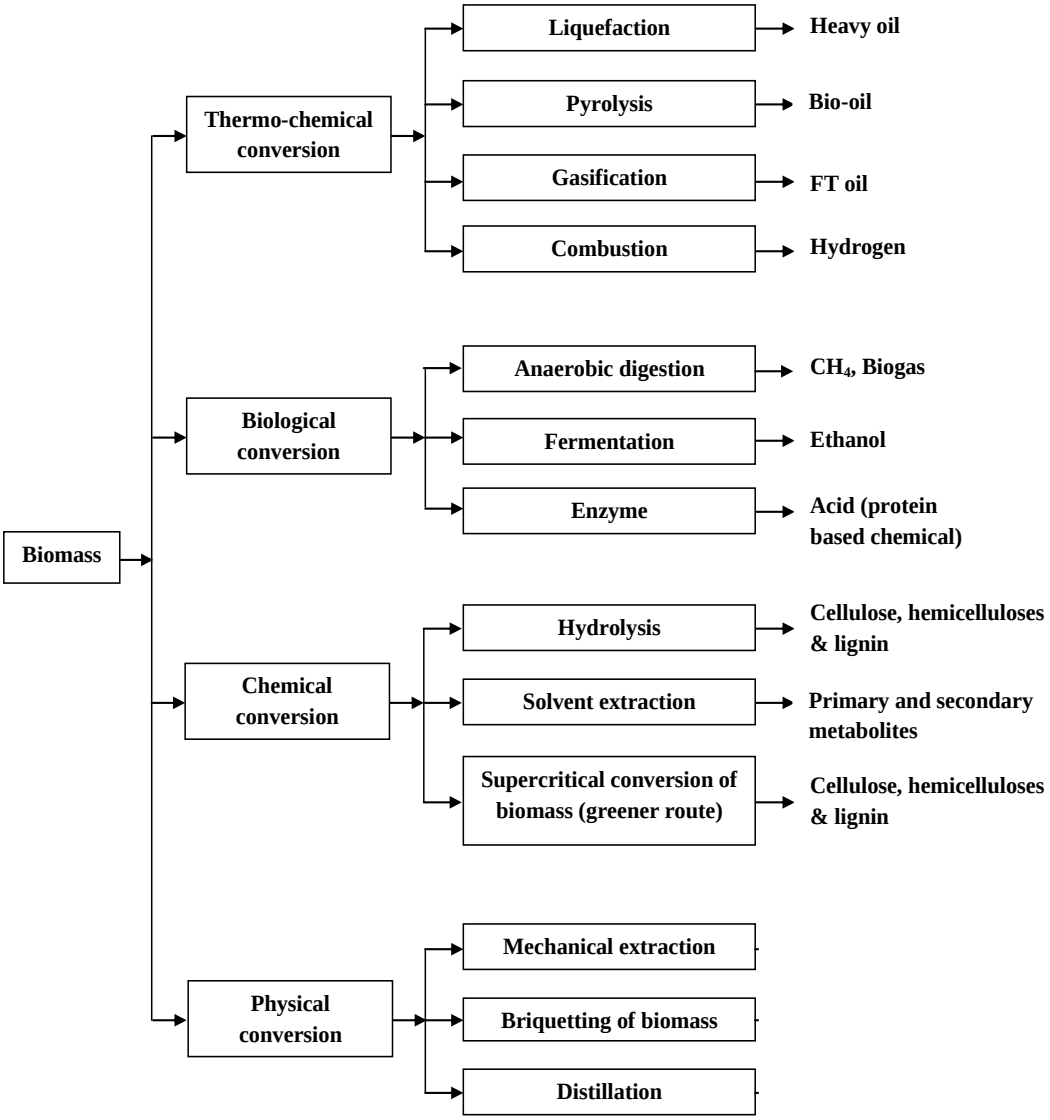

Figure 2.1: Biomass conversion processes [26]

2.1.1 Moisture Content

It is the amount of water in the biomass material, expressed as a percentage of the material's weight. The moisture content can be reported on a wet basis, on a dry basis, and on a dry-and-ash basis [22] as given:

$$MC_{wet} = \frac{WW-WD}{WW} \times 100\% \quad (2.1)$$

$$MC_{dry} = \frac{WW-WD}{WD} \times 100\% \quad (2.2)$$

where *WW* and *WD* represent the initial and final weight of biomass material. Usually, there are two methods to determine the moisture content of the biomass materials, direct and indirect. In the direct method, the moisture content of the material is removed and then the dry mass of the biomass is measured. This method is normally done by using ovens. On the other hand, the indirect method involves measurement of a property of the material that depends upon the moisture it contains, such as electrical and dielectric properties [28].

Moisture content of biomass material is considered as one of the important parameters of consideration on in gasification systems. It can greatly affect both the operation of gasifier and the quality of the producer gas [29, 30]. It is not desirable to use biomass material with high moisture content (>30%) in gasification systems. However, if the moisture content is excessive, many problems will arise. First of all, the producer gas may contain high water content that needs to be removed in order to make the gas combustible. Secondly, high moisture content reduces thermal efficiency of the gasification processes, because most of the heat is wasted for water evaporation, so that the producer gas will have low heating value. Finally, there will be difficulties in cooling and cleaning processes, such as increasing the pressure drop across the cooling and cleaning equipment. Table 2.1 shows acceptable range of moisture content for different gasifies.

Table 2.1: Acceptable moisture content for gasifier [22]

Type of gasifier	Moisture content% (wet basis)
Downdraft	Up to 25
Updraft	Up to 60
Open core	Up to 15

2.1.2 Ash Content

Ash content is an inorganic component (consists of carbonates and bicarbonates) in biomass fuel that is left as a solid residue when biomass is reacted. It is also expressed in the same methods as the moisture content (on wet basis, on a dry basis, and on a dry-and-ash basis), but generally it is expressed on dry basis [22]. The ash content of most biomass fuel is less than that of coals (less than 3%), but some biomass fuels have a high ash content [30]. It is reported that ash usually starts to melt at a temperature of around 1300^{o}C. The amount of ash content in biomass fuel and its chemical composition affect the gasifier operation process in many ways such as:

a) Slagging clinker formation in the gasifier that is caused by melting and agglomeration of ashes. This slagging can lead to excessive tar formation and/or complete blocking of the gasifier. Also, there is a possibility of air-channelling which can lead to a risk of explosion, especially in updraft gasifiers [31].

Melting the ashes at high temperature may hinder biomass and gas flow, as a result causing mal-functioning and sometimes causing shut down of the gasifier unit [28].

2.1.3 Volatile Matter

Volatile matter is a part of biomass that is released when the biomass is heated, up to 500^{o}C. Biomass fuels usually have high volatile matter content, about 70 – 90%, whereas coal has a low volatile matter content (around 20%) [22]. The amount of volatile matter content affects the gas quality of gasification process, however high volatile matter increases tar content in the producer gas [30].

2.1.4 Heating Value

The heating value, also known as calorific value or heat of combustion is defined as the amount of energy available in biomass fuel. The heating value is a function of the fuel's chemical composition and is used to indicate the usefulness of biomass as a fuel [28, 32]. The heating value is one of the important parameters of biomass fuels for

design calculations or numerical simulations of thermal conversion systems, planning and the control of power plants using this type of fuel [32, 33]. The heating value can be determined by two methods, experimentally by using an adiabatic bomb calorimeter, which measures the enthalpy change between reactants and products, or by calculation based on results from ultimate, proximate, structural analysis of the fuel [32, 34, 35]. Many formulas have been proposed to estimate the heating value of coal and some of the biomass fuels. Table 2.2 presents some of the formulas.

Generally, the heating value may be reported on two bases or according to two reference states, the higher heating value (HHV), also known as the gross calorific value and the lower heating value (LHV) or net calorific value. The higher heating value is more useful and refers to the heat released from combustion of biomass with the original and generated water in a condensed state. In other word, the reference state for HHV is the water in its liquid state [22, 28, 32], while the LHV is based on gaseous water as the product [32] or the reference state for this case is the water in its gaseous state [22].

Table 2.2: Equations for prediction HHV of biomass fuels

Equation	Biomass fuel	Based on	Ref.
$HHV = 146.76 + 621H - \frac{N + O - 1}{8} + 39.96S$	Coal	Ultimate analysis	[28]
$HHV = [33.4C + 143H - 15.4O - 14.5N] \times 10^{-2}$	Softwood and corncob	Ultimate analysis	[34]
$HHV = 0.196FC + 14.119$	Softwood and corncob	Proximate analysis	[34]
$\mathrm{HHV} = -3.0368 + 0.2218\mathrm{VM} + 0.2601\mathrm{FC}$	NA	Proximate analysis	[32]
$\mathrm{HHV} = 0.1739\mathrm{Ce} + 0.26631(1 - \mathrm{Ce}')$	NA	Structural analysis	[32, 36]
$\mathrm{HHV} = 0.0889\mathrm{L} + 16.8218$	Corncob	Structural analysis	[36, 37]

2.1.5 Bulk Density

Bulk density is defined as the weight of material per unit of volume. The bulk density of biomass is generally expressed in an oven dry basis (MC=0) or an as-is basis, with a corresponding moisture content (MC_w). The biomass fuels bulk densities show extreme variation in their value, ranging from 150 to 900 kg/m^3. In general, the bulk varies significantly with moisture content and particle size of the biomass fuel. The heating value and the bulk density of biomass determine the energy density (the potential energy available per unit volume) [22].

The bulk density of biomass fuel is very important for gasification process, especially in terms of handling and storage. However, biomass with high bulk densities needs less gasifier space for a given refueling time and represents high energy for volume value. On the other hand fuels with low bulk density give rise to insufficient flow under gravity, resulting in low heating value of the gas produced and low burning char in the reduction zone [30]. Table 2.3 shows average values of bulk densities of some biomass fuels.

Table 2.3: Average bulk densities of common biomass [38]

Fuel	Bulk density (kg/m^3)
Wood	110
Charcoal	223
Peat	197
Sawdust loose	134
Corn-cobs	202

2.1.6 Energy Content

The energy density is defined as the potential energy available per unit volume of biomass fuel. It is dependent on heating value and the bulk density of the fuel. Generally, the biomass energy density is about one-tenth of the fossil fuels [39].

2.1.7 Element Analysis

Biomass fuel has relatively uniform ash-free organic components. The major components are carbon, oxygen, hydrogen, and some biomass fuels have small amounts of nitrogen and Sulfur. Table 2.4 presents the major elemental components [22].

Table 2.4: Elemental composition of typical biomass as derived from ultimate analysis [22]

Element	Symbol	Wet percent (dry and ash-free basis)
Carbon	C	44 – 51
Hydrogen	H	5.5 – 6.7
Oxygen	O	41 – 50
Nitrogen	N	0.12 – 0.6
Sulfur	S	0.0 – 0.2

2.1.8 Particle Size

The particle size of biomass feedstock depends on the hearth dimensions but typically it is 10 – 20% of the hearth diameter. Larger particles of the feedstock can form bridges which prevent the feed from moving down, while the smaller size tends to clog the available air voidage, which leads to a high pressure drop and shutdown of the gasifier [40].

2.2 Oil Palm Fronds

Oil palm (Elaeis guineensis) grows well in wet, humid and tropical areas of the world, such as Asia, Africa and Central and South America. Currently, it has become one of the major economic and industrial crops in many countries that use it for producing edible oil [8]. Its fruits grow in large bunches; each bunch weighs about 10 – 40 kg. Each fruit contains a single seed known as palm kernel, which is surrounded by soft pulp. The edible oil used for cooking is extracted from the pulp, while the oil that is

extracted from the kernel is used mainly in soap manufacturing industries [7, 41]. At present, palm oil is the most dominant agricultural crops in Malaysia. Malaysia is the world's largest producer and exporter of palm oil, it contributes about 51% of the world palm oil production and 62% of the world exports [1, 42]. It is reported that, oil palm plantation represent about 56% of the total agriculture land and 11.75% of Malaysia's total land area [41]. Figure 2.2 shows Malaysia's oil palm production growth between 2004 and 2009 in million tons (MnT).

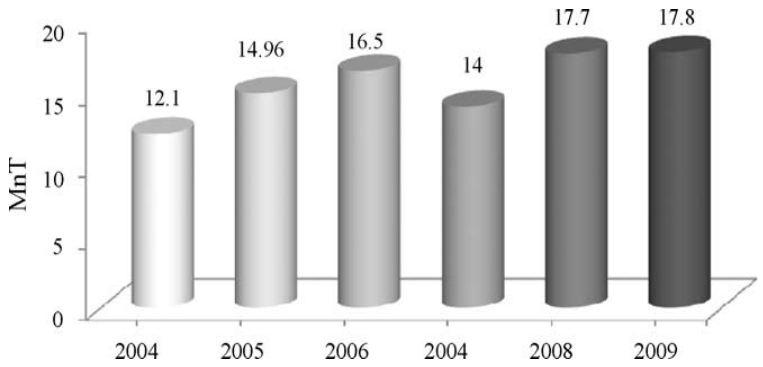

Figure 2.2: Palm oil production in Malaysia from 2004 to 2009 [8]

With the projected growth in the production of oil palm, there has been a concern on the tremendous quantities of palm wastes, that are produced from both plantation and processing industries. The types of the generated wastes include empty fruit bunch, oil palm fronds, oil palm trunk, palm kernel cake, oil palm shell, palm press fiber, palm oil mill effluent and oil palm stone. Most of these wastes are left to decompose in the plantation area and are used as soil conditioners [43] , and some of them, such as shell and fiber are used as the main source of fuels for power generation in oil palm mills [1].

At present, some of the oil palm wastes are converted into various types of valuable products, *e.g*. fibers from empty fruit bunch are used to make mattresses, seats, insulation *etc*, ashes produced from EFB are used as a good fertilizer or soil conditioner due to their high organic and nutrient content which is beneficial to the crops [41]. EFB belongs to the category of the fibrous crop residues (lignocellulosic residues), so that it can be converted into pulp [7]. Besides EFB, paper can be produced from oil palm wastes, and the palm fiber is used as a filter in thermoplastic

and thermoset composites. The oil palm ash is also used as an absorbent for removing pollutant gases such as sulfur dioxide and nitrogen dioxide.

It is reported that the amount of oil palm wastes produced annually is much more compared to that currently used for producing valuable products. The rest of the wastes such as fiber, shell, frond and EFB are burnt in an open area causing environment pollutants proving that the waste is still not managed properly. Moreover, as compared with other biomass materials generated in Malaysia, OPF is abundantly available at very low cost, especially in terms of cropping practice, collection and storage, which automatically reduce the overall cost of converting the OPF into energy related product [44]. The following paragraphs present the potential utilization of the OPFs.

Nowadays, OPF is one of the most abundant agricultural byproducts in Malaysia. OPF is obtained either during pruning for harvesting the fresh fruit bunch or during the replanting activities, and therefore it is available daily [45]. The availability of the OPF is about 26 million tons per year [46]. Up to now, almost all the generated fronds are left rotting in the plantations mainly for nutrient recycling, soil conservation and erosion control. However, this is the main disposal method for the fronds. The over-use of the OPFs on the plantations land results in both pollution of ground water and imbalance of nutrients in the soil. Thus, the huge surplus quantities of fronds produced by the plantations every year makes OPF a very promising source for both value added products and power generation.

The other alternative disposal method other than the natural decomposition of the OPFs in the plantations is direct combustion in fired boilers [47]. However, direct burning of any biomass material would generate toxic gases and impurities which create environmental problems such as air pollution [48]. The net conversion efficiency of biomass direct combustion is very low, ranging from 20% to 40%, though higher values may be obtained when the biomass material is co-combusted in coal-fired power plants [49].

OPF basically consists of petiole and leaflets as illustrated in Figure 2.3 and are categorized as fibrous crop residues [7]. Chemical and physical analyses show that

OPF is composed of approximately 70% fiber and 20% soluble carbohydrates [13], and the structure of the frond fibers is comparable to those of hardwood. OPF is also convert into pulp, which can be used as reinforcement component in newsprint production using softwood thermo-mechanical fibers (a kind of pulp produced via mechanical process) [7, 50]. Unfortunately, the production of pulp from OPF is still at research stage [7].

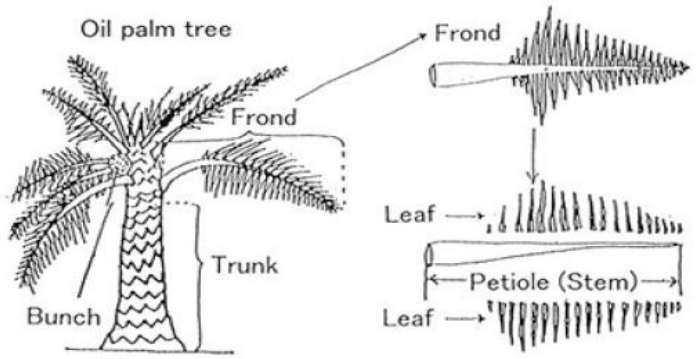

Figure 2.3: Oil palm frond [17]

As the nutritive value of the OPF is equivalent to that of rice straw, a number of studies were carried out to investigate suitable processing method for using the fronds as a roughage source for ruminants such as cattle and goats [13]. Chopping the whole fronds into pieces is the first step for producing ruminants' feed. Thereafter, the chopped fronds can be utilized as ruminants feed directly or mixed with other ingredients and conserved into cubes or pellets for use as a complete or balanced diet for fattening beef cattle [7, 13].

Because of its high amount of carbohydrates in the form of simple sugars, OPF has been used for the production of renewable sugars such as glucose, sucrose and fructose. Many studies have been carried out to investigate the conversion of the OPFs into glucose and xylose. However, the conversion may be through hydrothermal treatment followed by enzymatic hydrolysis [16, 44], or by pressing the fresh OPF into juice for the production of other valuable products such as lactic acid, bioethanol and biobutanol [45]. In addition, Saleh *et al.* [51] reported that hemicellulose can be extracted from oil palm frond fibres with autohydrolysis at 121^{o}C for 60 min, for

production of xylose and xylooligosaccharides, which can serve as functional food ingredients.

The OPF can be used as precursor for the production of activated carbon using physiochemical activation method. The effects of preparation variables, which were the activation temperature, activation time and chemical impregnation ratios (KOH: char by weight), on the carbon yield and bentazon removal were investigated by Salman and Hameed [52], they reported that activation temperature has the greatest effect on carbon yield, for which the optimum condition for the preparation of the activated carbon was obtained at the temperature of 850^{o}C, activation time of 1 h and KOH:char ratio of 3.75:1.

Nevertheless, the current utilization of OPF in these conversion processes does not consume the tremendous quantity of the fronds produced annually because some of these conversion methods are still in the research stage [7], and some of them have been found to have negative impact on the environment. Therefore, converting the wasted OPF into useful energy via gasification could be a good opportunity for the palm oil industries. This is due to the fact that OPF is abundantly available in Malaysia as compared to other biomass materials at a very low cost, especially in terms of cropping practice, collection and storage, which automatically reduce the overall cost of converting the OPF into energy related product [44].

2.3 Gasification

Gasification technology was first discovered independently in both France and England in 1798 [29], and by the year 1812, the technology had been developed to the point that the world's first coal gas company (Westminister Gaslight and Coke CO) was built in London [53]. Subsequently, gasification technology was rapidly developed, and by the year 1850 most of London was possible to be lighted with manufactured gas or town gas from coal [29]. In 1878, the gasification technology reached the point that it was possible to fire the internal combustion engine by the gas produced from gasifiers and the first attempt was accomplished by Dawson in

England [28]. After that, the technology has been almost forgotten when the fossil fuels became plentiful, available and cheap [28].

During the World War II (1939–1945) research and development of gasification units were speed up due to the shortage of petroleum, which occurred when oil imports were blockaded. It was reported that about one million units (vehicles, boars and generating power) were powered with the gas from gasification units that used many types of fuel such as coal, wood and charcoal. After the World War II, the technology was about to be forgotten again due to availability of inexpensive natural gas and crude oil which replaced the gas from coal units [28, 53]. But at the period of the oil crises (1970–1979) and due to the appearance of the effects of the rising oil prices on the economic and development sectors of oil-importing countries [54], many countries such as Sweden, South Africa and Philippines begun investigating in new design of gasification technology in safe, efficient and economical manner [28]. Currently, interest in developing large scale biomass gasification technology for power generation has been spread worldwide [55], this development made the technology more efficient, environmentally acceptable, convenient to use, and low in cost [4].

Gasification is a process that converts carbonaceous materials, such as coal, biofuel, or biomass, into synthetic gas or a mixture of combustible gas known as the producer gas. This is done by reacting the raw material at high temperatures with a controlled amount of a gasification agent such as air, oxygen, steam, carbon dioxide or a combination of any two of them [56]. The gasification process product composes of combustible gases such as hydrogen, carbon monoxide and methane and incombustible gases such as carbon dioxide and nitrogen in addition to solids (char) and condensable organic vapors known as tars [57, 58]. The relative proportion of each constituent and the energy content of the producer gas depend on numerous factors such as gasifying agent, geometry of the reactor, biomass type and composition, *etc*. Among all these factors the gasifying agent and gasifier design have the strongest influence on the gas composition and heating value [56, 57, 59].

The gasification process takes place in gasifiers which can be categorized in several ways according to the gasification agent such as air, oxygen, steam or carbon

dioxide; heat source such as auto-thermal or direct heat and all othermal or indirect heat; gasifier pressure such as atmospheric or pressurized; and gasifier design such as fixed bed, fluidized bed, entrained flow [23]. There are several types of biomass that have been used as a feedstock in gasification technology such as wood-based materials (woodchips, sawdust), energy crops (*e.g.* rice husk, cashew nut shell, sugar cane, empty fruit bunch, corn cob and olive kernels grass), agricultural residues and forestry wastes, some municipal solid wastes (sewage sludge), wastes from food processing, animal manure such as feedlot, chicken litter and cow dung.

2.4 Biomass Gasification Principles

Biomass gasification is a partial thermal oxidation process, which converts the biomass fuels into a high proportion of gaseous products. This results in gaseous product, known as a producer gas is a mixture of CO_2, CO, H_2, CH_4 and gaseous hydrocarbons, plus small quantities of char (solid product), ash and condensable compounds (tars and oils). The produced gas is more useful than the original solid biomass fuels and can be used for both heat and power generation as well as a chemical feedstock for the production of liquid fuels [23, 60]. Several oxidizing agents can be used for gasification process such as air, oxygen, steam, carbon dioxide or a mixture of these gases [57]. For economical reasons, air remains the most commonly utilized oxidizing agent. Gasification process takes place in gasifiers which differ in their design or biomass fuel used, but not in the chemical reactions. Regardless of gasifier type or oxidant agent, the biomass fuels must undergo drying, pyrolysis, oxidation, and reduction steps to convert the fuel from a solid phase into a gas phase [4].

2.4.1 Drying

The biomass fuels used in gasification have moisture content ranging from 5% to 35% [23]. Since the biomass fuels are introduced into the gasifier as moist materials, removal of the moisture occurs by using the heat in the zones below the drying zone [4, 30]. The rate of the moisture removal from biomass depends on the surface area

of biomass fuel, the temperature difference between the feeding fuel and the hot gases, the velocity and relative humidity of the gases as well as the internal diffusivity of moisture within the biomass fuel [30]. The drying process occurs at the temperature about 100 – 200^{o}C with a reduction in the moisture content of the biomass to less than 5% [23].

2.4.2 Pyrolysis

Pyrolysis (devolatilisation) is essentially the thermal decomposition of biomass in the absence of oxygen or air agent and always occurs at temperatures ranging from 200 to 600^{o}C [23]. However, pyrolysis of biomass starts at 350 – 550^{o}C and goes up to 700^{o}C. Pyrolysis is considered as the first step of thermochemical biomass conversions and plays a key role in product distribution. The main products are solids char, liquid tar, water and a mixture of gases (H_2, CO, CO_2, CH_4, C_2). The yield and the proportions of the pyrolysis product depend on the structure of the biomass, particle heating rate, gas residence time, and reactor temperature and pressure. Moreover, particle size affects the pyrolysis product yield due to heat diffusion limitation and gas conversion in freshly formed char [61]. Pyrolysis process occurs at different heating rates, categorized as slow, moderate and fast pyrolysis. The slow pyrolysis occurs at a heating rate of 10 K/s and leads to less liquid and gaseous product and more of char production, while the fast pyrolysis occurs generally at heating rate above 103 K/s [39].

2.4.3 Reduction

In the reduction zone (gasification zone), the char is converted into the gases by the reaction with the hot gases coming from the oxidation zone. These reactions occur in the absence or substoichiometric of oxygen, leading to a reduction between hot gases and chars. Generally, most of the reactions in this zone are endothermic reactions and occur in the temperature ranging from 800 to 1000^{o}C. The product gases leave this zone at temperatures between 200 and 300^{o}C [23, 30]. Reactions of the oxidation and reduction zones were discussed in Section 2.5.

2.4.4 Combustion

In this zone (called the oxidation zone), a reaction between solid pyrolysis products (char) and oxygen occurs resulting in a formation of CO_2. Hydrogen in biomass fuel reacts with oxygen to produce steam; as a result a large amount of heat is released due to the oxidation of carbon and hydrogen. This heat is used for drying, pyrolysis and reduction processes. If oxygen is present in substoichiometric value, partial oxidation of the carbon may occur to form carbon monoxide [23]. Generally, all reactions in the oxidation zone are highly exothermic reactions. The types and the quantities of the exothermic reactions depend on the temperature of the gasifier, type and quantity of oxidant agent [4].

2.5 Gasification Reactions (Chemistry of Gasification)

Biomass gasification is a complex process because a large number of reactions occur during the process, and a considerable number of biomass components are used. However, the gasification reactions inside the gasifier can be divided into three categories; combustion, gasification and pyrolysis. These reactions depend on the process parameters, biomass composition, gasifier type and the gasifying agent [62]. Air and steam are the most used agents in gasification; however, the overall gasification reaction with air and steam can be described by:

$$\underbrace{CH_xO_yN_zS_s}_{\text{Biomass}} + \underbrace{(79\%N_2 + 21\%O_2)}_{\text{Air}} \rightarrow \underbrace{CO_2 + CO + H_2 + CH_4 + N_2}_{\text{Gases}} + \underbrace{H_2O}_{\text{Steam}} + \underbrace{C}_{\text{Char}} + \underbrace{Tar}_{\text{Oil}} + \text{Ash} \quad (2.3)$$

The above equation is an overall reaction, and can be represented by the following sub-reactions:

$C + O_2 \rightarrow CO_2$	-393.5 kJ	complete oxidation	(2.4)
$C + 0.5O_2 \rightarrow CO$	-110.5 kJ	partial oxidation	(2.5)
$C + H_2O \rightarrow CO + H_2$	+131.3 kJ	water gas reaction	(2.6)
$C + CO_2 \rightarrow 2CO$	+172.4 kJ	boudouard reaction	(2.7)
$C + 2H_2 \rightarrow CH_4$	-74.8 kJ	methanation reaction	(2.8)

$CO + H_2O \rightarrow CO_2 + H_2$	-41.1 kJ	water gas shift reaction	(2.9)
$CH_4 + H_2O \rightarrow CO + 3H_2$	+206 kJ	steam reforming reaction	(2.10)
$2CO + 2H_2 \rightarrow CH_4 + CO_2$	-274.3 kJ	methanation reaction	(2.11)
$CO_2 + 4H_2 \rightarrow CH_4 + 2H_2O$	-165.0 kJ	methanation reaction	(2.12)
$CO + 3H_2 \rightarrow CH_4 + H_2O$	-206.1 kJ	methanation reaction	(2.13)

2.6 Gasifier Technology

As mentioned in Section 2.5, gasification process takes place in gasifiers, which can be defined as a device or a reactor for converting the solid fuel into combustible gases; however, all the chemical reactions for gasification processes take place in it. Currently, there are four types of gasifiers available for research and commercial use.

Gasifiers can be classified into fixed-bed, fluidized bed, entrained flow and cyclone type. The main difference between all these types of gasifier is concerned with how the biomass fuel and gasifying agent are moved in the gasifier [20].

2.6.1 Fixed Bed Gasifier

Fixed bed (sometimes called moving bed) gasifier consists of a fixed bed of solid carbonaceous fuel (coal or biomass) through which the gasifying agent and gas pass either up or down. They are considered as the simplest types of gasifier and are used efficiently for small scale application [29]. There are currently four types of fixed bed gasifiers, updraft, downdraft, cross-draft and open core gasifier.

2.6.1.1 Updraft or Counter-current Gasifier

It is the oldest and simplest type of gasifier, and can be designed to work at natural and forced draft. In this type of gasifiers [63], fuel is fed at the top of gasifier whereas the gasifying agent (*e.g.* air or steam) is taken at the bottom of the grate and diffused up through the bed of char. The produced gas leaves from the top of the gasifier but ash exits through the grate and is removed from the bottom. As the fuel moves

downward, it undergoes through drying, pyrolysis, gasification and combustion zones as shown in Figure 2.4 (a). The gas exits the gasifier at low temperature but contains high amount of tar (10 – 20%) [64].

The main advantages of an updraft gasifier are as follows [21]:

a. Simple and a low cost process
b. High thermal efficiency, due to high charcoal burn-out and internal heat exchange between the downward fuel and upward hot gases.
c. Low gas exit temperature.
d. Able to handle a fuel with high moisture content (up to 60%).
e. Able to handle a fuel with high ash content (up to 25%)
f. Flexible in the usable size of the biomass feedstock.

The major drawback of the updraft gasifier is that the producer gas contains high amount of tar, which requires extensive cleanup when the gas is to be used for internal combustion engine or turbines, but this drawback is of minor importance when the gas is to be used for direct heat applications [22, 65].

2.6.1.2 Downdraft or Co-current Gasifier

This type of gasifier has the same mechanical configuration as for the updraft gasifier except that the gasifying agent and the product gases flow downward the gasifier, as well as the biomass [63]. The fuel is fed at the top of the gasifier, but the oxidant intake is at the top or sides. The gas produced from this gasifier exits at the bottom of gasifier after passing through the hot zone (combustion zone) as shown in Figure 2.4 (b). This aids the cracking of tar [6], but at the same time increases the temperature of the gases, so lowers the overall gasification efficiency [40]. Downdraft gasifier has the same zone as updraft but the order is somewhat different [22]. Ash is collected and removed at the bottom of the reactor.

The major advantage of downdraft gasifier is that the producer gas contains low amount of tar, so this gasifier is suitable for internal combustion engine and turbine with minimal or no cleanup.

The disadvantages of downdraft gasifier may be summarized as follows [22]:

a. Low gasification efficiency due to the high temperature of the exit gas.
b. 4-7% of the carbon in the fuel remains unconverted.
c. The producer gas exiting the gasifier is at high temperature, requiring a secondary heat recovery system.
d. The producer gas contains a high amount of ash and dust particles because the gas has to pass through the oxidation zone. As a result, downdraft gasifier requires low ash fuel.
e. The moisture content of fuel must be less than 25% on the wet basis.
f. The fuel is relatively restricted in size; fuel must be sized from 4 – 10 cm.

2.6.1.3 Cross-Draft Gasifier

Cross-draft gasifiers are adopted for gasification of charcoal which results in very high temperatures (1500°C and higher) in the combustion zone, and these high temperature lead to material problems [22], but the insulation for the wall of the gasifier comes from the fuel and ash [29]. In this gasifier, both the gasifying agent entrance and the producer gas outlet are situated at the side and usually at the same level as shown in Figure 2.4 (c). Ash is removed at the bottom and the temperature of the gas leaving the gasifier is usually between 800 – 900^{o}C [40]. The main advantage of this gasifier lies in the small scale [22], but the major drawback is that this gasifier is suitable only for low ash fuel in order to avoid slag formation.

2.6.1.4 Open-Core Gasifier

It is designed for gasification of fine material with low bulk density such as rice husk. As shown in Figure 2.4 (d), the throat is not applied in open-core gasifier because of the low density of the fuel. As a result, this avoids the bridging of the fuel, which may prevent the flow of the fuel. In an open-core gasifier air and fuel are introduced at the top of the gasifier and both move down in co-currently. The product gases exit at the side of gasifier (immediately below the grate) whereas the bottom of the gasifier is set

in a basin of water which acts as a transport medium for the removal of ash. Rotating grate should be included in this gasifier to stir the fuel and remove the ash [22].

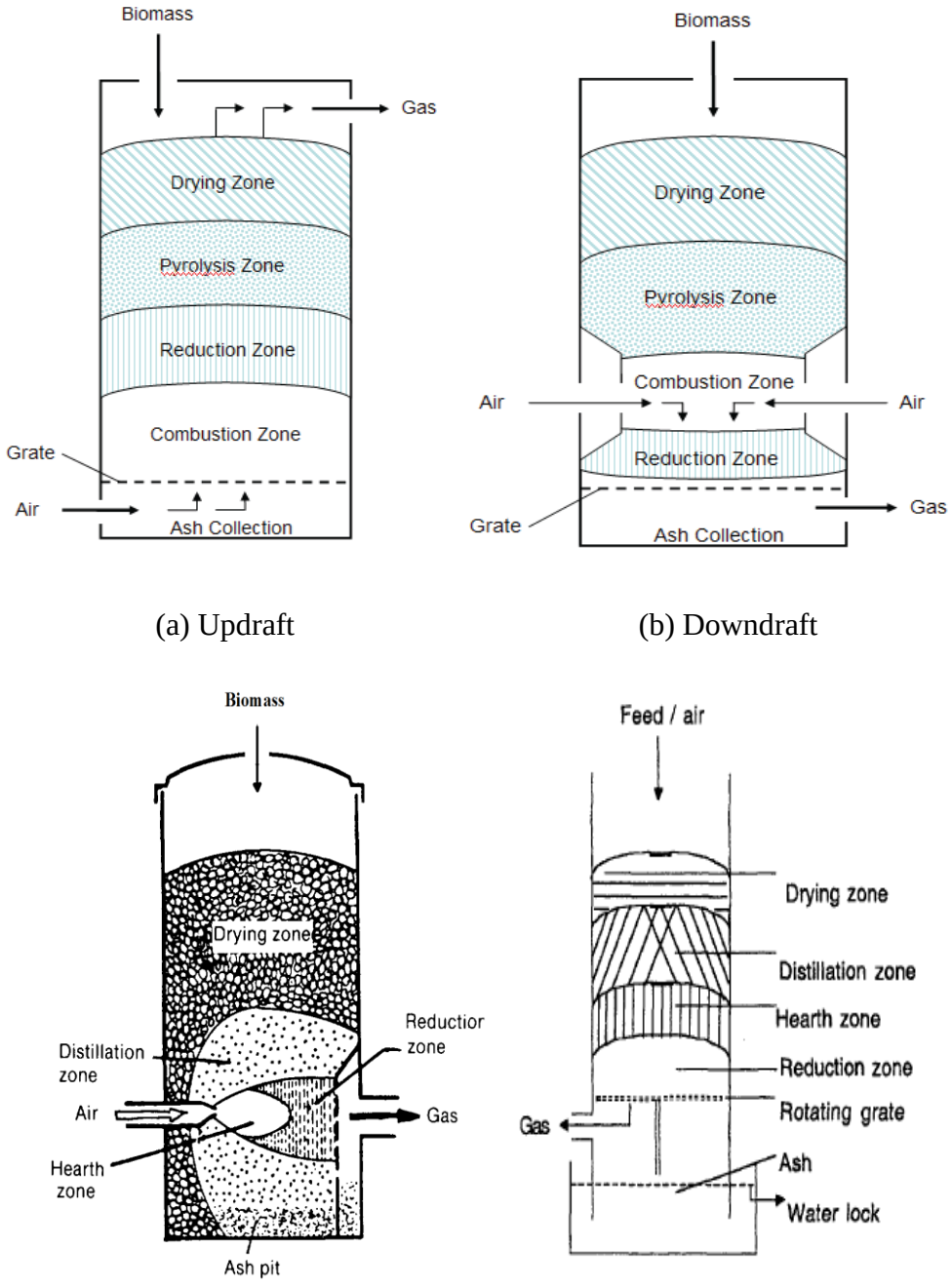

(a) Updraft (b) Downdraft

(c) Cross-draft (d) Open core

Figure 2.4: Fixed bed gasifiers with Air flow paths and reaction zones [22, 66]

2.6.2 Fluidized Bed Gasifier

This technology was developed to overcome the operational problems in fixed bed gasification with high ash fuels, in which the high temperature of fixed bed gasifiers develop a formation of ash slag. In general fluidized bed is more suitable for larger capacities (more than 10 MW_{th}) [22]. In fluidized bed gasifier, the fuel (usually fine particles) is fed into a suspended (bubbling fluidized-bed) or circulating (circulating fluidized-bed) hot solid material bed such as sand or ceramic. It is necessary that solid material must be fine and inert. The material bed behaves like a fluid and has some characteristics of the fluid. The particles of the fuel mix quickly with the hot bed material resulting in rapid drying and pyrolysis processes which produce a large amount of gases [39]. The gasifying agent (air or steam) enters the gasifier from the top with sufficient velocity through the bed of solid material and particles of fuel. Figure 2.5, shows both types of fluidized bed gasifier.

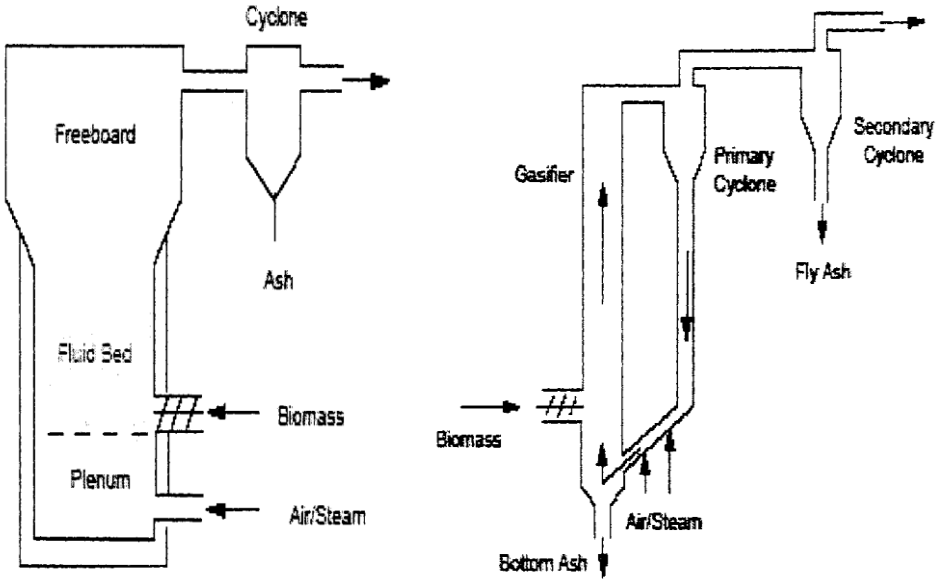

(a) Bubbling (b) Circulating

Figure 2.5: Types of fluidized bed gasifier

2.6.3 Entrained-flow Gasifier

An entrained-flow gasifier had been initially developed for coal gasification, but during the last decades, gasification process of an entrained flow gasifier has been investigated for wide variety of biomass [67]. However, due to the disadvantages of fixed bed and fluidized bed (lower rates of biomass conversion and higher tar yield), entrained flow gasifier became the promising technology, because entrained flow gasifier can operate at high temperature with fine particles of fuel and can achieve a high carbon conversion rate with low residence time, as a result an entrained-flow gasifier has a high capacity. Moreover, higher temperature impels the secondary-cracking of tar to reduce tar yield [68], so that the catalyst is no longer required. The disadvantages of an entrained flow gasifier are the complexity of the operational control and ash slagging [40]. Figure 2.6 shows the schemes of an entrained flow gasifier.

2.6.4 Cyclone Gasifier

Gas turbines are designed to be operated with a very clean fuel such as natural gas or light petroleum. However, the biomass gasification products have relatively high ash content which may form corrosive species that are considered thought to be the main cause of high temperature corrosion of gas turbine blades. This results in the increased maintenance costs and reduced equipment availability. Considerable amounts of research have been conducted to develop methods for the cleaning of the producer gas from biomass gasification to be suitable for the operation of a gas turbine, but most of these methods include extensive gas cleaning that requires high capital investment [69]. The alternative method is the use of cyclone gasifier, which achieves good ash separation and removes significant amounts of alkalis [70]. The fuel (usually in a powder form) and the gasifying agent enter together at the gasifier through a tangential inlet connected to the cylindrical part of the cyclone. As the fuel and its carrier enter the cyclone, it changes its motion to a cyclonic motion and twist down near the wall of the cyclone gasifier. The gasification processes can be divided into three steps as shown in Figure 2.7 as pyrolysis, oxidation and reduction. The stream

comes down till reaches the position (after reduction step) at which the gas and fly ash are separated from each other, resulting in the ash going down to the bottom of the gasifier while the gas exits through the central vent-pipe [71]. The advantages of this technique can be summarized as follows [72, 73]:

a. The gasification temperature could be kept at low level, resulting in keeping the alkali metals in the char.
b. Provides a proper mixing of gasifying agent and fuel and a long residence time of fuel particles in the gasifier.
c. Required lower investment compared to the other extensive cleaning methods.

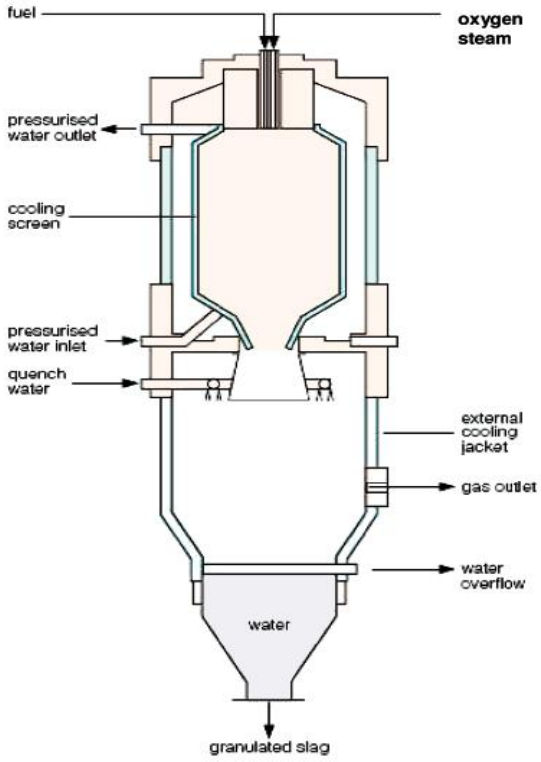

Figure 2.6: An entrained flow gasifier

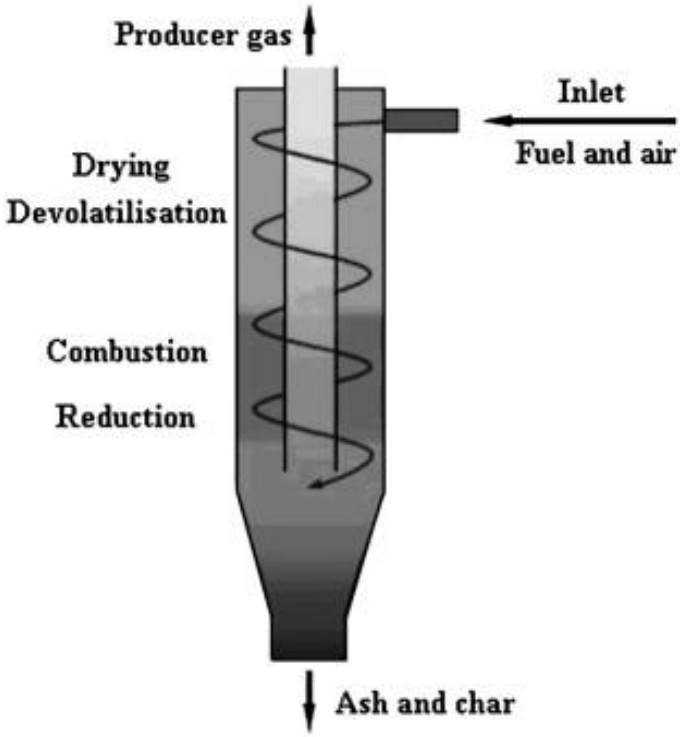

Figure 2.7: Cyclone gasifier [71]

2.7 Updraft Gasification

As mentioned in Section 2.6.1.1, the fuel particles are fed at the top of the gasifier in updraft gasification, while the gasification agent is introduced at the bottom of the gasifier. The fuel and the producer gas move in different direction, however the gas moves upwards while the fuel moves downwards and goes through drying, pyrolysis, gasification and combustion zones as shown in Figure 2.4 (a). Different reactions occur in each zone in order to convert the fuel and the gasification agent into gaseous mixture and ash residue. The evaporation of the fuel moisture content takes place in the drying zone as an endothermic reaction, given by:

$$\underbrace{CH_xO_yO_zS_s}_{\text{Wet biomass}} + \text{Heat} \rightarrow \underbrace{CH_xO_yO_zS_s}_{\text{Dry biomass}} + \underbrace{H_2O}_{\text{Steam}} \tag{2.14}$$

Pyrolysis or devolatization of biomass is a quite complex phenomenon, because it involves a large number of chemical reactions kinetics [74] with consideration of heat transfer. Moreover, the decomposition reactions of biomass are slightly endothermic

and slightly exothermic. Endothermic reactions occur at low temperature whereas the later occur at high temperature [75]. Pyrolysis process occurs at different heating rates, categorized as slow, moderate and fast, however the production of volatiles is highly influenced by the high temperature (fast pyrolysis). As a result of pyrolysis, the biomass fuel decomposes into gases, tar and charcoal, given by:

$$\underbrace{CH_xO_yO_zS_s}_{\text{Dry biomass}} + \text{Heat} \rightarrow \underbrace{CO_2 + CO + H_2 + CH_4}_{\text{Gases}} + \underbrace{C}_{\text{Char}} + \underbrace{\text{Tar}}_{\text{Liquid}} \quad (2.15)$$

Gasification or reduction zone contains many heterogeneous reactions and their reaction rate depends on mass transfer in the gas phase and diffusion or chemical reaction [74]. Finally, the charcoal moves downward to the combustion zone to be oxidized with the oxygen in the air to produce CO_2, CO and large amount of heat energy. This energy is useful and adequate for the other processes *e.g.* evaporation of the fuel moisture, pyrolyze the volatiles, heating the reacting air, maintain high temperature of the gasifier and providing the energy required for all endothermic reactions. The reactions of oxygen with charcoal are exothermic ones [75]. The updraft gasification may be categorized according to the following:

a. Status of the draft (natural draft and forced draft)
b. Oxidizing agent (air, air-steam, steam only and oxygen only)
c. Oxidizing temperature (normal temperature and high oxidizing temperature)
d. Bed temperature (ambient temperature and high temperature)
e. Gasifier pressure (pressurized and non-pressurized)
f. Position of the lit (bottom lit and top lit).
g. Using of catalyst (gasification with catalyst and without catalyst).

2.8 Factors Affecting Gasification

As it is known the objective of gasification process is to obtain desired composition of the product gas with small amount of impurities (tar) and to increase the net energy conversion. There are several factors influencing the gasification processes and thus affecting the final products. These factors can be categorized into three groups, gasifying agents (air, steam, air-steam), fuel characteristics, operation conditions.

Sections 2.8.1 to 2.8.3 describe the effects of these main factors on the quality and the quantity of the producer gas and on tar production.

2.8.1 Gasification Agent

2.8.1.1 Air Flow Rate or Equivalence Ratio (ER)

ER has a direct relationship with the flow rate of oxygen (or air), it is defined as the actual amount of oxygen (or air) supplied to the gasifier to the theoretical amount of oxygen (or air) required for stoichiometric combustion [5, 57] as shown in Eq. (2.16).

$$ER = \frac{AFR}{AFR_{stoich}} \tag{2.16}$$

where AFR and AFR_{stoich} represent the actual air (or oxygen) flow rate and air (or oxygen) flow rate at the stoichiometric condition, respectively. Oxygen is used as a gasifying agent. Nowadays, air is used instead of oxygen for economical purpose, but air has negative effect by diluting the producer gas due the presence of nitrogen [57], and therefore, there is an optimum value of ER to any biomass fuel. There is another expression for the equivalence ratio called modified equivalence ratio (ER_M) which is the ratio of stoichiometric oxygen to actual oxygen used in gasification of coal or biomass [76]. The modified equivalence ratio used when a mixture of air and steam was used as an oxidant. However, modified equivalence can be calculated as:

$$ER = \frac{\text{Stochiometric oxygen}}{\text{Actual oxygen through air and steam}} \tag{2.17}$$

Madhukar [57] found that as the ER increases from 0.2 to 0.6, both H_2 and CO yields decrease, while CO_2 increases. This is due to the oxidation of H_2 and CO to H_2O and CO_2, moreover with a low value of ER, solid carbon C(s) and CH_4 are formed in the gasifier, but both of them get oxidized if more oxygen (high ER) is available. Philippe [77] investigated the effects of oxygen factor (defined as the O_2 fraction of the stoichiometric O_2 amount used in the combustion process). However, oxygen factor is typical to ER. They reported that with an increase of oxygen factor from 20 to 50% (or increase ER from 0.2 to 0.5), CO and H_2 decrease from 28% to 15% and from 21% to 7%, respectively, while CO_2 and CH_4 remain fairly constant at

10% and almost zero, respectively. They also found that the best gasification efficiency is obtained when oxygen factor is 25%. Kim [78] observed an increase in producer gas yields, and more amount of H_2 and CO with a decrease of air flow rate from 0.076 to 0.056 m^3/min. Also the effects of ER on gasification process depend on other factors such as temperature and the presence of steam. The effects of ER with temperature will be discussed in Section 2.8.1.3.

Ningbo *et al*. [5] studied the effect of ER at constant steam feed rate, they found that an increase of ER from 0.0 to 0.3, decreased H_2 content from 44.45 to 23.56%. On the contrary, the CO_2 content increased from 23.7 to 48.74%, but CO first increased till ER equal to 0.05 then decreased, and the HHV of the producer gas follows the same trend as CO. The reason of decrease in HHV with higher ER was due to greater consumption of H_2 and CO, because as more O_2 (higher ER) is supplied to the gasifier, these reactions ($C + 0.5O_2 \rightleftharpoons 2CO$, $C + O_2 \rightleftharpoons CO_2$ and $2H_2 + O_2 \rightleftharpoons 2H_2O$) participate more in the gasification process. Another study was done by Gerardo and Kalyan [20] to investigate the of ER_M at constant feed rate of steam, they found that with increase of ER_M which means the decrease of O_2 supplied with the air, implies a decreasing of oxidation zone temperature as well as increasing the concentration of steam. The consequence, CO decreased whereas CO_2 and H_2 increased. This is due to the fact that as the oxidation temperature is lowered, the reaction ($C+O_2 \rightleftharpoons CO_2$) would be favored. Another explanation was that, increasing ER_M at constant steam feed rate increases steam-air ratio; therefore, it favored the reaction of char with H_2O rich mixture to produce H_2 and CO which reacted with H_2O to produce CO_2 and H_2.

2.8.1.2 Steam to Biomass Ratio (S/B)

Steam to biomass ratio (sometimes called steam to fuel ratio) is defined as the steam mole supplied to the reactor per empirical mole of biomass fuel [20]. It could be controlled in two ways, either by varying the steam feed rate and keeping the biomass feed rate [9] or *vice versa*. Supplying steam to gasifier has several advantages such as increasing the hydrogen production rate. Ningbo *et al*. [5] observed that an increase in

S/B from 1.05 to 3.47, causes CO_2 to decrease but H_2 and CO increase, while C_2H_2 and C_2H_6 remain constant at 7% and 1%, respectively. H_2 increased from 47.61% to 60.59%. Abuadala and Dincer [79] found that with an increase in S/B from 0.17 to 0.51, CO decreased from 35% to zero (CO would be negligible at S/B > 0.5), whereas H_2 and CO_2 increased. The same trend for H_2, CO_2 and CO was observed by Madhukar and Goswami [57]. With an increase in S/B from 0.4 to 0.8 at fixed ER_M of 1.6, Gordillo and Kalyan [20] reported an increase in H_2 by 57% whereas CO decreases by 26.6%. Moreover the gas LHV increases by 20%. The authors also reported that, S/B had more significant effect on LHV than that by ER. Gerardo *et al.* [76] investigated the effect of air steam ratio (ASTR) on gas composition. ASTR is defined as the ratio of oxygen in the air to the total oxygen in the air and steam in the oxidizer mixture and it is ranged from zero (steam only) to 1.0 (air only). They found that with a deceasing of ASTR (more steam) H_2 and CH_4 increased, while CO and CO_2 decreased. Effects of S/B on gas composition also depend upon other factors such as temperature and presence of catalyst. The catalytic steam gasification was studied by Jianfen *et al.* [9], they reported that with an increase in S/B from 0 to 2.67, both gas yield and H_2 yield increased, whereas CO, CH_4 and gas LHV decreased. However, H_2 content in the gas increased initially and decreased subsequently in S/B range; the decrease was due to excessive steam quantity that lowered the reaction temperature.

2.8.1.3 High Temperature Gasifying Agents

The use of highly preheated gasifying agent (air and steam) called High Temperature Agent Gasification, or HiTAG [27], provide additional energy into gasification processes [80]. However, it has significant advantages for the gasification of low-grate biomass fuels such as sludge. Yang *et al.* [27] reported that an increase of feed gas temperature would lower the tar yield, higher H_2 content of the producer gas, higher calorific value of the fuel gas, higher gasification efficiency and higher the production rate of the producer gas. The disadvantage of preheating air and steam is that, the system requires an additional energy source which has to be supplied by the regenerative preheated leading to an increase in the cost of the system [27, 80].

Weihong *et al.* [27] investigated the biomass gasification with high air temperature (up to 1473K) and reported that, an increase of air temperature resulted in higher gasification rate, higher molar fraction of H_2, CO and C_mH_n, thus a high LHV. They also found that, there was a critical value of air temperature above which preheating of air no longer efficient if the gasification purpose is to maximize the yield of gaseous products during the HiTAG process. This value was decided by the melting temperature of ash. Kentaro *et al.* [81] found that the high temperature of steam affected the reaction temperature, which in turn affected the gas composition strongly. However, the H_2 fraction in the synthesis gas was varied between 35–55% vol. at the outlet of the gasifier.

2.8.2 Fuel Characteristics (type, properties and size)

Biomass elemental composition has a significant effect on the producer gas composition. The release of pyrolysis from biomass fuel is highly dependent on hydrogen/carbon and oxygen/carbon ratio, and it increases as these ratios increase, but it increases more with an increase in Hydrogen/Carbon ratio. The concentration of oxygen in biomass affects the ER for gasification, *i.e.* biomass with higher amount of oxygen concentration needs lower ER, because this inherent oxygen will be available for gasification process. Ash content in biomass is also one of the important factors that affect the gasification process. Although the high ash content (above 5%) causes slagging, and consequently ash agglomeration due to fusion [82], a successful updraft gasification with biomass ash-content up to 24.1% is reported in the literature [20, 83, 84].

Another important factor is particle size of the biomass feedstock. The acceptable size depends on a certain extent of the design of the unit. Usually, particle size of less than 50 mm would be recommended for the fixed bed gasifier. The earlier studies on updraft gasifiers were confined to small size. For example, Khummongkol and Arunlaksalmmron [85] studied the gasification of sun-dried mangrove wood with size of 2–5 cm long and 5 cm in diameter in an updraft gasifier. Recently, larger size of biomass was gasified in an updraft gasifier. Saravanakumar *et al.* [86-88] gasified

long wood sticks with length of 68 cm and diameter of 6 cm in an updraft gasifier. They reported that, long wood sticks could be successfully gasified in a top lit updraft gasifier and a bottom lit updraft gasifier, and also found that the efficiency of gasifier was 73% and 75%, respectively. Increase in gas yield and hydrogen yield were observed with a decrease in particle size. Jianfen *et al.* [9] reported that both gas yield and hydrogen yield improved as the particle size decreased from 5–2 mm to below 0.15 mm. It is also observed that decrease in particle size resulted in less char and tar production. Siyi *et al.* [89] studied the effect of three particle sizes small, medium and large with size of (below 0.075 mm), (0.075–0.6 mm) and (0.6–1.2 mm) respectively and reported that production of char and heavy tar were negligible with the smallest size.

2.8.3 Operation Conditions

2.8.3.1 Reactor Temperature

To achieve high reactor temperature (above 1000^{o}C), heat must to be provided to the reactor directly or indirectly. This procedure is always associated with adjustment of the reactor design or reactor configuration [80]. It has been observed that gas quality would be generally influenced by a high reaction temperature especially the hydrogen yield. Several researchers reported an increase in gas yield and hydrogen yield corresponding to the increase in the reaction temperature [5, 90, 91], because both carbon and methane reformed at high temperature and were converted to H_2 and CO, but at high temperature (above 1000 K) the hydrogen content decrease as the temperature increased [56, 57, 79, 92]. This might be due to Le-Chatelier's principle, "high temperature favors reactants in an exothermic reaction thus explaining the increase in CO and reduction in H_2 (and CO_2 yield) at higher temperature" [57].

2.8.3.2 Reactor Pressure

"High-pressure gasification reduces the size of the reactor for the same amount of feedstock and can act to reduce the need for further compression when the

gasification products are intended for subsequent use in Fischer-Tropsch process or other chemical synthesis which requires high pressure" [82]. Madhukar and Goswami [57] have studied the effect of pressure upon the producer gas composition. Their research aimed to study the effect of both increasing the pressure to above 1 atm (up to 25 atm) and reducing the pressure to below 1 atm (till 0.1 atm). With increase in pressure to above 1 atm, a decrease in CO and H_2 were observed, while CO_2 increased. They also observed an insignificant improvement in gas composition for reducing the pressure to below 1 atm. The effect of reaction pressure on gasification product at high temperature (923 K) was investigated by Hanaoka *et al.* [91]. They reported that with an increase in pressure from 0.3 – 8.4 MPa, the H_2 yield and conversion to gas increased with an increase in reactor pressure up to 0.6 MPa, and subsequently both H_2 yield and conversion to gas decreased as the pressure increased to 8.4 MPa. Other authors like Agus *et al.* [93] studied the effect of pressure with different reactor temperature, and found no considerable change in gas composition by increasing the pressure at temperature less than 600 K. They, however, reported that with an increase in the pressure from 1 – 3 atm at temperature high temperature (above 900 K), a significant increase was in H_2, CH_4 and CO_2. Insignificant changes in H_2, CH_4 and CO_2 were observed with further increase in pressure.

2.9 Studies of Biomass Gasification in Updraft Gasifier

As mentioned in Section 2.6.1.1, updraft gasification is the oldest form of gasification that used for coal and biomass, and it is still used for both coal and biomass gasification. However, the first commercial updraft gasifier was installed in 1839 for gasification of coke. By the end of the Second World War and due to the energy crisis of 1970s', an interest in biomass gasification was renewed. Therefore, many institutes in Europe began to develop updraft gasifiers. One of those institutes was the Technical Research Centre of Finland (VTT) which developed an updraft gasifier for peat and wood. However, in 1989 Kurkela *et al.* [94] developed a gasifier in VTT to gasify the low-grade fuel such as peat, wood chips, MSW (briquetted) and straw in an updraft gasifier. The analysis of the producer gas gas was as follows: CO, 25-27%; H_2, 13-15%; CH_4, 2.4-2.8%; CO_2, 8-10%; N_2, 47-50%, whereas the H_2O content in the gas

was calculated from the material balances and it was in the range of 19-23% on volume basis.

Thereafter, many studies of biomass updraft gasification have been carried out. A successful updraft gasification of mangrove wood was accomplished in 1990, and maximum value of 3.666 MJ/m^3 was reported on the energy content [85]. A cylindrical updraft gasifier of constant diameter of 76 mm and a height of 1500 mm above the grate was used for the gasification jute-stick in 1994, and the heating value of the product gas was in the range of 4.106-4.689 MJ/m^3 [95]. In 1996, a counter-current reactor of total length 1650 mm and constant diameter 76 mm was used for updraft gasification of jute stick with air as the gasifying agent. The performance was evaluated for a different particle size of the biomass fuel at different superficial velocities of inlet air (0.0337-0.1011 m/s). The calorific value of the producer gas was in the range of 4.306- 4.912 MJ/m^3 [96]. While in 1999, Di Blasi *et al.* [58] designed and constructed a laboratory-scale updraft gasification plant for the gasification of wood and agricultural residues (nutshells, olive husks, grape residues, and straw pellets). The optimum heating value of the syngas of gasification of wood and agricultural residues was in the range of 5-5.5 MJ/Nm^3 with 28-30% CO, 5-7% CO_2, 6-8% H_2, 1-2% CH_4, and small amounts of C_2- hydrocarbons.

In 2003, Carlos *et al.* [97] used the gasification facility that was built at the Royal in Institute of Technology (KTH) to investigate the updraft gasification of three types of biomass fuels, which were bark, wood chips and wood pellets. The experiments were performed with preheat feed gas. The high temperature gasification contributed to many advantages such as maximizing the gaseous product yield and minimizing the tar generation in an updraft fixed bed gasifier. Another study was establish by Jae *et al.* [98] in which the pelletized waste (a mixed of plastic and cellulosic materials) was gasified a temperature range of 1100–1450^oC. The authors reported that the cold gas efficiency was around 61%, while the heating values of product the gases were in the range of 11.72–14.40 MJ/Nm^3.

In 2004, the disposal of high amount of waste generated from the food industries posed a major issue to companies. The annual cost of American's food industries to dispose the waste was about $1 billion [19]. Therefore, the Oklahoma State University

proposed a study in which an updraft gasification technology was used as an alternative solution for disposing the food processing byproduct such as cardboard, inedible meat and sludge. The heating value and cold gas efficiency were in the range of 9.7-13.8 MJ/kg and 47-71%, respectively. While the total potential saving was about $822,109/year. Another study was carried out in 2004 by Kalisz *et al.* [99] in which a continuous high temperature air/steam gasification (HTAG) was used to investigate the updraft gasification of wood pellet using preheated (up to 1600^{o}C) air and steam as a gasifying agent. Two different gasification processes were studied *i.e.* gasification with preheated air only and gasification with preheated air and steam. For both cases, the lower heating value of the producer gas remain stable and relatively at high level, namely about 8 MJ/Nm^{3}. On the other side, the tar content had been affected in a negative direction and many problems had been occurred, *i.e.* clogging of pebble bed.

A producer gas from updraft gasification of sun dried wood (*Subabool*) was used for hardening steel in 2005 [100]. The system consisted of a batch type updraft gasifier, an air swirling type PG burner and a hardening furnace. The furnace attained a uniform temperature of 900^{o}C within 30 min and able to hardening 20 kg of steel in 2 hour by consuming 15 kg of biomass.

An updraft gasification of biomass using high-temperature air up to 1473 K was investigated by Yang *et al.* in 2006 [27]. The authors did not report an improvement in a gas quality only, but they found that there was a critical limit for preheating the air, above which the preheating of the air was no longer efficient to improve the gas yield and quality.

Recently, a number of studies were carried out on an updraft fixed bed gasifier to extract the available energy form different types of biomass in the previous five years. Table 2.5 presents several investigations conducted on updraft fixed bed gasifier. In 2007, Kim *et al.* [78] studied the gasification of rice husk in an updraft gasifier in order to quantify combustible gases from the rice husks gasification. The effect of air flow rates on combustible gases was studied and observed that the major combustible gases were CO, H_2 and total hydrocarbon (THC) and the total percentage of these gases were about 36.18% of the total gas produced. In the same year, updraft

gasification experiments of a woody stick biomass with a size of 6 cm in diameter and 68 cm in length were carried out by Saravanakumar *et al*. [88], and the results showed a yielding gasifier efficiency of 73%.

During the year 2008 to 2011, many studies were conducted to investigate the gasification products of several biomass such as pine sawdust [5], palm wastes [9], wood pellets [65], softwood pellets [74, 101], rape straw, corn straw, sunflower stem [65] cattle manure [102] and woody biomass [103] by using different gasification mediums such as air, oxygen, steam, high air-steam temperature and enriched air. These materials proved to be suitable for gasification in an updraft gasifier under different operating conditions. However, most of the materials produced a synthetic gas with a heating value in the range of 4 – 13 MJ/m^3 for different operating conditions.

In 2012, investigation of the gasification characteristics of mesquite (*Prosopis glandulosa*) and redberry juniper (*Juniperus pinchotii*) were carried out in an updraft fixed bed gasifier by using air as an oxidizing agent [104]. The study showed that both types of biomass generated high quality gas. The effects of equivalence ratio, particle size and moisture content were also studied. Segiani *et al.* [105] carried out sewage sludge gasification and co-gasification (sewage sludge with wood pellets) experiments at a pilot-scale plant operating at atmospheric pressure using air as media. It was reported that, it would be possible to co-gasify sewage sludge with wood pellets in an updraft fixed-bed gasification installations, and the gas composition and heating value of the experiments are shown in the same table. Joseph *et al.* [103] performed gasification experiments for chicken litter in updraft gasifier with air as a medium gasifying agent, and the results obtained confirmed that the gasification process is a vital method of chicken litter disposal.

Although several studies were carried out to investigate experimentally the updraft gasification of several types of biomass fuels, in order to explore their feasibility and suitability as a feedstock in updraft gasifier, no attention has been paid on the updraft gasification (with air, oxygen, steam, CO_2 or high temperature air-steam gasification) of the oil palm fronds produced in Malaysia or anywhere else.

Table 2.5: Various investigations conducted on updraft fixed bed gasifier

System configuration and Operation parameters		Investigated parameters	Optimum obtained results	Date-Ref.
Rice husk ID: NA H: NA	Feeding batch: 50kg GA: Air AFR: 0.056-0.076 m^3/min	Effect of air flow rate on: Gas composition Gas production	Gas composition (vol. %): CO:28; H_2:7.5; THC: 0.68 Gas production (kg): 39.6 AFR (m^3/min): 0.056	2007 [78]
Long stick wood Length: 75 cm Breadth: 60 cm H: 134 cm Rectangle in cross section	Particle size: 68x6 – 65x5 cm Initial fuel: 65 kg GA: Air AFR: 24.11 – 24.45 m^3/h	Effect of AFR on: Gas composition HHV Gasification efficiency Turn down ratio Tar yield	Gas composition (vol. %): CO:12; H_2:15; CO_2: 14; HHV (MJ/m^3 dry gas): 4.5 Gasification efficiency (%):73 Turn down ratio (%): 1.5 Tar yield (g): 0.189 AFR (m^3/h): 24.45 Particle size (cm): 68x5 Final charcoal (g): 1000	2007 [88]
Shell, fibre and EFB ID: 20 cm H: 40 cm	Particle size: 5 to less than 0.15 mm MC: 5.73-8.75% S/B: 0-2.67 BT: 800^oC GA: Steam No Catalyst:	Effect of S/B and particle size on: Gas yield HHV Hydrogen yield Tar yield	Gas yield (m^3 gas/kg biomass): 1.21 LHV (MJ/m^3 dry gas): 12.37 Hydrogen yield g H_2/kg biomass): 39.75 Tar yield (g/Nm3): 37.8 S/B: 1.33 Particle size (mm): 0.15-2 Gasifier temperature (^oC): 800	2008 [106]

Table 2.5 continued: Various investigations conducted on updraft fixed bed gasifier

System configuration and Operation parameters		Investigated parameters	Optimum obtained results	Date-Ref.
Pine sawdust ID: 8.75 cm H: 150 cm	Feed rate: 0.48 (kg/h) S/B: 1.05- 3.47 at 850^{o}C GA: Air	Effect of gasifier temperature, ER, S/B and porous ceramic reforming on: Gas density Gas yield LHV Residence time	Gas density (kg/m^3): 0.73 Gas yield (m^3/kg): 2.33 LHV (MJ/Nm^3): 12.87 Hydrogen yield (g H_2/kg biomass): 86.08 Residence time (sec): 4.07 Gasifier temperature (^{o}C): 850 S/B (%): 2.53	2008 [5]
Eastern redcedar ID: 20 cm H: 100 cm	Particle size: 0.25x0.25x1 – 1x3x1 inch MC: 11.38% ER: 0.138-0.246 GA: Air	Effect of ER on: Gas composition HHV CGE Tar and water production	Gas composition (vol. %): CO: 22.80-24.34; H_2: 4.32-4.72; CO_2: 8.10-8.54; HHV (MJ/m^3 dry gas): 8.486-8.911 CGE (%): 45-47 Tar yield (g/m^3): 83-125 ER: 0.177 to 0.215	2008 [107]
Dairy biomass ID: 13.9 cm H: 72 cm	Particle size: 5 6.35 mm ER_M: 1-4 ASTR: 0.2-0.8 GA: Air AT: 298 K	Effect of ER and S:F on: Gas composition HHV	Gas composition on mole fraction (dry basis): H_2: 0.072, CO: 0.23, CO_2: 0.101, CH_4: 0.02, C_2H_6: 0.015 HHV (MJ/m^3 dry gas): 5.15 ER_M (%): 1.9	2009 [76]

Table 2.5 continued: Various investigations conducted on updraft fixed bed gasifier

System configuration and Operation parameters		Investigated parameters	Optimum obtained results	Date-Ref.
Pine sawdust ID: 13.9 cm H: 72 cm	Particle size: 0.075-1.2 mm BT: 600 to 900 ^{o}C GA: Steam	Effect of particle size: Gas composition Gas yield CCE Hydrogen yield Char and tar content	Gas composition (vol. %): H_2:51.2; CO:22.4; CO_2: 14.8; CH_4: 4.9 Gas yield (m^3/kg): 1.67 CCE (%): 99.87 Hydrogen yield (m^3/kg): 0.82 Char and tar content: negligible Particle size (mm): < 0.075 BT (^{o}C): 900	2009 [89]
Dairy biomass ID: 13.9 cm H: 72 cm	Particle size: 5 6.35 mm ER_M: ER_M: 1.6-6.4 ASTR: 0.4-0.8 GA: Air+steam AT: 298 K ST: 373 K	Effect of ER and S:F on: Gas composition HHV ECE Tar	Gas composition (vol. %): CO: 4.77; H_2: 25.45; CO_2: 25. HHV (MJ/m^3 dry gas): 4.585 ECE (%): 69 Tar (kg/kg of biomass): 1.8 ER_M (%): 6.4 S:F (%): 0.8	2010 [20]
Softwood pellets ID: 12.5 cm H: 60 cm	Particle size: 2-6 mm MC: 60 g kg w.b. GA: Air A/F: 1.1 – 1.6	Effect of air flow rate on: Gas composition CGE Tar	Gas composition (vol. %): CO:26.6; H_2:6.3; CO_2: 5; CH_4: 1.7 CGE (%): 88.3 Tar (g/m^3): 199	2011 [101]

Table 2.5 continued: Various investigations conducted on updraft fixed bed gasifier

System configuration and Operation parameters		Investigated parameters	Optimum obtained results	Date-Ref.
Woody biomass ID: 10.23 cm H: 100 cm	Feeding rate: 0.25 kg/20 min Particle size: 6.5-8.5 mm MC: 4.64% GA: Air AFR: 20 L/min	Effect of air flow rate on: Gas composition LHV CGE CCE Tar generation	Gas composition (vol. %): CO:28; H_2:5; CO_2: 5.5; CH_4: 1.2 HHV (MJ/m^3 dry gas): 4.8 CGE (%): 76 Tar (g/m^3): 132.4	2011 [103]
Dairy biomass ID: 13.9 cm H: 72 cm	MC: 14.95% GA: Air+steam	Effect of enriched oxygen (24-28%) and ER on: Gas composition LHV Gasification efficiency	Gas composition (vol. %): CO:22.79; H_2:3.99; CO_2: 14.62; CH_4: 1.15, C_2H_6: 0.48 LHV (MJ/Nm^3): 4.167 Gasification efficiency (%): 73 ER: 2.1 Oxygen concentration (%): 21	2011 [102]
Wood pellets ID: 25 cm H: 60 cm	FR: 4.1-16 kg/h MC: 7-16% GA: Air AFR:5.5-19 m^3/h Excess air ratio: 0.31	Effect of air to fuel ratio on: Gas composition HHV CGE	Gas composition (vol. %): CO:25.02; H_2:10.73; CO_2: 8.68; CH_4: 2.57 LHV (MJ/m^3 dry gas): 5.38 CGE (%): 64.3 A/F: 1.89 MC (%): 7.0	2011 [65]
Juniper ID: 13.9 cm H: 72 cm	Particle size: 2-9.5 mm MC: 12.6-20.15% GA: Air ER: 2.7 – 4.2	Effect of ER, particle size and MC on: Gas composition LHV	Gas composition (vol. %): CO:25; H_2:3.3; CO_2: 11; CH_4: 1.7 LHV (MJ/m^3 dry gas):3.9 Gas yield (m^3 gas/kg biomass):2.4 ER: 2.7 Particle size (mm): 4-6	2012 [104]

Table 2.5 continued: Various investigations conducted on updraft fixed bed gasifier

System configuration and Operation parameters		Investigated parameters	Optimum obtained results	Ref.
Mesquite ID: 13.9 cm H: 72 cm	Particle size: 2-6 mm MC: 12.6-20.15% GA: Air ER: 2.7 – 4.2	Effect of ER, particle size and MC on: Gas composition LHV	Gas composition (vol. %): CO:21; H_2:3; CO_2: 11; CH_4: 1.5 LHV (MJ/m^3 dry gas):3.5 Gas yield (m^3 gas/kg biomass):2.2 ER: 2.7 Particle size (mm): 4-6 MC (%): 12.6	2012 [104]
Sewage sludge ID: 16.5 cm H: 200 cm	MC: 20% GA: Air ER: 0.15-0.25	Effect of ER, particle size and MC on: Gas composition LHV Gas yield CGE CCE	Gas composition (vol. %): CO:11.2; H_2:4.4; CO_2: 12.7; CH_4: 1.1 LHV (MJ/Nm^3): 3.96 Gas yield (m^3 gas/kg biomass):0.51 CGE (%): 21 CCE (%):39.1 ER: 2.1	2012 [105]
Chicken litter ID: NA H: NA	FR: 4.1-16 kg/h MC: 8.99-14.01% GA: Air AFR:65.33-96.77 m^3/h	Effect of AFR and MC on: Gas composition LHV Gasification efficiency	Gas composition (vol. %): CO:9.5; H_2:7.8; CO_2: 14; CH_4: 1.7 LHV (MJ/m^3 dry gas):2.9 Gasification efficiency (%): 19.6 AFR (m^3/h): 95.85 MC (%): 11.42	2012 [48]

ID: internal diameter, H: height of gasifier, GA: gasifying agent, ER: equivalence ratio MC: moisture content, FR: feeding rate, AFR: air flow rate, A/F: air to fuel ratio, BT: bed temperature, AT: air temperature, ST: steam temperature, HHV: higher heating value, LHV: lower heating value, CGE: cold gas efficiency, CCE: carbon conversion efficiency, ECE: energy conversion efficiency, Ref.: reference

2.10 Tar Removal

Tar is a general name used to define all hydrocarbons with a molecular weight greater than that of benzene. It consists of polycyclic aromatic hydrocarbons (PAH) including benzene. Tar is present in gasification product as gas phase hydrocarbon compounds. The yield of tar from gasification processes depends upon a number of parameters such as gasifier operation conditions, feedstock characteristics *etc.*, [108]. The presence of tar in producer gas is undesirable because it is associated with various problems in downstream equipments as well as in the end use applications such as engines and turbines [109].

Milne and Evans [110] proposed a tar classification system in order to characterize it from biomass gasification reactors and four classes were identified as below:

- Primary tars: characterized by cellulose, hemicelluloses and lignin-derived products.
- Secondary tars: the products of conversion of primary tar and consist of phenolics and olefins.
- Alkyl tertiary tars: these include methyl derivatives of aromatics (methyl acenaphthylene, methylnaphthalene, toluene, and indene.)
- Condensed tertiary tar: the polyaromatic hydrocarbons without substituent.

Tar removal can be achieved by two main methods depending on where the tar is removed from; these methods can be outlined as follows:

- Primary methods are used to remove or convert the tar into light gases after production inside the gasifier, and include the following techniques:
    - Optimizing the operating conditions such as high temperature gasification [80, 97, 99], increasing ER [111] and using feedstock with small particle size [89].
    - Addition of catalyst (In-bed catalysts) [89].
    - Gasifier modification such as two-stage biomass gasifier (FIB) [112], injection of secondary air or oxygen (FIB and cyclone gasifier) [71, 113], top-lit updraft gasifier [87] and updraft gasifier with an embedded combustor [64].

- Secondary methods are used to remove the tar from the product gas outside the gasifier and can be chemical or physical and include the following techniques:
    - Mechanical separation methods by using cyclone, filters, scrubber and electrostatic precipitators (ESP), these methods are effective ways of removing tar from producer gas but the useful energy in tar is lost. The rest of the methods convert the useful energy in tar into combustible gases and increase the efficiency of gasification process.
    - Thermal cracking such as partial combustion in swirl burner [114].
    - Catalytic cracking in the second reforming reactor [5, 9].

Due to the high tar content of the producer gas (up to 150 g/m^3), a number of improvements have been made in an updraft fixed bed gasifier to remove or reduce the amount of tar that is produced during the gasification process. Jeng-Chyan [64] developed an updraft fixed bed gasifier with an embedded combustor. The unique feature of this modified gasifier is the embedded combustor inside. Therefore, the embedded tube with numerous small holes on its lower wall inserted inside the gasifier at its pyrolysis zone allows the generated syngas to be introduced inside the tube and mixed with the secondary combustion air in order to be fully combusted. The combination of an updraft gasifier with embedded combustor is capable to produce a clean gas, but with a high temperature of 1320^oC.

Saravanakumar *et al.* [87] used a top lit updraft gasification (TLUG) to reduce the amount of tar during the gasification process. In this type of gasification the reaction zone is at the top and air is fed to the bottom of the reactor. However, the top lit updraft gasifier is considered as "tar burning, char making" gasifier. The advantage of this gasifier is that tar is much lower (1-5%), which is due to the fact that volatile and tar pass through a layer of a hot charcoal at the top of the gasifier, then cracked at this high temperature.

Recently, Fajri *et al.* [115] carried out simulation using CFD to find out the effect of recirculation of the pyrolysis gas into combustion zone and the product gas release from reduction zone at updraft gasifier, by using an ejector to entrain the secondary fluid flow. However, the study investigated the variation of nozzle exit position, diameter of ejector, diameter of mixing area and length of mixing area on flow

phenomena and the maximum flow of updraft gasifier. Their results showed that the change of nozzle diameter gives great influence at the total flow of recirculation compared to the other parameters.

More recently, Pedroso *et al.* [116] modified traditional updraft fixed bed gasifier especially in the way of feedstock feeding. In the modified gasifier, the feedstock was feeding continuously through a conduit in the base of the gasifier over the grate. The modified updraft gasifier (named, bottom feed gasifier) showed a tar content of about 26.9 mg/Nm^3. Considering all the previous works, it was observed that there were no studies on reducing the tar produced in an updraft gasification process by using air staged gasification approach (injection of the secondary air).

2.11 Chapter Summary

OPF are considered as one of the most abundant agricultural waste in Malaysia, and are estimated to be produced at 26 million tons per year. Most of these fronds are left rotting in the plantations mainly for nutrient recycling, soil conservation and erosion control. But as the OPFs have slow degradation rate and require longer time to decompose, thus remaining long time in the plantations causing mobilization problems and threaten the life of the workers. Moreover, the over-use of the OPFs on the plantations land causes both the pollution of ground water and imbalance of nutrients in the soil. In addition, the direct burning of the wasted fronds resulted in serious environmental problems. Therefore, a proper way of disposal of the OPFs needs to be developed and improved. A review of literature showed that recently OPF is used to be converted to pulp, used for the preparation of activated carbon and production of renewable sugar. All these studies are still at the research stage. In addition, OPF can also be used as a roughage source for animals. The current use of fronds doesn't consume the tremendous quantity produced annually. Therefore, converting the wasted OPF into useful energy via gasification could be a good opportunity for the palm oil industry and could contribute to the solution of energy problems, mobilization problems within the plantations, ground water pollution and imbalance of nutrients in the soil.

From literature review, it is apparent that there are no published studies on the use OPF as a feedstock in an updraft fixed gasifier. Moreover, detailed studies on the nature of the fresh OPF (large in size, high moisture content, suspended dust and impurities), properties and chemical composition of the OPFs showed that updraft gasification is the most promising technology for converting the huge quantities of the wasted fronds, with very less pretreatment, therefore minimum preparation cost.

CHAPTER 3

RESEARCH METHODOLOGY

This chapter describes the material and methods that used in this study. Section 3.1 focuses on the raw material and its characterization. In relation to moisture content, density, ultimate and proximate analysis, heating value, surface morphology and mineral analysis, Fourier Transform Infrared Spectroscopy (FTIR) and thermogravimetric analysis. The gasifier design, fabrication and the whole gasification system used in this work are presented in Section 3.2, whereas Section 3.3 is dedicated to describe the general procedure of gasification experiments.

3.1 Material Characterization

The biomass material investigated in this study was oil palm fronds collected from an oil palm plantation, located in Bota Kanan in the state of Perak in Malaysia. The leaflets were shredded and only petioles were used in this study. In order to evaluate the suitability of biomass material for gasification process, the following properties were considered: moisture content, density, proximate and ultimate analysis, heating value, FTIR, thermogravimetric analysis, mineral content analysis and ash content.

3.1.1 Moisture Content

Determination of moisture content was carried out using a Carbolite 450 oven at 105^{o}C for 24 hours, according to ASTM D 3173-73. Two independent drying experiments were conducted. The first experiment was performed to investigate the moisture removal rate for a certain period of time at a constant temperature. 45 samples (15 for each section of the tips, middle and hubs) were used in this experiment. The second experiment was conducted to investigate the relationship

between moisture content and the density of the fronds. 147 samples (49 for each section of the tips, middle and hubs) were prepared to conduct an experiment for the determination of moisture content versus density relationship. For both cases, the experiments were carried out only on freshly pruned fronds.

3.1.2 Proximate Analysis

Proximate analysis was used to determine the weight percentages (wt. %) of moisture content (MC), volatile matter (VM), fixed carbon (FC) and ash of the fronds. The proximate analysis of the samples was carried out in thermogravimetric analyzer (TG) (Model: Perkin-Elmer, Pyris 1) following the ASTM E870 - 82(2006). However, for estimating the percentage of MC and the VM, the samples were heated with N_2 from room temperature to 600^{o}C at rate of 10^{o}C/min, and then the temperature was increased up to 860^{o}C with O_2 at rate of 10^{o}C/min to estimate the percentage of FC. The residue is considered as the ash content.

3.1.3 Ultimate Analysis

Ultimate analysis was used to determine the weight percentages of chemical elemental carbon (C), hydrogen (H), nitrogen (N), sulfur (S) and oxygen (O) of the fronds. The oxygen content was determined by difference in the solid fuel. The ultimate analysis was performed on dry basis, because the ultimate analysis on wet basis may indicate a presence of more hydrogen and oxygen. The ultimate analysis of the samples was carried out using Leco CHNS-932 elemental analyzer in accordance to ASTM D3176-09.

3.1.4 Surface Morphology and Elemental Composition (SEM/EDX Analyses)

The surface structure (morphology) of OPF and inorganic materials in original OPF and OPF ash, such as potassium, calcium, magnesium, phosphorus, sodium and iron, were estimated by using the Variable Pressure Field Emission Scanning Electron

Microscope (Model: VPFESEM, Zeiss Supra55 VP). The surface morphology and elemental composition analyses were performed by using Scanning Electron Microscope (SEM) and Electron Dispersive X-ray Spectroscopy (EDX) techniques, respectively.

3.1.5 Fourier Transform Infrared (FT-IR) Spectroscopy

The FT-IR spectra were carried out for the samples of the OPF by using Shimadzu FTIR-84005 spectrophotometer to investigate the functional group of the fronds. Spectra analyses were obtained over a wave number range of 4000–650 cm^{-1}.

3.1.6 Heating Value

The higher heating value (HHV) represents the quantitative energy content of biomass fuels in terms of MJ/kg. The higher heating value of the samples was measured using the IKA Werke C5000 bomb calorimeter in accordance to ASTM D2015.

3.1.7 Heating Value Models

Regression analysis was used to develop an empirical equation for the higher heating value of oil palm fronds produced in Malaysia. The fronds parameters were divided into two groups, dependent variables and independent variables. The independent variable was the higher heating value of biomass, while the dependent variables were the elemental composition of biomass fuel (carbon, hydrogen and oxygen).

3.1.8 Thermogravimetric Analysis (TGA)

Kinetic analysis of thermal decomposition of biomass fuel is an essential step in its thermochemical conversion processes. Moreover, the kinetic parameters are essential for designing the equipment in which the thermal decomposition takes place. The thermogravimetric experiments of the samples were carried out on thermogravimetric

analyzer (Model: Perkin-Elmer, Pyris 1). The experiments were performed in both an inert gas (nitrogen) and oxidant gas (oxygen) at different heating rates (20, 30 and 40^{o}C/min) and the temperature range from 30 to 860^{o}C.

3.2 Gasification System

3.2.1 Gasifier Design and Description

The gasifier must be designed and constructed to study the feasibility of gasifying OPF and to produce the necessary producer gas to be used for the domestic cooking stove. Based on this thought the design of the gasifier should be simple, easy to operate and possess a power of 50 kW_{th} (thermal). An updraft gasifier configuration was selected due to its simplicity, low cost, versatility and suitable for thermal applications. Moreover, updraft gasifier would be easy to operate. In addition, updraft gasifier has a high thermal conversion rate and can handle biomass fuel with moisture content of up to 60%.

Designing a gasifier involves selecting the type of gasifier and obtaining the dimensions of all the components such as diameter, height *etc*. However, the gasifier components was designed as per existing design presented by many researchers [87, 114, 117-119] and the data needed for calculations was either gathered from the literature or measured by the author. It is found from previous works [119] that most of the design was based on empirical data, but there were many factors that should be considered for the design of gasifiers in order to achieve the desired performance. Those factors are the properties of the biomass feedstock, mode of operation, final use of the gas, insulation of the reactor and location of the firing. The design of the gasifier was as follows:

3.2.1.1 Assumptions for Gasifier Design

Considering was given to the characteristics of the feedstock, the power (capacity) of the gasifier and the end use of the gas generated from the gasifier. Recommended

values for some parameters are required to be obtained from the literature. Table 3.1 shows the assumptions made for the design of an updraft gasifier.

Table 3.1: Assumptions for updraft gasifier design

Description	Value	Remark
Gasifier output (P_g)	50 kW	Assumed
Gasifier efficiency (η_g)	70%	From [119]
Lower heating value of producer gas (LHV_g)	4 MJ/m^3	From [120]
Specific gasification rate (SGR)	110 kg/m^{2}h	From [117]
Duty hours (T)	6	Assumed
Equivalence ratio (ε)	0.3	From [119]
Density of air (ρ_a)	1.25 kg/m^3	From [119]
Biomass molecular formula	$CH_{1.28}O_{0.92}$	Calculated
Boimass higher heating value (HHV_{OPF})	17.01 MJ/kg	Measured

3.2.1.2 General Calculations

As the expected output power of the gasifier is 50 kW, the power input (in terms of biomass fuel) can be determined as:

$$P_g = Q_i \times \eta_g \tag{3.1}$$

where Q_i and P_g are the input and output power of the gasifier (kW), while η_g is the gasifier efficiency (%). Therefore, the input power was determined to be 71 kW. The fuel consumption rate which is the amount of energy needed for the gasifier in terms of biomass fuel in order to produce the required output power can be determined as [114, 118]:

$$\mathrm{FCR} = \frac{\mathrm{P_g}}{\mathrm{HHV_{OPF}} \times \eta_g} \tag{3.2}$$

where FCR is the fuel consumption rate (kg/h) and HHV_{OPF} is the higher heating value of biomass fuel (MJ/kg). Therefore, the fuel consumption rate was determined to be 15 kg/h. The amount of air flow rate (Q_{air}) needed to gasify biomass fuel can be

determined based on the fuel consumption rate, recommended equivalence ratio (ε), air density (ρ_{air}) and stoichiometric air of biomass fuel (*SA*) as follow [119]:

$$\mathrm{Q_{air}} = \frac{\varepsilon \times \mathrm{FCR} \times \mathrm{SA}}{\rho_{\mathrm{air}}} \tag{3.3}$$

The stoichiometric air (*SA*) can be determined as:

$$\mathrm{SA} = \overline{\mathrm{AF}} \left(\frac{\mathrm{M_{air}}}{\mathrm{M_{fuel}}} \right) \tag{3.4}$$

where *AF* is the air to fuel ratio on molar basis, M_{air} and M_{fuel} are the molecular weight of air and fuel, respectively. The air to fuel ratio on molar basis was determined from the combustion reaction of oil palm frond (Eq. 3.5):

$$\mathrm{CH_{1.28}O_{0.92}} + \mathrm{a}(\mathrm{O_2} + 3.76\mathrm{N_2}) = \mathrm{bCO_2} + \mathrm{cH_2O} + \mathrm{dN_2} \tag{3.5}$$

Thus, the constants *a*, *b*, *c* and *d* can be calculated from the elemental balance of carbon, hydrogen, oxygen and nitrogen. Therefore, the air to fuel ratio on molar basis and the stoichiometric air were determined to be 5.8 and 6.1 kg of air per kg of fuel, respectively. Based on that, the air flow rate was determined to be 21.3 m^3/h.

3.2.1.3 Gasifier Geometries

The gasifier diameter refers to the size of the gasifier in terms of the cross-section of the cylinder where the biomass fuels are being burned. As suggested by Belonio and Anderson [119], the gasifier diameter is a function of the amount fuel consumption rate and the specific gasification rate as described by the equation below,

$$\mathrm{D} = \left(\frac{4 \times \mathrm{FCR}}{\pi \times \mathrm{SGR}} \right)^{0.5} \tag{3.6}$$

where *D* is the gasifier diameter, which is determined to be 0.44 m in this case. Due to the difficulty of fabrication the gasifier and the cost issue, the cross sectional area was changed to the square shape according to the equation below,

$$\mathrm{A} = \frac{\pi}{4}\mathrm{D}^2 = \mathrm{L}^2 \tag{3.7}$$

where *A* is the gasifier cross section area. The height of gasifier refers to the total distance from the top and the bottom end of the gasifier. This is a function of several variables such as specific gasification rate, density of the biomass fuel and the time required to operate the gasifier as expressed below [118, 119]:

$$\mathrm{H} = \frac{\mathrm{SGR} \times \mathrm{T}}{\rho_{\mathrm{OPF}}} \tag{3.8}$$

where *H, T* and ρ_{OPF} are the gasifier height, time required to operate the gasifier and density of OPF, respectively. In the view of the above, the height of gasifier was determined to be 0.93 m, but the actual height was fixed at 1.2 m in order to provide space at the top of gasifier for the producer gas to be collected through the exit pipe, and to provide space at the bottom of the gasifier for ash collection.

3.2.1.4 Air Nozzle Design

This is referring to size and number of the air nozzle which provide a suitable air velocity for gasification process. Both high and low air velocities lead to formation of central dark zone in the oxidation zone and inefficient tar cracking [38]. The area of the nozzles can be calculated using the formula below,

$$\mathrm{A_{noz}} = \frac{\mathrm{Q_{air}}}{\mathrm{v}} \times \frac{10^3}{3.6} \tag{3.9}$$

where A_{noz} and *v* are the cross section areas (mm^2) of the nozzles and the air velocity (m/s), respectively. Assuming that the air velocity is 8 m/sec, which is recommended for updraft gasifier [100, 107], the area of the nozzles should be about 739.6 mm^2.

3.2.1.5 Fabrication of Updraft Gasifier

The gasifier was fabricated in a local workshop. The gasifier body consisted of main four main parts, namely gasifier cover, fuel chamber, grate, ash container and primary and secondary air inlets (Figure 3.1). The chamber of the gasifier was constructed from mild steel and refractory cement. However, the internal and external wall was made from 4 mm mild steel sheet with 17 mm of refractory cement between the walls

as shown in Figure 3.2. The purpose of the refractory cement is to reduce the heat loss from the gasifier. The gasifier has one opening on the top for feeding of the fuel. The gasifier fuel chamber was in square cross section with an internal length of 0.4 m and made of mild steel and cement with 25 mm thickness. The height from the top of the gasifier to the grate (fuel chamber) was 1.0 m .The length of the lower part of the fuel chamber was reduced from 0.4 to 0.3 m, and then connected to the gasifier grate. However, the lower portion of the gasifier included the grate, two inlet air nozzles, ash receptacle and ash cleanout port. The grate was made of mild steel and is directly supported to the combustion zone and must be capable of letting the ash fall through, without loss of fuel. Moreover, the grate is used as an air distributor; however the holes are distributed across the whole section of the grate. The ash receptacle was made in square shape and is fixed below the grate, has a height of 0.2 m and outside length of 0.45 m.

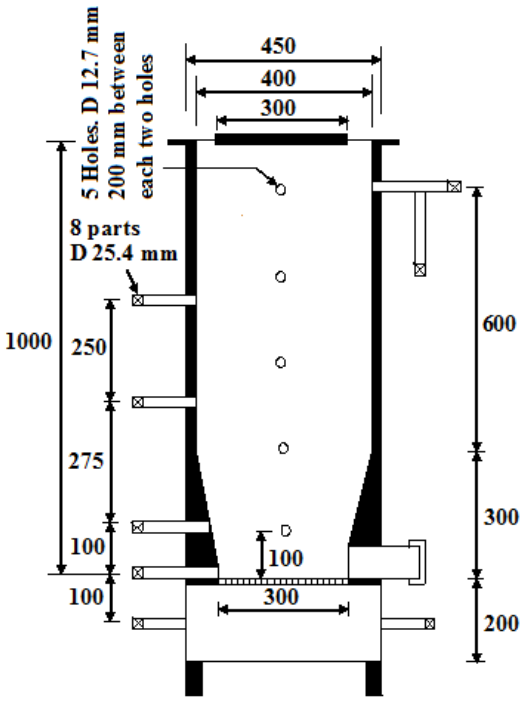

Figure 3.1: Designed updraft gasifier (All dimensions in mm)

The upper part of the gasifier includes the feedstock feeding portion and the producer gas exhaust pipe. The feeding open is in square shape and has a cross section area of about 0.09 m^2. The producer gas exhaust pipe is made from Galvanized Iron (GI pipe) and it includes three other parts. The first part is a dirt leg which used for tar

and condensate removal, while the second part is a temperature probe to measure the temperature of the outlet syngas. The last part is a pipe with a ball value which use to check the combustibility of the producer gas (named, flare point No.1).

Regarding the air inlet, there were three primary air inlets, two of them were located at about 10 cm below the grate and the third one was located exactly through the grate, while there were three inlets for the injection of secondary air located at oxidation zone, reduction zone and pyrolysis zone. However, they were located at 10 cm, 37.5 cm and 62.5 cm above the grate.

Figure 3.2: Semi-finished parts of the gasifier

Five Type-K thermocouples were inserted into the gasifier through 12.7mm diameter tubes into the gasifier body at 10, 30, 50, 70 and 90 cm above the grate. The purpose of these tubes was to protect the thermocouples from direct contact with the feedstock in the gasifier. All temperatures were recorded during system operation using a data logger (USB TC08) connected to a computer.

3.2.2 Facilities of Gasification System

3.2.2.1 Air Supply Unit

The primary air and secondary air were supplied into the gasifier by using an electric blower. The primary air was fed into the gasifier through two points under the grate while the secondary air was fed to the gasifier through three point above the grate (10, 37.5 and 62.5 cm above the grate, of which the secondary air was considered to be introduced to the gasifier through oxidation, reduction and pyrolysis zone).

A blower of 185 W was used to introduce the air to the gasifier, and the air was regulated and measured by the control valve and flowmeter, respectively. The blower was selected according to the minimum and maximum air requirement for gasification and pressure inside the gasifier and also on operation type (blowing or sucking). Table 3.2 shows the specifications of the blower used in this system.

Table 3.2: Specifications of the blower

Parameter	Value
Type	Hailea vortex blower
Type of fans	Centrifugal
Speed	2900 rpm
Flow rate	0.95 m^3/min
Power	185 W, 220 V
Pressure	950 mm H_2O

3.2.2.2 Data Acquisition and Monitoring System

The data collected from each experiment can be categorized into, gas sample, flow rate, temperature and material accumulation.

a. Gas sample: After separating the particulates carried by the producer gas, the gas was passed through the heat exchanger for cooling. After that, the sample of the producer gas transferred to another gas filter for further cleaning to prevent damage on the gas analyzer. The sample was analyzed online immediately by using X-STREAM gas analyzer (Figure 3.3). The gas analyzer was used to analyze five gases of the producer gas: CO, CO_2, CH_4, H_2 and N_2.

b. Flow rate: The flow rate of the gasification air (primary and secondary air) and the producer gas were measured by the flowmeters. A flowmeter was used to measure the air. It was capable in measuring air flow rate between 60 – 700 L/min, while the one used to measure the producer gas was capable to measure up to 1400 L/min. The flowmeters used for air and producer gas are Dwyer flowmeter series, model VFC-131 and UV-C112, respectively.

c. Temperature: The temperatures were monitored from five positions of the gasifier, from the exit of gasifier, from the flare and from the exit of the heat exchanger. The temperature was measured every 30 seconds using Type-K thermocouples placed at eight locations in the system as mentioned above. All thermocouples had temperature range from 0^{o}C to 1200^{o}C. The thermocouples were connected to the data logger (USB TC08) which was connected to the computer.

d. Byproduct material accumulation: The material accumulation consisted char, ash, tar and condensate formed during the experiment. The amount of these materials could not be measured during the experiment, so their accumulation was measured at the end of the experiment and then was divided by the time to obtain the production rate.

Figure 3.3: X-STREAM gas analyzer

3.2.2.3 Cyclone

The cyclone is the most commonly used technique to separate the solid particles (dust, ash and char) from the gas produced by an updraft gasifier. Cyclones are relatively inexpensive, simple in design and their operational and maintenance cost is low. Cyclones use centrifugal force to separate particles from a gas stream.

The cyclone body diameter was determined based on the gasifier gas flow rate (Q_c) and gasifier's gas outlet velocity which considered as the gas inlet velocity of the cyclone (V_i). Therefore, a cyclone diameter could be determined as follow [121]:

$$D_C = \sqrt{\frac{8Q_C}{V_i}} \tag{3.10}$$

where D_c is the cyclone body diameter, which is determined to be 180 mm. As the cyclone body diameter has geometrical proportion to all other cyclone's dimensions. Therefore, other cyclone's dimensions could easily determine based on the cyclone body diameter as shown in Table 3.3. A schematic diagram of a cyclone separator is shown in Figure 3.4.

Table 3.3: Typical cyclone dimensions [121]

Cyclone Geometry	Symbol	geometrical proportion
Height of cyclone inlet duct	H_c	$0.5D_c$
Width of cyclone inlet duct	W_c	$0.25D_c$
Height of cyclone outlet duct	S_c	$0.625D_c$
Diameter of clean gas outlet	D_e	$0.5D_c$
Diameter of dust outlet	J_c	$0.25D_c$
Length of cyclone body	L_c	$2D_c$
Length of cone	Z_c	$2D_c$

The cyclone separator was connected to the exit of the gasifier to capture the particles from the stream gas as shown in Figure 3.5. The cyclone was made by 1.2 mm thick of stainless steel metal sheet. It consisted of two sections, cylindrical and conical. The cylindrical section had 180 mm diameter and 360 mm height. The conical section had a height of 360 mm and the diameter decrease from 180 mm to the 45 mm. The cyclone had a tangential inlet connected to the cylindrical part of the cyclone, as the gas brought into the cyclone through this inlet, a vortex was created and the particles in the gas flow were subjected to the centrifugal force which moved them to the cyclone wall where they leave the gas stream, then the particles moved

down to the exit port and were collected in the particulate collector but the clean gas escaped at the top of the cyclone.

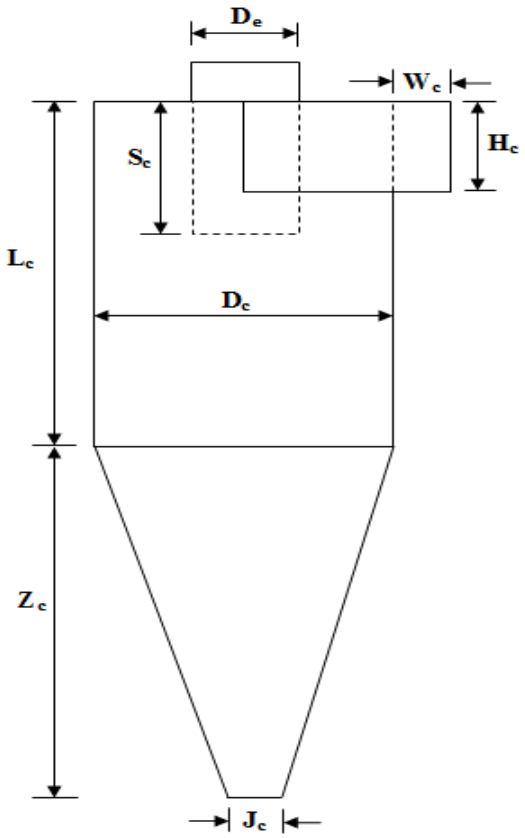

Figure 3.4: A schematic diagram of a cyclone separator

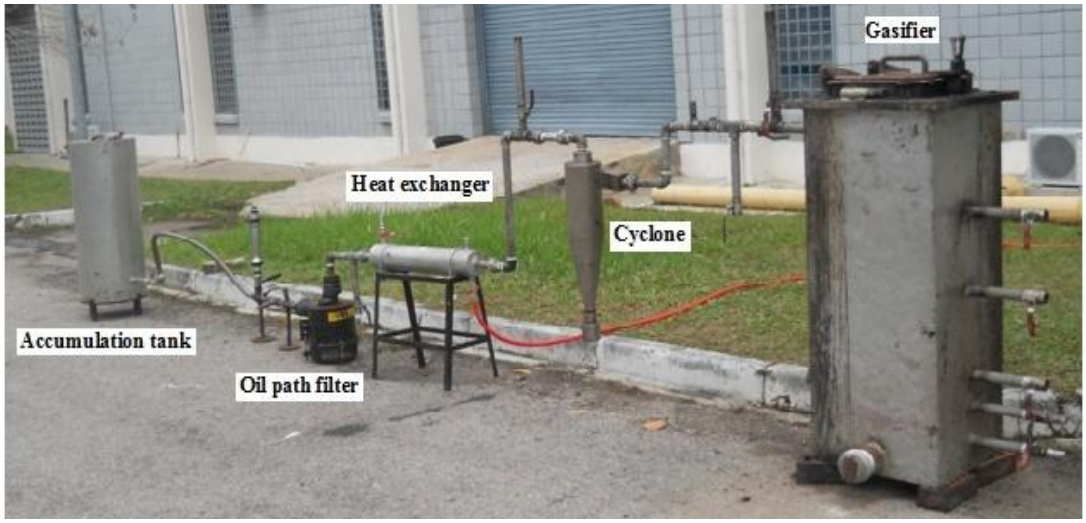

Figure 3.5: Photograph of gasification system

3.2.2.4 Heat Exchanger

Counter flow double pipe heat exchanger was designed and constructed to cool the producer gas to the temperature suitable for gas analyzer as well as suitable for the end use. The heat exchanger was designed based on the inlet and outlet temperature of the producer gas and cooling water, pipes used to convey the producer gas and cooling water as well as the properties of both streams. A copper pipe with an internal and external diameter of about 25.4 mm and 26.3 mm, respectively was used to convey the producer gas, whereas a Galvanized Iron pipe (GI tube pipe) with an internal diameter of about 76.2 mm was used for a cooling water as shown in Figure 3.6. Table 3.4 shows the properties of the producer gas (air) and water at mean temperature (T_m).

Table 3.4: Properties of producer gas and water

Gas	Producer gas	Water
Mean temperature, T_m (^oC)	120	27.5
Heat capacity, Cp (kJ/kgk)	1.013	4.2
Thermal conductivity, K (w/m.k)	0.0328	0.609
Dynamic viscosity, μ (kg/m.s)	2.27×10^{-5}	0.841×10^{-6}
Density, ρ (kg/m^3)	0.898	1000
Prandtl number, p_r	0.7	5.77

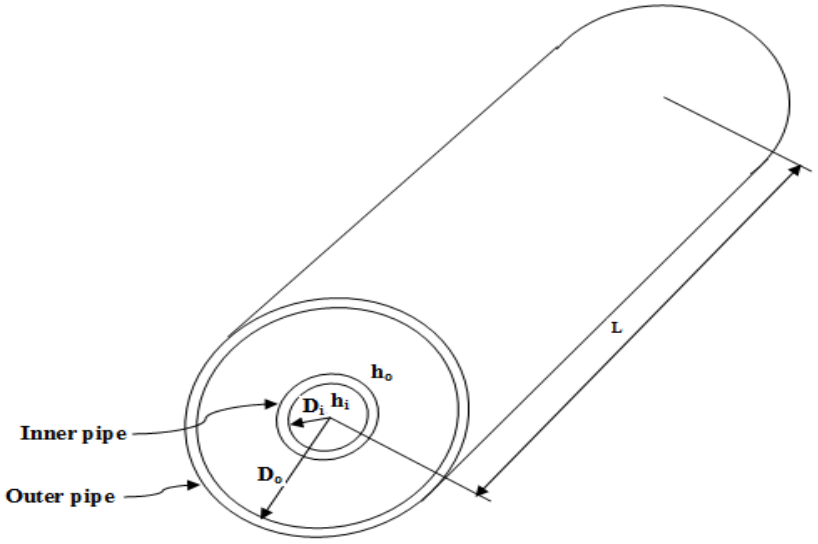

Figure 3.6: View of double pipe heat exchanger

The design was initially started by performing an energy balance of each stream,

$$Q = \dot{m}_w Cp_w \Delta T_w = -\dot{m}_g Cp_g \Delta T_g = U_o A \Delta T_{LMTD} \quad (3.11)$$

where Q is the amount of heat loss from the hot gas and gained by the cold water which determined to be 3.216 kW, $\dot{m}_w$ and $\dot{m}_g$ represent the mass flow rate of the cold water and hot gas, Cp_w and Cp_g represent the heat capacity of the cold water and hot gas, while ΔT_w and ΔT_g represent the temperature difference for the cold water and hot gas, U_o is the overall heat transfer coefficient based on inside tube area, A is the inside tube area and ΔT_m represent the log mean temperature difference (LMTD) which can be determined as follow,

$$\Delta T_{LMTD} = \frac{\Delta T_1 - \Delta T_2}{\ln \frac{\Delta T_1}{\Delta T_2}} \quad (3.12)$$

For the countercurrent flow, the ΔT_1 and ΔT_1 can be determined from Figure 3.6 as follow,

$$\Delta T_1 = T_{g,in} - T_{w,out} \quad (3.13)$$

$$\Delta T_2 = T_{g,out} - T_{w,in} \quad (3.14)$$

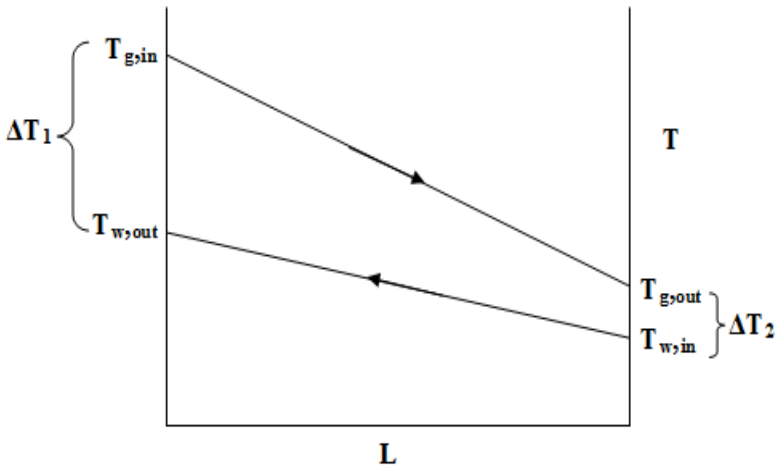

Figure 3.7: Hot and cold streams for the counter current flow heat exchanger

Therefore, ΔT_m was determined to be 70.58. The overall heat transfer coefficient based on inside tube area can be determined as follow,

$$\frac{1}{U_o} = \frac{1}{h_i} + \frac{1}{h_o} \tag{3.15}$$

where h_i and h_o represent the convective heat transfer coefficient of each stream, therefore, U_o was found to be 412.6 W/m^{2}K, and finally the length of the heat exchanger can be computed from Eq. 3.16 as A is expressed by the following equation,

$$A = 2\pi DL \tag{3.16}$$

Therefore, the length of the heat exchanger (L) was determined to be 0.7 m. In the gasification system, the heat exchanger was connected after the cyclone separator as shown in Figure 3.5.

3.2.2.5 Flare

The producer gas exiting the gasifier can be either delivered to the storage for other uses or to the gas flare whose purpose is to minimize air pollution during the run and to confirm the combustion capability of the gas. The system was provided by three flare points, one is placed directly after the gasifier, and the others are placed after the cyclone and after the accumulation tank. Figure 3.5 shows the positions of the flare points in the gasification system, while Figure. 3.8 show an example of the flare status during the experiment.

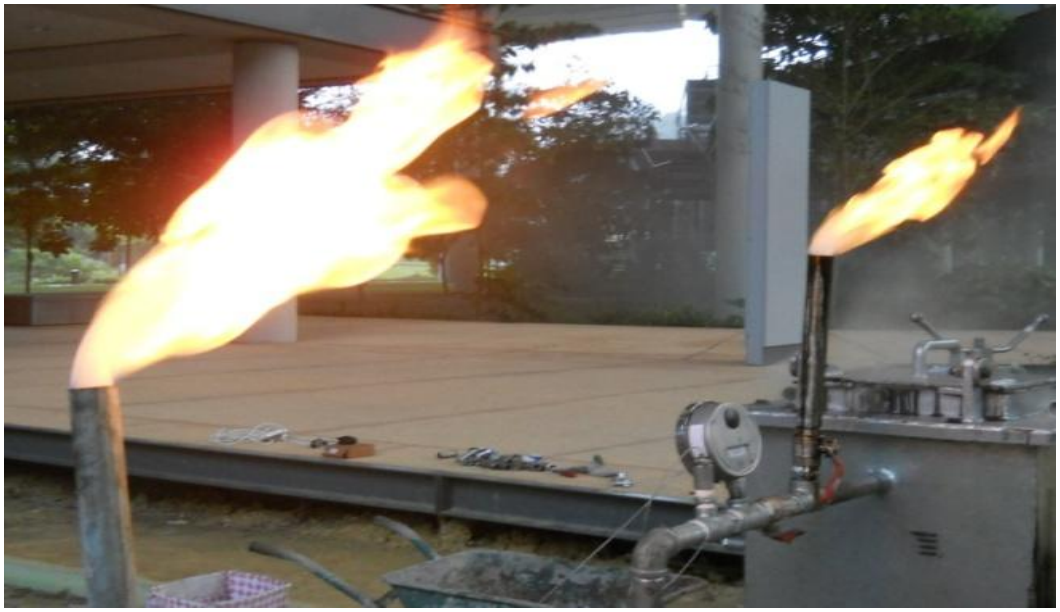

Figure 3.8: Photograph of the flare points

3.2.2.6 Accumulation Tank

After cleaning and cooling the producer gas, some of the gas was sampled for analyzing and the rest of the gas is delivered to the gas storage tank for the end use. The tank shown in Figure 3.5 was made of 3 mm thick mild steel plate and had 400 mm diameter and 1.0 m height. The storage tank can store a gas of one hour operation of the gasifier. The stored gas in the tank is either used to run the domestic cooking stove or to be channeled to the flare.

3.3 Experimental Procedure

A series of experiments were performed on updraft fixed-bed gasifier using OPF as feedstock material to investigate the effects of equivalence ratio, particle size, moisture content, position of primary air (below the grate, through the grate and above the grate) and secondary air (effect of the secondary air position and secondary to primary air ratio) on gasification performance of OPF. The schematic diagram of an updraft gasification system used in this study is shown in Figure 3.9

The biomass material used for this study was obtained from a plantation in the state of Perak, Malaysia. The fresh OPF (after removing leaves) were cut into the required size. Then about five samples of the OPF dried in a dryer oven at a temperature of 105^{o}C for 24 hours to determine the initial moisture content of the sample. Thereafter, the whole samples dried for certain time to achieve the required moisture content. This time is estimated from the graph of moisture content *vs*. time by knowing the initial and the final (required) moisture content. For reliability, the samples of the dryer OPF are then dried in a dryer oven at a temperature of 105^{o}C for 24 hours to determine the final moisture content by using Eq. 4.1.

Before starting up the gasifier, the temperature monitoring system was initialized. The temperature monitoring system was USB data logger acquisition system (USB TC08 connected to the computer). The gasification experiments started with uploading the gasifier with about one kilogram of charcoal (usually a residue from previous experiment) in order to preheat the gasifier. The charcoal was dumped above the grate and ignited with kerosene and flame, and then the air blower was turned on to introduce the atmospheric air to the gasifier at the rate of 0.95 m^3/min in order to facilitate the burning of the charcoal and OPF. Charcoal and OPF were allowed to burn until the temperature at the distance of 10 cm above the grate reached the desired temperature (usually 600^{o}C), then the OPF for the experiment was added to the gasifier through the top of the gasifier and the air was adjusted to the required experimental conditions, then the cover of the gasifier was closed. The time, at which the cover was closed, was considered as the starting point of the experiment.

After about 10 – 15 minutes as biomass started to be gasified, the height of the fuel bed started to decrease and the gas started to produce and accumulate at the top of the gasifier. The producer gas, left the gasifier at the top, and was sent to the accumulation tank via gas line, and in its way to the tank, the gas was passed through the cyclone, oil path filter and heat exchanger, in order to be cooled, cleaned and ready for analyzing. Gas samples were taken at every five minutes during the experiment run. This was done when the temperature was stabilized and the flare appeared more consistent. The gas sampling line is connected to the X-STREAM gas analyzer; however the producer gas were analyzed immediately after sampling. There

are six Type-K thermocouples located at different locations to measure the temperature profile across the gasifier and the producer gas temperature, while the producer gas flow rate was measured by using a flowmeter (Dwyer UV Series flowmeter, Model UV-C112).

When all the feedstock was gasified and all the flares disappeared, the blower was turned off and the gasifier was allowed to cool, after that char and ash were collected from the gasifier and ash container, respectively, and then weighed and analyzed. Tar and condensate were collected in order to be weighed and analyzed. The amount of the feedstock gasified and the time of the run were used to give a rough flow rate for the gasification experiment run. Finally the gasifier was prepared for the next experiment. Tar and ash collected from the gasifier were sent for further analysis to investigate their characteristics, while the char collected from the gasifier used as a charcoal for preheating the gasifier in the beginning of the next experiment.

3.4 Chapter Summary

The first section on this chapter described the material used in this study which is the OPF. Moreover, it described the methods, equipments and standards used to characterize the OPF. The second section focused on the gasifier design and fabrication. Furthermore, it focused on the design and fabrication on the other parts of gasification system such as cyclone, heat exchanger and accumulation tank. The last section presented in details the general procedure of the gasification experiments.

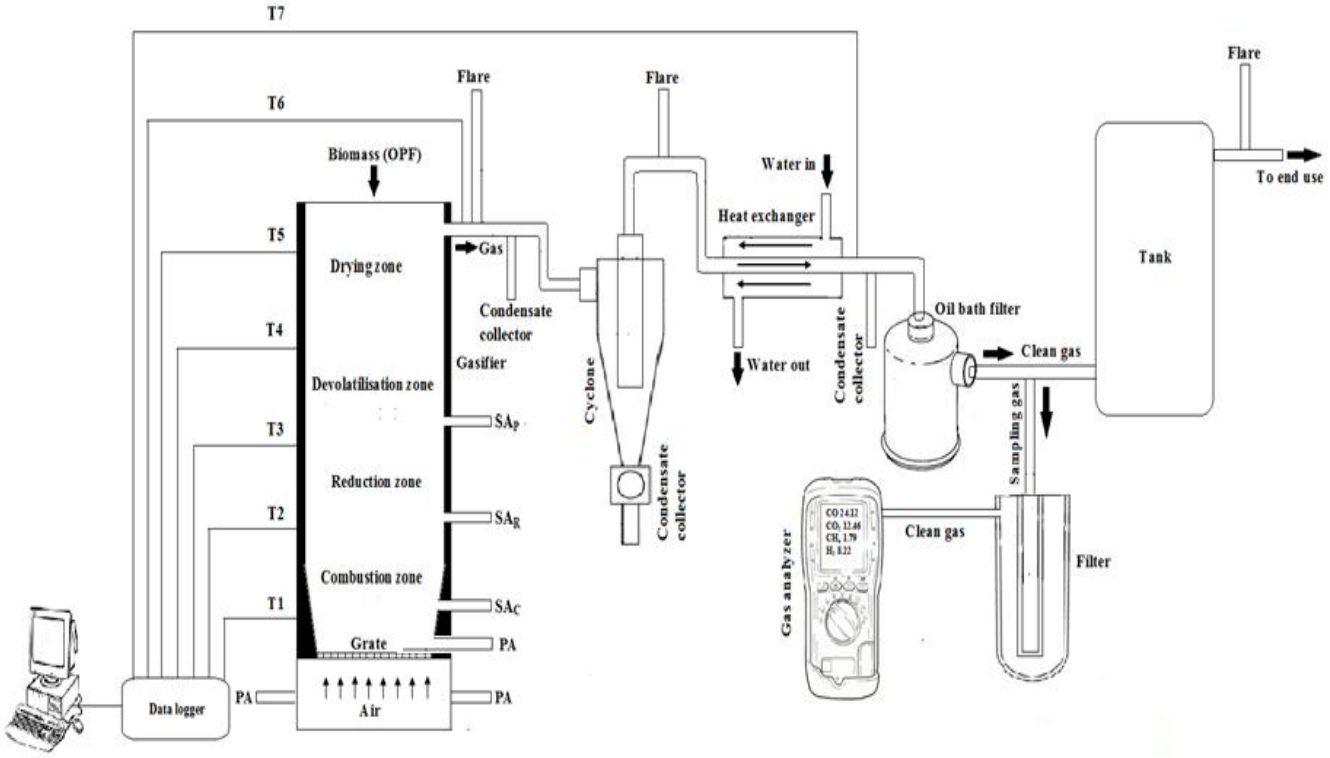

Figure 3.9: The schematic diagram of an updraft gasification system

CHAPTER 4

THEORTICAL FRAMEWORK

In this chapter, all the theories employed in this study are described in details. Sections 4.1 and 4.2 present the equations that were used to calculate the moisture content and the lower heating value of the raw material. In Section 4.3, the regression parameters criteria are presented, while the procedure and equations that were used for calculating the parameters of the reaction kinetics are discussed in Section 4.4. Sections 4.5 to 4.10 are dedicated for equations related gasification parameters such as equivalence ratio, gas production yield and gas heating value *etc*, while the last Section present the total uncertainty of the gasification experiments.

4.1 Moisture Content of OPF

Moisture content tests were performed on the freshly pruned OPF by oven drying method (Carbolite 450 oven). The drying process was performed at 105^{o}C for 24 hours. The weight measurement of each sample was taken at an interval of 30 minutes, till the weights of the samples remained constant (usually in the first 12 hours). Thereafter, the samples were kept in the oven for the rest of the time to ensure constant weight (no weight loss), and the moisture content of the samples was calculated on the wet basis as:

$$\mathrm{MC_{wet}} = \frac{\mathrm{WW-WD}}{\mathrm{WW}} \times 100\% \tag{4.1}$$

where *WW* and *WD* represent the mass weight of the fronds before and after the drying process, respectively, while MC_{wet} represents the moisture content on wet basis.

4.2 Lower Heating Value of OPF

Bomb calorimeter is used to measure the higher heating value (*HHV*) of biomass material, which is defined as the total amount of energy that available in the biomass material. The lower heating value (*LHV*) which is defined as the amount of energy in biomass material when subtracting the energy embodied in the water vapor can be calculated by subtracting the heat of vaporization from the higher heating value. Thus the LHV is computed using the following equation.

$$\mathrm{LHV_b} = \mathrm{HHV_b} - (\mathrm{F_w} \times \mathrm{h_w}) \tag{4.2}$$

where F_w represents the weight fraction of moisture content in the combustion gas (0.2228), h_w represents the heat of vaporization of water (2.283MJ/kg), whereas the HHV_b and LHV_b represent the higher and lower heating value of biomass fuel, respectively.

4.3 Regression Parameters

4.3.1 Correlation Coefficient (R^2)

The Pearson's regression coefficient (R^2) ranges between 0 and 1.0. A value above 0.5 would be valid and that above 0.7 would be the best R^2 value for a given correlation. It is widely used in statistical and regression analysis to quantify the accuracy of a model and can be calculated as:

$$\mathrm{R^2} = 1 - \sum_{\mathrm{i=1}}^{\mathrm{n}} \left| \frac{(\mathrm{HHV_M} - \mathrm{HHV_C})^2}{(\overline{\mathrm{HHV}}_{\mathrm{M}} - \mathrm{HHV_M})^2} \right| \tag{4.3}$$

where HHV_C and HHV_M are the calculated and measured higher heating value of biomass, respectively, while $\overline{HHV_M}$ is the measured average higher heating value of all the samples and n is the number of samples.

4.3.2 Average Absolute Error (AAE)

The average absolute error of the correlation indicates the correlation accuracy.

$$\mathrm{AAE} = \frac{1}{n}\sum_{i=1}^{n}\left|\frac{\mathrm{HHV_C} - \mathrm{HHV_M}}{\mathrm{HHV_M}}\right| \times 100\% \quad (4.4)$$

The average absolute error takes the total absolute error instead of the total squared error as in Pearson's regression coefficient. It is actually quantifies how close the predicted values of the *HHV* are to the experimental value of *HHV* of the samples. The lower the *AAE* value, the higher would be the accuracy of the correlation model.

4.3.3 Average Bias Error (ABE)

Average bias error describes the average deviation of the correlation. The *ABE* value is either be a positive or negative. A positive value of *ABE* means an overall over-estimation of the sample population, while a negative value indicates an overall under-estimation of the sample population. The smaller the absolute value of *ABE*, the smaller would be the bias of the correlation. The *ABE* is equal zero for a perfect correlation.

$$\mathrm{ABE} = \frac{1}{n}\sum_{i=1}^{n}\frac{\mathrm{HHV_C} - \mathrm{HHV_M}}{\mathrm{HHV_M}} \times 100\% \quad (4.5)$$

4.4 Parameters of Reaction Kinetics

The parameters of the reaction kinetics were determined using the following procedure [122]. The global kinetics of the vitalization reaction can be written as:

$$\frac{d\alpha}{dt} = A\exp\left(-\frac{E}{RT}\right)(1-\alpha)^{n} \quad (4.6)$$

where *A* is the pre-exponential factor of the reaction, *E* is the activation energy, *R* is the gas constant (8.3145 J/mol K), *T* is the temperature and *n* is reaction order. The fractional reaction α can be defined as follows:

$$\alpha = \frac{w_o - w}{w_o - w_f} \quad (4.7)$$

where w_o and w_f refer to the initial and final mass of sample, while *w* is the actual mass of sample at any temperature.

Determination of the kinetic parameters from the TGA data under non-isothermal conditions was expressed by using the Arrhenius equation as follows:

$$\frac{d\alpha}{dT} = \frac{A}{\beta} \exp\left(-\frac{E}{RT}\right)(1-\alpha)^n \tag{4.8}$$

where β is the heating rate (^oC/min)

By arranging Eq. (4.6), the following expression can be obtained:

$$\frac{1-(1-\alpha)^{1-n}}{1-n} = \frac{A}{\beta}\int_0^T \exp\left(-\frac{E}{RT}\right) dT \tag{4.9}$$

Although $\int_0^T \exp\left(-\frac{E}{RT}\right) dT$ has no exact integration, the term $\exp\left(-\frac{E}{RT}\right)$ can be expressed by:

$$\frac{1-(1-\alpha)^{1-n}}{1-n} = \frac{ART^2}{\beta E}\left[1-\frac{2RT}{E}\right] \exp\left(-\frac{E}{RT}\right) \tag{4.10}$$

As the value of $2RT/E$ is much smaller than 1.0, it can be assumed that $1-\frac{2RT}{E}$ is approximately equal to 1.0, Eq. (4.10) becomes:-

$$\ln\left[\frac{1-(1-\alpha)^{1-n}}{T^2(1-n)}\right] = \ln\left[\frac{AR}{\beta E}\right] - \frac{E}{RT} \text{ (for } n \neq 1.0) \tag{4.11}$$

If $n = 1.0$, Eq. (4.11) can be rewritten as:

$$\ln\left[-\frac{\ln(1-\alpha)}{T^2}\right] = \ln\left[\frac{AR}{\beta E}\right] - \frac{E}{RT} \text{ (for } n = 1.0) \tag{4.12}$$

Thus, plotting the left term of Eqs. (4.11) and (4.12) against $\frac{1}{T}$ for n^{th} and first order reactions, respectively. The resultant would be a straight line, and the kinetic parameters (*E* and *A*) can be estimated by the slope and intercept of the linear equation using a spreadsheet program.

Although, the model-fitting method is simple as it is usually used to determine the kinetic parameters for a single heating rate, there is a disadvantage that a single heating rate is not always sufficient to determine the kinetic parameters. This is due to the fact that the activation energy varies with the heating rate because of the mass

and/or energy transfer. Recently [123], model-free methods have appeared to be preferable and reliable for thermal analysis due to the following reasons:

a. The flexibility is greater allowing the mechanism to be changed during the reaction process.
b. Reduced mass transfer limitations, due to the use of multiple heating rates.
c. Allows the activation energy (E) to be determined as a function of conversion (α), without any assumption on the reaction model [124].

These methods calculate the activation energy at progressive conversion values (α), and require several kinetic curves to perform the analysis; therefore they have been called "multi-curve methods" as shown in Figure 5.14 (a–d). Moreover, the name is-conoversional comes from the calculation of the activation energy from several curves at different heating rates and the same value of conversion (α).

For the model-free method, the following expressions can be used. Eq. (4.8) can be rewritten as:

$$\frac{d\alpha}{dT} = \frac{A}{\beta}\exp\left(-\frac{E}{RT}\right)f(\alpha) \tag{4.13}$$

by integrating up to conversion α, Eq. (4.12) gives:

$$\int_0^{\propto}\frac{d\alpha}{f(\alpha)} = g(\alpha) = \frac{A}{\beta}\int_{T_0}^{T}\exp\left(-\frac{E}{RT}\right)dT \tag{4.14}$$

For the isoconversional method (model-free), a series of experiments have to be conducted at different heating rates. For solving Eq. (4.14), several approximation methods were introduced; these methods lead to a direct isoconversional method in the form of:

$$\ln\frac{\beta}{T^k} = C - \frac{E}{RT} \tag{4.15}$$

For each value of α, the corresponding temperature and heating rate were used to plot $\ln\left(\frac{\beta}{T^k}\right)$ vs. $\frac{1}{T}$, where k is constant. Then, the activation energy could be estimated from the slope of the straight line. Flynn–Wall–Ozawa (FWO), Kissinger–Akahira–Sunose (KAS), Tang (T) and Straink are the most accurate representatives of the

isoconversional methods [125]. All the above mentioned methods were used in this work.

The Flynn-Wall-Ozawa (FWO) is one of the popular methods used to determine the value of the activation energy without knowledge of the reaction order [126-129]; and it uses Doyle's approximation of p(x). The correlation corresponding to this method is given by:

$$\ln(\beta) = C_W - 1.052\frac{E}{RT} \tag{4.16}$$

Thus, by plotting $\ln(\beta)$ vs. $\frac{1}{T}$, the activation energy can be estimated from the slope of the straight lines at different conversion values (α).

Kissinger–Akahira–Sunose (KAS) is one of the best iso-conversional methods and is given by [125, 128-130]:

$$\ln\left(\frac{\beta}{T^2}\right) = C_K - \frac{E}{RT} \tag{4.17}$$

By plotting $\ln\left(\frac{\beta}{T^2}\right)$ vs. $\frac{1}{T}$, the activation energy can be calculated for different conversion values.

The Tang method is assumed to be the most precise expression for the temperature integral, and the equation corresponding to this method is [129]:

$$\ln\left(\frac{\beta}{T^{1.894661}}\right) = C_T - 1.00145033\ \frac{E}{RT} \tag{4.18}$$

The activation energy for each conversion (α) can be estimated from the slope of the straight line obtained by plotting $\ln\left(\frac{\beta}{T^{1.894661}}\right)$ vs. $\frac{1}{T}$.

According to the method proposed by Starink, the correlation given by [129]:

$$\ln\left(\frac{\beta}{T^{1.92}}\right) = C_S - 1.0008\frac{E}{RT} \tag{4.19}$$

Plotting $\ln\left(\frac{\beta}{T^{1.92}}\right)$ vs. $\frac{1}{T}$, gives the slope for calculation of the activation energy.

Kissinger proposed a kinetic analysis method for reaction-order models $(\alpha) = (1-\alpha)^n$, in which the kinetic parameters can be calculated without knowing the reaction mechanism. In this method, kinetic parameters for each conversion (α) do not need to be calculated. Instead, the Kissinger method is based on the fact that the reaction rate is dependent on the peak temperature, which varies with heating rate [131, 132]. Therefore, it is possible to determine the kinetic parameters using equation (4.19):

$$\ln\left(\frac{\beta}{T_p^2}\right) = -\frac{E}{RT_p} + \ln\left(\frac{AR}{E}\right) \tag{4.20}$$

The activation energy can be estimated from the slope of the plot.

Similarly, another equation in which the reaction rate is dependent on the peak temperature was postulated by Ozawa as:

$$\ln(\beta) = -\frac{E}{RT_p} + \ln\left(\frac{AR}{E}\right) \tag{4.21}$$

4.5 Equivalence Ratio (ER)

The equivalence ratio reflects the combined effect of the air flow rate, flow rate of OPF feedstock and duration of the test. The equivalence ratio for this study was calculated by [133]:

$$ER = \frac{Q_{air} \times t}{M_{fuel} \times AF_{stoich}} \tag{4.22}$$

where Q_{air} is the air flow rate (m^3/h), t is the duration of the experiment (h), M_{fuel} is mass input of biomass fuel (kg) and AF_{stoich} is the air fuel ratio at stoichiometric condition (6.1 m^3 of air per kg of OPF).

4.6 Fuel Gas Production

The dry gas yield, Y_{gas}, is calculated from the material balance of nitrogen and is expressed as [134]:

$$Y_{Gas} = \frac{\mathrm{Q_{Air}} \times 0.79}{\dot{\mathrm{m}}_{\mathrm{OPF}} \times \mathrm{N_2}\%} \quad (4.23)$$

where $N_2\%$ represents the N_2 concentration in the fuel gas. Q_{Air} and $\dot{m}_{OPF}$ represent flow rate of air (Nm^3/h) and OPF consumption rate (kg/h), respectively.

4.7 Heating Value of the Product Gas

The higher and lower heating values of the producer gas are determined from the chemical composition of the gas and HHV or LHV of individual components as follow:

$$\mathrm{HHV_{Gas}} = \sum \text{volume\% of component} \times \text{HHV of the component} \quad (4.24)$$

$$\mathrm{LHV_{Gas}} = \sum \text{volume\% of component} \times \text{LHV of the component} \quad (4.25)$$

where the considered components volumetric percentage are CO, H_2 and CH_4.

4.8 Carbon Conversion Efficiency

Carbon conversion efficiency is one of the common performance indicators that are used for gasification process and it is defined as the weight of carbon content in the producer gas to the weight of carbon content in the biomass material. The carbon conversion could be calculated [134]:

$$\eta_{\mathrm{C}} = \frac{12 \times \mathrm{Y_{Gas}} \times (\mathrm{CO} + \mathrm{CO_2} + \mathrm{CH_4})}{22.4 \times \mathrm{C}\%} \quad (4.26)$$

where *C%* is air dried based carbon content in OPF ultimate analysis. High carbon conversion efficiency means that most of carbon content in the biomass fuel converted to gaseous fuel rather than being converted to char and tar. It is an important parameter in deciding the performance of a gasifier. Low carbon conversion is an adverse condition. However, it reduces both the gas yield and energy efficiency [135]. For efficient gasification, a typical value should be in the range of 95% – 99%.

4.9 Gasification Efficiency

Gasification efficiency is one of the important factors that determine the actual technical operation. It usually depends on the gasifier type and design as well as on the characteristics of the biomass fuel [31]. The gasification efficiency in this study was expressed in terms of cold gas efficiency [84]:

$$\mathrm{CGE} = \frac{\mathrm{Y_{gas} \times HHV_{gas}}}{\mathrm{HHV_{OPF}}} \times 100 \tag{4.27}$$

where Y_{gas} is the fuel gas production, HHV_{gas} is the higher heating value of the producer gas and HHV_{OPF} is the higher heating value of the fronds.

4.10 Mass Balance

Mass balance or material balance is essential to validate the experimental results of the gasifier. However, to perform a mass balance for an updraft gasifier, input and output materials should be visualized. The input streams to the gasifier include dry OPF, dry air and their moistures, whereas the output streams include producer gas, char and condensate.

Applying the law of conservation of mass to the gasification process yields [84].

$$\sum M_i = \sum M_o \tag{4.28}$$

Where the total mass input (M_i) and total mass output (M_o) are given by:

$$\mathrm{M_i} = \mathrm{M_{i,f}} + \mathrm{M_{i,a}} + \mathrm{M_{i,w}} \tag{4.29}$$

$$\mathrm{M_o} = \mathrm{M_{o,g}} + \mathrm{M_{o,c}} + \mathrm{M_{o,t}} + \mathrm{M_{o,l}} \tag{4.30}$$

where subscript *i* stands for the process input or input constituents and subscript *o* stands for the process output or output constituents. The subscripts *f, a, w, g, c, t,* and *l* denotes for mass of output fuel, air, water, gases, char, tar and condensate, and losses.

To apply the Eqs. (4.29) and (4.30), the dry air is assumed to consist only oxygen and nitrogen, with a molar ratio of 21:79%. The air is also assumed to have 2%

moisture content (by weight). The producer gas is assumed to be dry, ideal and composed of CO, CO_2, CH_4, H_2 and N_2.

4.11 Uncertainty Analysis

There is no any physical quantity can be measured with perfect certainty in an experiment test. There are always errors in any measurement. Therefore, the experimental investigation work is not complete without the estimation of the uncertainties associated with the measured quantities and the final calculated values. The uncertainty of each measured parameter was evaluated by applying the standard uncertainty evaluations [136]. Two errors were considered in the evaluation the total uncertainty (u_t), systematic error uncertainty which was estimated by instrument uncertainty (u_i) and random error uncertainty (u_e) which was measured from the experiments data.

The systematic uncertainty remain constant when the data obtained under the same conditions and can be obtained based on the accuracy of the instrument as,

$$u_i = \pm DA \times FS \tag{4.31}$$

where *DA* and *FS* represent the device accuracy and full scale of the device, respectively.

The random uncertainty is estimated using the *t*-distribution table [137]. For a confidence level of about 95%, the *t* value can be obtained for the degree of freedom ($g = m - 1$). Hence, the random uncertainty can be determined as,

$$u_e = \pm \frac{t \times SD}{\sqrt{m}} \tag{4.32}$$

where *m* is the samples size, and *SD* is the standard deviation of the sample. The total uncertainty can be calculated as [136, 137],

$$u_t = \sqrt{u_i^2 + u_e^2} \tag{4.33}$$

The uncertainty propagation analysis was also applied in the case of output parameter (gas heating value, gas yield, gasification efficiency *etc.*) obtained from the calculation of multiple measured parameters [138].

.

CHAPTER 5

RESULTS AND DISCUSSIONS

In this chapter, the results of the experiments for OPF characterization and gasification are presented. The characterization of the OPF includes determination of moisture content, density, proximate analysis, ultimate analysis, heating value, thermogravimetric analysis, fourier transform infrared, surface morphology and mineral content analysis. Then, a relationship between biomass moisture content and density is developed, and an empirical correlation for the prediction of the heating value of oil palm fronds based on the ultimate analysis is also presented. The later Sections present the results of the second batch of the experiments which investigated the thermal behavior of OPF under different operating conditions such as equivalence ratio, moisture content and particle size. Thereafter, the results of study on thermal behavior of the gasifier using various inlets air positions and the secondary air approach (secondary air position and secondary to primary air ratios) are presented. Finally, using of OPF synthetic gas in a demotic cooking stove and characterization of gasification byproducts such as char and ash are presented at the end of this chapter.

5.1 Characterization of OPF

The OPF samples were characterized by means of ultimate analysis, proximate analysis, heating value, mineral content, moisture content, density, fourier transform infrared, surface morphology and ash content. In addition, thermal decompositions of the samples were investigated under nitrogen and oxygen atmosphere, in order to determine and analyze the reaction kinetics. A correlation for calculating the higher heating value from elemental composition is presented in this section.

5.1.1 Moisture Content

As the block of cut fronds are not in uniform size, the samples were categorized in three different parts, *i.e*. tip, middle and hub as shown in Figure 5.1. Moisture content tests were performed on freshly pruned OPF by oven drying method (Carbolite 450 oven). The drying process was performed at a temperature of 105^{o}C for 24 hours. The weight measurement of each sample was taken at an interval of 30 minutes, till the weights of the samples remain constant (usually in the first 13 hours). Thereafter, the samples were kept in the oven for the rest of the time to insure constant weight (no weight loss), and the moisture content of the samples was calculated on the wet basis as shown in Eq. (4.1).

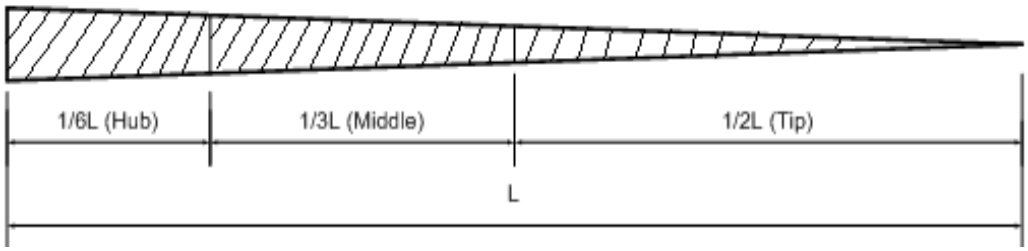

Figure 5.1: Sections of frond

It was found that the final weight of the completely dried sample was about 28.1%, 30.4% and 31.4% of the original weight for the hub, middle and the tip, respectively as shown in Table A.1 (Appendix A). The average moisture content of the OPFs on the weight basis was about 70% as shown in Figure 5.2.

Determining the moisture content by drying the biomass samples in an oven for 24 hour is both time and energy-consuming. Thus, prediction of the moisture content with an easy and fast method within an acceptable tolerance is highly preferable. Therefore, investigating the moisture content-density relationship is considered as the quick prediction method to determine the moisture content for the purpose of gasification process. For this reason, about 147 samples (49 for each section of the tips, middle and hubs) were prepared to conduct an experiment for the determination of moisture content versus density relationship. After each 15 minutes, the samples were taken out of the oven then the volume and mass of the samples were measured. The volume of the samples was measured with graduated cylinder and a known

amount of sand (250 ml), while the mass of the samples were measured using Ohaus precision standard weight balance.

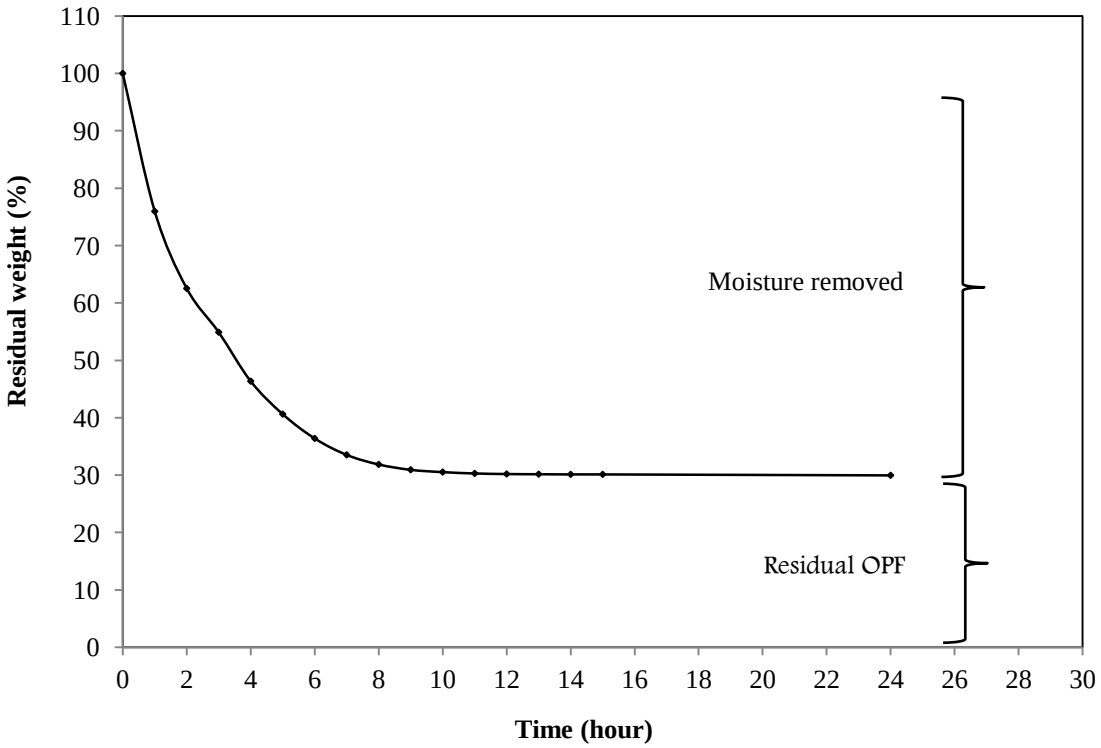

Figure 5.2: Average percentage weight reduction in OPF samples during drying process

The results show that the density of the OPF samples decreases as the moisture content decreases as shown in Figure 5.3. This is simply due to the fact that density is weight per unit volume, and as the samples dried further, weight and volume also reduced, but the weight reduction is faster than the volume reduction and hence, the density will decrease when the moisture content decreases. In general, the experimental results showed that the average values of the density is in the range of 0.25 to 1.0 kg/m^3 for the completely dried and fresh OPF, respectively as illustrated in Figure 5.4.

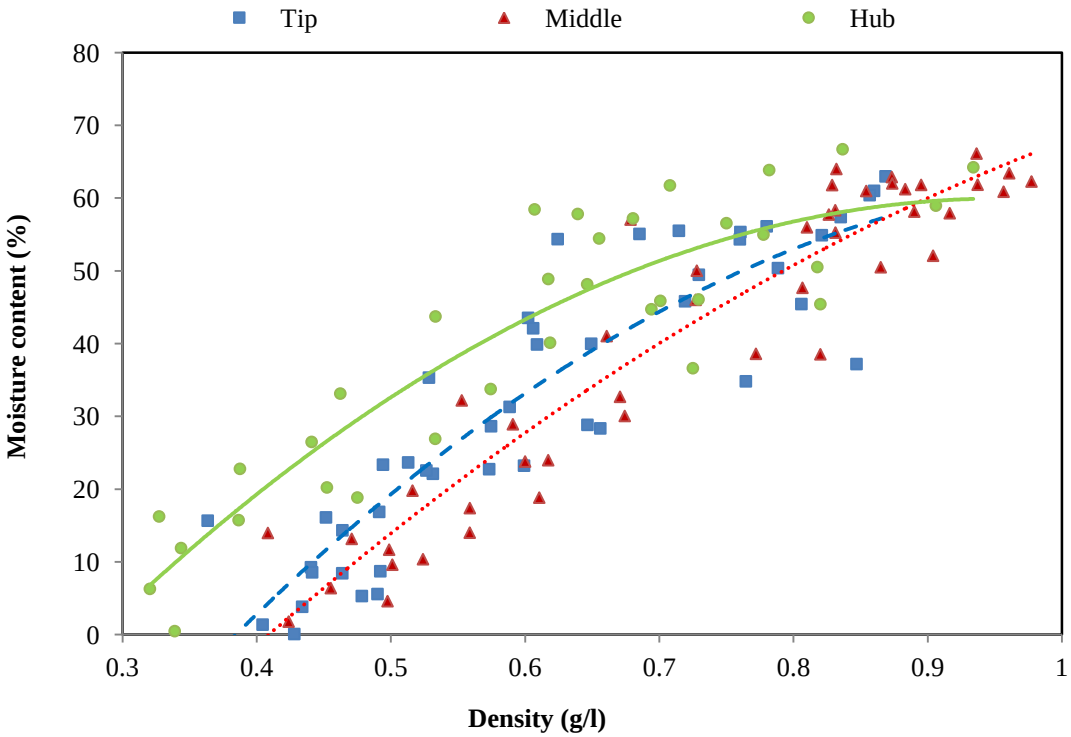

Figure 5.3: Variation of moisture content with density of the frond section

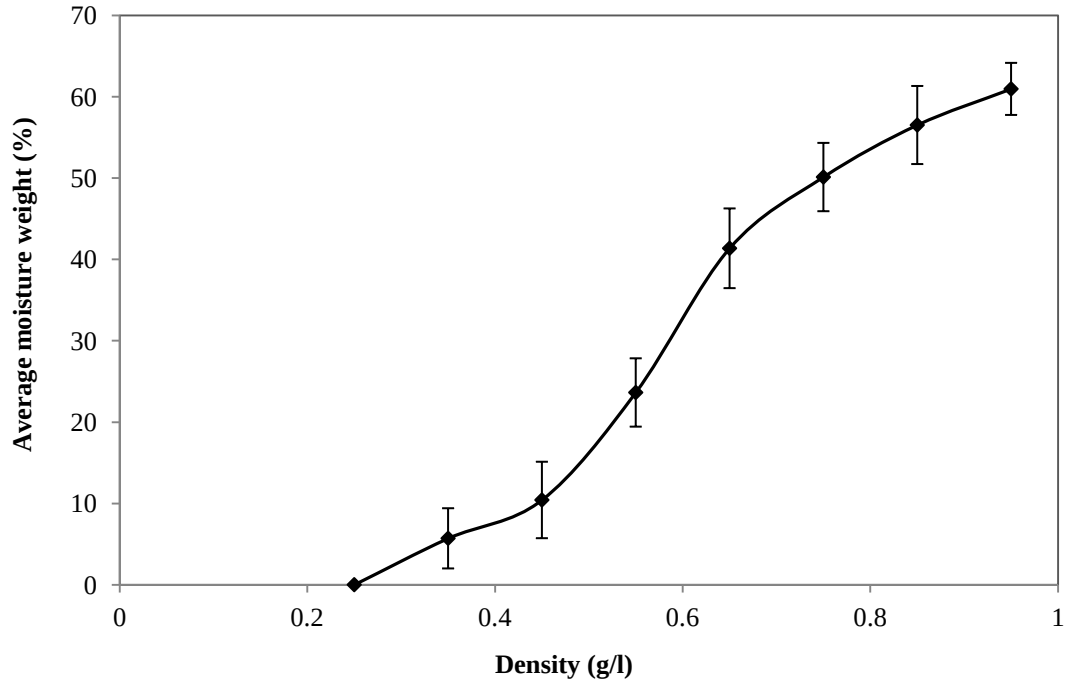

Figure 5.4: Variation of average density with moisture content

As the density increase linearly with an increase in moisture content, a linear relationship as shown in Eq. 5.1 with a correlation coefficient (R^2) of about 0.97 was

developed to predict the moisture content of the OPF based on its density. Then the developed correlation was used to predict the moisture content of the OPF in order to confirm the validity and reliability of the developed correlation. The results of the predicted and measured value are shown in Table 5.1. It was found that the correlation is capable of predicting the OPF moisture content with an average error less than 10% for the OPF moisture content in the range of 10% to 60%, which is the possible range for updraft gasification. Therefore, the developed correlation has a good capability for predicting the OPF moisture content based on its density.

$$MC = 97.3 \times \rho - 27.3 \tag{5.1}$$

where MC and ρ represent the OPF moisture content (%) and density (kg/m^3), respectively.

Table 5.1: Comparison between the measured and the predicted OPF moisture content

Density (kg/m^3)	Moisture content (%)		Error (%)
	Experimental value	Predicted value	
0.25	0.0	2.9	-
0.35	5.7	6.7	17
0.45	11	16	3.6
0.55	24	26	8
0.65	41	37	9.7
0.75	50	46	8
0.85	57	55.4	4.4
0.95	61	65	8.2

5.1.2 Proximate Analysis

As shown in Table 5.2 and Figure 5.5, the OPF contains low percentage of volatile matter (69.32%) as compared to wood and EFB, and contains a reasonable percentage of fixed carbon (18.77%) and ash (3.14%), and low amount of moisture content, around 7.86% are also observed. The volatile matter in biomass significantly affects

the tar content in the product gas; however, biomass with lower volatile matter produces a gas with less tar content. Therefore, as OPFs have lower volatile matter compared to other biomass that gasified in updraft gasifier, such as woody biomass (76.85%), palm shell (73.74%) and EFB (82.58%), the product gas of OPF fuel is expected to have relatively lower tar content, which can reduce the cost of the intensive cleaning that would be required for ordinary updraft product gas.

Table 5.2: Proximate analysis of OPF as compared to other biomass fuel

Variable	Ultimate analysis (Dry basis %)			
	OPF	EFB [139]	Wood [5]	Coal [76]
Moisture content	7.86	5.18	3.93	22.80
Volatile matter	69.32	82.58	76.85	37.30
Fixed carbon	18.77	8.97	18.88	34.50
Ash	3.14	3.45	0.34	5.50

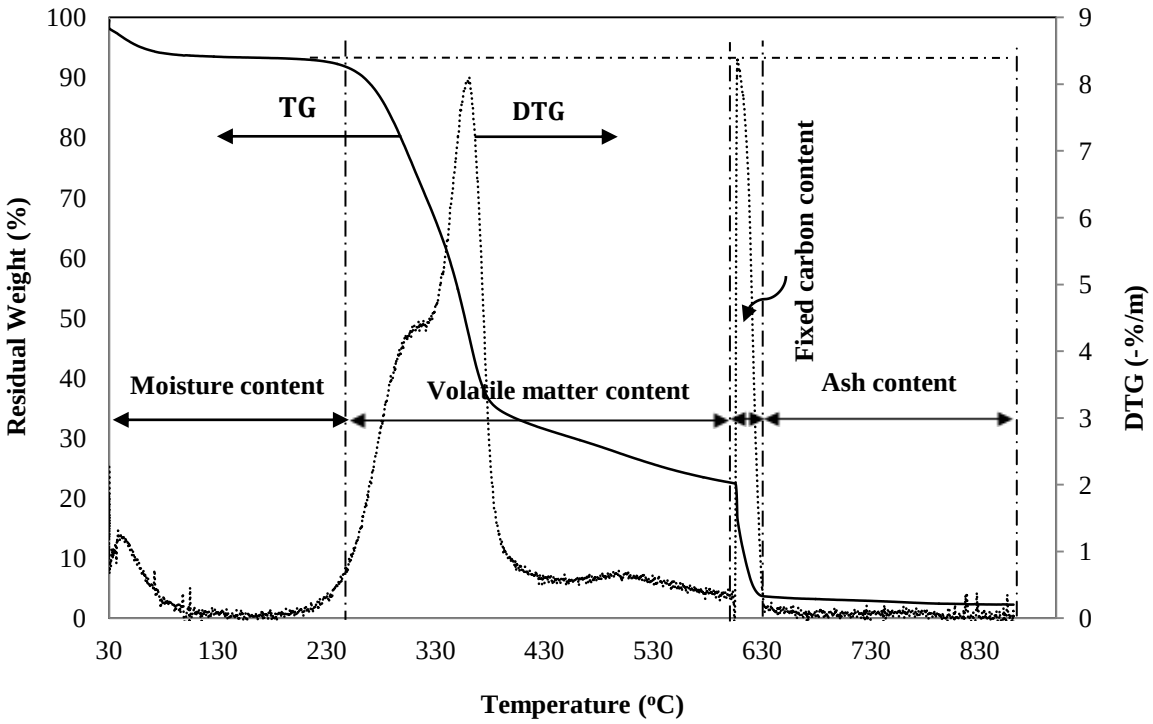

Figure 5.5: Proximate analysis of OPF

5.1.3 Ultimate Analysis

The ultimate analysis was conducted to determine the chemical composition of the OPF and the results were expressed in dry basis term. It determines the weight percentages of carbon (C), hydrogen (H), nitrogen (N), sulfur (S) and oxygen content (estimated by difference). The ultimate analysis of the OPF samples showed an average value of 42.48%, 4.52%, 0.61%, 0.05%, and 52.34% for carbon, hydrogen, nitrogen, sulfur and oxygen content, respectively, as shown in Table 5.3. The *N* content in OPF is much lower than those in coal, wood and EFB. Therefore, the possibility of NO_x generation during updraft gasification process would be smaller. The *S* content in OPF is shown to be much lower than that of coal and exactly equal to that of woody biomass, thus reducing the possibility of acid species formation which is associated to the formation of ‘‘acid rain’’ in the ambience. High *S* content also causes corrosion on the metallic parts of the gasification installation. As a conclusion, the ultimate analysis indicates that OPF is environmental friendly, with only negligible amounts of nitrogen and sulfur.

The average value of hydrogen/carbon (H/C) and oxygen/carbon (O/C) ratios of the samples are 0.11 and 1.23, respectively, which reflect a hydrocarbon combustible property of biomass [140]. Compared to the typical mean values for woody biomass and coals, the OPF samples show much higher value for *O/C* ratio and lower value for *H/C* ratios. Therefore, OPF is expected to have low gasification efficiency than woody biomass and coal. Actually, this is not the only factor that affects the gasification process; there are many other factors that should be considered such as low sulfur and nitrogen content. Moreover, as OPF has the highest oxygen and lowest carbon contents, it is expected to have lowest heating value, due to the fact that a higher oxygen concentration (carbon–oxygen bonds) tends to decrease the heating value. The elemental composition of the samples indicates that the OPF is environmental friendly as it is expected to generate very small traces of nitrogen and sulfur. By considering the main elements C, H and O in Table 5.3 which represent about 99% of the OPF organic mass, the molecular formula can be written as $CH_{1.28}O_{0.92}$.

Table 5.3: Ultimate analysis of OPF as compared to other biomass fuel

Variable	Ultimate analysis (Dry basis %)			
	OPF	EFB [139]	Wood [5]	Coal [76]
C	42.48	46.62	44.75	54.1
H	4.52	6.45	6.31	3.4
N	0.61	1.21	1.68	0.81
S	0.05	0.035	0.05	0.39
O	52.34	45.66	47.21	13.1
H/C	0.11	0.14	0.14	0.063
O/C	1.23	0.98	1.05	0.24

5.1.4 Surface Morphology and Elemental Composition (SEM/EDX Analyses)

To gain additional insight into the OPF structure, scanning electron microscopic (SEM) was performed on the OPF samples to analyze the surface structure. Figure 5.6 presents high resolution SEM micrographs of OPF at magnification of 100x, 200x, 500x and 1000x.

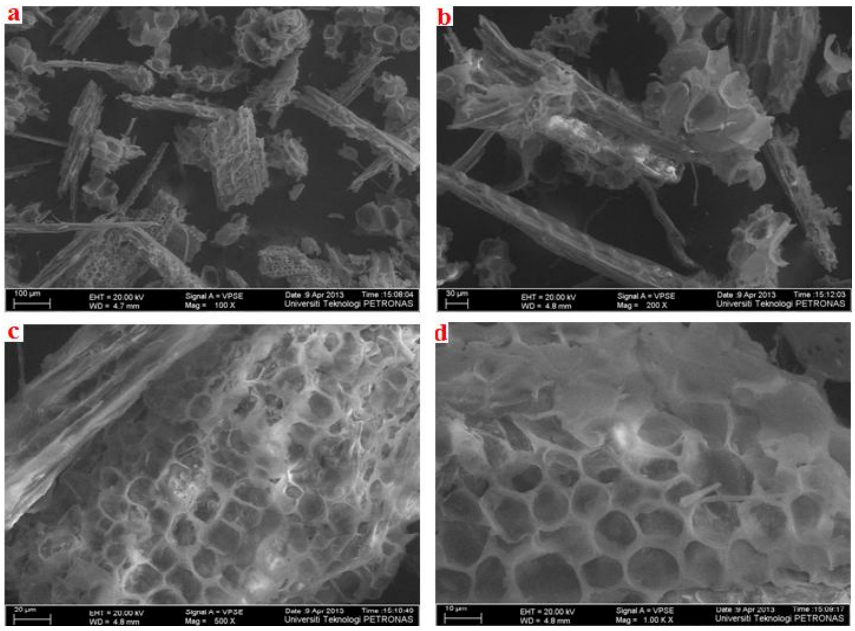

Figure 5.6: SEM image of OPF at different magnification (a) 100x (b) 200x (c) 500x (d) 1000x

The image shows the presence of pores on the surface which may lead to an ease release of volatiles matter from the surface. However, results in a rapid thermal degradation in relatively low temperature.

Table 5.4 presents average results of elemental analyses of OPF material and OPF ash by using the Electron Dispersive X-ray Spectroscopy (EDX). A noteworthy observation is that elements with high percentage such potassium, chlorine, calcium, silicon and sulfur was observed in both OPF material and ash, while some elements such as magnesium, sodium and phosphors were observed in OPF ash only and not detected in the origin OPF material, this may be due to their small concentration. Another observation is that aluminum was detected in the origin OPF material only. This may be attributed to the melting of aluminum during the combustion and gasification processes, as it is known that the aluminum melting point is about 660^{o}C.

Table 5.4: Elemental composition of OPF material and OPF ash

Main components	Symbol	Value (wt. %)	
		OPF	OPF ash
Carbon	C	38.99	29.83
Oxygen	O	51.89	37.39
Magnesium	Mg	-	1.54
Silicon	Si	1.07	2.02
Phosphors	P	-	0.49
Chlorine	Cl	1.32	3.68
Potassium	K	3.33	13.11
Calcium	Ca	1.96	6.68
Sodium	Na	-	0.69
Sulfur	S	0.18	1.72
Iron	Fe	-	2.85
Aluminum	Al	2.26	-

It was also observed that the OPF ash contains a relatively high weight percentage of potassium (13.11%), calcium (6.68%) and iron (2.85%) while magnesium and

sodium weight percentages are comparatively low. As the potassium is considered as one of the main sources of agglomeration of biomass in the gasifier bed [139], which may probably clog the air voidage (grate holes). This problem is basically related to the content of the fuel ash and the operating temperature within the bed [141]. Therefore, the operating temperature for a fuel with high potassium should be in the range of 900-1000^{o}C, in order to avoid the agglomeration problem.

In the view of the above, an updraft gasifier could be a suitable candidate to gasify the OPF. However, as the oxidation temperature in updraft gasifier mostly in the range of 800-1000^{o}C, therefore, might be acceptable for fuel with high percentage of potassium.

5.1.5 Fourier Transform Infrared (FT-IR) Spectroscopy

Figure 5.7 illustrates the spectra for oil palm fronds samples. The spectra were performed over a frequency range of 4000–650 cm^{-1}. The peak at 3316 cm^{-1} can be assigned to the C–H stretching region. The peak at 2907 cm^{-1} can be assigned to methylene (CH_2) asymmetric stretch of aliphatic hydrocarbons or can be assigned to the CH stretching vibrations in cellulose [142], while the C–O and C–C stretching at about 1031 cm^{-1} indicates the presence of aliphatic and alicyclic eight-member ring (levoglucosan) alcohols which could originate from the decomposition of trace bedding material (wood) in the manure. Additionally, the bands at 1238 and 1501cm^{-1} may suggest the presence of aromatic compound, while the bands at 1593 cm^{-1} could be attributed to the existence of C=C stretching vibration in aromatic rings. Moreover, the peak at 1422 cm^{-1} resulted in C–N stretch of primary amide. In conclusion, the FT-IR profiles of OPF samples showed the characteristic of a typical ligno-cellulosic material as well as the cellulosic wastes derived from chicken farms [48], EFB [143], and wood chips [142] and indicated that the OPF might contain some carbohydrates, alkene, aromatics, ketone, alcohol and inorganic compounds, with different oxygen-containing functional groups such as OH, C–O–C and C=O.

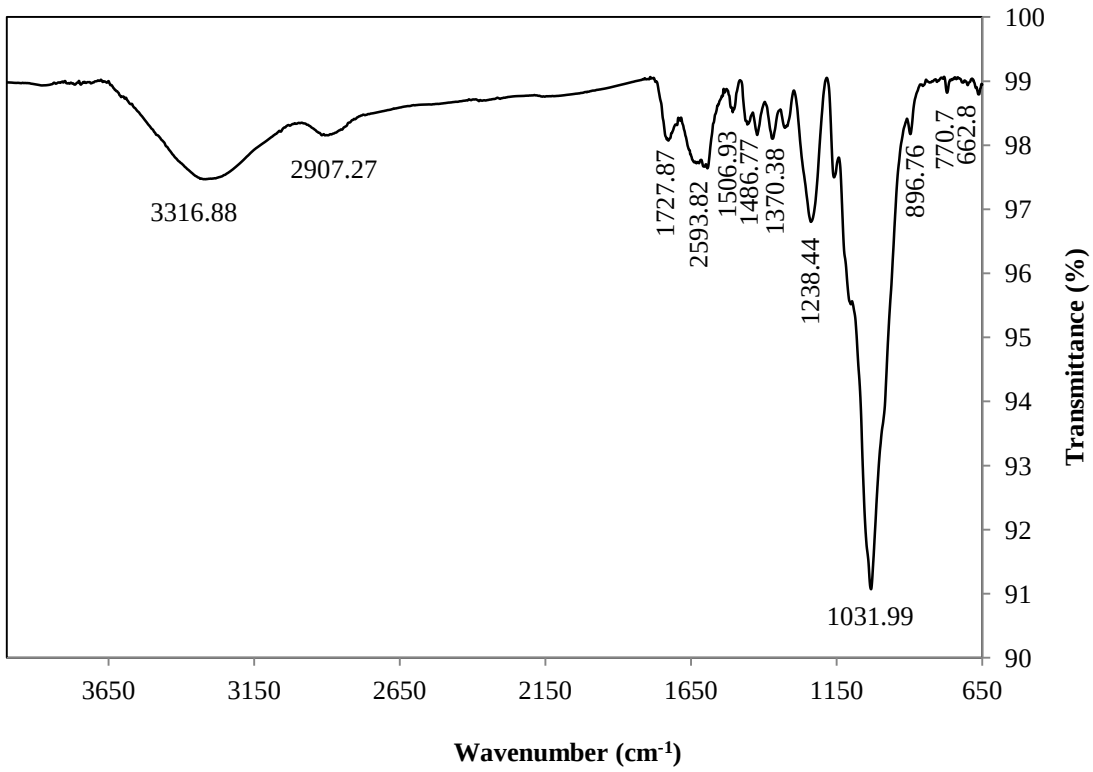

Figure 5.7: FT-IR spectra of OPF

5.1.6 Heating Value

Knowledge of heating value of OPF is essential when determining the thermal efficiency of the gasifier for producing syngas. The higher heating value of OPF was found to be about 17.01 MJ/kg, which is slightly lower than that reported in the literature for wood (18.47 MJ/kg) and coal (21.39 MJ/kg) [5, 76], but the value falls in the range of various type of woody biomass fuel, which is between 15.3 MJ/kg and 21.2 MJ/kg on dry fuel basis [144].

5.1.7 Heating Value Model

As the correlations based on the ultimate analysis were considered the most accurate and reliable models to predict the heating value of biomass material [32], elemental analysis were used to predict the heating value for the OPFs. In developing the model, 36 samples were used. 30 of the samples were used in the regression analysis to

develop the models, while the remaining 6 samples were used to validate the developed model. Development of the models, selection of the best model and validation of the model were the steps used to develop the correlation.

The results of the ultimate analysis showed that the OPF composed the elements C, H, O, N and S, of which the first three elements represented about 97-99% of the OPF organic mass. Sulfur was found in a very small amount (less than 0.17%), and therefore it was not considered in the model.

It is observed from Table A.3 (Appendix A) that there is a linear relationship between the heating value and carbon, hydrogen and oxygen. However, the heating value increased with an increase in carbon and hydrogen contents, which agreed with the results obtained by Sheng [32] for biomass fuel. The heating values decreased with an increase in oxygen content, and this correlates well with the fact that oxygen is not a reactive element [32]. However, increasing the non reactive elements in biomass fuel means a decreasing of the reactive elements such as carbon and hydrogen. On the other hand, there was no trend observed between heating values and nitrogen content. Therefore, in calculating the higher heating value of the OPF, only three elements were selected, which were carbon, hydrogen and oxygen. For the current experimental data, and confidence level of 95%, there were significant correlations between the biomass heating value and the carbon, oxygen and hydrogen components; for which the correlation coefficients (R^2) are 0.903, 0.817 and 0.523, respectively. There is no correlation between biomass heating value and nitrogen components (0.026) as shown in Table 5.5. Therefore, and from the same table it can be noted that the computed correlation coefficients for carbon, oxygen and hydrogen are greater than the critical correlation coefficients for the number of samples [137].

Table 5.5: The calculated and critical correlation coefficient for the biomass component

Factor	R^2	rt
C	0.903	0.361
H	0.523	0.361
O	0.817	0.361
N	0.026	0.361

R^2: computed correlation coefficient, rt: critical correlation coefficient

In order to develop the model, multiple linear regression analysis was used; however, carbon, hydrogen and oxygen were taken as input independent variables, while the actual heating values were taken as an output dependent variable. Thus, four empirical equations were proposed to determine the heating values using the elements of the ultimate analysis. These equations were developed based on the fact that the heating value of OPF biomass is a function of carbon, carbon and hydrogen, carbon and oxygen, and also as a function of a combination of carbon, hydrogen and oxygen. However, carbon was included in all proposed models; this is because of its nature as the major reactive element present in the biomass. The proposed models are shown in Table 5.6.

Table 5.6: Proposed models based on the ultimate analysis element

	Independent variable	Equation	R^2	AAE (%)	ABE (%)
M1	C	$HHV = 0.924C - 22.403$	0.903	1.6	-0.0016
M2	C, H	$HHV = 0.824C + 0.2894H - 19.427$	0.916	1.5	0.16
M3	C, O	$HHV = 0.886C + 0.0324O - 19.086$	0.903	1.6	0.19
M4	C, H, O	$\mathrm{HHV} = 0.879\mathrm{C} + 0.3214\mathrm{H} + 0.056\mathrm{O} - 24.826$	0.917	1.4	0.16

In selecting the best model, the developed equations were evaluated and compared with the fitting performance criteria, which evaluated the accuracy and validity of the model. The considered performance criteria were the correlation coefficient (R^2),

average absolute error (*AAE*) and average bias error (*ABE*), which can be computed by the Eqs. 4.3, 4.4 and 4.5, respectively.

The correlation coefficient (R^2) is widely used in statistical and regression analyses to quantify the accuracy of the model. The higher value of the correlation coefficient, indicates the better estimation (A perfect model has an R^2 of 1.0). The average absolute error (*AAE*) of the correlation indicates the correlation accuracy. The lower the *AAE* value, the higher would be the accuracy of the correlation model. *ABE* describes the average bias error of the correlation. A positive value of *ABE* means an overall over-estimation, while a negative value indicates an overall under-estimation of the sample population. The lower the absolute value of *ABE*, the smaller would be the bias of the correlation. As shown in Table 5.6, model M4 gives the maximum R^2 and minimum *AAE* performance. Based on that, the best model of predicting the heating value of the OPF by using the ultimate analysis could be:

$$\mathrm{HHV} = 0.879\mathrm{C} + 0.3214\mathrm{H} + 0.056\mathrm{O} - 24.826 \qquad (5.2)$$

The validation of the selected model was carried out by comparing the predicted heating values with those obtained experimentally. The calculated and measured values are shown in Figure 5.8. It can be seen from the same figure that the calculated values were quite consistent with the experimental measurements. Figure 5.9 shows the scatter plot of the standard residuals against the predicted heating values. It can be seen that the standard residuals were randomly distributed along the predicted heating values, and most of the values lay within ±0.8

The developed model was also tested with other six samples of oil palm fronds (not included in developing the model) to confirm the reliability of the model. Table 5.7 shows the comparison between the measured and calculated heating values for the tested samples. However, the developed model is capable of predicting the heating value of OPF with an average absolute error of less than 6%, indicating its good predicting capability.

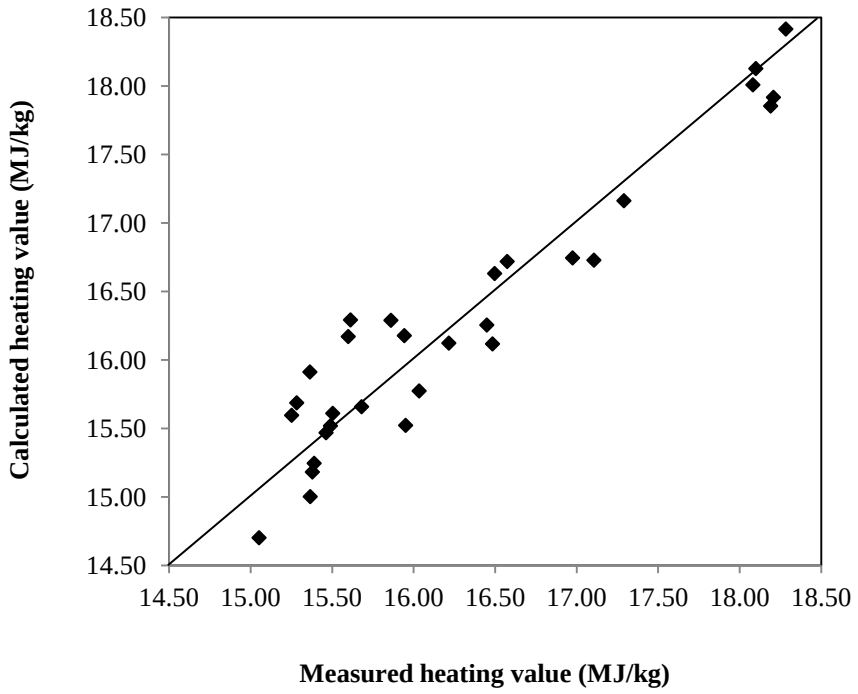

Figure 5.8: Comparison between the measured and calculated heating values of OPF

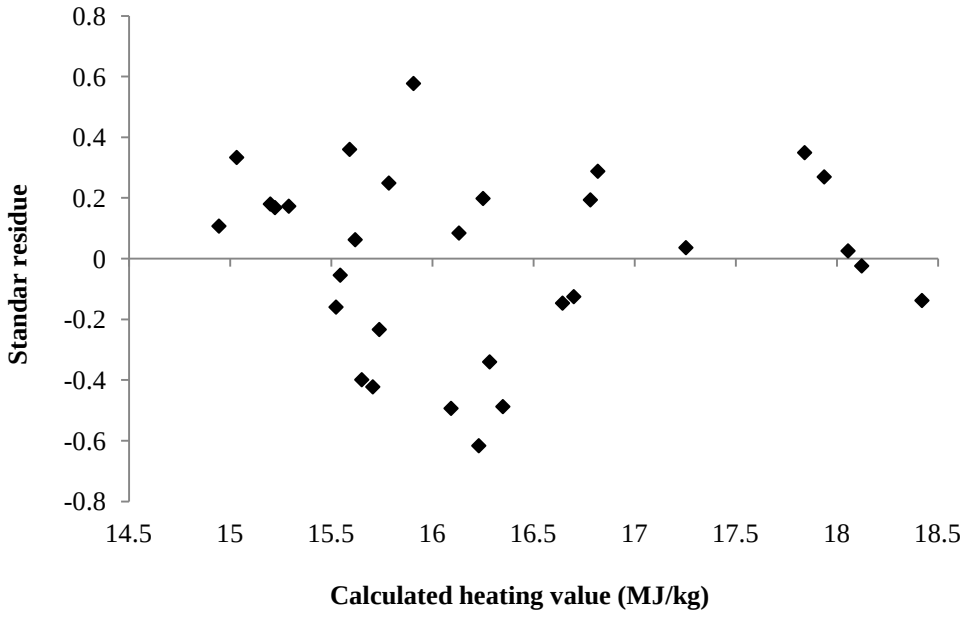

Figure 5.9: Standard residuals against the predicted heating values

Table 5.7: Comparison between the measured and the predicted heating values of the OPF

Sample	Ultimate analysis (wt %)					HHV_m	HHV_c	AAE (%)
	C	H	N	S	O			
1	42.290	3.924	0.770	0.060	52.956	16.014	16.572	3.485
2	40.800	3.937	0.498	0.015	54.774	15.774	15.367	-2.580
3	42.360	4.069	0.538	0.024	53.009	16.385	16.683	1.819
4	42.290	4.780	0.722	0.047	54.161	15.833	15.156	5.236
5	42.080	4.143	0.603	0.036	53.138	15.981	16.468	3.047
6	40.970	5.000	0.744	0.078	53.208	15.409	15.771	2.351

HHV_m: measured heating value, HHV_p: calculated heating value

5.1.8 Thermogravimetric Characterization and Kinetics Analysis

Thermogravimetric analyses were conducted in order to study the various physio-chemical changes that occur when samples of the OPF were heated in atmospheres of nitrogen and oxygen. The investigation of thermogravimetric behavior of the samples was examined at different heating rates of 20, 30 and 40^{o}C/min at temperatures between room temperature and 860^{o}C. The residual weight % (TG) and its derivative (DTG), with respect to the temperature and time were recorded using the TGA software, and the data used to determine the kinetic parameters (activation energy, frequency factor and order of reaction). Moreover, the kinetic parameters were evaluated from the TGA profiles by using two model approaches; *i.e.*, model-fitting and model-free approaches.

5.1.8.1 Thermogravimetric Analysis in Nitrogen (inert) Atmosphere

Figure 5.10 shows a typical thermogravimetric profile of oil palm fronds in a nitrogen atmosphere. For all heating rates, three distinct stages of thermal decomposition could be distinguished. In the first stage, about 5-8% of the weight loss could be observed at

temperatures of about 150°C. As biomass drying usually takes place at the temperature about 100°C, the stage implied removal of moisture content. After the first stage, there was negligible weight loss (<3%) in the temperature range of 150-250°C. The second stage of the weight loss, occurred at between 250 and 410°C, showed sharp weight loss. However, about 60% of the weight loss of the sample occurred in this stage. As suggested by Lapuerta *et al*. [145], this may be due to the decomposition of the light volatile matter (hemicellulose and cellulose). In a later stage, there was small reduction in weight by about 6-8% at temperature range of 390-600°C. This stage represented the degradation of lignin. The remaining constant value at the temperature between 600 and 860°C implied the weight of char and ash.

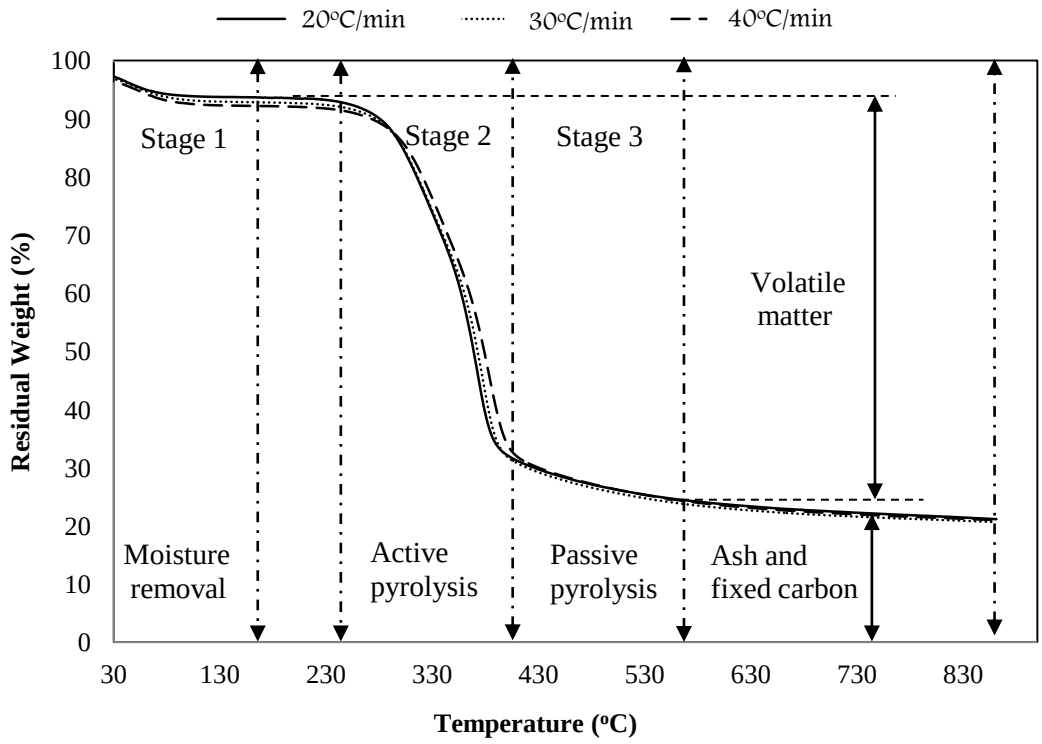

Figure 5.10: Identification of decomposition stages of OPF by TGA in nitrogen atmosphere at different heating rates

a) ***Thermal Degradation Rate (TDR) of OPF under Nitrogen Atmosphere***

As discussed in Section 5.1.8.1, with a nitrogen atmosphere, the volatile matter of the OPF samples decompose in distinct decomposition stages as shown in Figure 5.10. It was found that the thermal degradation rate in all decomposition stages increase

linearly as the heating rate (β) increases. However, as the heating rate increases from 20°C/min to 40°C/min, the thermal degradation rates increase linearly from 9.0 % min^{-1} to 17.05 % min^{-1} and from 1.1 % min^{-1} to 1.73 % min^{-1} for holocellulose (hemicellulose and cellulose) decomposition stage and lignin decomposition stage, respectively as shown in Figure 5.11. As the thermal degradation rate of OPF samples increases linearly with heating rate in nitrogen atmosphere, a linear relationship is obtained between the thermal degradation rates and heating rates for the same stages. As noted from the same figure, the thermal degradation rates for the active pyrolysis stage and passive pyrolysis stage are fitted respectively with the correlations below:

$TDR = 0.4028\beta + 0.9472$, with a coefficient $R^2 = 1.0$. For active pyrolysis (5.3)

$TDR = 0.0333\beta + 0.4338$, with a coefficient $R^2 = 0.99$. For passive pyrolysis (5.4)

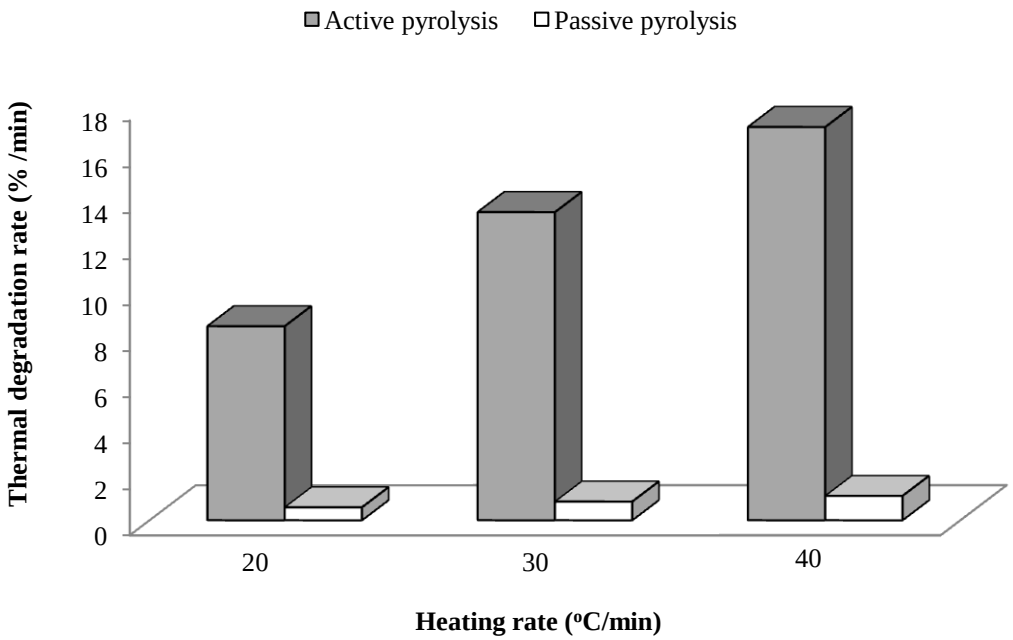

Figure 5.11: Thermal degradation rate for the different heating rates

b) ***Effect of Nitrogen Heating Rate on Thermogravimetric of OPF***

Figures 5.10 and 5.12 show the thermogravimetric (TG) and derivative thermogravimetric (DTG) profiles for the OPFs under different heating rates (20-40°C/min). The samples were heated from room temperature to 860°C at gas (N_2) flow rate of 20 ml/min. The TGA curves revealed an initial slight weight loss at

between 30°C and 150°C. Probably it might be due to loss in moisture content from the samples. This was followed by the major and rapid weight loss (about 60%), in the temperature range of 250-410°C. The high and rapid weight loss might be due to the release of light volatile matter that existed in the biomass material. Moreover, this zone was referred to as an active pyrolysis zone [146, 147]. Another change in the TGA curves was observed within a temperature range of 420-600°C depending on the heating rate; this could be indicated as the initiation of the second reaction zone which terminated completely at around 600°C. This could be considered as the passive pyrolysis zone. Several studies in the past provided strong evidence for attributing the active pyrolysis zone to the evolution of the volatile compounds that were generated during the decomposition of the primary hemicelluloses and cellulose [148, 149], while the continued weight loss in the passive pyrolysis zone was attributed to the lignin conversion [149].

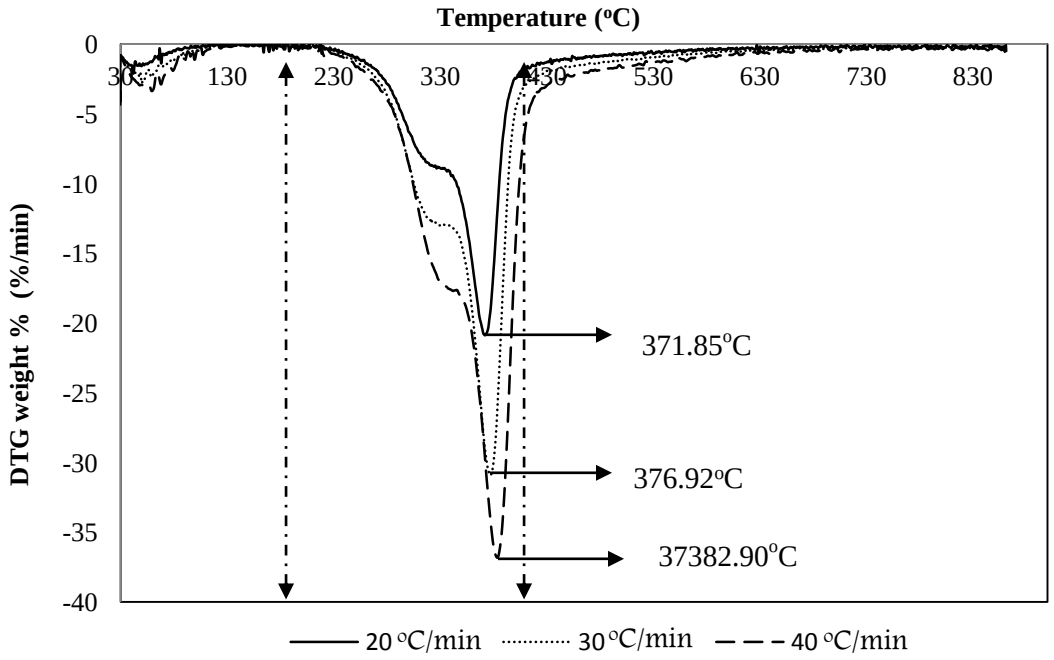

Figure 5.12: Derivative thermogravimetric of OPF under nitrogen atmosphere

As shown in Figure 5.12 for all the heating rates, the DTG profiles consisted of a peak value, and appeared at the range of 370-390°C. It was reported that this peak value represented the hemicelluloses and cellulose decomposition [122, 150, 151]. It was also shown in the previous work [152] that as the heating rate increased, the onset

temperature shifted slightly to the right; as shown in Table 5.8. This temperature shift might be due to heat transfer effect. It can be seen from Figure 5.10 that there was a lateral shift in the TG curves for different heating rates. Moreover, this was an effect of the heating rate on the total weight loss. The same phenomenon was observed by other researchers for different biomass materials [147, 152, 153]. It was also observed that the faster the heating rate, the higher the temperature at which weight loss starts. This phenomenon can be observed clearly in Figure 5.10.

Table 5.8: The DTG peak temperature of OPF at N_2 atmosphere

Heating rate (^oC/min)	Temperature (^oC) at presence of DTG peak
20	371.85
30	376.92
40	382.90

c) ***Parameters of Reaction Kinetics***

Based on the model-fitting approaches, the kinetic parameters of the weight loss at different heating rates were determined by using the Coats-Redfern method [131] one of the most widely used methods in non-isothermal kinetic analysis. The results of the kinetic parameters such as activation energy (*E*), frequency factor (*A*) and order of reaction (*n*) with their corresponding correlation coefficients (R^2) were evaluated for the two reaction zones separately, and listed in Table 5.9. Higher thermal degradation was observed in the first reaction zone, and this was due to the rapid release of the volatile compound in this zone as compared to the second reaction zone. The activation energies for the first order kinetics were found to be in the range of 72.1-73.3 kJ/mol for the first reaction zone (active pyrolysis), while the activation energy was almost the same for the second reaction zone (passive pyrolysis). Moreover, the total of the activation energy of the OPFs appeared to decrease with the increasing heating rate, which indicated that the sample decomposed at a faster rate with an increase in the heating rate. This finding agrees with that reported in the literature for palm fibre [151]. The correlation coefficients were found to be higher than 0.94 for all heating rates and for both reaction zones.

Table 5.9: Kinetic parameters from the TG curve at different heating rates

TG curve	Stage 2 (Active pyrolysis) 250-400°C			Stage 3 (Passive pyrolysis) 400-600°C		
β (°C/min)	A^*	E (kJ/mol)	R^2	A^*	E (kJ/mol)	R^2
20	11.26	73.30	0.94	-2.40	6.47	0.90
30	11.08	72.07	0.95	-2.51	6.30	0.93
40	11.05	72.66	0.94	-3.72	6.18	0.93

$A^* = \ln\left[\frac{AR}{\beta E}\right]$

In order to evaluate the activation energy by using the model-free approach, several degrees of conversion (α) along the thermal decomposition of the samples were marked crossing the TG curves corresponding to each heating rate (β). It can be observed that the faster the heating rate, the higher would be the temperature at which weight loss starts. Therefore, five different degrees of conversion (20, 30, 40, 50 and 60%) are pointed out from the TG curve of the OPFs as shown in Figure 5.14 which shows the plots of $\ln(\beta)$ vs. $\frac{1}{T}$, $\ln\left(\frac{\beta}{T^2}\right)$ vs. $\frac{1}{T}$, $\ln\left(\frac{\beta}{T^{1.894661}}\right)$ vs. $\frac{1}{T}$ and $\ln\left(\frac{\beta}{T^{1.92}}\right)$ vs. $\frac{1}{T}$ corresponding to the several conversion degrees (α) of the process according to the Flynn–Wall–Ozawa (FWO), Kissinger–Akahira–Sunose (KAS), Tang and Starink isoconversional methods, respectively. Straight lines with the angular coefficients $\frac{E}{R}$ are shown in Figure 5.13 from which series of activation energy values were evaluated by using Eqs. 4.16 – 4.19.

For the Kissinger and Ozawa methods (model-free methods but not isoconversional), the activation energy was not obtained at the progressive values of (α), but rather a single value of the activation energy was obtained at the peak temperature, which corresponds to the maximum weight loss for each heating rate. Figure 5.13 (e and f) also shows the plot of $\ln\left(\frac{\beta}{T_p^2}\right)$ versus $\frac{1}{T_p}$ and $\ln(\beta)$ versus $\frac{1}{T_p}$ for the different heating rates corresponding to Kissinger and Ozawa methods, respectively.

The activation energies corresponding to the FWO, KAS, Tang and Starink methods were found to be 134.17, 131.16, 131.51 and 131.47 kJ/mol, respectively, with correlation coefficients of 0.86-0.99 for all degrees of conversion (α). In addition, the single values of the activation energy evaluated by Kissinger and Ozawa methods were found to be 85.41 and 95.96 kJ/mol respectively, which were consistent with the range of values obtained by free-model isoconversional methods as presented in Table 5.10.

Table 5.10: Activation energy (E) and correlation coefficients (R^2) at different conversion (α) for the FWO, KAS, Tang, Straink, Kissinger and Ozawa methods

α (%)	FWO		KAS		Tang		Straink	
	E (kJ/mol)	R^2	E (kJ/mol)	R^2	E (kJ/mol)	R^2	E (kJ/mol)	R^2
20	113.68	0.88	109.98	0.87	110.32	0.87	110.28	0.87
30	106.33	0.88	101.89	0.86	102.61	0.86	102.20	0.86
40	119.45	0.91	115.36	0.90	115.74	0.90	115.68	0.90
50	140.15	0.96	136.87	0.96	137.23	0.96	137.19	0.96
60	191.72	0.99	191.72	0.97	192.01	0.97	192.00	0.99
Average	134.27	-	131.17	-	131.51	-	131.47	-
Kissinger	85.41	0.96						
Ozawa	95.88	0.96						

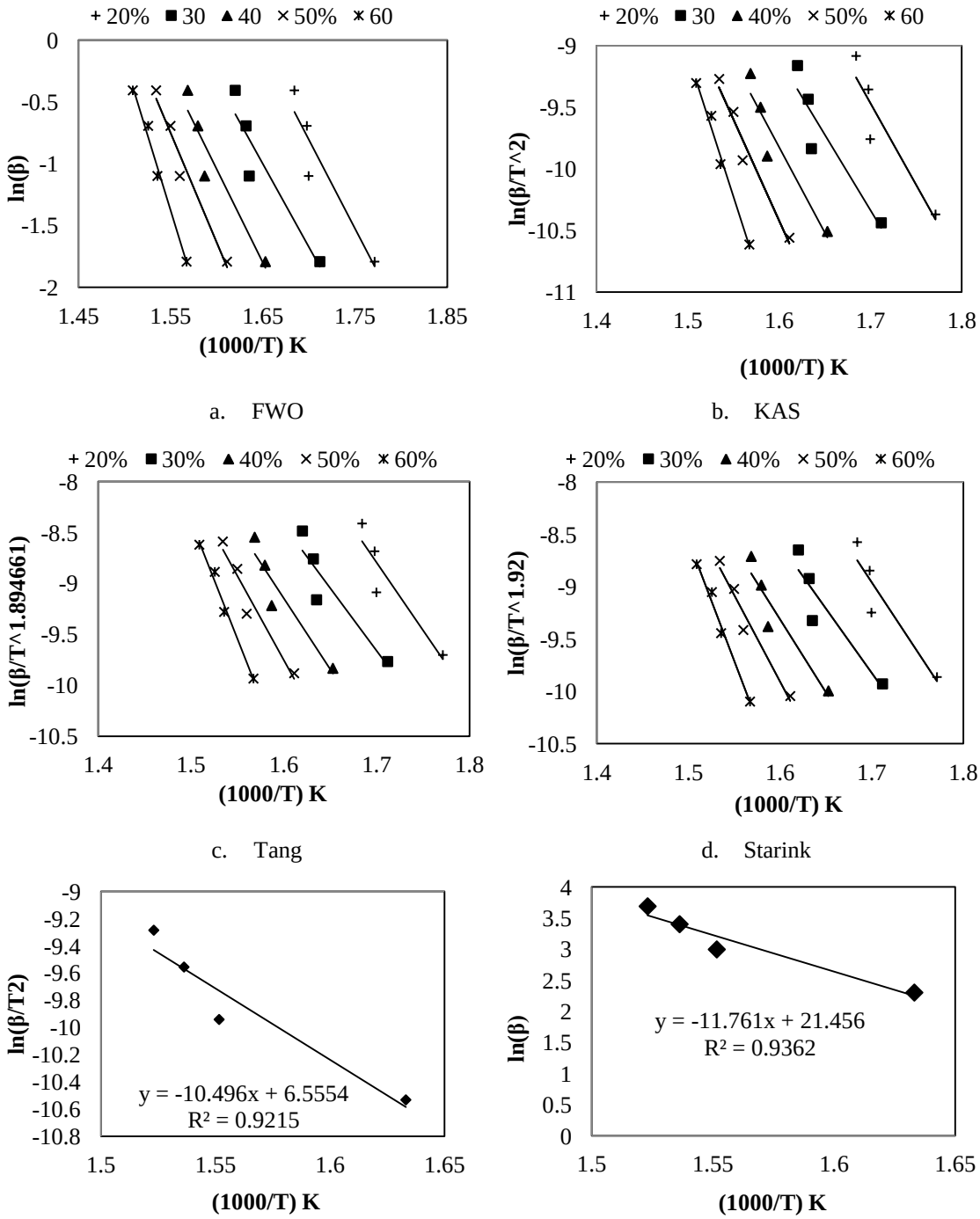

a. FWO

b. KAS

c. Tang

d. Starink

e. Kissinger

f. Ozawa

Figure 5.13: Linearization slopes according to the FWO, KAS, Tang, Starink, Kissinger and Ozawa Methods for the OPF

5.1.8.2 Thermogravimetric Analysis in Oxygen Atmosphere (oxidizing)

Several stages of decomposition could be distinguished for all heating rates as shown in Figure 5.14. In the first stage, a small amount of weight loss was observed at a temperature of less than 150^{o}C. Signifying the removal of moisture content from the samples. In the second and third stage, for temperatures between 250-380^{o}C and 380-450^{o}C, respectively, volatile matter began to release. The second stage represents decomposition of the light volatile matter (hemicellulose and cellulose), while the third stage represents decomposition of the heavy volatile matter (lignin). The fourth stage of degradation occurred between 440^{o}C and 555^{o}C and this corresponds to char oxidation. Thereafter, the remaining constant value, at temperatures between 555^{o}C and 860^{o}C, was considered as ash content. For all cases, the total weight loss of the OPF samples in the first three stages (second, third and fourth) was in the range of 86-92%, which is an indication of the easy burning or gasifying of the OPF compared to other types of biomasses [139].

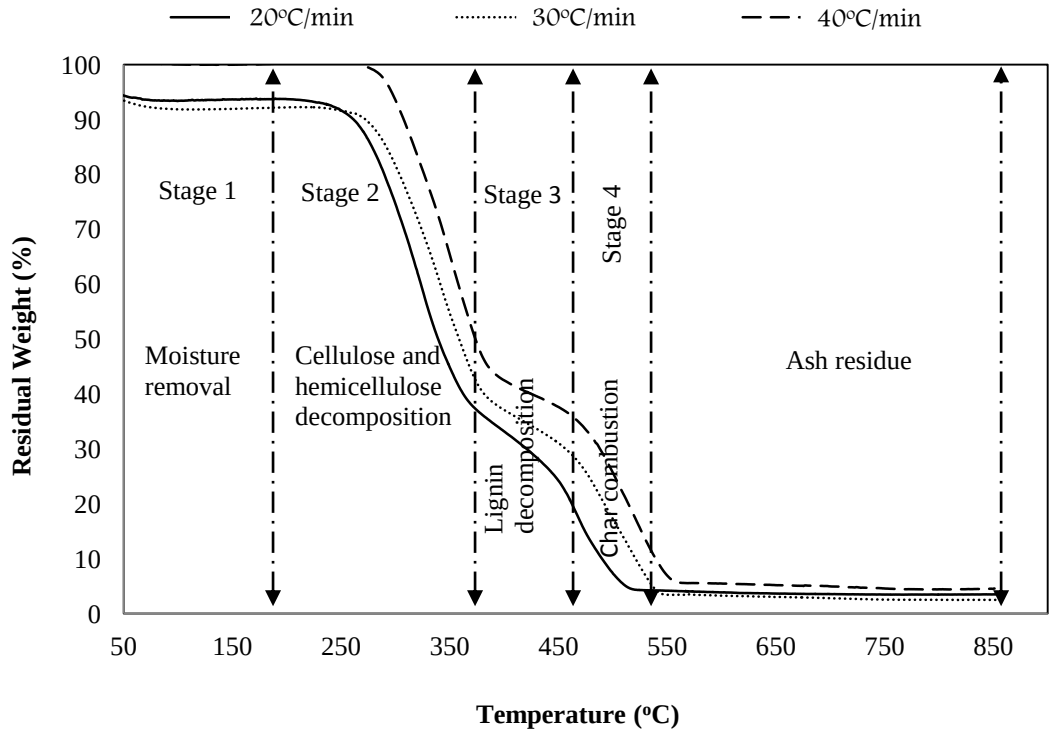

Figure 5.14: Identification of decomposition stages of OPF by TGA in oxygen atmosphere

a) ***Thermal Degradation Rate (TDR) of OPF under Oxygen Atmosphere***

As mentioned earlier, during thermal degradation of OPF samples, three distinct decomposition stages could be observed such as holocellulose (cellulose and hemicellulose) decomposition, lignin decomposition and char oxidation. It is found that, the thermal degradation rate in all decomposition stages increases linearly as heating rate (β) increases. However, the thermal degradation rates increase from 8.84 to 21.25, 2.84 to 4.92 and from 6.56 to 13.76 % min^{-1} for holocellulose decomposition stage, lignin decomposition stage and char oxidation stage, respectively as shown in Figure 5.15. As the thermal degradation rate of OPF samples increases linearly with heating rate in oxygen atmosphere, a linear relationship is obtained between the thermal degradation rates and heating rates for holocellulose decomposition stage, lignin decomposition stage and char oxidation stage. As noted from the same figure, the thermal degradation rates for the decomposition stages are fitted respectively with a correlation of:

$$TDR = 0.6025\beta - 4.341, \text{ with a coefficient } R^2 = 0.96, \text{ for stage 2} \quad (5.5)$$

$$TDR = 0.1036\beta + 0.5673, \text{ with a coefficient } R^2 = 0.99, \text{ for stage 3} \quad (5.6)$$

$$TDR = 0.3601\beta - 0.8355, \text{ with a coefficient } R^2 = 0.91, \text{ for stage 4} \quad (5.7)$$

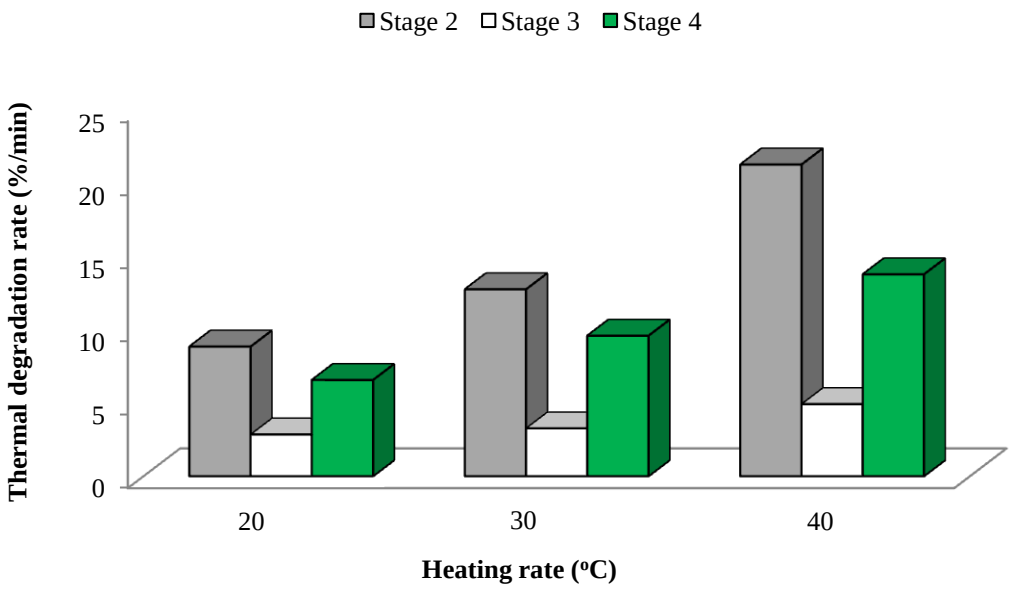

Figure 5.15: Thermal degradation rate for the different heating rate

b) ***Parameters of Reaction Kinetics***

Table 5.11 represents the calculated kinetic parameters such as activation energy (*E*) and the pre-exponential factor (*A*) with their corresponding correlation coefficients (R^2) for the different heating rate. It is observed that the activation energies change during the degradation process of OPF. However, the kinetic analysis of holocellulose decomposition stage showed that the activation energy increases from 66.68 to 75.83 kJ/mol as the heating rate increases from 20 to 40^{o}C/min. This suggested that the higher heating rate, the easier and faster would be the release of the light volatile matter. The kinetic analysis of lignin decomposition stage showed that the activation energies varied between 14.03 kJ/mol and 17.49 kJ/mol. However, for char oxidation stage, the activation energies were increased from 70.24 to 77.63 kJ/mol for the same heating rates. The results showed a higher correlation coefficient in the range of 0.88-0.94 for all decomposition stages as well as all heating rates.

Table 5.11: Kinetic parameters during decomposition stages in an oxygen atmosphere

TG curve	Stage 2 First reaction zone 250-384^{o}C			Stage 3 Second reaction zone 370-470^{o}C			Stage 3 Third reaction zone 450-560^{o}C		
β (^{o}C/min)	A	E (kJ/mol)	R^2	A	E (kJ/mol)	R^2	A	E (kJ/mol)	R^2
20	13.25	66.68	0.94	12.76	17.49	0.88	25.51	70.24	0.91
30	13.80	66.87	0.92	16.59	14.66	0.90	33.52	73.11	0.92
40	14.25	75.83	0.92	21.73	14.03	0.90	25.75	77.63	0.94

c) ***Effect of Oxygen Heating Rate on Thermogravimetric of OPF***

Heating rate had an effect on the start and end of each stage. However increases in a heating rate appear to increase the start and end temperatures of each stage, as well as the onset temperatures as shown in Figure 5.14 and 5.16. This may be due to the heat and mass transfer limitations, and the results of these experiments agreed with those obtained by Kumar [147] for corn stover biomass. The weight losses at the second and third stages are almost the same for all heating rates, while it increases as the

heating rate increases at the fourth stage. However, the weight losses ranged between 49.94% and 53.66%, and 9.16-13.79% for the second and third stage, respectively. As the heating rate increased from 20 to 40^{o}C/min, the weight loss at the fourth stage increases from 18.61 to 28.43%, which may explain that the combustion of OPF was incomplete for less heating rate up to 470^{o}C. While at the end of the fourth stage, whatever the heating rate was, the residual weight at the temperature of 555^{o}C was almost the same at a value less than 5% of the original mass, and this value was considered as the amount of ash in the OPF. For all heating rates, the DTG profiles consisted of two peak values, the first peak value appeared at the range of 320-350^{o}C, while the second peak value appeared at the range of 470-510^{o}C as shown in Figure 5.16.

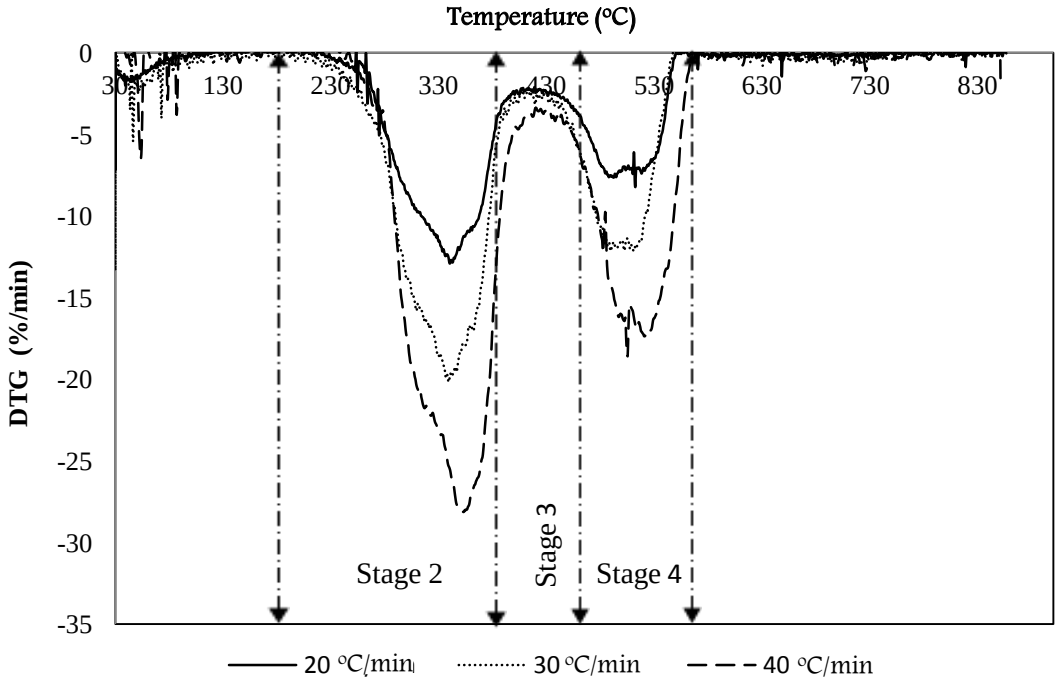

Figure 5.16: DTG of OPF by TGA under oxygen atmosphere

d) ***Effect of Particle Size***

The TGA profiles of different OPF particle sizes under oxygen atmosphere and at a heating rate of 30^{o}C/min are compared in Figure 5.17. As shown in the same figure, there is no significant change for the temperatures of the starting and ending of each stage. The starting and ending temperatures for the all particle size are almost the

same, while the DTG peak temperature increased slightly as the particle size increased. The peak temperatures were about 335^{o}C for particles with diameter less than 212 mm, 357^{o}C for 300-415mm particles diameter, 360^{o}C for 600-1.18 mm particles diameter and 370^{o}C for larger than 1.18 mm particles diameter.

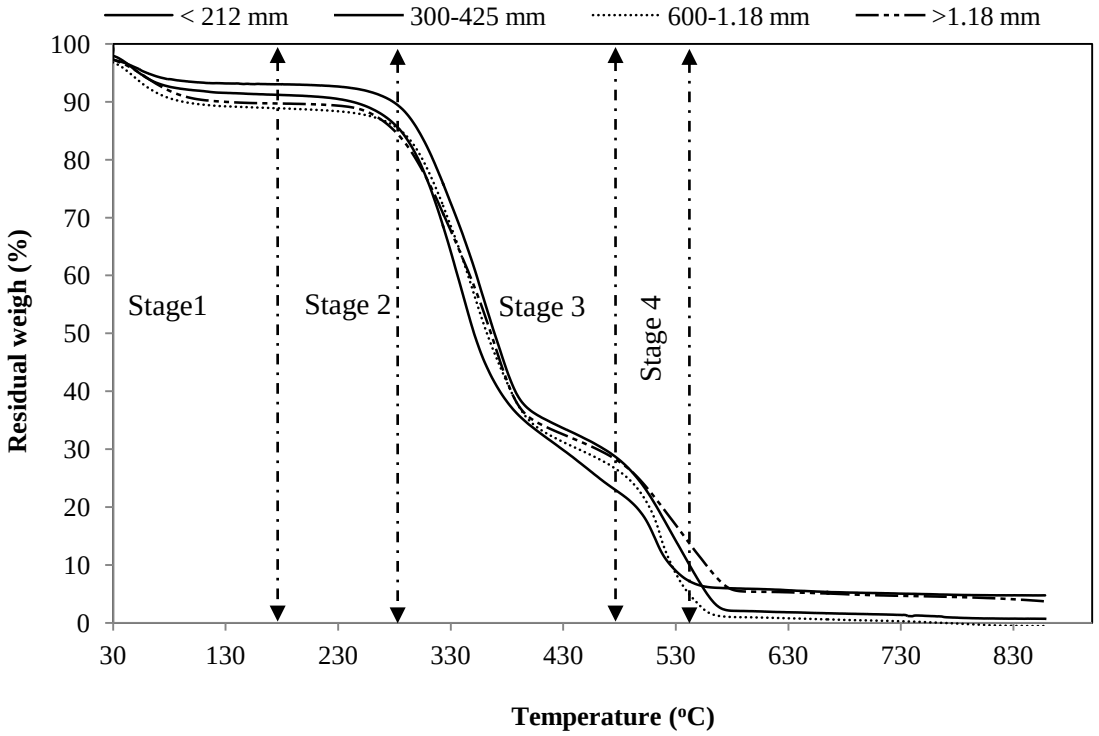

Figure 5.17: Thermal degradation characteristics of OPF at different particle sizes

5.2 Gasification Analysis

This section presents the results of experiments which performed on gasification performance of OPF using air as an oxidant (gasification agent). Tables B.1 to B.7 (Appendix B) summarize the experimental conditions. For all the gasification conditions, the gasification performance was investigated in terms of temperature profile, gas quality (gas composition and gas heating value) and other performance parameters such as gas production yield, carbon conversion efficiency and cold gas efficiency. Additionally, the accumulated char-ash and condensate materials were also measured. In the first series of experiments, gasification test was conducted to

investigate the effects of air equivalence ratio. Five levels of air equivalence ratios (0.18, 0.22, 0.29, 0.35 and 0.4) were used in this study. The second and third series of experiments were performed to establish the effect of OPF moisture content and particle size, respectively. However, five levels of OPF moisture content (0%, 15%, 30%, 40% and 60%) and five particle size in the range of 5 mm to larger than 250 mm were used in this study. In the fourth series, experiments were carried out to investigate the impact of air location on the gasification of OPF. Finally, gasification experiments were conducted to examine the effect of secondary air injection on the gasification of OPF. The experiments were performed to investigate the effect of both the injection position and ratio of the secondary air. However, consideration is given to the improvement in gas quality and tar reduction.

5.2.1 Analysis of Preliminary Data

The aims of preliminary experiments were to demonstrate the feasibility of the overall experimental approach, to figure out if a newly built fixed-bed updraft gasifier does what it is meant to do, and to get information for modifying experimental procedure as well as to determine the practical range of air flow rate that needed for the updraft gasification of OPF. The gasification tests were carried out at five level of air flow rate in the range of 12 to 18 m^3/h, while the gasification performance was investigated in terms of temperature profile, fuel consumption rate and specific gasification rate as well as the combustibility and suitability of the produced gas.

For all the tests, the air was supplied to the gasifier through two points at about 10 cm below the grate and its rate was measured by the flowmeters (Dwyer VFC Flowmeter). The gasifier temperature was measured every 30 seconds at five locations above the grate using Type-K thermocouples probes. However, the temperature was measured at 10, 30, 50, 70 and 90 cm above the grate. The thermocouples have a temperature range from 0^oC to 1200^oC. All thermocouples were connected to the data logger (USB TC-08) which is connected to the computer.

In the case of air flow rate of 12 m^3/h, there was no gas produced from the gasifier, this attributed to the fact that at a very low flow rate of air (deficient oxygen)

would result in incomplete combustion of the fuel and process would behaved like pyrolysis and produced high amount of char and tar; therefore, this experiment was excluded from the discussions. For other cases, after 10 to 15 minutes from starting the experiment, the producer gas started to be produced and the gas was fired in the three flare points (after the gasifier, after the cyclone and after the accumulation tank) to confirm its combustibility and it was found that the temperature of the flared gas was in the range of 286-470^{o}C.

The variation of gasifier temperatures at different air flow rates were presented in Figures 5.19 to 5.22. It was also observed that after 15 minutes from starting the experiment a constant temperature with an average value in range of 800 to 1007^{o}C was recorded at T_1 indicating that the fuel in this region was undergoing oxidation process. The reactions in this zone are highly exothermic producing large amount of heat energy that required for other endothermic gasification processes. Another observation was that the temperatures at T_4 and T_5 are almost the same at a value of 130–200^{o}C indicating that the fuel in these regions was undergoing drying process. The average temperatures at T_2 and T_3 were ranged between440–690 and 200–360^{o}C, respectively, indicating that these regions represented the reduction and pyrolysis zone, respectively.

The fuel consumption rate was varied between 9 to 14 kg/h, the consumption rate was lowest with air flow rate of 14.4 m^3/h, and highest with air flow rate of 16.8 m^3/h. Specific gasification rate (SGR) is defined as the amount of fuel that can be gasified per sq. m grate area per hour, and it was reported that the specific gasification rate for an updraft fixed bed gasifier ranged between 100–200 kg/h m^2. It was observed that the specific gasification rate of OPF in an updraft fixed bed gasifier was varied between 100 – 156 kg/h m^2, however the reported specific gasification rate of OPF was fall within that reported in the literature [84].

The newly built fixed-bed updraft gasifier gasifier was found to be suitable for gasification of OPF to produce a synthetic gas that can be used for thermal applications. The gasifier was modified by adding more three ports for the injection the secondary air. Those ports were located at the middle of combustion, reduction and pyrolysis zone. However, they were located at 10, 37.5 and 62.5 cm above the

grate.

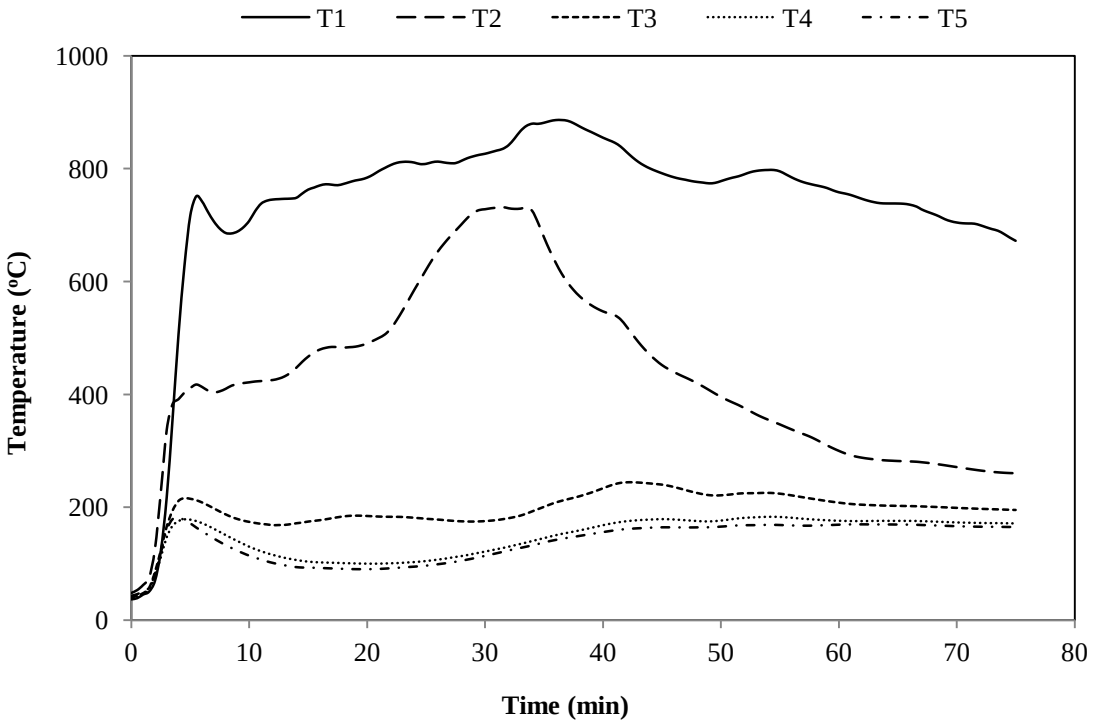

Figure 5.18: Temperature profile inside the gasifier at flow rate of 12 m^3/h

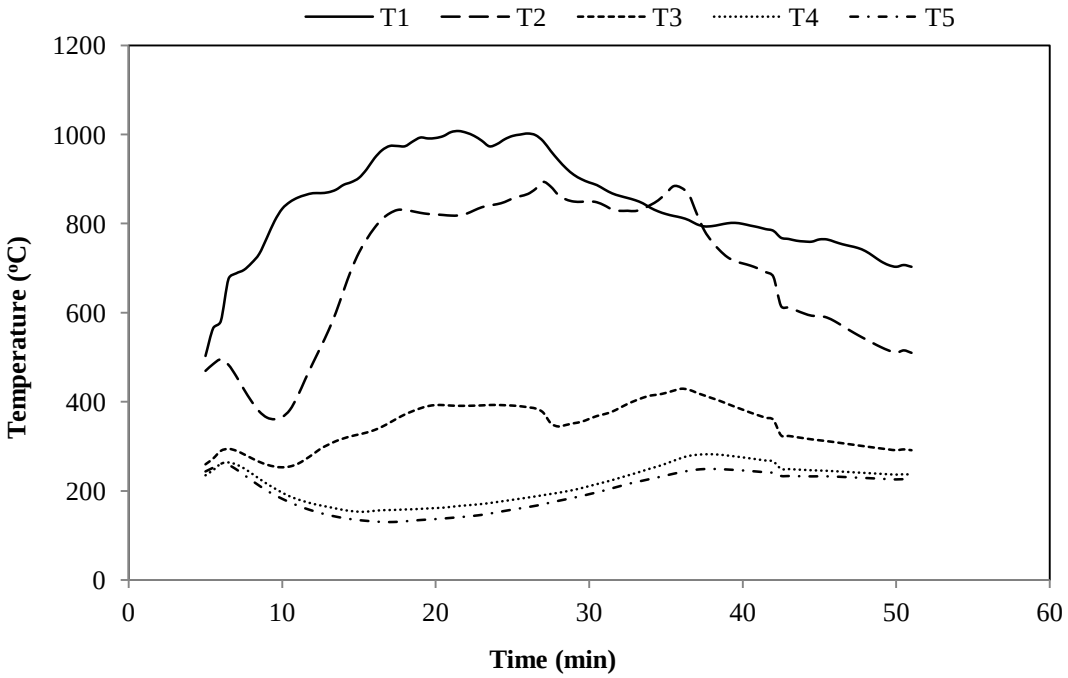

Figure 5.19: Temperature profile inside the gasifier at flow rate of 14.4 m^3/h

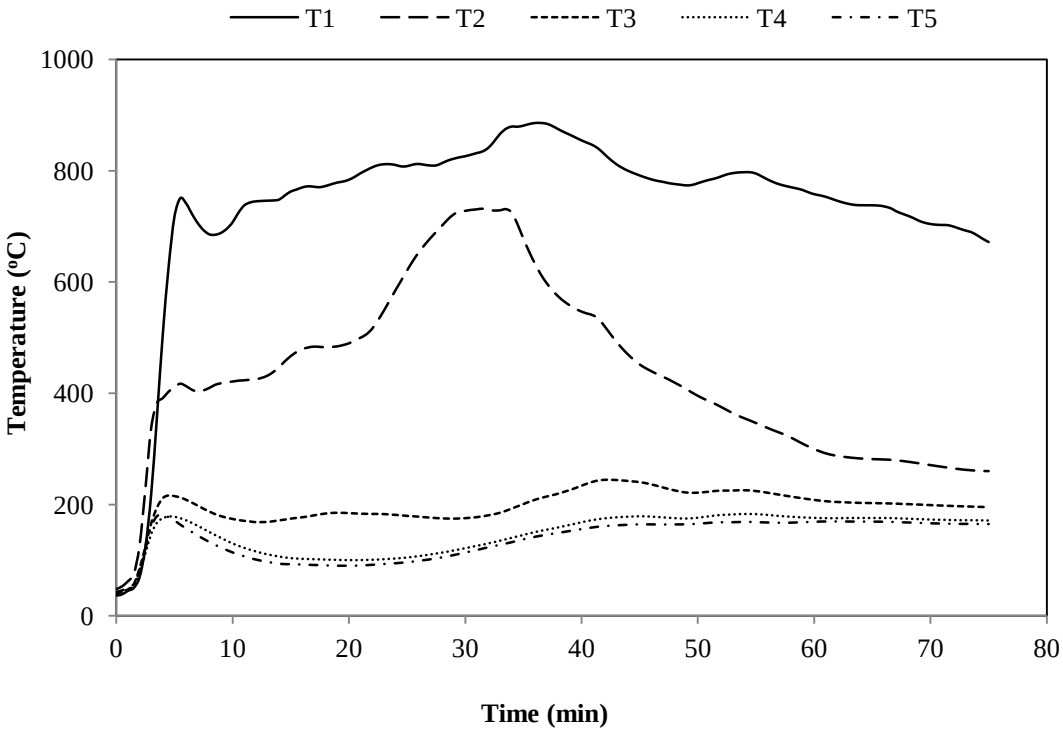

Figure 5.20: Temperature profile inside the gasifier at flow rate of 16.8 m^3/h

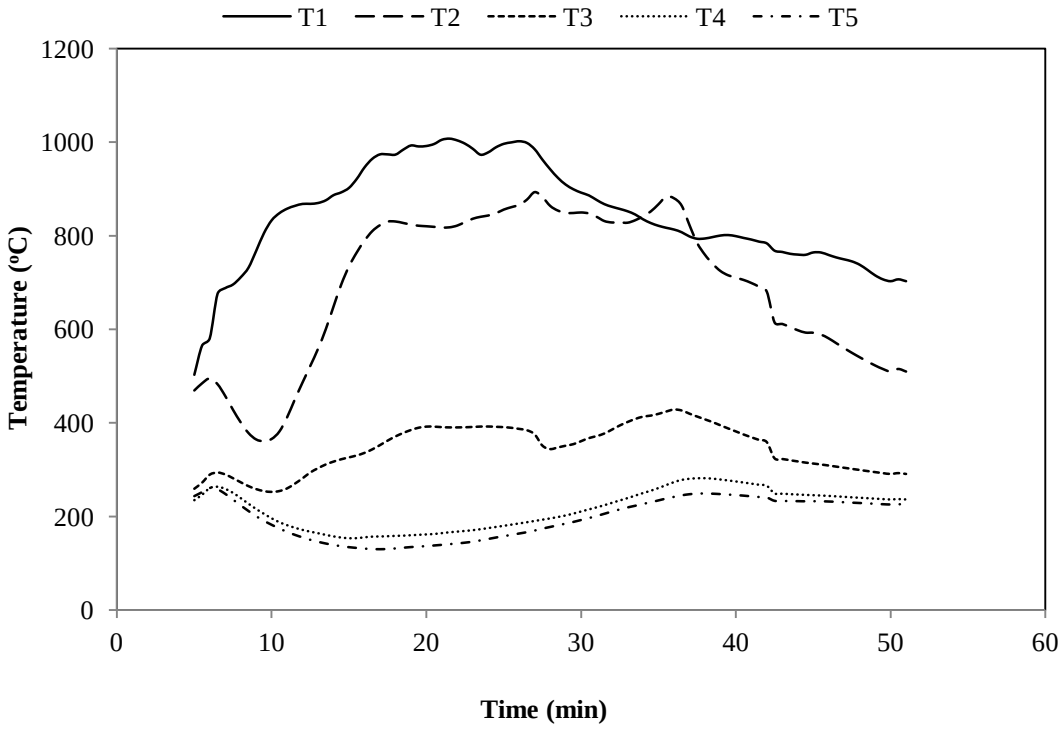

Figure 5.21: Temperature profile inside the gasifier at flow rate of 18 m^3/h

5.2.2 Influence of Equivalence Ratio (*ER*)

The equivalence ratio reflects the combined effect of the flow rate of air, OPF feedstock and duration of the test. The equivalence ratio for this study was calculated using Eq. 4.22. The equivalence ratio was found to be in the range of 0.18 – 0.4. Table 5.12 summarizes the gasification performance with the employed equivalence ratio.

Table 5.12: Experimental results of different equivalence ratios

Measured parameters	Equivalence Ratio				
	0.18	0.22	0.29	0.35	0.4
CO (vol. %)	17.73	21.09	23.10	20.20	14.17
CO_2 (vol. %)	13.97	12.27	10.41	10.70	18.87
CH_4 (vol. %)	1.36	1.47	1.20	0.91	0.29
H_2 (vol. %)	5.50	6.54	6.66	5.79	2.33
N_2 (vol. %)	61.44	58.63	58.63	62.40	64.34
Combustible gas (CO, H_2 and CH_4)	24.59	29.10	30.96	26.90	16.79
Syngas (CO+H_2)	23.23	27.63	29.76	25.99	16.50
CO/CO_2 (%)	1.27	1.72	2.22	1.89	0.75
H_2/CO (%)	0.31	0.31	0.30	0.30	0.16
CH_4/H_2 (%)	0.25	0.22	0.18	0.16	0.12
Calorific value (MJ/Nm^3)	3.48	4.09	4.26	3.65	2.20
Fuel gas production (Nm^3/kg)	1.12	1.90	2.02	2.07	2.04
Carbon conversion rate (%)	48.31	86.13	94.24	83.03	65.54
Cold gas efficiency (%)	23.08	45.80	50.56	44.61	27.01
Tar and condensate (g/Nm^3)	28.35	19.10	13.61	12.62	9.84
Char and ash	1.88	1.07	0.48	0.61	0.64

5.2.2.1 Temperature Profile

The temperature profile inside the gasifier was measured at every 30 seconds by a set of thermocouples located at different heights in the gasifier. T_1 is measured at 10 cm, T_2 at 30 cm, T_3 at 50 cm and T_4 at 70 cm above the grate. As found in the preliminary experiments (Figures 5.18 to 5.21), the location of these thermocouples represents the

temperature profile for the updraft gasification of OPF. Temperatures at T_1, T_2, T_3 and T_4 represent the oxidation, reduction, pyrolysis and drying zone, respectively. Typical plots of variation of temperatures inside the gasifier with time, as recorded using the four thermocouple points are shown in Figure 5.22.

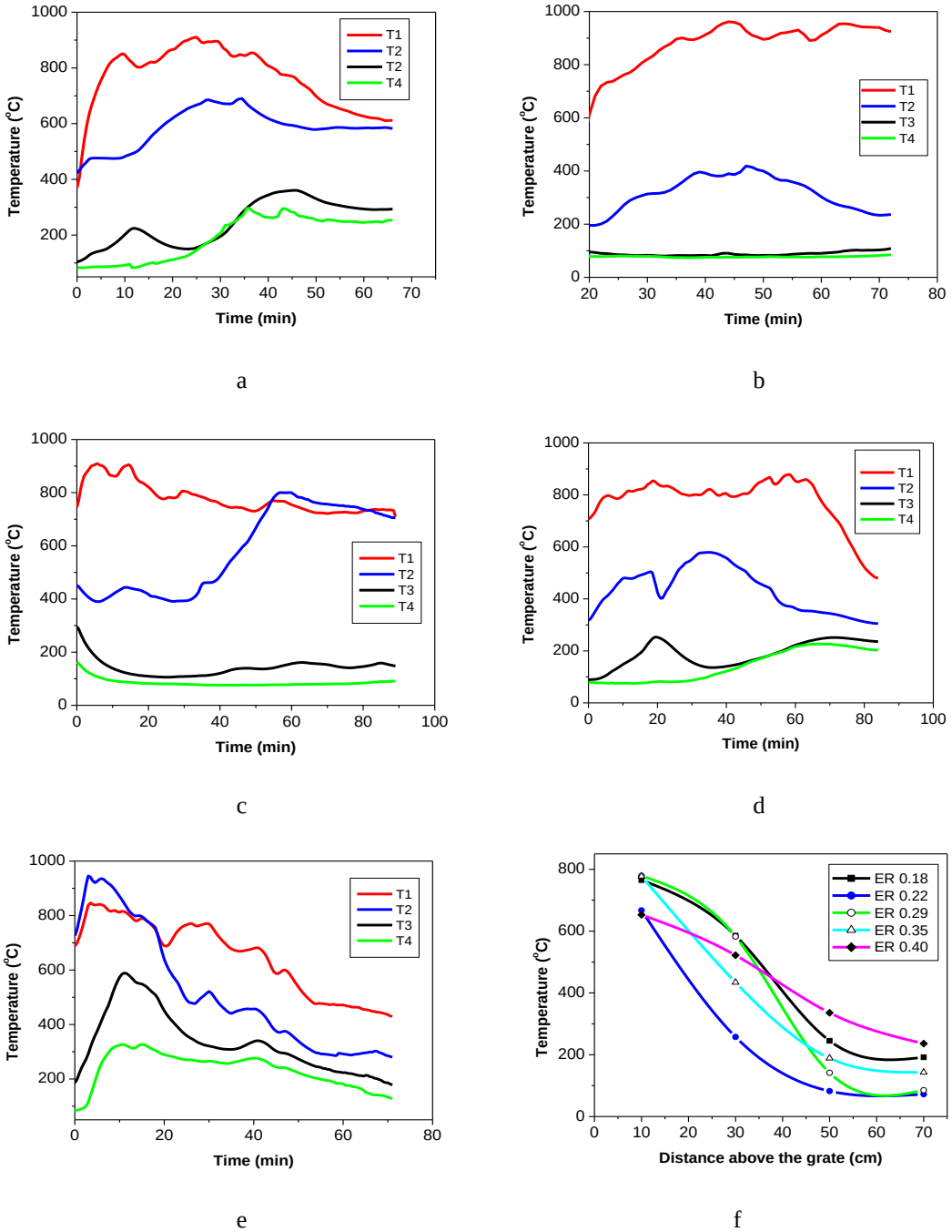

Figure 5.22: Temperature profile during operation time for a. ER 0.18 b. ER 0.22 c. ER 0.29 d. ER 0.35 e. ER 0.4 and f. Average temperature profile along the gasifier axis for several ERs

It was observed that the temperature profiles near the grate (T_1) showed a temperature range of between 700^{o}C and 950^{o}C, indicating that this region was undergoing oxidation process. Heterogeneous oxidation reactions (char with oxygen in air) occurred in this region to produce the heat required for gasification process.

It was also observed that an increase in the equivalence ratio from 0.18 to 0.35 resulted in an increase in the average oxidation zone temperature, while further increase in the equivalence ratio provided more nitrogen which acted as a heat carrier. The lower oxidation zone temperature and higher temperature of the other zones compare to other equivalence ratios could be observed as shown in Figure 5.22 (e and f). Rowland [107] showed that at high air flow rate (above 0.23 m^3/min) the temperature in the oxidation zone may raise and fall rapidly due to the turbulence in the gasifier, and as a result, a non-steady state condition could be obtained. The temperatures at the top of the gasifier, 70 cm above the grate (T_4) were lower than 200^{o}C, *i.e*. the feedstock was undergoing drying process. Above the combustion zone and below the drying zone were the reduction and pyrolysis zones, where the temperatures were lower than that of combustion zone, due to the fact that the most endothermic reactions occurred there.

5.2.2.2 Gas Production Yield (Y_{gas})

The evaluation behavior of gas yield produced from the gasification of OPF is also shown in Table 5.12, which shows the effect of the equivalence ratio on the fuel gas yield per unit of biomass (Nm^3/kg). It is shown that the gas yield increased with the equivalence ratio of up to 0.35, and then decreased a little bit with further increase in equivalence ratio. This was due to fact that an increase in equivalence ratio resulted in the increases of temperature; therefore it enhances the conversion of the solid fuel into gaseous fuel. Moreover, a higher equivalence ratio signifies the air flow rate for specific biomass consumption.

The gasification of OPF at an optimum equivalence ratio (highest heating value) produced gas yield of 2.02 Nm^3/kg which was higher (by around 19.5%) than the theoretical gas yield of 1.64 Nm^3/kg calculated using Eq. 5.8. The lowest value of

equivalence ratio (0.18) produced gas yield of 1.12 Nm^3/kg, which was less than the theoretical value by about 32%. A reasonable explanation is that as the equivalence ratio was decreased, less OPF fuel was converted to gaseous fuel and instead, it remained as char residue.

$$CH_{1.28}O_{0.92} + 0.04O_2 \rightarrow CO + 0.64H_2 \quad (5.8)$$

5.2.2.3 Gas Composition and Higher Heating Value

The producer gas was analyzed online at a five-minute interval during the experiment run, by using X-STREAM gas analyzer to determine its composition. The gas analyzer was used to analyze four gases of the producer gas; these gases were CO, CO_2, CH_4 and H_2, while N_2 could be calculated by the difference from the total volume. Figure 5.23 shows the profile of syngas composition during the gasification operation for equivalence ratio in the range of 0.18 – 0.40. Figure 5.24 presents the average concentration of generated syngas. The syngas composition at optimum equivalence ratio of 0.29 was found to be similar to that reported by other researchers [58, 65, 84, 105] and the average compositions of gases in this work were 23.10% CO, 10.41% CO_2, 1.20% CH_4 and 6.66% H_2. The remaining gases were mostly nitrogen originated from air.

It can be seen in Figure 5.23 (b and c) that for equivalence ratios of 0.22 and 0.29, the syngas compositions were quite stable during the gasification operation, but unstable for the rest of the employed equivalence ratios. Table 5.12 also shows that the total amount of combustible gases (H_2, CO and CH_4) increased from 24.59 to 30.96% with increase in equivalence ratio up to 0.29 then decreased to 16.79% with further increase in equivalence ratio up to 0.4, this could be due to the fact that at low equivalence ratio the process behaved like pyrolysis and produced high amount of char and tar. At a higher equivalence ratio, more oxygen was supplied into the gasifier and hence enhanced the degree of combustion reactions that lead to improved char burning to produce CO_2 at the expense of combustible gases such as CO, H_2 and CH_4.

As expected, the N_2 content in the producer gas increased gradually with an increase in equivalence ratio. A reasonable explanation is that, as the equivalence ratio was increased (air flow rate increased) the nitrogen content increased too.

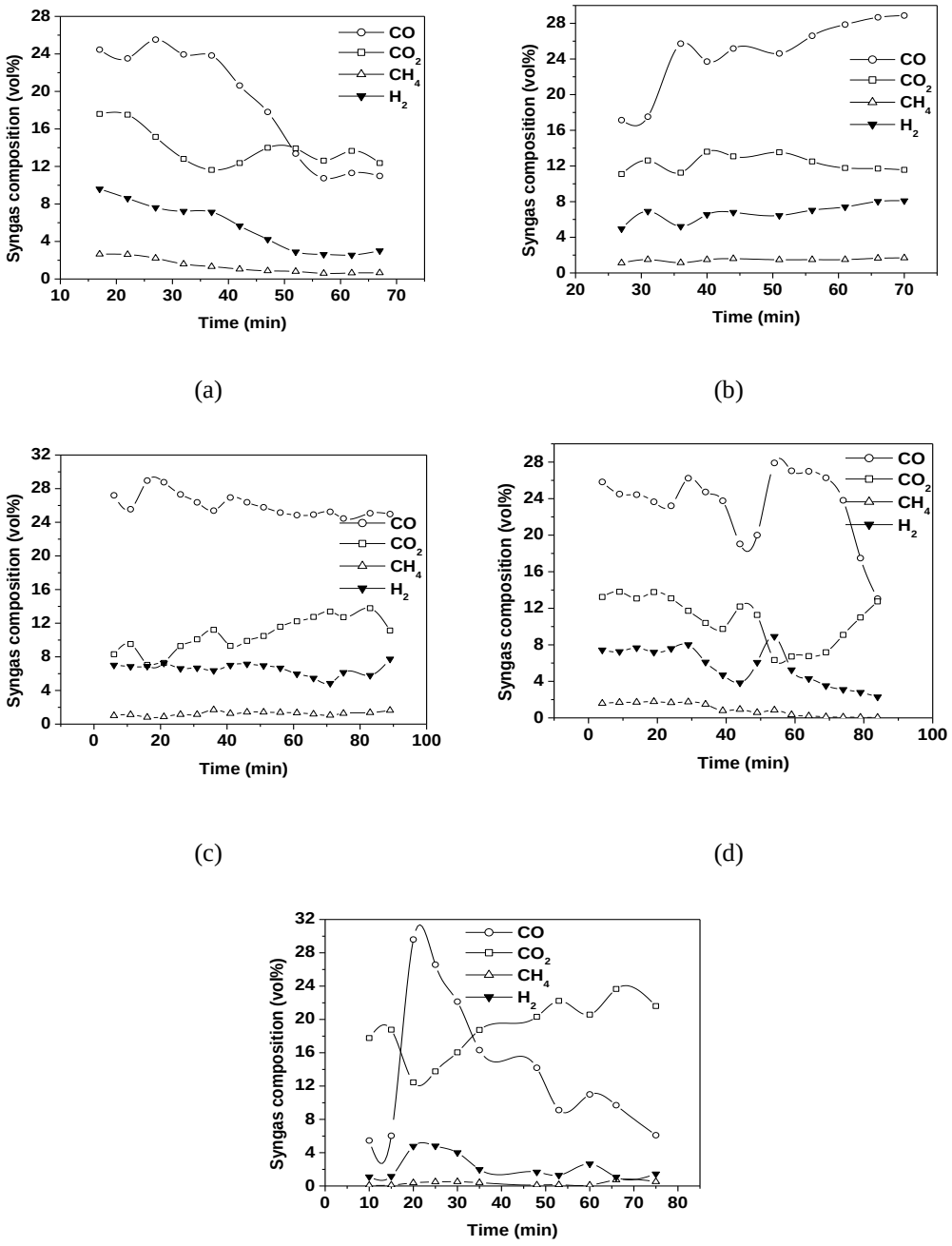

Figure 5.23: Syngas composition profiles with the elapsed time at (a) ER=0.18 (b) ER=0.22 (c) ER=0.29 (d) ER=0.35 and (e) ER=0.4

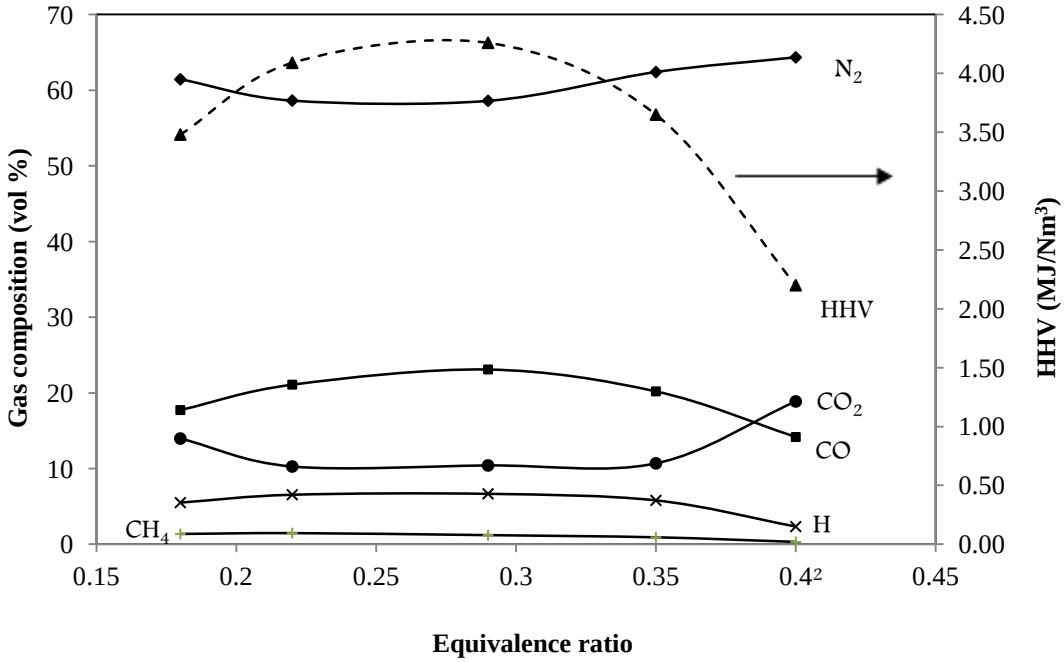

Figure 5.24: Effect of equivalence ratios on syngas composition and higher heating value

As the equivalence ratio increased from 0.18 to 0.29, the CO content in the producer gas increased from 17.73% to 23.10%, while the CO_2 content decreased from 13.97% to 10.41%. This was mainly due to the incomplete oxidation reaction ($C+0.5O_2 \rightleftharpoons CO$) and Boudouard reaction ($C+CO_2 \rightleftharpoons 2CO$). A further increase in equivalence ratio of up to 0.4 resulted in a decrease of CO to 14.17%, whereas the CO_2 content increased up to 18.87% following an opposite trend. This was due to the fact that a further increase in O_2 promoted the oxidation reactions ($C+O_2 \rightleftharpoons CO_2$) and ($CO+0.5O_2 \rightleftharpoons CO_2$), and enhance the oxidation of the produced CH_4 content ($CH_4+O_2 \rightleftharpoons CO_2+H_2O$). Therefore, leading to an increase in the CO_2 content and a decrease in CO content.

When the equivalence ratio increased from 0.18 to 0.29, the H_2 content in the producer gas increased gradually from 5.5% to 6.66%, and then decreased to 2.33% for an increase in equivalence ratio up to 0.4. The CH_4 content decreased with an increase in the equivalence ratio. This may be due to the fact that, more oxygen enhancing the oxidation reaction of the produced CH_4.

The amount of syngas ($CO+H_2$) and combustible spices ($CO+H_2+CH_4$) in the producer gas are of the important parameters that define the volume of the valuable products in the product gas, characterizing its ideal product selectivity [154]. Table 5.12 shows that both syngas and combustible spices in the product gas follow the trend of CO and H_2, which are the major combustible components in the product gas.

Table 5.12 shows the change of H_2/CO, CO/CO_2 and CH_4/H_2 molar ratio in the product gas with the employed equivalence ratio. It was observed that the molar ratio of H_2/CO and CH_4/H_2 decreased from 0.3 to 0.16, and from 0.25 to 0.12, respectively, with an increase of equivalence ratio, while the molar ratio of CO/CO_2 increase from 1.27 to 2.22 as the equivalence ratio increased up to 0.35 then decreased sharply to 0.75 with equivalence ratio of 0.4. This could be attributed to the fact that less equivalence ratio favors incomplete oxidation reaction of char and Boudouard reaction, while at a higher equivalence ratio (more oxygen is available), complete oxidation reaction ($C+O_2 \rightleftharpoons CO_2$) and carbon monoxide oxidation reaction ($CO+0.5O_2 \rightleftharpoons CO_2$) take place and become stronger due to the higher quantity of oxygen. The trend of the H_2/CO of the syngas during the gasification operation time with equivalence ratio is illustrated in Figure 5.25. It can be seen that the average value of H_2/CO varied from 0.3 to 0.16, which is reasonable for air gasification. It can be concluded that it is preferable to run the gasifier at equivalence ratio in the range of 0.22 – 0.29 in order to obtain smooth operation for the equipment that uses the produced synthesis gas.

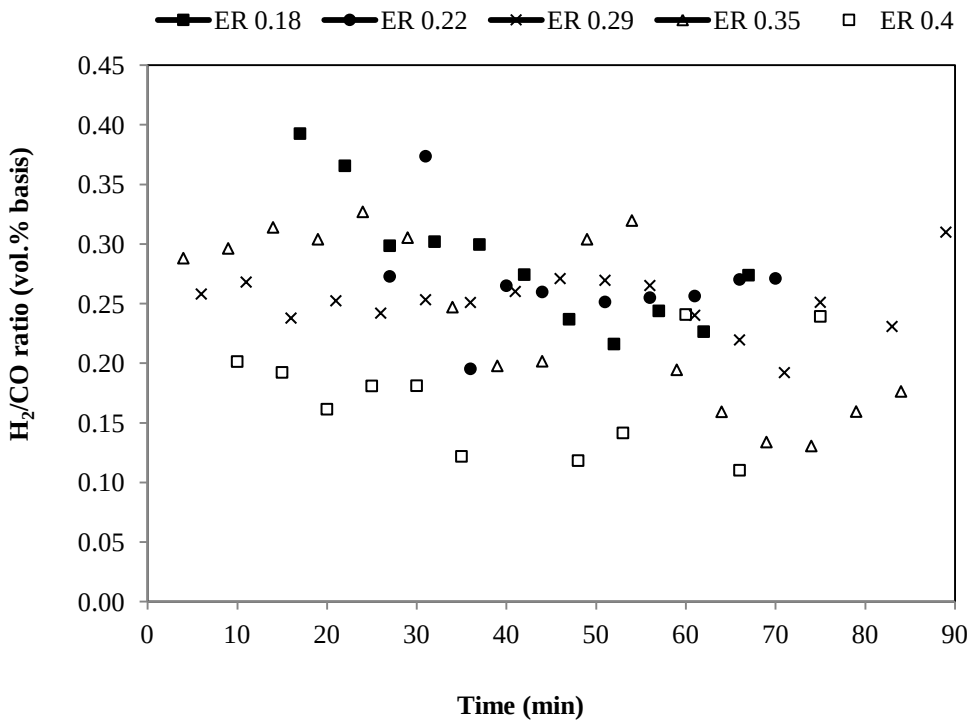

Figure 5.25: Profile of molar ratio of H_2/CO with time at different equivalence ratio

The higher heating value (HHV) of the producer gas was determined considering the volumetric percentage of the gas constitutes (CO, H_2 and CH_4). Figure 5.24 shows the effect of equivalence ratios on the HHV of the producer gas. The HHV of the gas increased with the equivalence ratio up to a peak value of 0.29. This was due to the increase in CO and H_2, and then started to decrease, which was caused due to the consumption of CO, H_2 and CH_4. On the other hand, increasing the equivalence ratio meant more O_2 was available for gasification which increased the gasification temperature. Hence, accelerating the gasification process and improving the gas quality. Further increase in the equivalence ratio provided more N_2 with air and diluted the producer gas, which degraded the gas quality [155]. Furthermore, it was also known that more O_2 drives the gasification reactions towards oxidation reactions; however, more CO_2 and lower amount of combustible gases will be produced.

It is also shown in Figure 5.24; the heating value of the producer gas was in the range of 2.30 – 4.26 MJ/Nm^3. The heating value of 4.09 – 4.26 MJ/Nm^3 was obtained for the equivalence ratio of 0.22 – 0.29 appeared to be at the range reported in the

literature [87, 96, 105] for air gasification of several types of biomass fuels in updraft gasifiers.

5.2.2.4 Carbon Conversion Efficiency and Gasification Efficiency

The influence of the equivalence ratio on the carbon conversion efficiency (CCE) is shown in Figure 5.26. It is reported that the carbon conversion efficiency was strongly influenced by the equivalence ratio, with an increase in the equivalence ratio from 0.18 to 0.4, the carbon conversion efficiency increased from 48.31 to 94.25% as the equivalence ratio increased up to 0.29, and then decrease to 65.54% for a further increase in equivalence ratio. It was also observed that the carbon conversion depended upon the gas yield and the volumetric percentage of CO, CO_2 and CH_4 in the producer gas. It can be seen that the carbon conversion efficiency had the same trend as that of the gas yield. However, the effect of the gas yield on the carbon conversion efficiency was stronger than the effect of the volumetric percentage of CO, CO_2 and CH_4 in the producer gas.

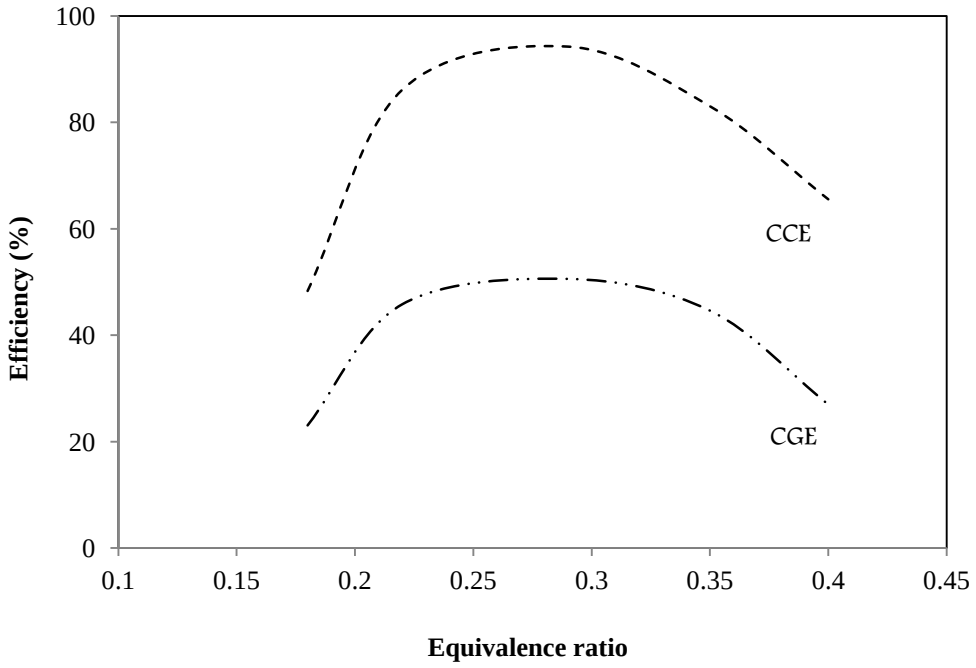

Figure 5.26: Effect of equivalence ratios on cold gas efficiency and carbon conversion efficiency

The influence of the equivalence ratio on cold gas efficiency (CGE) is also shown in Figure 5.26. As mentioned previously, the amount of gas yield has a peak value of 2.07 Nm^3/kg at an equivalence ratio of 0.35, which is almost equal to the value of the gas yield at an equivalence ratio 0.29 (2.02 Nm^3/kg), while the gas heating value increased up to a peak value at the equivalence ratio of 0.29 and decreased thereafter. It was observed that the cold gas efficiency had the same trend as that of the heating value. The maximum cold gas efficiency was 50.56% which was observed at the optimum equivalence ratio of 0.29.

5.2.2.5 Tar and Condensate Yield

Figure 5.27 shows the influence of the equivalence ratio on tar and condensate generation. It was observed that an increase in the equivalence ratio led to a decrease in tar yield. This can be attributed to the fact that as the equivalence ratio increased, more oxygen was available for cracking the residual species; therefore, the tar cracking was more effective. A similar study [156] using a coir pith and circulating fluidized bed gasifier reported a decrease of tar yield from 11 to 7.8 g/Nm^3 as the equivalence ratio increased from 0.18 to 0.31. Observation from the present study revealed a value of 13.61 g/Nm^3 at the optimum equivalence ratio.

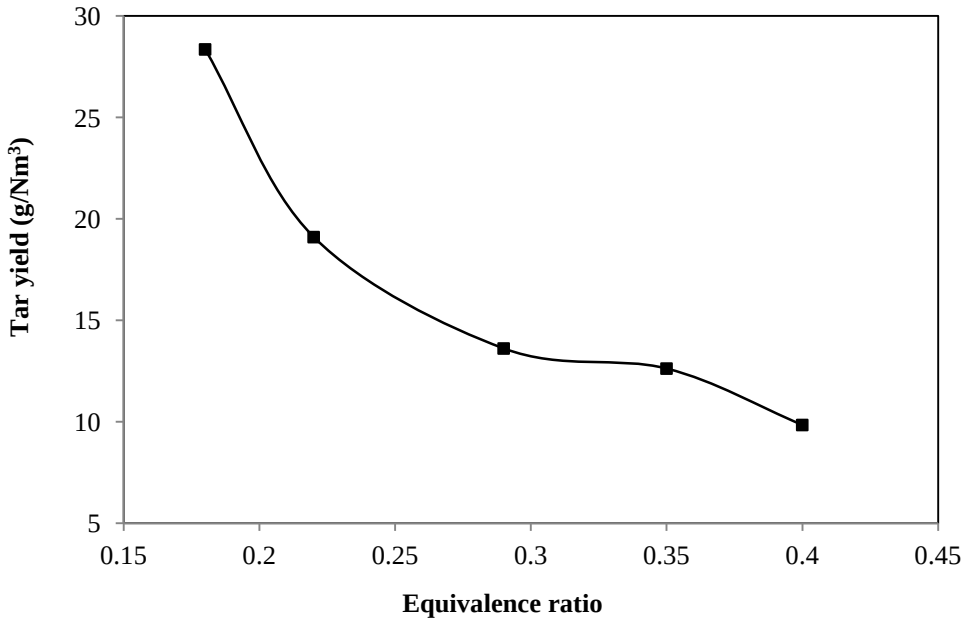

Figure 5.27: Effect of equivalence ratio on tar production yield

5.2.3 Influence of Moisture Content

Shown in Table B.2 (Appendix B) are the results summary of the second series of gasification experiments, in which the effects of OPF moisture content on gasification performance behavior have been studied. Figures 5.28 and 5.29 show the effect of moisture content on producer gas yield, volume fraction of the producer gas, higher heating value, carbon conversion efficiency and cold gas efficiency. In this work, the actual moisture content of OPF material was varied from 0% to 60% (wet basis). The variation in temperature profile during the gasification process related to the variation of OPF moisture content are shown in Figures B.1 to B.5, while the difference in synthetic gas composition profiles related to the variation in OPF moisture content are shown in Figures B.6 to B.10 (Appendix B). All the gasification experiments in this section were carried out at the same value of air flow rate of 16.8 m^3/h.

It was observed that OPF with high moisture content (about 60%) was difficult to be ignited and the temperatures (reaction temperatures) inside the gasifier were very low and not sustained at the same value during the whole experiment period (non-steady state temperature) as shown in Figure B.5. Another observation was that the gas produced from the gasification of OPF with high moisture content was not combustible any more. This might be attributed to the high amount of non-combustible gases in the synthetic gas (12.5% CO_2 and 72.63% N_2) correspondingly to 14.87% of the combustible gases (CO, H_2 and CH_4) as shown in Table B.2. Generally, as shown in the Figures B.1 to B.5, the temperature inside the gasifier decrease with an increase in moisture content, due to the fact that evaporation of the moisture content from the OPF consumes a lot of energy which would otherwise be used for the other gasification processes (drying, pyrolysis and reduction). The consequence is a reduction in gasification efficiency, carbon conversion efficiency and fuel consumption rate.

Effects of OPF moisture content on the constituents of gas product and gasifier performance behavior are studied by gasification of five samples of OPF with different moisture content (0, 15, 30, 40, and 60%) and the results are shown in Table B.2 and Figures 5.28 and 5.29. As discussed earlier, gasifier temperature plays the dominant role in controlling the formation of the constituents of the product gas.

However, a lower temperature inside the gasifier results in a decrease in the rate of endothermic reactions between carbon dioxide and char (Boudouard reaction), and between water vapor and char (water gas reaction). Moreover, decreasing the gasifier temperature as a result of increasing the OPF moisture content enhances the reaction rate of the exothermic reaction of water-gas shift reaction. Thus, the above scenario is a reasonable explanation why the increasing of OPF moisture content results in decreasing CO and increasing CO_2, char and water in the producer gas as shown in Table B.2. However, as illustrated in Figure 5.28 increasing OPF moisture content from 0 to 40% wet basis resulted in an increase in CO_2 and H_2 from 9.3 to 13.1% and from 6.22 to 6.42%, respectively, whereas the CO decreased from 25.4 to 15.4%. The percentages of CH_4 remained almost constant in small volume in the range of 1.11 to 0.92% for all OPF moisture content.

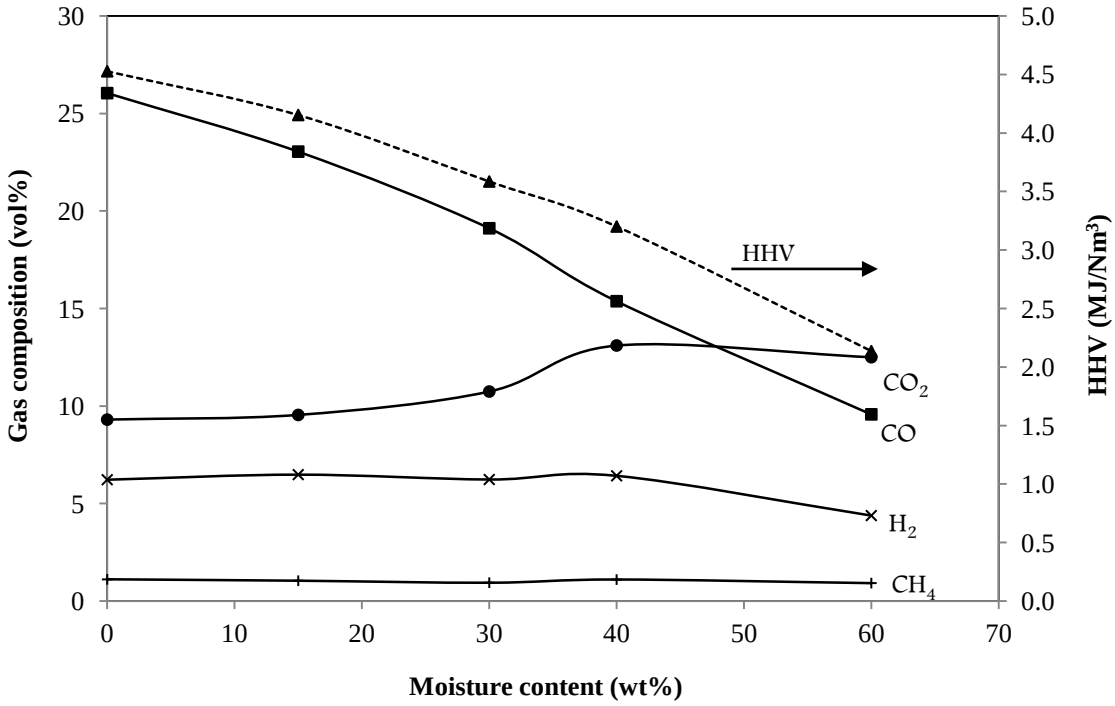

Figure 5.28: Effect of OPF moisture content on gas composition and heating value

It was also observed that the higher heating value of the producer gas decreased with an increase of OPF moisture content. This can be attributed to the lower amount of CO in the producer gas with an increase of moisture content. Although the CH_4 in the producer gas remained constant and in small volume with an increase in OPF moisture content, the decrease in CO is more pronounced compare to the increase in

H_2 with the same change in moisture content. However, the CO content decreased by about 39.5% whereas the H_2 content increase by about 3.2% for an increase in moisture content from 0 to 40%. This is why the higher heating value of the producer gas followed the trend of CO as shown in Figure 5.28. Moreover, as shown in Figure 5.30 the carbon conversion efficiency and cold gas efficiency decreased from 99.21 to 88.77% and from 58.2 to 44.86%, respectively as the moisture content of OPF increased from 0 to 40%. This is due to the fact that most of the energy (heat) being used for evaporating the moisture content rather than to be used for gasification processes.

As expected, the increase in the moisture content in the OPF increase both tar-condensate and char-ash residues (Table B.2). The increasing of tar-condensate might be due low reaction temperatures inside the gasifier as a result of high moisture content in OPF, as the low reaction temperatures in the pyrolysis zone is not favorable for tar cracking. The increasing of char-ash as a result of increasing moisture content in the OPF might be due to the decrease of carbon conversion rate.

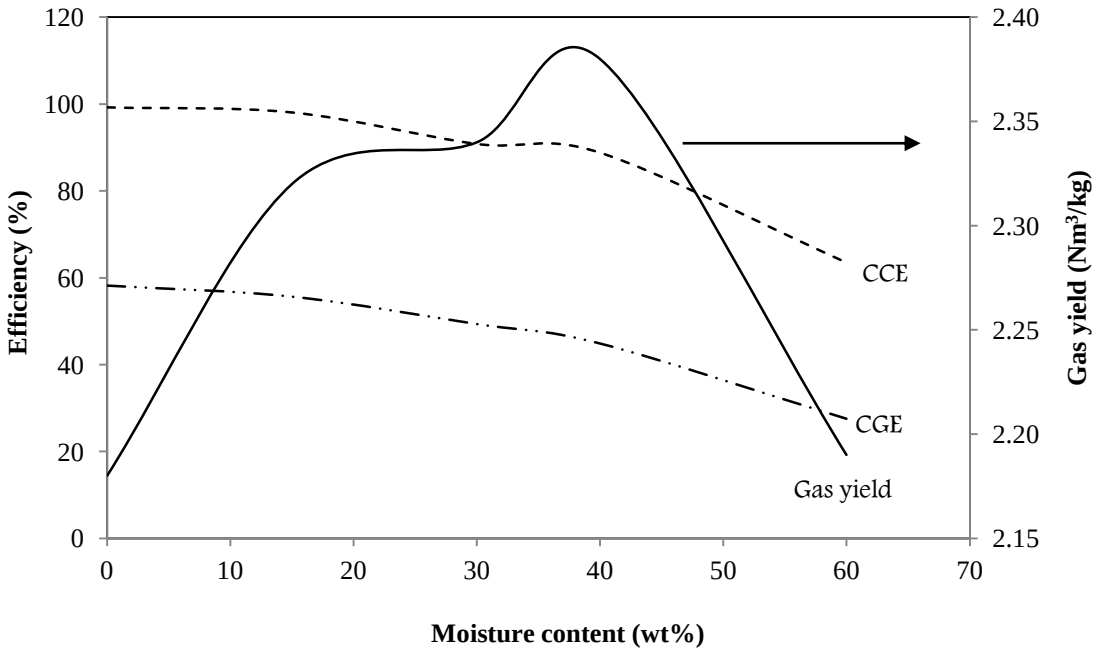

Figure 5.29: Effect of OPF moisture content on cold gas efficiency, carbon conversion efficiency and gas yield

5.2.4 Influence of Particle Size

The third series of gasification experiment was performed to establish the effect of biomass particle size on the gasification of OPF. In this research, the experiments were conducted by using five size ranges of biomass particles (<5, 13-25, 38-50, 64-90, >250 mm) while the other conditions were kept constant. Figure 5.30 shows the different particle sizes that were used in these experiments. The experiment results are presented in Table B.3, while the variation in temperature profile and synthetic gas composition profiles related to the difference in OPF particle size are shown in Figures B.11 to B.20 (Appendix B).

Figure 5.30: OPF particle size (a) <5mm (b) 13-25mm (c) 38-50 mm (d) 64-90 mm (e) >250 mm

Most of the gasification parameters (dry gas yield, calorific value, CGE *etc*.) increased as the particle size increased from <5 mm to 13-25 mm, then started to decrease for the larger particles. This was due to the fact that, with the smallest particle size (<5 mm) that seem like sawdust contain a lot of fibers which may cause a bridging that leads to the reduction in H_2 and CO and an increase in CO_2 of the synthetic gas due to combustion of some of the gas generated, thus resulting in low calorific value and gasification efficiency. On the other hand, smaller particles may clog the available air voidage, and then increase the pressure drop inside the gasifier which may affect the gasification performance negatively and sometimes lead to shutdown the gasifier. Therefore, the explanation in this section should include the particle size in the range of 13-25 to larger than 250 mm

Figure 5.32 illustrates the influence of biomass particle size on gas production yield. Shown in the same figure is that, as the particle size varied from below 5 mm to larger than 250 mm, the gas yield increased gradually from 1.72 to 2.08 Nm^3/kg, then declined to 1.35 Nm^3/kg. The maximum gas yield of 2.08 Nm^3/kg was obtained at the particle size of 13-25 mm, thereafter the gas yield decreased as the OPF particle size increased, while char-ash and condensate yields increased with an increasing in OPF particle size. A possible explanation for this occurrence is that with smaller particle sizes (which is related to a higher surface area per unit mass) the gasification processes are under kinetic control and therefore, more effective mass and heat transfer reached in the particles (lower diffusion resistance coefficient) and thus allows the reaction to take place through the whole particles rather than just through the surface areas, which leads to improved the gas yield. Moreover, smaller particle size resulted in higher H_2 and CO and less CO_2 as illustrated in Figure 5.31, therefore resulted in an increase in gas heating value, carbon conversion efficiency and gasification efficiency as shown in Figures 5.31 and 5.32.

As shown in Figure 5.33, it can be seen that the average value of H_2/CO varied from 0.22 to 0.30, which is reasonable for air gasification. Although the particle size of 13-25 mm has a low value (0.22) of H_2/CO ratio compare to some particle sizes, but contributed the most stable ratio during the whole gasification time, with standard deviation of about ± 0.05. The same figure shows that it is preferable to run the

gasifier with particle size in the ranges of 13-25 and 38-50 mm in order to obtain smooth operation for the equipment that utilizes the produced synthesis gas.

On the other hand, larger particle size and their greater heat and mass transfer resistance causes the internal particle core temperature to become lower than the temperature at their surfaces (greater temperature gradient inside the particles), and thus results in incomplete pyrolysis. Moreover, it is more difficult for the gas produced inside the particle to diffuse out and the gasification processes are mainly under diffusion control. Therefore, a lower gas yield and higher amount of char and liquids (tar and condensate) was observed with an increase in particle sizes as shown in Table B.3.

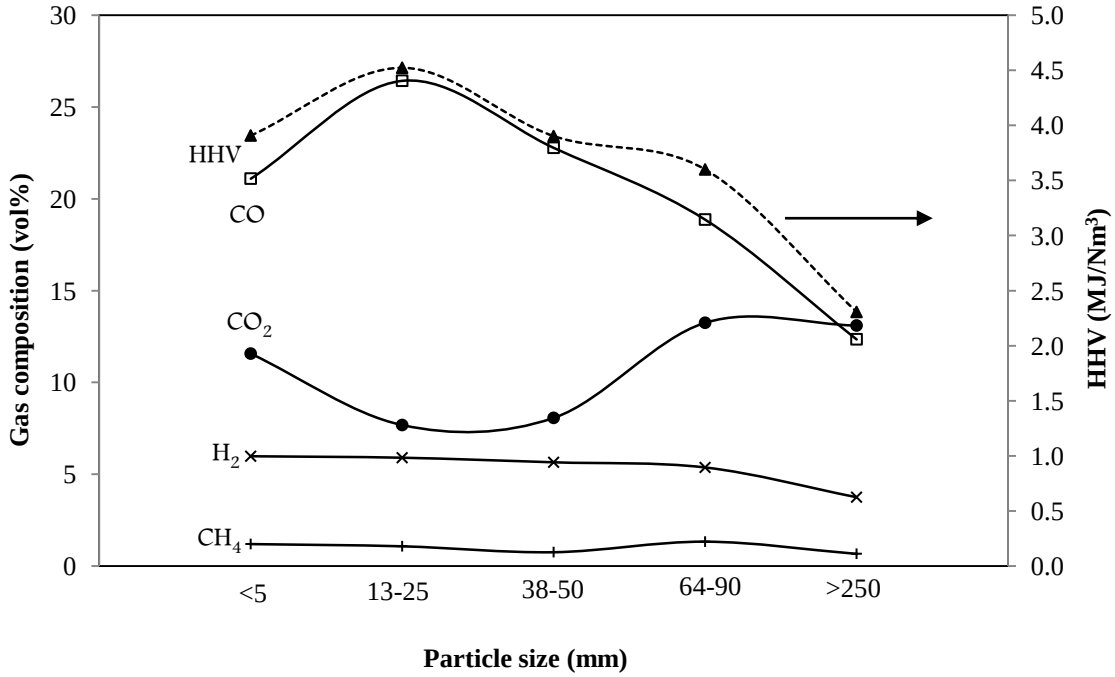

Figure 5.31: Effect of particle size on gas composition and heating value

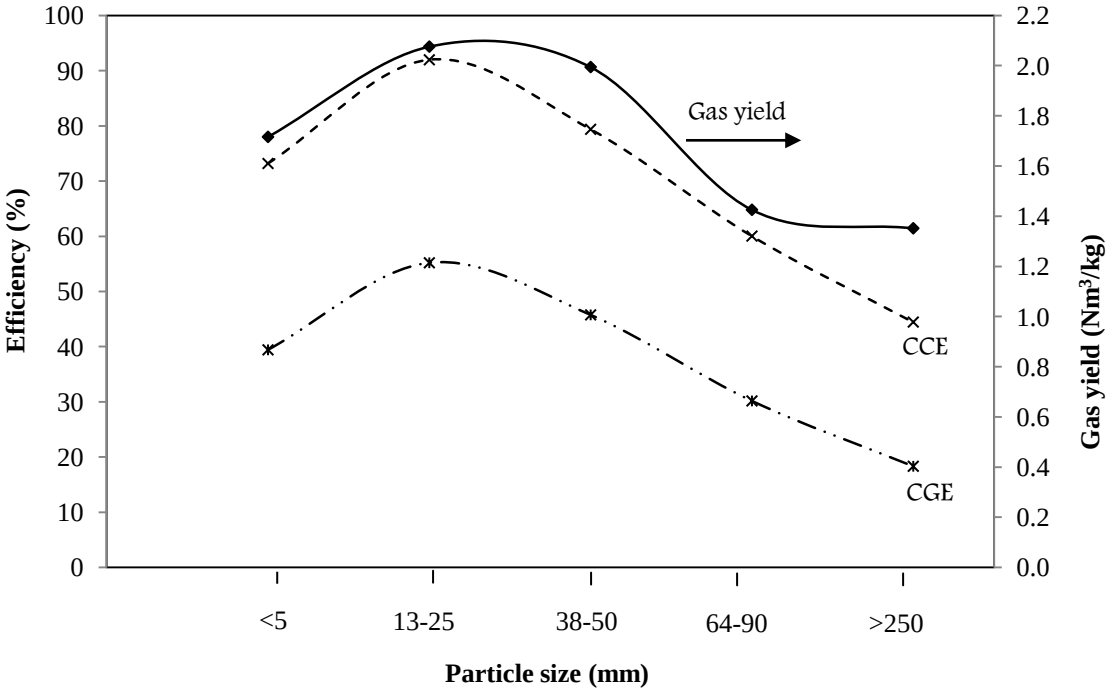

Figure 5.32: Effect of particle size on cold gas efficiency, carbom conversion efficiency and gas yield

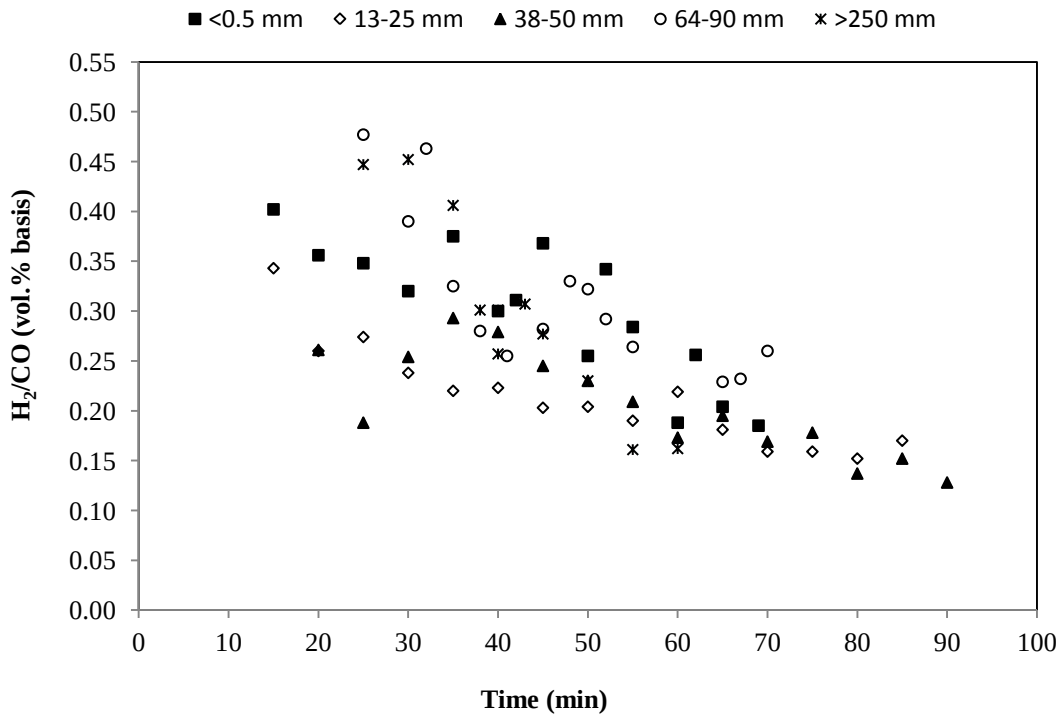

Figure 5.33: Profile of molar ratio of H_2/CO with time at different particle size

5.2.5 Influence of Gasification Air Position

As known, updraft is co-current flow gasifier, in which fuel is fed at the top of gasifier whereas the gasifying agent (*e.g* air) is taken at the bottom of the grate and diffuses up through the bed of char. The generated producer gas leaves at the top of the gasifier while ash exits through the grate and is removed from the bottom. As the fuel moves downward, it undergoes through drying, pyrolysis, reduction and combustion zones (Figure 5.34).

The current gasifier was provided with three points for feeding the gasification air, the first point was located at 10 cm below the grate, and the second point was located immediately above the grate (named, through the grate) while the last point was located at 10 cm above the grate. The aim of the innovative configuration is to investigate the effect of primary air position on gasification performance of OPF. However, initially three experiments were performed by changing the location (below, through and above) of gasifying agent, while the other conditions were kept constant. After analyzing the result, two more experiments were added to overcome the disadvantages of using single feeding point and to investigate the effects of introducing the air through two couple feeding points.

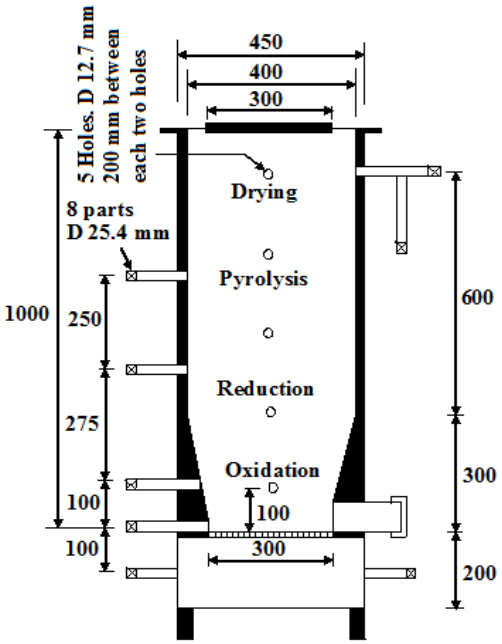

Figure 5.34: Gasification air positions in the designed gasifier

Each feed point was 25.4 mm diameter and the air was fed at the rate of 16.8 m^3/h. Therefore, the velocity of the air through the feedstock in the cases of feeding the air through the grate and above the grate was 9.21 m/sec (when using single feeding point), which was higher than the recommended value. This high velocity of air led to non-steady state temperature in the oxidation zone, and as a result, non-steady state gas product components as shown in Figures 5.35 and 5.36. Moreover, increasing the air velocity might increase the oxidation of the OPF and resulted in the high production of CO_2. On the other hand, in the case of feeding the air below the grate, the grate was used as an air distributor; however the holes in the grate were used to distribute the air across the whole grate, leading to almost uniform temperature through the axis of the gasifier as shown in Figure B.21 (Appendix B).

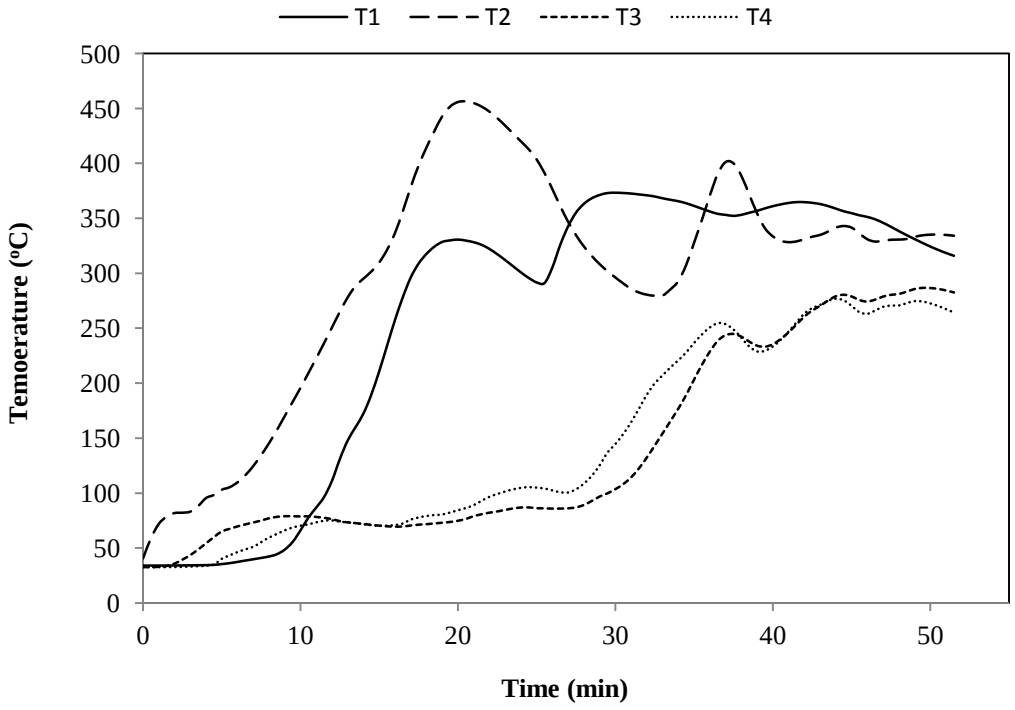

Figure 5.35: Temperature profile in the case of feeding the air through the grate

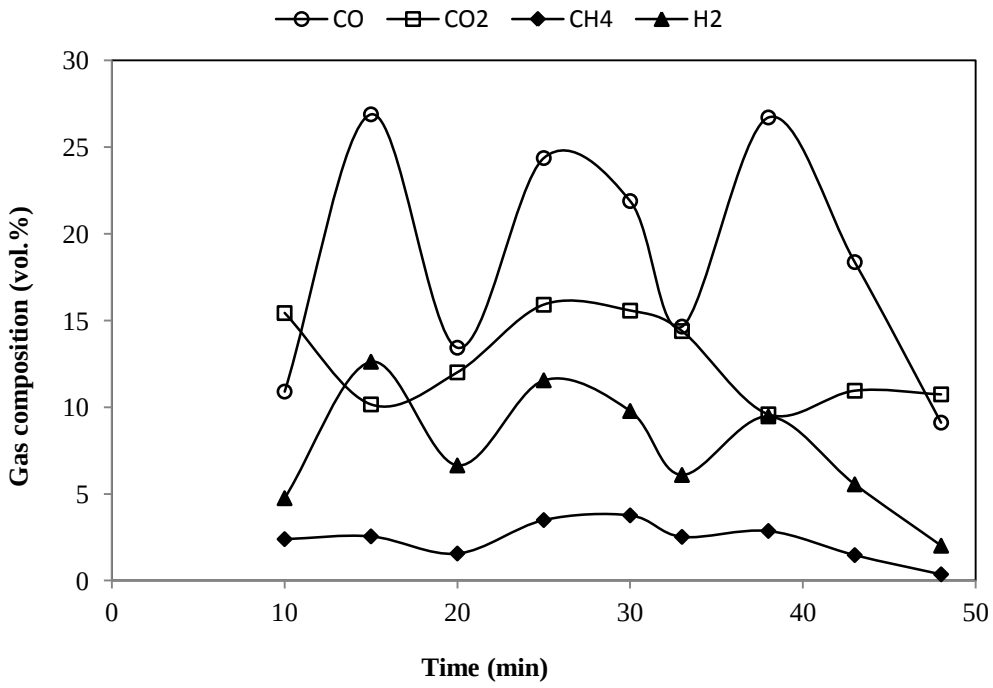

Figure 5.36: Variation of syngas composition with time in the case of feeding the air through the grate

Another disadvantage of feeding the air through and above the grate was that, it might result in higher amount of feedstock remaining as char or unreactant fuel at the end of the experiment as shown in Table 5.13. A reasonable explanation was that, due to fact that the dry OPF had low density, therefore as the gasification process was going on, the height of the fuel bed decreased, and then the high air velocity might lead the fuel to be in a turbulence state or might turn out the fire. The consequence was that the production of combustible gases might stop due to non-continues burning of the OPF fuel. This also might be a reason of why feeding the air above and through the grate resulted in non-steady state temperature along axis of the gasifier after a certain time from starting the gasification experiment.

Table 5.13: Experimental results of OPF gasification as a function of primary air position

Measured parameters	Air position				
	Case 1	Case 2	Case 3	Case 4	Case 5
CO (vol. %)	22.61	18.84	19.57	24.73	20.54
CO_2 (vol. %)	9.51	12.75	13.13	9.05	13.69
CH_4 (vol. %)	1.2	2.33	2.96	1.17	2.32
H_2 (vol. %)	6.48	7.61	8.02	7.26	8.19
N_2 (vol. %)	59.2	58.83	56.32	58.55	55.27
Combustible gas (CO, H_2 and CH_4)	30.56	30.78	31.72	33.12	32.66
Syngas (CO+H_2)	29.09	26.45	27.59	31.99	28.73
Calorific value (MJ/Nm^3)	4.10	4.23	4.67	4.57	5.56
Fuel gas production (Nm^3/kg)	2.37	2.10	2.02	2.31	2.44
Cold gas efficiency (%)	0.57	0.52	0.56	0.62	0.64
Char and ash (g)	532	2138	2651	1014	2256

Case 1: below the grate, Case 2: through the grate, Case 3: above the grate, Case 4: 50% below and 50% through the grate, Case 5: 50% below and 50% above the grate

In order to overcome the disadvantages of feeding the air through or above the grate, two other experiments were carried out. In which the total amount of air flow rate was divided into two parts, 50% of the air was fed below the grate and the other 50% was fed through and above the grate, respectively. The results of the two experiments were attached in the same table. In those new experiments, the gasification parameters such as the amount of combustible gases, quality of the producer gas and cold gas efficiency were improved significantly, while the char residue was considered to be high if compared to that obtained in the case of feeding the air below the grate.

5.2.6 Influence of Secondary Air Injection on Gasification Performance

The schematic diagram of the innovative modified updraft fixed bed gasifier with secondary air configuration is illustrated in Figure 5.37. As shown in the same figure, the biomass was fed in at the top of the gasifier, while the gasification air was introduced through several holes on the grate. During the gasification tests, the

biomass fuel moved down in an opposite direction to the gaseous fuel. In its downward movement the biomass fuel passed through four distinct reaction zones, which were drying zone, the pyrolysis zone, the reduction zone and the combustion zone. In the drying zone, feedstock was dried by heat generated in the zones below. In the pyrolysis zone (devolatilization zone), the feedstock was decomposed into solids char, liquid tar, water and a mixture of volatile gases (H_2, CO, CO_2, CH_4, C_2). The heat for this process was delivered by both the upward flowing gas and the radiation from the combustion zone. In the reduction zone (gasification zone), char and water vapor were converted to gases by reacting with the hot gases coming from the combustion zone. The main reactions that occur in this zone were Boudouard reaction, water gas reaction, water-gas shift reaction and methanation reactions. In the combustion zone (oxidation zone), the solid char was oxidized resulting in the formation of CO_2, CO and heat. Moreover, hydrogen in biomass fuel reacts with oxygen to produce steam. Generally, all the reactions in the oxidation zone are highly exothermic reactions (produce large amount of heat), and the large amount of heat generated in this zone is used for drying, pyrolysis and reduction processes.

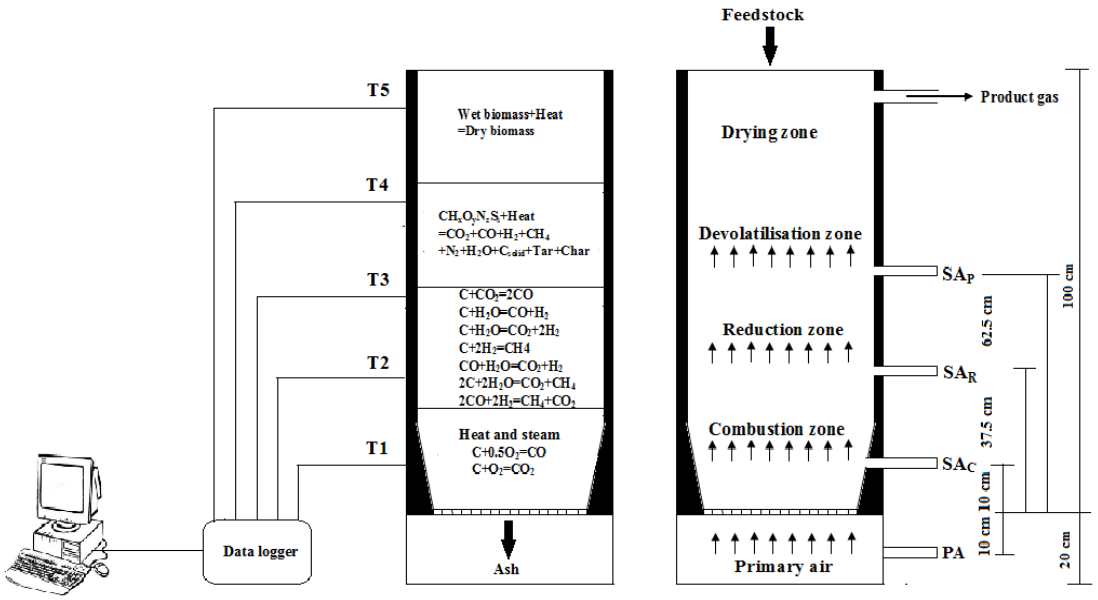

Figure 5.37: Schematic diagram of an updraft gasifier with the positions of secondary air

Injection of the secondary air in those zones is expected to serve two purposes: decreasing the gasification air, thus enhancing the formation of CO instead of CO_2 in the oxidation zone, and increasing the temperature at the upper zone due to the oxidation of char in these zones, thus resulting in cracking the tars.

It is also shown in Figure 5.37 that the distance from the grate to the top of the gasifier is 1.0 m. The primary air (gasification air) was fed to the gasifier at 10 cm below the grate; however, the holes on the grate were used to distribute the air across the whole section of the grate, whereas the injection of the secondary air entrance was either to be at 10, 37.5 or 62.5 cm above the grate, which considered to be fed through the combustion zone, reduction zone or pyrolysis zone, respectively.

5.2.6.1 Effect of the Secondary Air Position

In order to study the effects of secondary air positions in an updraft fixed bed gasifier with OPF as a biomass feedstock, four experiments were performed by changing the location of entrances of the secondary air while the other conditions were kept constant. However, the secondary to primary air ratios were kept at 17%. The variation in temperature profile and variation of synthetic gas composition profiles during the gasification process related to the variation of injection of secondary air position are shown in Figures B.31 to B.34 and B.35 to B.38 (Appendix B), respectively.

Figure 5.38 shows the average temperature of the gasifier versus the gasifier height for the four experiments that were performed in this section. The first experiment (case 1) was performed without injection of secondary air, while the second (case 2), third (case 3) and the fourth (case 4) experiment were performed with the injection of the secondary air at combustion zone, reduction zone and pyrolysis zone, respectively. It can be observed from the same figure that injection the secondary air at the upper zones resulted in an increase of the gasifier temperature at T_1, T_2, T_3 and T_4. Increasing the temperature at T_1 as a result of secondary air injection might be due to the decrease of primary air [71], while the significant increase of temperature at T_2 and T_3 when the secondary air was injected at the

reduction and pyrolysis zone was probably due to the partial oxidation of char as a result of the presence of oxygen (O_2 introduced with secondary air).

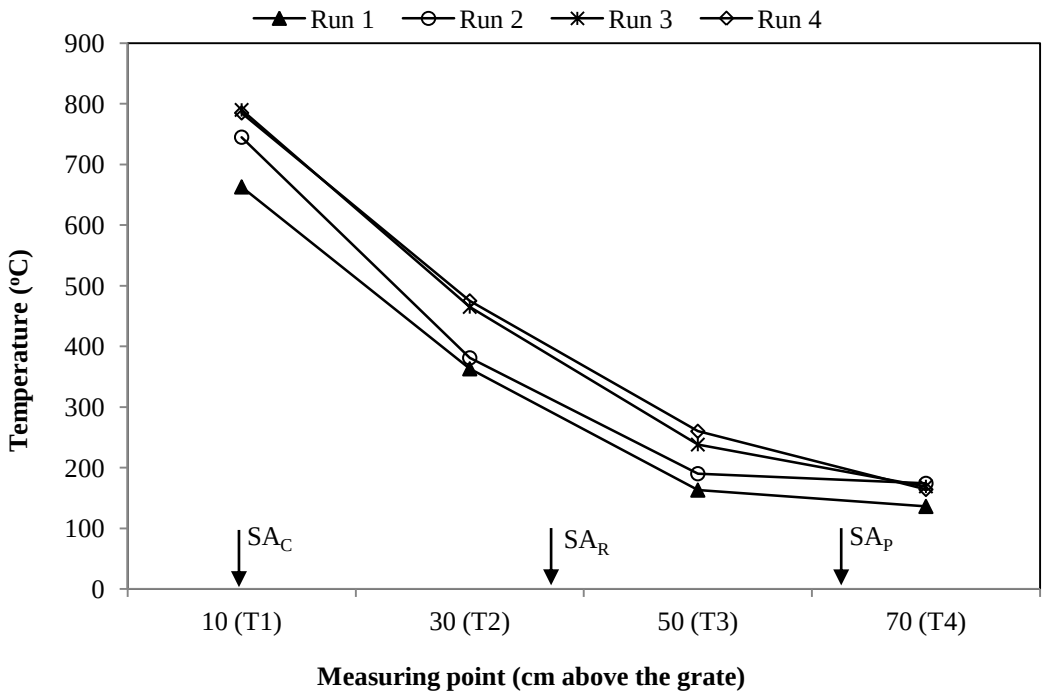

Figure 5.38: Effect of secondary air position on gasifier temperature profile along the gasifier axis

Table 5.14 shows the results summary of the four experiments that were performed in this section. It was observed that, with injection the secondary air at different zones, there was an increase in CO, H_2 and CH_4 content and slightly decrease in CO_2 content. The highest concentration of CO and lowest concentration of CO_2 was observed when the secondary air was injected at reduction zone. This may be due to the fact that the availability of oxygen at reduction zone might be favorable for the Boudouard reaction, however, most of the carbon dioxide that was produced in the reduction zone by the following reactions: $C+2H_2O \rightleftharpoons CO_2+2H_2$ and $2C+H_2O \rightleftharpoons CO_2+CH_4$ might be consumed by Boudouard reaction ($C+CO_2 \rightleftharpoons 2CO$). Moreover, the availability of shortage oxygen at the oxidation zone might enhance the incomplete oxidation reaction ($C+0.5O_2 \rightleftharpoons CO$). Moreover, the partial oxidation of char ($C+0.5O_2 \rightleftharpoons CO$) at the reduction zone as a result of the presence of oxygen might be a reasonable explanation of increasing the temperature at T_2 and T_3 when the

secondary air was injected at the reduction zone (Figure B.33 in Appendix B). On the other side, this high temperature was favorable for tar-condensate cracking.

Table 5.14: Experimental results of different secondary air positions

Measured parameters	Secondary air position			
	Case 1	Case 2	Case 3	Case 4
CO (vol. %)	22.04	23.46	24.70	23.29
CO_2 (vol. %)	9.54	8.91	8.33	8.97
CH_4 (vol. %)	1.24	1.79	1.72	1.27
H_2 (vol. %)	6.48	7.32	7.91	6.25
N_2 (vol. %)	59.90	58.62	55.37	59.64
Combustible gas (CO, H_2 and CH_4)	30.56	32.47	34.30	31.69
CO/CO_2 (%)	2.31	2.63	2.97	2.79
H_2/CO (%)	0.29	0.31	0.33	0.26
H_2/CO_2 (%)	0.68	0.82	0.95	0.71
CH_4/H_2 (%)	0.19	0.24	0.22	0.21
Calorific value (MJ/Nm^3)	4.11	4.60	4.89	4.25
Fuel gas production (Nm^3/kg)	2.36	2.26	2.28	2.29
Fuel consumption rate (kg/h)	9.23	10	8.72	8.18
Carbon conversion rate (%)	95.96	97.09	99.70	95.93
Cold gas efficiency (%)	57.18	61.21	65	57.64
Tar and condensate (g)	240	179	180	600
Char and ash (g)	532	695	1105	1324

Case 1: without secondary air, Case 2: through combustion zone, Case 3: through reduction zone, Case 4: through pyrolysis zone

There was a high increase in the concentration of H_2 and CH_4 when the secondary air was injected through the combustion and reduction zone which might be due to the fact that higher temperature created by the secondary air always favors the tars and hydrocarbons cracking [71]. The molar ratios such as CO/CO_2, H_2/CO, H_2/CO_2 and CH_4/H_2 ratios might be used to investigate the importance of the reactions and characterize the syngas composition. An increase of CO/CO_2 ratio with the injection of secondary air could be attributing to the fact that, as less oxygen was supplied below the grate for the oxidation process, favored the formation of CO instead of oxidizing the carbon to CO_2, thus caused an increase in CO/CO_2 ratio. Moreover,

injection of the secondary air at any zone favored the formation of CO in that zone. The same table shows a slight increase in H_2/CO molar ratio; however the H_2/CO increased from 0.28 in the case of no secondary air to 0.31 and 0.33 for the case of injecting the secondary air through the combustion and reduction zone, respectively, while decreased to 0.26 when the secondary air was injected at the pyrolysis zone. It seemed that both Boudouard reaction and water gas reaction played more prevailing role when the secondary air was injected in the combustion and reduction zone, but Boudouard reaction was the most prevailing. However, the molar ratio of CO/CO_2 increased by 14% and 27% when secondary air was injected through combustion and reduction zone, respectively, while the molar ratio of H_2/CO increased by 7% and 14% for the same cases. The molar ratios H_2/CO_2 and CH_4/H_2 show an increase for the cases of the secondary air injection.

Gasification parameters such as higher heating value, cold gas efficiency and carbon conversion efficiency might be used to investigate the effect of the secondary air injection on the gasification of OPF. However, as the secondary air was injected at combustion, reduction and pyrolysis zone, the higher heating value of the producer gas improved by 12%, 19% and 3.42%, whereas the cold gas efficiency increased by 7.1%, 13.68% and 0.8%, respectively. This is due to the increase of total amount of combustible gases (CO, H_2 and CH_4). Therefore, the optimum condition is that the secondary air should be injected at the reduction zone in order to improve the gas quality and reduce the tar-condensate production yield.

It was found that injection of the secondary air at the pyrolysis zone did not contribute much to the improvement in gas quality or gasification performance. This could be due to the fact that, as the gasification process was going on, the feedstock decreased and it became below the position of secondary air injection, so that there would be no chance for the secondary air to react with char. Moreover, as the temperature at pyrolysis zone was very low (about 300^{o}C), endothermic reactions between the secondary air and the upward flowing gas might not be achievable. Therefore, injecting the secondary air at the pyrolysis zone is not useful for the whole gasification time when using batch type updraft gasifier.

5.2.6.2 Effect of the Secondary Air Ratio

As mentioned at Section 5.2.6.1, injecting the secondary air at combustion zone, reduction zone and pyrolysis zone improved the higher heating value of the producer gas by 12%, 19% and 3.42%, whereas the cold gas efficiency increased by 7.1%, 14% and 0.8%, respectively. Therefore, studying the influence of secondary air ratios (secondary to primary air ratio) would be implemented only for the reduction zone and combustion zone, in which the higher heating value and gasification efficiency were improved significantly.

a) **Influence of Secondary Air Ratios: Reduction Zone**

To study the effect of the secondary air ratio on the quality of the producer gas and gasifier performance in the reduction zone, four tests were performed by setting the secondary air ratios to 17%, 27%, 40% and 56%, while the other conditions were kept constant. However, the total amount of air was kept constant, thus increasing the secondary air means decreasing of the primary air. The summary of the experiment results, the temperature profiles inside the gasifier and the synthetic gas composition profiles during the gasification process related to the variation of secondary air ratios are shown in Table B.6, Figures B.39 to B.42 and Figures B.43 to B.46 (Appendix B), respectively.

As the secondary air was injected at 37.5 cm above the grate, the amount of primary air (below the grate) was supposed to be enough for gasification processes. Therefore, in order to improve the syngas quality and tar-condensation reduction, the secondary air ratio at the reduction zone would be less than 27% as shown in Figures 5.39 and 5.40. Under the conditions of secondary air ratio of 17% and 27%, the fuel production rate are 2.28 and 2.27 Nm^3/kg, the higher heating value is 4.9 and 4.6 MJ/Nm^3 and cold gas efficiency of the gasifier is 65% and 60.13%, respectively. In which the higher heating value of the producer gas improved by 19% and 12% and the cold gas efficiency of the gasifier improved by 14% and 5.20%, respectively. Further increase in the secondary air means further decrease in the primary air that made the main process seemed like pyrolysis and therefore, produced high amount of char and condensate beside the product gas. Additionally, as the air was injected in

the reduction zone, tar-condensate generation was decreased by about 22% as compared to the case of no secondary air (Case 1 as mentioned in Section 5.2.6.1).

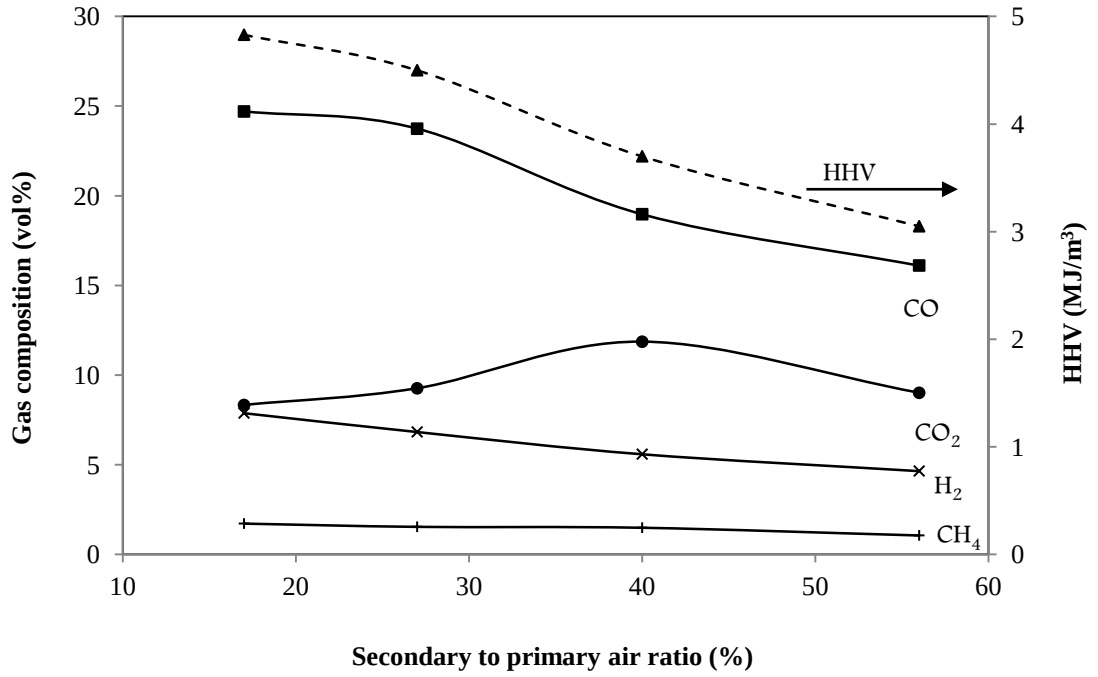

Figure 5.39: Effect of secondary air ratio in reduction zone on gas composition and heating value

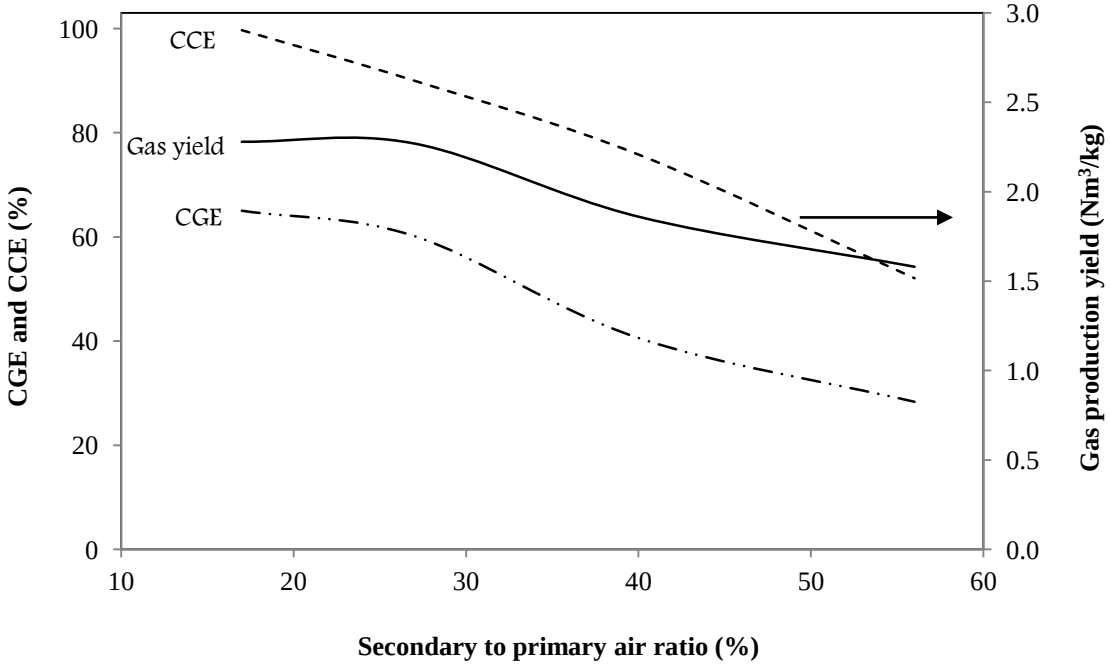

Figure 5.40: Effect of secondary air ratio in reduction zone on cold gas efficiency, carbon conversion efficiency and gas production yield

b) **Influence of Secondary Air Ratios: Combustion Zone**

To study the effect of the secondary air ratio on the quality of the producer gas and gasifier performance in the combustion zone, four tests were performed by setting the secondary air ratios to 17%, 27%, 56%, and 100% for each test respectively, while the other conditions were kept constant. Table B.7 in Appendix B shows the composition of producer gas, fuel consumption rate and gasifier performance for different cases, while Figures B.47 to B.57 illustrates the temperature profile inside the gasifier and variation of synthetic gas composition profiles.

As shown in the same table and Figures 5.41 and 5.42, the secondary air had an impact on the components of the producer gas and gasifier performance. As the secondary air increased, the temperature of the upper zones increased, resulting in the formation of H_2 and CH_4. Moreover, higher temperature at the upper zone was favorable to the cracking of hydrocarbons and tar. Therefore, increasing the secondary air resulted in an increase in H_2, CH_4, higher heating value and cold gas efficiency. Moreover, the molar ratios of H_2/CO, H_2/CO_2 and CH_4/H_2 were also improved.

Although the injection of higher amount of secondary air improved the gasification performance of OPF, but resulted in higher amount of feedstock remaining as char. This could be attributed to the fact that, as the secondary air was fed to the gasifier at about 10 cm above the grate, and due to the decrease of fuel bed in the gasifier with time. Therefore, when the fuel bed reached the level of below than 10 cm, char residue may stop to be combusted and gasified in the bottom region of the gasifier. Additionally, another explanation was that, due to fact that the dry OPF had low density, therefore as the gasification process was going on, the height of the fuel bed decreased, and then the high air velocity as a result of high secondary air might lead the fuel to be in a turbulence state or might turn out the fire. The sequence was that the production of combustible gases might stop due to non-continues burning of the OPF fuel. Therefore, the usage of higher secondary air ratio through the combustion zone may be favorable for continuous feeding updraft gasifier rather than batch type updraft gasifier.

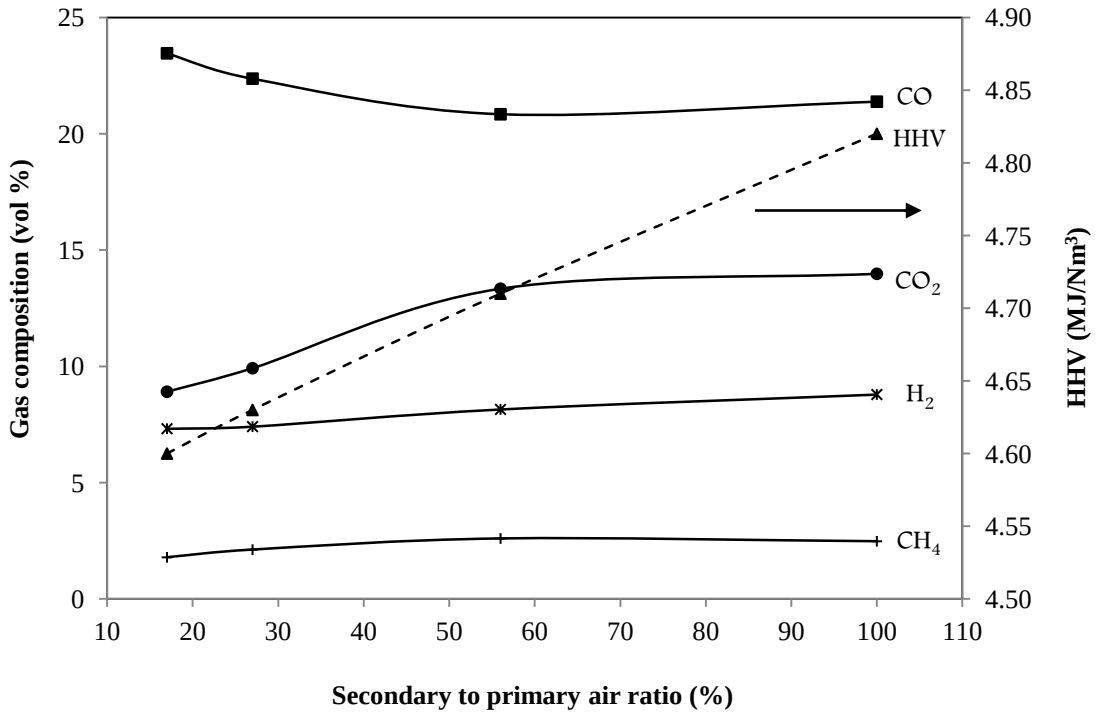

Figure 5.41: Effect of secondary air ratio in combustion zone on gas composition and heating value

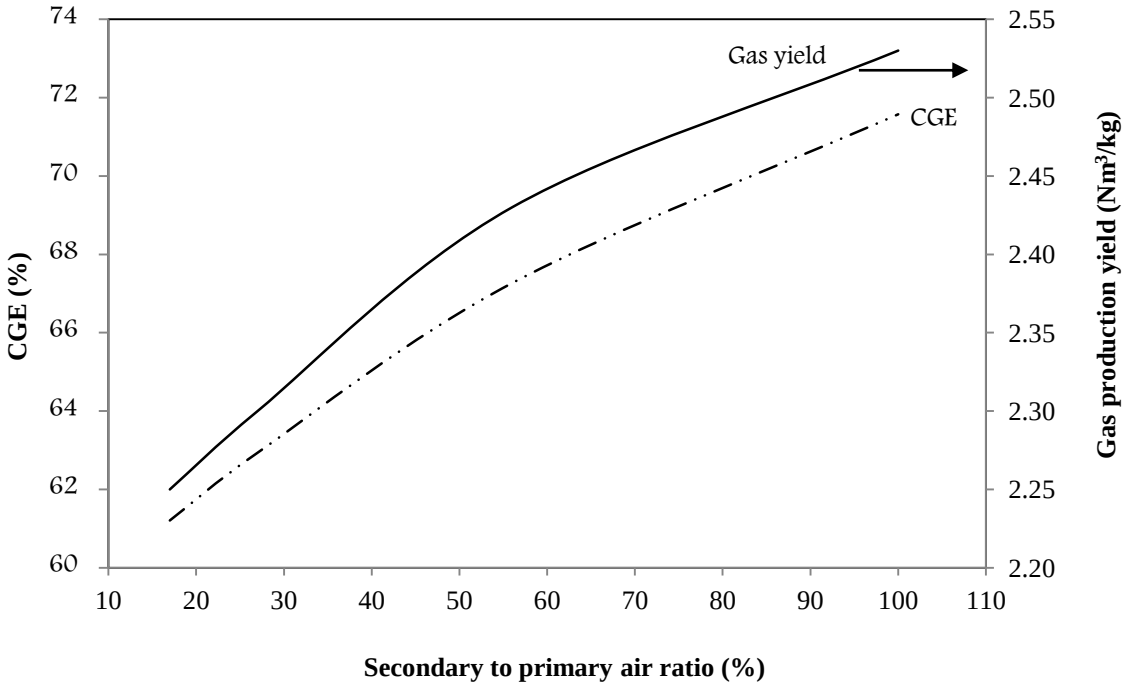

Figure 5.42: Effect of secondary air ratio in reduction zone on cold gas efficiency, carbon conversion efficiency and gas production yield

5.2.7 Mass Balance

Total mass balance is one of the methods that used to examine the reliability of collected data [30]. During this study, total of 32 gasification experiments were carried out. However, the material mass balance was conducted for each experiment in order to validate experimental results of the gasifier. The mass inputs include the feedstock, air and their moisture content, while the mass outputs comprise dry gas product, char-ash and condensate. The mass balance closure which is defined as the percentage of the total mass output to that of the total mass input is obtained for all the experiments and presented in Table C.1 in Appendix C. The results of overall mass balance closure were observed to be in the range of 81-101%, with an average of about 90%. This result indicates the reliability of collected data measurements. An overall mass balance closure of 100% was not easy to be obtained, due to the following reasons:

- Leakage of the system
- Error in measurements
- Neglecting the water, oxygen and hydrocarbons (C_2H_2, C_2H_4, C_2H_6, *etc.*) in the product gas.

5.2.8 Comparison of OPF Gasification Results with Literature Results of Different Feedstock

Table 5.15 shows the optimum results of an updraft gasification of OPF as compared with updraft gasification of other biomass fuel such as wood, sewage sludge *etc*. The results were presented in terms of gas composition and gas heating value, gas production yield and cold gas efficiency. The woody biomass (beech wood and wood pellets) and dairy biomass produced a gas with heating values in the range of 4.99 – 6.8 MJ/Nm^3 which higher than that obtained by OPF (4.9 MJ/Nm^3), while the other types of biomass such as sewage sludge and chicken litter showed a heating value of about 3.96 and 2.9 MJ/Nm^3, respectively. The amount of gas production yield of OPF was in the range of that obtained by other biomass fuel such as RDF pellets, mesquite and juniper wood.

Table 5.15: Comparison of gasification OPF results with literature results of different feedstock with air as an oxidant

Biomass type	HHV_b (MJ/kg)	ER	CO	CO_2	CH_4	H_2	HHV_{gas} (MJ/m^3)	Ygas (kg/m^3)	CGE (%)	Ref.
				(% vol.)						
OPF	17.01	0.33	24.7	8.33	1.88	7.91	4.90	2.27	65	a
Long stick	na	na	12	14	na	15	4.50	na	73	[88]
Dairy biomass	17.19	1.9[b]	23	10.1	2.0	7.2	5.15	na	na	[76]
RDF pellets[c]	na	0.35	25.5	5.3	1.9	18.5	5.58	2.35	73.2	[84]
Mangrove	na	na	28.8	na	5.0	na	3.67	na	na	[85]
Wood pellets	17.68	0.29	27.5	6.2	3.2	7.1	4.99	na	54.7	[65]
Beech wood	na	na	30	5.5	1.8	7	5.25	na	na	[58]
Sewage sludge	15	0.15	11.2	12.7	1.1	4.4	3.96	0.51	21	[105]
Chicken litter	na	na	14	9.4	1.7	7.8	2.90	na	na	[48]
Wood pellets	na	1.2	25.1	5.2	1.6	4.9	6.80	na	na	[74]
Mesquite	20.13	2.7[b]	21	15	1.5	3	3.50	2.22	na	[104]
Juniper	20.58	2.7[b]	25	12	1.8	3.5	3.90	2.34	na	[104]

a: this study, b: modified equivalence ratio, c: Refuse Derived Fuel pellets, HHV_b: higher heating value of biomass fuel

The cold gas efficiency in the case of OPF gasification was about 65%, which was in range to that obtained by other biomass fuels. The gas composition of the producer gas was about 24.7% CO, 8.33 CO_2, 1.88 CH_4 and 7.91% H_2 which was in the range of that obtained by the gasification of woody biomass as shown in Table 5.15. Therefore, the gaseous fuel produced by updraft gasification of wasted OPF could consider as a promising fuel for thermal applications such as boilers and kiln, instead of using expensive woody biomass in those applications.

5.3 OPF Synthetic Gas Applications

5.3.1 Synthetic Gas Flare

To examine the capability of using the OPF synthetic gas as a fuel for engine and heat applications, the producer gas of an updraft gasification system was flared through three provided ports in the system. However, the first flare point was located at the producer gas exhaust pipe and the second flare point was located at the exit pipe of

the cyclone, while the last point was located at the exit of the accumulation tank. The producer gas was able to be flared at the three points with different phenomenon.

Figure 5.43 (a) shows the photo of the gas flare at the first point, where the gas was at high temperature (120-200^{o}C). It was observed that the gas at this point was flared with yellow orange flame. On the other side, shown in the Figure 5.43 (b) is the producer gas flare at the second flare point (after dirt leg and cyclone cleaning). The flare of the producer gas at the second flare point was found in a bluish color. This might be due to the removal of some condensate (water and tar) and contaminants. Moreover, it might also be due to the decrease of the gas temperature which happens due to the centrifugal movement of the gas in the cyclone.

Figure 5.43 (c) shows the flare of the gas at the third point, in which the gas was flared with blue flame. This type of flame referred to the cooled filtered gas and the quality of the gas which seems it's the quality that needed for thermal and engine applications. It was observed that the producer gas may still contain some water vapor, which resulted in some orange dots in the flared flame. However, the gas is still need to be cleaned to operate the engine in safety mode.

Figure 5.43: OPF gas flame in updraft gasifier a. flared gas at first and second flare point b. flared gas at the exit of the accumulation tank (third flare point)

5.3.2 Domestic Cooking Stove

The aims of this experiment were to examine the capability of using OPF synthetic gas in a domestic cooking stove and to estimate the total energy used in boiling the water from ambient temperature. The stove used in this experiment was not designed to be used with the synthetic gas; instead it was designed to be used with domestic cooking gas (Liquefied Petroleum Gas, LPG). In order to examine the capability of using the domestic cooking stove with OPF gas, the stove was disassembled and then the gas was ignited in the burner by showing the flame through the holes in the burner as shown in Figure 5.44 (a). Thereafter, the stove was assembled and then connected to the supply of the producer gas.

In the water boiling test, the producer gas with a known flow rate (0.9 m^3/h) was allowed to flow naturally to the stove burner and then the stove was ignited by cigarette lighter. Thereafter, a known quantity of water of about one liter was taken in cooking pot and then put in the stove stand and left to boil as shown in Figure 5.44 (b). The time of boiling the water was then used to estimate the energy used for boiling the water.

Actually, the water in the pot was boiled in about six minutes consuming about 0.09 m^3 of the OPF synthetic gas. As mentioned earlier, the average gas yield was about 2.29 Nm^3 per kg of OPF. Therefore, and via updraft gasification technology each kilogram of OPF was expected to boil about 25 liters of water. As known the energy needs to boil the water can be determined as follow:

$$Energy = \text{specific heat of water} \times \text{mass} \times \text{temperature rise} \qquad (5.9)$$

Hence, the energy needed to boil 25 liters was found to be 8.37 MJ. Theoretically, as the Malaysian LPG has a calorific value of about 45.9 MJ/kg. Therefore, via updraft gasification each kilogram of OPF could save about 0.2 kg of LPG.

Figure 5.44: The use of OPF synthetic gas a. Synthetic gas flare in the stove burner b. boiling water with domestic cooking stove using OPF synthetic gas

5.4 Characterizations of Gasification Byproducts

5.4.1 Char Analysis

Char derived from the updraft gasification of OPF was characterized in term of proximate analysis, ultimate analysis and determination of the higher heating value in order to provide a comprehensive understanding of its combustion properties. As evidenced from the proximate analysis results of OPF char (Table 5.16), the OPF gasification char showed a decrease in the volatile matter accompanied by an increase in the fixed carbon and ash content as compared to the original OPF. Moreover, the results of elemental analysis showed an increase in carbon content, and a decrease in both hydrogen and oxygen contents, which might be due to the decrease of volatile matter. The higher heating value was about 22.87 MJ/kg, which is higher than the heating value of the original OPF by more than 5 MJ/kg.

Table 5.16: Properties OPF char and ash residue as compared to origin OPF material

Properties	OPF	OPF char	OPF ash
Proximate analysis (wt.% db)			
Moisture content	7.860	10.201	4.520
Volatile matter	68.320	35.754	14.590
Fixed carbon	18.770	49.191	9.510
Ash	2.250	4.854	71.310
Ultimate analysis (wt.% db)			
C	42.480	65.100	17.160
H	4.52	1.617	0.680
N	0.610	0.845	0.440
S	0.050	0.029	0.010
O (by difference)	52.340	32.409	81.710
Calorific value (MJ/kg)	17.01	22.87	-

The above results encourage the research on pyrolysis of both original and briquetted OPF in order to produce OPF char fuel for the gasification purpose. The produced char from the pyrolysis of both original and briquetted OPF is expected to have high percentage of fixed carbon and carbon content, which are the main reason for increasing the higher heating value. The sequence is that the gasification of the

produced char is expected to produce gaseous fuel with high heating value and low tar content.

5.4.2 Ash Analysis

The ash residue derived from the gasification of OPF was physically and chemically characterized in order to investigate its properties. However, the OPF ash was characterized in terms of proximate analysis, CHNS analysis, SEM/EDX and FTIR analysis. However, as shown in Table 5.16, the results of proximate and ultimate analyses of OPF ash residues showed that the percentage of unburned carbon in terms of fixed carbon and carbon element were about 9.51% and 17.16%, respectively. A comparison of these results with that reported for fly ash [157], showed that the unburned carbon in OPF gasification ash was much lower than that reported for fly ash generated in Dishergarh Thermal Power Station (DIPS). That means almost the whole carbon in the OPF was converted to gaseous fuel. However, the disposal of OPF ash which contained a low amount of unburnt carbon might not cause any environmental damages. Nitrogen and sulfur content in ash residue were about 0.44% and 0.01%, respectively. The amount of nitrogen and sulfur content in the ash residue was lower than that of OPF material; this indicates the release of nitrogen and sulfur gases during the gasification process, but as expected the production of these gases during the updraft gasification of OPF was negligible, as the amount of nitrogen and sulfur content in the OPF material was much lower compared to other fuels such as coal and wood.

Figure 5.45 shows the micrograph of OPF ash which appears to be porous, non smooth surface and tendency to cohesion properties. As mentioned earlier, Table 5.4 shows an average result of elemental analysis of OPF ash using Electron Dispersive X-ray Spectroscopy (EDX). A noteworthy observation was that OPF ash contains a relatively high weight percentage of potassium (13.11%), calcium (6.68%) and iron (2.85%) while magnesium and sodium weight percentages were comparatively low. The high potassium was considered as one of the main sources of agglomeration of biomass in the gasifier bed, due to decreasing its melting point [139], which might

probably clog the air voidage (grate holes). This problem was basically related to the content of the fuel ash and the operating temperature within the bed [141]. Therefore, as the problem is expected to be more announced in high temperature, the operating temperature for a fuel with high potassium should be in the range of 900-1000^{o}C, in order to avoid the agglomeration problem.

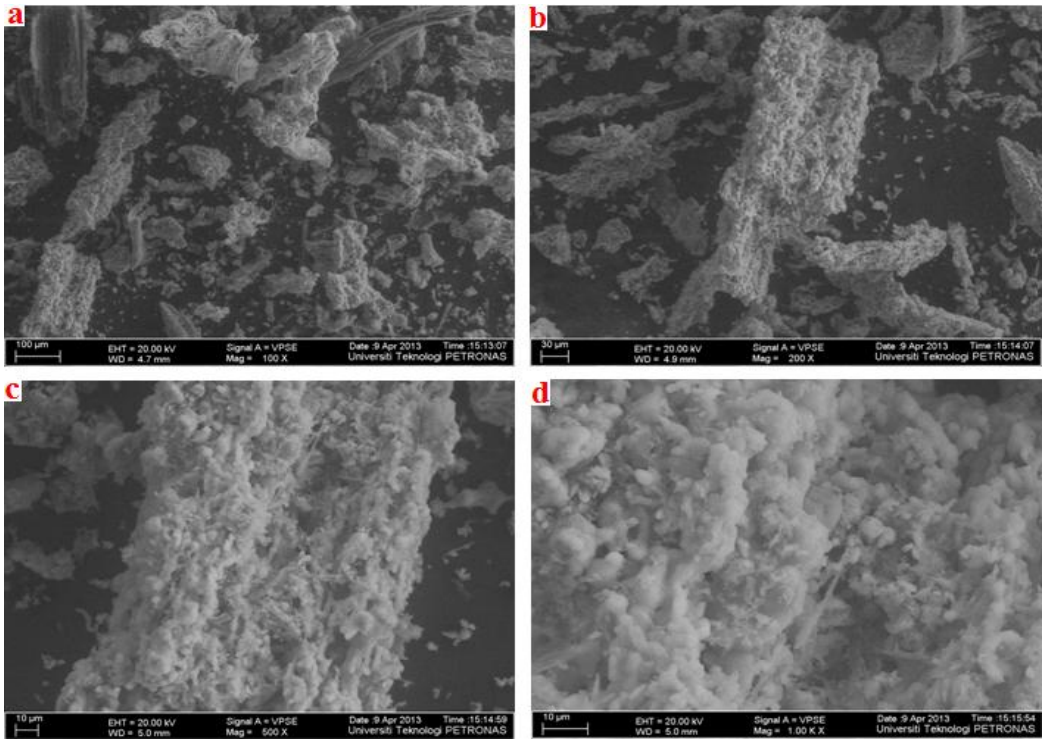

Figure 5.45: SEM image of OPF at different magnification (a) 100x (b) 200x (c) 500x (d) 1000x

Figure 5.46 illustrates the spectra for OPF ash residue samples as compared with the origin OPF material. The spectra were performed over a frequency range of 4000–650 cm^{-1}. The spectrum of the OPF ash appeared to be very similar to the FTIR spectrum of the OPF fuel in terms of location of most peaks. A significant change was appeared in the FTIR spectrum in the range of 1729–1177 cm^{-1}. However, instead of seven small peaks in the OPF material in this range, three significant peaks were observed at the same range for the ash samples. A significant peak appeared at around 1625.86 cm^{-1} was commonly assigned to the O-H. The peaks at around 1106, 870, 665.9 cm^{-1} were assigned to Si-O bonds (silica traces), Al-O and Si-O or Al-O respectively [158, 159].

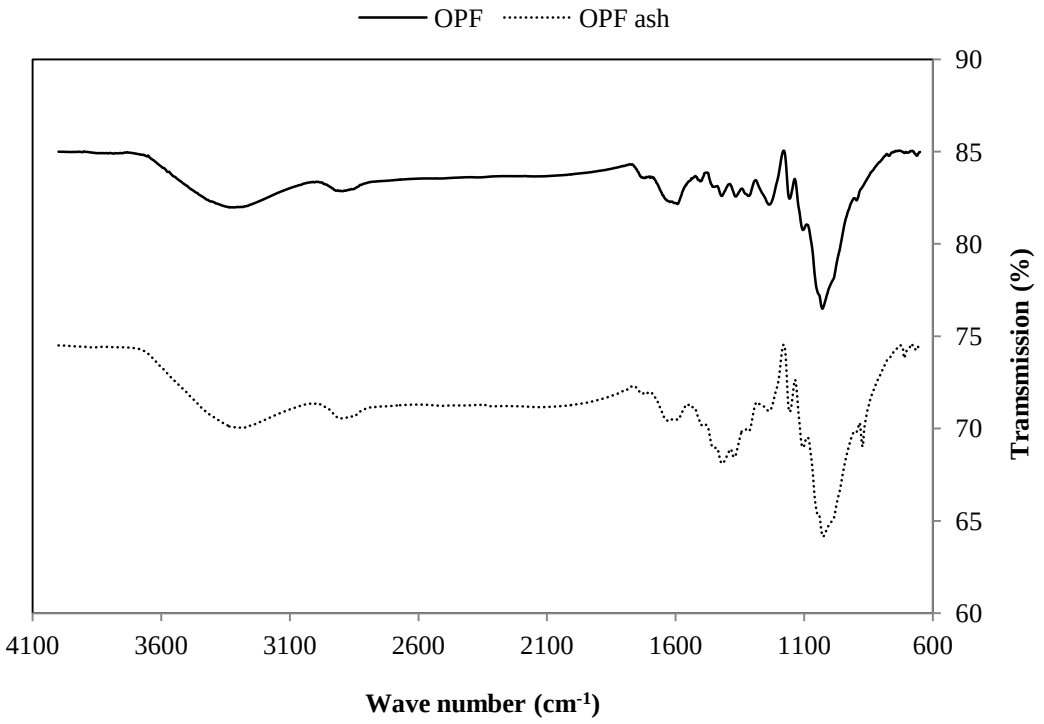

Figure 5.46: FT-IR spectra of OPF ash as compared to OPF fuel

5.5 Uncertainty Analysis

In the experiments of updraft gasification of OPF, the flow rates, temperatures, gas percentages, tar-condensate content and char-ash content were measured with appropriate instruments. However, the average of the total uncertainties arisen from the measurement of air flow rate, temperatures, total combustible gas percentages, tar-condensate content and char-ash content were calculated based on the theory stated at Section 4.11. The average uncertainties are shown in Table 5.17.

The uncertainty propagation analysis was also applied in the case of output gasification parameters such as equivalence ratio, gas production yield, gas heating value, carbon conversion efficiency and cold gas efficiency. However, the total uncertainties of the output gasification parameters were affected by the uncertainties of the instruments used to measure the flow rates, combustible gas percentages, *etc* and the values of the total uncertainties are presented in the same table.

Table 5.17: Total uncertainties

Total uncertainties in air flow rate and OPF weight measurement		
Total uncertainty	U_{AFR}	M_{OPF}
Comments (%)	±1.13	±3.81

Total uncertainties in each temperature					
Total uncertainty	U_{T1}	U_{T2}	U_{T3}	U_{T4}	U_{T6}
Comments (^{o}C)	±14.36	±16.24	±8.01	±7.14	±4.28

Total uncertainties in total combustible gas, tar-condensate and ash tar amount							
Total uncertainty	U_{CO}	U_{CO2}	U_{CH4}	U_{H2}	U_{N2}	U_{t-c}	U_{c-a}
Comments (%)	±0.27	±0.36	±0.85	±0.53	±1.10	±6.4	±3.8

Total uncertainties in the indicators of gasification parameters					
Total uncertainty	U_{ER}	U_{yield}	U_{HHV}	U_{CCE}	U_{CGE}
Comments (%)	±3.97	±4.14	±0.97	±4.25	±4.25

CHAPTER 6

CONCLUSIONS AND RECOMMENDATIONS

6.1 Conclusions

The OPF samples were characterized by means of ultimate analysis, proximate analysis, heating value, mineral content, moisture content, density, fourier transform infrared, surface morphology and ash content. In addition, thermal decompositions of the samples were investigated under nitrogen and oxygen atmosphere, in order to determine and analyze the reaction kinetics. Moreover, two empirical equations have been developed by using multiple linear regression analysis. The first equation was developed for the prediction of OPF moisture content based on its density and it has a correlation coefficient (R^2) of about 0.97 and has capability for predicting the OPF moisture content in the range of 10% to 60% with an average error less than 10%. The second equation was developed for the prediction of OPF heating value based on the ultimate analysis and has correlation coefficient (R^2) of 0.92 indicating its good capability.

A 50 kW batch type updraft gasifier was designed and constructed from mild steel and cement refractory as lining wall and insulation, respectively. The gasifier is a part of small gasification system to produce a gas for thermal application and the gasifier has a thermal input of about 71 kW_{th} (15 kg/h OPF) and produces product gas with heating value of 4-5 MJ/Nm^3. The gasifier was modified to be very flexible allowing the gasification air to be fed through several locations as well as allowing the secondary air to be injected at several positions; these positions represent the combustion, reduction and pyrolysis zones.

Experimental studies were successfully conducted on an updraft fixed bed gasifier to investigate the effect of various operation conditions such as equivalence ratio (0.18 - 0.4), OPF moisture content (0% - 60% wet basis) and particle size (<5 mm - >250 mm) on producer gas quality and gasifier performance. The gasification performance was investigated in terms of temperatures profile, product gas composition, product gas heating value, gas production yield, fuel consumption rate, carbon conversion efficiency, gasification efficiency, char-ash content and tar-condensate content as well as gas molar ratios.

Four air locations at about 10 cm below the grate, 1.0 cm above the grate (called through the grate) and 10 cm above the grate were selected. Results showed that producer gas composition, gas heating value and cold gas efficiency were significantly influenced by the air location. The best gas heating value in the range of 4.6-5.6 MJ/Nm^3 and cold gas efficiency in the range of 62-64% was obtained when the air was divided into two parts, 50% below-50% through the grate and 50% below-50% above the grate, respectively.

Injection of the secondary air showed gasification performance and tar generation were strongly affected by both the injection position and ratio of the secondary air. For injection the secondary air in the reduction zone, the secondary air ratio should not exceed 27%. Under the conditions of secondary air ratio of 17% and 27%, the gas heating values were improved by about 20% and 12% and cold gas efficiencies of the gasifier were increased by about 14% and 5.2%, respectively as compared to the case of no secondary air. Moreover, the tar-condensate generation was decreased by about 22-25% as a result of secondary air injection.

The gas produced from updraft gasification of OPF was used in a domestic cooking stove in order investigate the capability of using OPF synthetic gas in a domestic cooking stove and to estimate the total energy used in boiling the water from ambient temperature. However, one liter of water was boiled in six minutes consuming about 0.09 m^3 of the OPF synthetic gas. Therefore, it was estimated that gasification of one kilogram of OPF (via updraft gasification) could save about 0.2 kg of liquefied petroleum gas (LPG).

Based on these experiments, the updraft gasification of the frond appears to be a feasible alternative to the use of fossil fuels in thermal applications, and the gasification byproducts such as char and ash appear to be reusable and contained insignificant unburnt carbon, respectively.

6.2 Recommendations

As discussed, the measurement of temperature profile along the axis of the gasifier would be of great guidance to be able to understand the gasification processes. Moreover, the experimental results of temperature profiles inside the gasifier showed some inconsistencies. Currently, the temperature profiles inside the gasifier were measured by four thermocouples, inserted to about 4 inch inside the gasifier from the external wall. Additional thermocouples are required to be placed along the gasifier. Moreover, for most accurate temperature profiles, the thermocouples should be able to measure the temperature at the center of the gasifier.

Since the current gasifier was manually loaded due to the feedstock, it is recommended to attach continuous feeding mechanism system to the gasifier in order to obtain an easy loading of feedstock during the operation of the gasifier. On the other hand, most accurate data could be collected with the continuous feeding updraft gasifier rather than batch type updraft gasifier.

A study on the effect of gasification air velocity on updraft gasification of OPF would give information about the applicable velocity on gasification of OPF in updraft gasifier. Moreover, updraft gasification of OPF with preheating air and other gasification agents such as oxygen, steam is required to investigate the effect of those parameters on the gasification of OPF and compare with the current results.

The characterizations of char residue encourage the research on pyrolysis of both original and briquetted OPF in order to produce OPF char fuel for the gasification purpose. The produced char from the pyrolysis of both original and briquetted OPF is expected to have high percentage of fixed carbon and carbon content, which are the main reason for increasing the higher heating value. The sequence is that the

gasification of the produced char is expected to produce gaseous fuel with high heating value and low tar content. Moreover, a comprehensive characterization of OPF ash residue is required in order to provide a comprehensive understanding of its specific properties in terms of toxicity and reusability. Additionally, tar analysis should be performed in order to study its properties and to examine the method of disposal.

REFERENCES

[1] T. L. Chew and S. Bhatia, "Catalytic processes towards the production of biofuels in a palm oil and oil palm biomass-based biorefinery," *Bioresource Technology,* vol. 99, pp. 7911-7922, 2008.

[2] M. S. Juraščík, Anna Ptasinski, Krzysztof J., "Exergy analysis of synthetic natural gas production method from biomass," *Energy,* vol. 35, pp. 880-888, 2010.

[3] P. Sheth and B. Babu, "Production of hydrogen energy through biomass (waste wood) gasification," *International Journal of Hydrogen Energy,* vol. 35, pp. 10803-10810, October 2010 2010.

[4] L. Wei, "Experimental study on the effects of operational parameters of a downdraft gasifier," M.S. 1457997, Mississippi State University, United States -- Mississippi, 2005.

[5] N. Gao, A. Li, C. Quan, and F. Gao, "Hydrogen-rich gas production from biomass steam gasification in an updraft fixed-bed gasifier combined with a porous ceramic reformer," *International Journal of Hydrogen Energy,* vol. 33, pp. 5 4 3 0 – 5 4 3 8, 2008.

[6] P. Sheth and B. Babu, "Experimental studies on producer gas generation from wood waste in a downdraft biomass gasifier," *Bioresource Technology,* vol. 100, pp. 3127-3133, June 2009 2009.

[7] S. H. Shuit, K. T. Tan, K. T. Lee, and A. H. Kamaruddin, "Oil palm biomass as a sustainable energy source: A Malaysian case study," *Energy,* vol. 34, pp. 1225-1235, 2009.

[8] M. A. A. S. Mohammed, A. , W. A. K. G. M. A. Wan Azlina, M. S. Fakhru'l-Razi, A. , and Y. H. Taufiq-Yap, "Hydrogen rich gas from oil palm biomass as a potential source of renewable energy in Malaysia," *Renewable and Sustainable Energy Reviews,* vol. 15, pp. 1258-1270, 2011.

[9] J. Li, Y. Yin, X. Zhang, J. Liu, and R. Yan, "Hydrogen-rich gas production by steam gasification of palm oil wastes over supported tri-metallic catalyst," *International Journal of Hydrogen Energy,* vol. 34, pp. 9108-9115 2009.

[10] Y. Uemura, W. N. Omar, T. Tsutsui, and S. Yusup, "Torrefaction of oil palm wastes," *Fuel,* vol. 90, pp. 2585–2591, 2011.

[11] L. F. Gutiérrez, Ó. J. Sánchez, and C. A. Cardona, "Process integration possibilities for biodiesel production from palm oil using ethanol obtained from lignocellulosic residues of oil palm industry," *Bioresource Technology,* vol. 100, pp. 1227-1237, 2009.

[12] H. Yang, R. Yan, H. Chen, D. H. Lee, D. T. Liang, and C. Zheng, "Pyrolysis of palm oil wastes for enhanced production of hydrogen rich gases," *Fuel Processing Technology,* vol. 87, pp. 935-942, 2006.

[13] H. Kawamoto, W. Z. Mohamed, N. I. Mohd Shukur, M. S. Mohd Ali, Y. Ismail, and S. Oshio, "Palatability, Digestibility and Voluntary Intake of Processed Oil Palm Fronds in Cattle," Malaysian Agricultural Research & Development Institute and Japan International Cooperation Agency 2001.

[14] M. I. B. Yakari, "Oil Palm Frond (OPF) as an alternative Source of Pulp and Paper Production Material," Bachelor, Chemical Engineering, Universiti Malaysia Pahang, 2008.

[15] J. M. Salman, V. O. Njoku, and B. H. Hameed, "Batch and fixed-bed adsorption of 2,4-dichlorophenoxyacetic acid onto oil palm frond activated carbon," *Chemical Engineering Journal,* vol. 174, pp. 33-40, 2011.

[16] A. Fazilah, M. N. Azemi, A. A. Karim, and M. N. Norakma, "Physicochemical properties of hydrothermally treated hemicellulose from oil palm frond," *J. Agric Food Chem,* vol. 57, pp. 1527–1531, 2009.

[17] M. F. Mohideen, M. Faiz , H. Salleh, H. Zakaria, and R. Vijay, "Drying of Oil Palm Frond via Swirling Fluidization Technique," in *The World Congress on Engineering*, London, UK, 2011.

[18] V. Belgiorno, G. De Feo, C. Della Rocca, and R. M. A. Napoli, "Energy from gasification of solid wastes," *Waste Management,* vol. 23, pp. 1-15, 2003.

[19] B. R. Rao, "Gasification of food processing byproducts: An economic waste handling alternative," M.Sc. 1424889, Oklahoma State University, United States, Oklahoma, 2004.

[20] G. Gordillo and K. Annamalai, "Adiabatic fixed bed gasification of dairy biomass with air and steam," *Fuel,* vol. 89, pp. 384-391, 2010.

[21] D. S. Deshpande, A. D. Phadke, S. L. Patil , A. G. Ghadge, and V. N. Raibhole, "Testing And Parametric Analysis Of An Updraft Biomass Gasifier," in *International Conference on Global Scenario in Environment and Energy*, 2013, pp. 753-760.

[22] P. Quaak, H. Knoef, and H. Stassen, *Energy from Biomass-A Review of Combustion and Gasification Technologies* vol. Paper No 422-Energy Series: World Bank Technical 1999.

[23] M. Puig-Arnavat, J. C. Bruno, and A. Coronas, "Review and analysis of biomass gasification models," *Renewable and Sustainable Energy Reviews,* vol. 14, pp. 2841-2851, 2010.

[24] P. C. Roy, A. Datta, and N. Chakraborty, "Assessment of cow dung as a supplementary fuel in a downdraft biomass gasifier," *Renewable Energy,* vol. 35, pp. 379-386, February 2010.

[25] T. Damartzis and A. Zabaniotou, "Thermochemical conversion of biomass to second generation biofuels through integrated process design--A review," *Renewable and Sustainable Energy Reviews,* vol. 15, pp. 366-378, 2011.

[26] S. N. Naik, V. V. Goud, P. K. Rout, and A. K. Dalai, "Production of first and second generation biofuels: A comprehensive review," *Renewable and Sustainable Energy Reviews,* vol. 14, pp. 578-597, 2010.

[27] W. Yang, A. Ponzio, C. Lucas, and W. Blasiak, "Performance analysis of a fixed-bed biomass gasifier using high-temperature air," *Fuel Processing Technology,* vol. 87, pp. 235 – 245, 2006.

[28] J. N. D. Silva, "Tar Formation in Corncob Gasification," Ph.D. 8423427, Purdue University, United States, 1984.

[29] T. B. Reed and A. Das, *Handbook of biomass downdraft gasifier engine system*. Golden, Colorado, 1988.

[30] M. Dogru, C. R. Howarth, G. Akay, B. Keskinler, and A. A. Malik, "Gasification of hazelnut shells in a downdraft gasifier," *Energy,* vol. 27, pp. 415-427, 2002.

[31] F. Department, "Wood Gas as Engine Fuel," in *FAO Forestry Paper*, ed, 1986.

[32] C. Sheng and J. L. T. Azevedo, "Estimating the higher heating value of biomass fuels from basic analysis data," *Biomass and Bioenergy,* vol. 28, pp. 499-507, 2005.

[33] A. Friedl, E. Padouvas, H. Rotter, and K. Varmuza, "Prediction of heating values of biomass fuel from elemental composition," *Analytica Chimica Acta,* vol. 544, pp. 191-198, 2005.

[34] A. Demirbas, "Calculation of higher heating values of biomass fuels," *Fuel,* vol. 76, pp. 431-434, 1997.

[35] C.-Y. Yin, "Prediction of higher heating values of biomass from proximate and ultimate analyses," *Fuel,* vol. 90, pp. 1128-1132, 2011.

[36] R. Saidur, E. A. Abdelaziz, A. Demirbas, M. S. Hossain, and S. Mekhilef, "A review on biomass as a fuel for boilers," *Renewable and Sustainable Energy Reviews,* vol. 15, pp. 2262-2289, 2011.

[37] A. Demirbas, "Relationships between lignin contents and heating values of biomass," *Energy Conversion and Management,* vol. 42, pp. 183-188, 2001.

[38] I. Rudakova, "Use of Biomass Gasification for Transport," MSc, Bioenergy technology, Lappeenranta University of Technology, 2009.

[39] C. O. Akudo, "Quantification of tars and particulates from a pilot scale, downdraft biomass gasifier," MSc, Biological and Agricultural Engineering, Federal University of Technology Minna, 2008.

[40] P. McKendry, "Energy production from biomass (part 3): gasification technologies," *Bioresource Technology*, vol. 83, pp. 55-63, 2002.

[41] T. L. Kelly-Yong, K. T. Lee, A. R. Mohamed, and S. Bhatia, "Potential of hydrogen from oil palm biomass as a source of renewable energy worldwide," *Energy Policy*, vol. 35, pp. 5692-5701, 2007.

[42] M. A. A. S. Mohammed, A. and W. A. K. G. M. A. Wan Azlina, M. S. Fakhru'l-Razi, A., "Air gasification of empty fruit bunch for hydrogen-rich gas production in a fluidized-bed reactor," *Energy Conversion and Management*, vol. 52, pp. 1555-1561, 2011.

[43] R. F. Razuan, K. N. Chen, Q. Sharifi, V. N. Swithenbank, J., "Pelletised fuel production from palm kernel cake," *Fuel Processing Technology*, vol. 92, pp. 609-615, 2011.

[44] C. S. Goh, K. T. Lee, and S. Bhatia, "Hot compressed water pretreatment of oil palm fronds to enhance glucose recovery for production of second generation bio-ethanol," *Bioresource Technology*, vol. 101, pp. 7362-7367, 2010.

[45] M. A. Zahari, M. R. Zakaria, H. Ariffin, M. N. Mokhtar, J. Salihon, Y. Shirai, *et al.*, "Renewable sugars from oil palm frond juice as an alternative novel fermentation feedstock for value-added products," *Bioresource Technology*, vol. 110, pp. 566-571, 2012.

[46] M. M. Rahman, M. Lourenço, H. A. Hassim, J. J. P. Baars, A. S. M. Sonnenberg, J. W. Cone, *et al.*, "Improving ruminal degradability of oil palm fronds using white rot fungi," *Animal Feed Science and Technology*, vol. 169, pp. 157-166, 2011.

[47] http://oilpalmproducts.com/index_files/PalmBurning.htm.

[48] P. Joseph and S. M. Tretsiakova-McNally, S., "Characterization of cellulosic wastes and gasification products from chicken farms," *Waste Management*, vol. 32, pp. 701-709, 2012.

[49] A. C. Caputo, M. Palumbo, P. M. Pelagagge, and F. Scacchia, "Economics of biomass energy utilization in combustion and gasification plants: effects of logistic variables," *Biomass and Bioenergy*, vol. 28, pp. 35-51, 2005.

[50] W. D. Wanrosli, Z. Zainuddin, K. N. Law, and R. Asro, "Pulp from oil palm fronds by chemical processes," *Industrial Crops and Products,* vol. 25, pp. 89-94, 2007.

[51] S. Sabiha-Hanim, M. A. Noor, and A. Rosma, "Effect of autohydrolysis and enzymatic treatment on oil palm (Elaeis guineensis Jacq.) frond fibres for xylose and xylooligosaccharides production," *Bioresource Technology,* vol. 102, pp. 1234–1239, 2011.

[52] J. M. Salman and B. H. Hameed, "Effect of preparation conditions of oil palm fronds activated carbon on adsorption of bentazon from aqueous solutions," *Journal of Hazardous Materials,* vol. 175, pp. 133-137, 2010.

[53] M. L. Hobbs, "Modeling countercurrent fixed-bed coal gasification," Ph.D. 9108050, Department of Chemical Engineering, Brigham Young University, 1990.

[54] A. Midilli, M. Dogru, G. Akay, and C. R. Howarth, "Hydrogen production from sewage sludge via a fixed bed gasifier product gas," *International Journal of Hydrogen Energy,* vol. 27, pp. 1035-1041, 2002.

[55] H. Ahmad, N. A. Farid, N. D. Amer, M. Hamdan, A. Saiful, and A. M., "Thermochemical Behaviour of Empty Fruit Bunches and Oil Palm Shell Waste in A Circulating Fluidized-Bed Combustor (CFBC)," *Journal of Oil Palm Research,* vol. 18, pp. 210 - 218, 2006.

[56] A. D. Abuadala, I. Naterer, G. F., "Exergy analysis of hydrogen production from biomass gasification," *International Journal of Hydrogen Energy,* vol. 35, pp. 4981-4990, 2010.

[57] M. R. Mahishi and D. Y. Goswami, "Thermodynamic optimization of biomass gasifier for hydrogen production," *International Journal of Hydrogen Energy,* vol. 32, pp. 3831-3840, 2007.

[58] C. D. Blasi, G. Signorelli, and G. Portoricco, "Countercurrnt Fixed-bed Gasification of Biomass at Laboratory Scale," *Ind. Eng. Chem,* vol. 38, pp. 2571 - 2581, 1999.

[59] A. Midilli, M. Dogru, C. R. Howarth, M. J. Ling, and T. Ayhan, "Combustible gas production from sewage sludge with a downdraft gasifier," *Energy Conversion and Management,* vol. 42, pp. 157-172, 2001.

[60] P. McKendry, "Energy production from biomass (part 2): conversion technologies," *Bioresource Technology,* vol. 83, pp. 47-54, 2002.

[61] A. Dufour, P. Girods, E. Masson, Y. Rogaume, and A. Zoulalian, "Synthesis gas production by biomass pyrolysis: Effect of reactor temperature on product distribution," *International Journal of Hydrogen Energy,* vol. 34, pp. 1726-1734, 2009.

[62] P. Basu, *Combustion and Gasification in Fluidized Beds*: CRC Press,Taylor & Francis Group, 2006.

[63] P. Jared, J. Ciferno, and J. Marano. (2002). *Benchmarking Biomass Gasification Technologies for Fuels, Chemicals and Hydrogen Production*.

[64] J. M. Lin, "Development of an Updraft Fixed Bed Gasifier with an Embedded Combustor Fed by Solid Biomass " *Journal of the Chinese Institute of Engineers,* vol. 29, pp. 557-562, 2006.

[65] P. Plis and R. K. Wilk, "Theoretical and experimental investigation of biomass gasification process in a fixed bed gasifier," *Energy,* vol. 6, pp. 3838–3845, 2011.

[66] G. Pilon, "Utilization of Arecanut (Areca catechu) Husk for Gasification," MSc, Department of Bioresource Engineering, McGill University, Montreal, 2007.

[67] L. Hu, X. Wang, G. Yu, F. Wang, and Z. Yu, "Study on gas-liquid phase mass transfer coefficient of entrained flow reactor," *Chemical Engineering Journal,* vol. 141, pp. 278-283, 2008.

[68] J. Zhou, Q. Chen, H. Zhao, X. Cao, Q. Mei, Z. Luo, *et al.*, "Biomass-oxygen gasification in a high-temperature entrained-flow gasifier," *Biotechnology Advances,* vol. 27, pp. 606-611, 2009.

[69] M. Gabra, A. Nordin, M. Öhman, and B. Kjellström, "Alkali retention/separation during bagasse gasification: a comparison between a fluidised bed and a cyclone gasifier," *Biomass and Bioenergy,* vol. 21, pp. 461-476, 2001.

[70] C. Syred, W. Fick, A. J. Griffiths, and N. Syred, "Cyclone gasifier and cyclone combustor for the use of biomass derived gas in the operation of a small gas turbine in cogeneration plants," *Fuel,* vol. 83, pp. 2381-2392, 2004.

[71] S. Sun, Y. Zhao, F. Ling, and F. Su, "Experimental research on air staged cyclone gasification of rice husk," *Fuel Processing Technology,* vol. 90, pp. 465-471, 2009.

[72] M. Gabra, E. Pettersson, R. Backman, and B. Kjellström, "Evaluation of cyclone gasifier performance for gasification of sugar cane residue: Part 1: gasification of bagasse," *Biomass and Bioenergy,* vol. 21, pp. 351-369, 2001.

[73] M. Moghiman, T. Hashemi, I. Zahmatkesh, and Y. Daghighi, "Effects of particle size and equivalence ratio on cyclone gasification of wood powder," *Journal of the Energy Institute,* vol. 80, pp. 29 - 34, 2007.

[74] C. Mandl, I. Obernberger, and F. Biedermann, "Modelling of an updraft fixed-bed gasifier operated with softwood pellets," *Fuel,* vol. 89, p. 3795, 2010.

[75] F. A. Payne, "The Conversion of Corncobs into Thermal Energy for Drying Grain using A gasification and Combustion Process," PhD, University of Kentucky, 1980.

[76] G. Gordillo, K. Annamalai, and N. Carlin, "Adiabatic fixed-bed gasification of coal, dairy biomass, and feedlot biomass using an air-steam mixture as an oxidizing agent," *Renewable Energy,* vol. 34, pp. 2789-2797, 2009.

[77] P. Mathieu and R. Dubuisson, "Performance analysis of a biomass gasifier," *Energy Conversion and Management,* vol. 43, pp. 1291-1299.

[78] Y. J. Kim, Y. K. Kang, Y. S. Ryou, G. C. Kang, and Y. Paek, "Gasification Characteristics of Rice Husks in Batch Operation," *Agri. & Biosys. Eng,* vol. 8, pp. 1 - 5, 2007.

[79] A. Abuadala and I. Dincer, "Efficiency evaluation of dry hydrogen production from biomass gasification," *Thermochimica Acta,* vol. 507–508, pp. 127-134, 2010.

[80] S. Kalisz, R. Abeyweera, D. Szewczyk, A. Jansson, C. Lucas, and W. Blasiak, "Energy Balance of High Temperature Air/Steam Gasification of Biomass in Up-Draft, Fixed Bed Type Gasifier," presented at the IT3'04 Conference, Phoenix, Arizona, 2004.

[81] K. Umeki, K. Yamamoto, T. Namioka, and K. Yoshikawa, "High temperature steam-only gasification of woody biomass," *Applied Energy,* vol. 87, pp. 791-798, 2010.

[82] G. Gautam, "Parametric Study of a Commercial-Scale Biomass Downdraft Gasifier: Experiments and Equilibrium Modeling," MSc, Graduate Faculty, Auburn University, 2010.

[83] S. Priyadarsan, K. Annamalai, J. M. Sweeten, M. T. Holtzapple, and S. Mukhtar, "Co-gasification of blended coal with feedlot and chicken litter biomass," *Proceedings of the Combustion Institute,* vol. 30, pp. 2973–2980, 2005.

[84] M. S. Rao, S. P. Singh, M. S. Sodha, A. K. Dubey, and M. Shyam, "Stoichiometric, mass, energy and exergy balance analysis of countercurrent fixed-bed gasification of post-consumer residues," *Biomass and Bioenergy,* vol. 27, pp. 155 – 171, 2004.

[85] D. Khummongkol and W. Arunlaksadamrong, "Performance of an updraft mangrove-wood gasifier," *Energy,* vol. 15, pp. 781 - 784, 1990.

[86] A. Saravanakumar, T. M. Haridasan, T. B. Reed, and R. K. Bai, "Operation and modelling of an updraft long-stick wood gasifier," *Energy for Sustainable Development,* vol. 9, p. 25, 2005.

[87] A. Saravanakumar, T. M. Haridasan, T. B. Reed, and R. K. Bai, "Experimental investigation and modelling study of long stick wood gasification in a top lit updraft fixed bed gasifier," *Fuel,* vol. 86, p. 2846, 2007.

[88] A. Saravanakumar, T. M. Haridasan, T. B. Reed, and R. K. Bai, "Experimental investigations of long stick wood gasification in a bottom lit updraft fixed bed gasifier," *Fuel Processing Technology,* vol. 88, pp. 617–622, 2007.

[89] S. Luo, B. Xiao, Z. Hu, S. Liu, X. Guo, and M. He, "Hydrogen-rich gas from catalytic steam gasification of biomass in a fixed bed reactor: Influence of particle size on gasification performance," *International Journal of Hydrogen Energy,* vol. 34, pp. 1260-1264, 2009.

[90] C. Franco, F. Pinto, I. Gulyurtlu, and I. Cabrita, "The study of reactions influencing the biomass steam gasification process " *Fuel,* vol. 82, pp. 835-842, 2003.

[91] T. Hanaoka, T. Yoshida, S. Fujimoto, K. Kamei, M. Harada, Y. Suzuki, *et al.*, "Hydrogen production from woody biomass by steam gasification using a CO2 sorbent," *Biomass and Bioenergy,* vol. 28, pp. 63-68, 2005.

[92] A. Abuadala and I. Dincer, "Efficiency evaluation of dry hydrogen production from biomass gasification," *Thermochimica Acta,* vol. 507-508, pp. 127-134, 2010.

[93] A. Haryanto, S. D. Fernando, L. O. Pordesimo, and S. Adhikari, "Upgrading of syngas derived from biomass gasification: A thermodynamic analysis," *Biomass and Bioenergy,* vol. 33, pp. 882-889, 2009.

[94] E. Kurkela, P. Ståhlberg, P. Simell, and J. Leppälahti, "Updraft gasification of peat and biomass," *Biomass,* vol. 19, pp. 37-46, 1989.

[95] T. K. Kayal, M. Chakravarty, and G. K. Biswas, "Mathematical modelling of continuous updraft gasification of bundled jute stick -- a low ash content woody biomass," *Bioresource Technology,* vol. 49, pp. 61-73, 1994.

[96] T. K. Kayal, M. Chakravarty, and G. K. Biswas, "Mathematical modelling of steady state updraft gasification of jute stick particles of definite sizes packed randomly -- An analytical approach," *Bioresource Technology,* vol. 60, pp. 131-141, 1997.

[97] C. Lucas, D. Szewczyk, W. Blasiak, and R. Abeyweera, "Gasification of Biomass Wastes in Updraft Fixed Bed Gasifier with High Temperature Air and Steam," presented at the Regional Conference on Energy Technology towards a Clean Environment, Phuket, Thailand, 2003.

[98] J. I. Na, S. J. Park, Y. K. Kim, J. G. Lee, and J. H. Kim, "Characteristics of oxygen-blown gasification for combustible waste in a fixed-bed gasifier," *Applied Energy,* vol. 75, pp. 275–285, 2003/8// 2003.

[99] S. C. Kalisz, A. J. Lucas, and W. Blasiak, "Continuous High Temperature Air/steam Gasification (HTAG) of Biomass," presented at the 6th Int. Conference on Science in Thermal and Chemical Biomass Conversion, Victoria, Canada, 2004.

[100] P. V. Ramana, R. N. Singh, and K. N. Patil, "Development and performance evaluation of a producer gas based system for hardening of steels," *Renewable Energy,* vol. 30, pp. 773-782, 2005.

[101] C. Mandl, I. Obernberger, and I. R. Scharler, "Characterisation of fuel bound nitrogen in the gasification process and the staged combustion of producer gas from the updraft gasification of softwood pellets," *Biomass and Bioenergy,* vol. 35, pp. 4595-4604, 2011.

[102] S. S. Thanapal, K. Annamalai, J. M. Sweeten, and G. Gordillo, "Fixed bed gasification of dairy biomass with enriched air mixture," *Applied Energy,* vol. 97, pp. 525–531, 2012.

[103] Y. Ueki, T. Torigoe, H. Ono, R. Yoshiie, J. H. Kihedu, and I. Naruse, "Gasification characteristics of woody biomass in the packed bed reactor," *Proceedings of the Combustion Institute,* vol. 33, pp. 1795-1800, 2011.

[104] W. Chen, K. Annamalai, R. J. Ansley, and M. M., "Updraft fixed bed gasification of mesquite and juniper wood samples," *Energy,* vol. 41, pp. 454-461, 2012.

[105] M. Seggiani, S. Vitolo, M. Puccini, and A. Bellini, "Cogasification of sewage sludge in an updraft gasifier," *Fuel,* vol. 93, pp. 486-491, 2012.

[106] J. Li, Y. Yin, X. Zhang, J. Liu, and R. Yan, "Hydrogen-rich gas production by steam gasification of palm oil wastes over supported tri-metallic catalyst," *International Journal of Hydrogen Energy,* vol. 34, pp. 9108-9115, 2009.

[107] S. Rowland, "Design and Testing of A Small-Scale Updraft Gasifier for Gasification of Eastern Redcdar," MSc, Biosystems and Agricultural Engineering, Oklahoma State University, 2008.

[108] S. V. B. Paasen, M. K. Cieplik, and N. P. Phokawat, "Gasification of Non-woody Biomass: Economic and Technical Perspectives of Chlorine and Sulphur Removal from Product Gas," Energy Research Center of the Netherland2006.

[109] C. Xu, J. Donald, E. Byambajav, and Y. Ohtsuka, "Recent advances in catalysts for hot-gas removal of tar and NH3 from biomass gasification," *Fuel,* vol. 89, pp. 1784–1795, 2010.

[110] T. A. Milne and R. J. Evans, "Biomass Gasifier “Tars”: Their Nature, Formation, and Conversion," National Renewable Energy Laboratory, Golden, Colorado, USA 1998.

[111] R. Aldas, "Integrated bioenergy conversion concepts for small scale gasification power systems," PhD 3362471, University of California, Davis, United States, California, 2009.

[112] Y. Cao, Y. Wang, J. T. Riley, and W. P. Pan, "A novel biomass air gasification process for producing tar-free higher heating value fuel gas," *Fuel Processing Technology,* vol. 87, pp. 343-353, 2006.

[113] Y. G. Pan, X. Roca, E. Velo, and L. Puigjaner, "Removal of tar by secondary air in fluidised bed gasification of residual biomass and coal," *Fuel*, vol. 78, pp. 1703-1709, 1999.

[114] T. A. Hoeven, "Partial product gas combustion for tar reduction," PhD, Eindhoven University of Technology, 2007.

[115] V. Fajri, S. Adi, and S. N. Yulianto, "CFD Analysis of External Recirculation Flow at Updraft Gasifier Using Ejector," presented at the The 4th International Meeting of Advances in Thermofluids, Melaka, Malaysia, 2011.

[116] D. T. Pedroso, E. B. Machín, J. L. Silveira, and Y. Nemoto, "Experimental study of bottom feed updraft gasifier," *Renewable Energy,* vol. 57, pp. 311-316, 2013.

[117] N. S. Rathore, N. L. Panwar, and Y. C. Vijay, "Design and techno economic evaluation of biomass gasifier for industrial thermal applications," *African Journal of Environmental Science and Technology,* vol. 3, pp. 6 - 12, 2009.

[118] N. L. Panwar and N. S. Rathore, "Design and performance of a 5 kW producer gas stove," *Biomass and bioenergy,* vol. 32, pp. 1349 – 1352, 2008.

[119] A. T. Belonio and P. S. Anderson, *Rice husk gas stove handbook*: Appropriate Tehcnology Center Central Philippine University, Iloilo City, Philippines, 2005.

[120] P. Basu, *Biomass Gasification and Pyrolysis: Practical Design and Theory*: Elsevier Inc, 2010.

[121] L. Wang, "Theoritical Study of Cyclone Design," PhD, Biological & Agricultural Engineering, Texas A&M University, 2004.

[122] A. Chouchene, M. Jeguirim, B. Khiari, F. Zagrouba, and G. Trouvé, "Thermal degradation of olive solid waste: Influence of particle size and oxygen concentration," *Resources, Conservation and Recycling,* vol. 54, pp. 271-277, 2010.

[123] I. Mohoriè, M. Krajnc, and U. Šebenik, "Model-free Kinetics Analysis of Thermal Degradation of Polysiloxane Lubricant," *Chem. Biochem.*, vol. 23, pp. 493–496, 2009.

[124] A. Khawam, "Application of solid-state kinetics to desolvation reactions," PhD, University of Iowa, 2007.

[125] M. Z. Sphoorti Srivastava, A. K., "Study of Crystallization Kinetics in Glassy Se100-xBix Using Iso-Conversional Methods " *Journal of Non-Oxide Glasses,* vol. 2, 2010.

[126] T. Ozawa, "A new method of analyzing thermogravimetric data," *Chem. Soc. Jpn,* vol. 38, pp. 1881–1886, 1965.

[127] A. K. Galway and M. E. Brown. (1999). *Studied in physical and theortical chimistry: Thermal decomposition of ionic solids*.

[128] M. Otero, L. F. Calvo, M. V. Gil, A. I. Garcıa, and A. Moran, "Co-combustion of different sewage sludge and coal: A non-isothermal thermogravimetric kinetic analysis," *Bioresource Technology,* vol. 99, 2008.

[129] M. A. El-Oyoun, "An investigation of the kinetic transformation mechanism of Ge12.5Te87.5 chalcogenide glass under non-isothermal regime," *Journal of Non-Crystalline Solids,* vol. 357, pp. 1729-1735, 2011.

[130] H.-M. Xiao, X.-Q. Ma, and Z.-Y. Lai, "Isoconversional kinetic analysis of co-combustion of sewage sludge with straw and coal," *Applied Energy,* vol. 86, pp. 1741-1745, 2009.

[131] K. A. Ross, A. Leung, D. V. Godfrey, and G. Mazza, "Evaluation of Thermal Decomposition and Antioxidant Activity of Crop Residues and Ionic Liquid Extracted Lignin," *World Applied Sciences Journal,* vol. 16, pp. 160-176, 2012.

[132] K. Slopiecka, P. B., and F. Fantozzi, "Thermogravimetric analysis and Kinetic study of poplar wood pyrolysis," presented at the Energy Solutions for a Sustainable World - Proceedings of the Third International Perugia, Italy, 2012.

[133] Z. A. Zainal, A. Rifau, G. A. Quadir, and K. N. Seetharamu, "Experimental investigation of a downdraft biomass gasifier," *Biomass and Bioenergy,* vol. 23, pp. 283-289, 2002.

[134] F. Ju, H. Chen, H. Yang, X. Wang, S. Zhang, and D. Liu, "Experimental study of a commercial circulated fluidized bed coal gasifier," *Fuel Processing Technology,* vol. 91, pp. 818-822, 2010.

[135] Q. Zhang, D. Liran, D. Fenigshtein, W. Yang, and W. Blasiak, "Gasification of municipal solid waste in the Plasma Gasification Melting process," *Applied Energy,* vol. 90, pp. 106-112, 2012.

[136] K. Jaojaruek, S. Jarungthammachote, M. K. B. Gratuito, H. Wongsuwan, and S. Homhual, "Experimental study of wood downdraft gasification for an improved producer gas quality through an innovative two-stage air and

premixed air/gas supply approach," *Bioresource Technology,* vol. 102, pp. 4834-4840, 2011.

[137] J. W. Anthony and R. G. Ahmad, *Introduction to Engineering Experimentation*, Second Edition ed.: Pearson Education, Inc., 2004.

[138] M. Dogru, A. Midilli, and C. R. Howarth, "Gasification of sewage sludge using a throated downdraft gasifier and uncertainty analysis," *Fuel Processing Technology,* vol. 75, pp. 55-82, 2002.

[139] M. A. A. Mohammed, A. Salmiaton, W. A. K. G. Wan Azlina, and M. S. Amran, "Gasification of oil palm empty fruit bunches: A characterization and kinetic study," *Bioresource Technology,* vol. 110, pp. 628-636, 2012.

[140] M. A. Sukiran, L. S. Kheang, N. A. Bakar, and C. Y. May, "Production and Characterization of Bio-Char from the Pyrolysis of Empty Fruit Bunches," *American Journal of Applied Sciences* vol. 8, pp. 984-988, 2011.

[141] P. Lahijani and Z. A. Zainal, "Gasification of palm empty fruit bunch in a bubbling fluidized bed: A performance and agglomeration study," *Bioresource Technology,* vol. 102, pp. 2068-2076, 2011.

[142] M. Grube, J. G. Lin, P. H. Lee, and S. Kokorevicha, "Evaluation of sewage sludge-based compost by FT-IR spectroscopy," *Geoderma,* vol. 130, pp. 324-333, 2006.

[143] S. B. Azhari, A. A. R. Nor', K. M. S. Umi, A. H. Mohd, W. Minato, and S. Yoshihito, "Evaluation of pressed shredded empty fruit bunch (EFB)-palm oil mill effluent (POME) anaerobic sludge based compost using Fourier transform infrared (FTIR) and nuclear magnetic resonance (NMR) analysis," *African Journal of Biotechnology*, vol. 41, pp. 8082-8089, 2011.

[144] M. A. Miskam, "Performance Characteristic of a Cyclone Gasifier for Power Generation," MSc, Mechanical Department, Universiti Sains Malaysia, 2008.

[145] M. Lapuerta, J. J. Hernández, and J. Rodríguez, "Kinetics of devolatilisation of forestry wastes from thermogravimetric analysis," *Biomass and Bioenergy,* vol. 27, pp. 385-391, 2004.

[146] K. G. Mansarary and A. E. Ghaly, "Thermal Degradation of Rice Husk in Nitrogen Atmosphere," *Bioresourse Technology,* vol. 65, 1998.

[147] A. Kumar, "Biomass Thermochemical Gasification: Experimental Studies and Modeling," PhD, Agricultural and Biological Systems Engineering, University of Nebraska, 2009.

[148] R. J. Evans, R. A. Knight, M. Onischak, and S. P. Babu "Development of biomass gasification to produce substitute fuels," Institute of gas technology, Pacific Northwest Laboratory Richland, Washington1988.

[149] H. Yang, R. Yan, H. Chen, D. H. Lee, and C. Zheng, "Characteristics of hemicellulose, cellulose and lignin pyrolysis," *Fuel*, vol. 86, pp. 1781-1788, 2007.

[150] Z. Khan, S. Yusup, and M. M. Ahmad, "Thermogravimetric analysis of palm oil wastes decomposition," presented at the IEEE first conference on clean and energy technology (CET), 2011.

[151] P. T. Luangkiattikhun, C. Tangsathitkulchai, M., "Non-isothermal thermogravimetric analysis of oil-palm solid wastes," *Bioresource Technology*, vol. 99, pp. 986-997, 2008.

[152] L. Sangmook and S. J. Byung, "Thermal Degradation Kinetics of Antimicrobial Agent, Poly(hexamethylene guanidine) Phosphate," *Macromolecular Research*, vol. 14, 2006.

[153] H. Ahmad, N. A. Farid, N. Amer, and A. Zainal, "Thermogravimetric and Thermochemical Studies of Malaysian Oil Palm Shell Waste," *Jurnal Teknologi*, vol. 45, pp. 43–53, 2006.

[154] H. Chen, "Integarted Analysis of Biomass Gasification in Fluidized Beds," PhD, Department of Chemical and Biochemical Engineering, The University of Western Ontario, 2007.

[155] X. Guo, B. Xiao, S. Liu, Z. Hu, S. Luo, and M. He, "An experimental study on air gasification of biomass micron fuel (BMF) in a cyclone gasifier," *International Journal of Hydrogen Energy*, vol. 34, pp. 1265-1269, 2009.

[156] K. N. Sheeba, J. S. C. Babu, and S. Jaisankar, "Air gasification characteristics of coir pith in a circulating fluidized bed gasifier," *Energy for Sustainable Development*, vol. 13, pp. 166-173, 2009.

[157] Surabhi, G. Udaybhanu, and N. Suresh, "Characterization of Unburnt Carbon Recovered From Fly Ash by Froth Flotatioin," in *International Seminar on Mineral Processing Technology*, Chennai, India, 2006.

[158] S. Andini, R. Cioffi, F. Colangelo, T. Grieco, F. Montagnaro, and L. Santoro, "Coal fly ash as raw material for the manufacture of geopolymer-based products," *Waste Management*, vol. 28, pp. 416-423, 2008.

[159] J. Bai, W. Li, and B. Li, "Characterization of low-temperature coal ash behaviors at high temperatures under reducing atmosphere," *Fuel*, vol. 87, pp. 583-591, 2008.

LIST OF PUBLICATIONS

1. Elneel, R., A. Sulaiman, S. A and A. Bambang, 2011. Feasibility study of gasification oil palm fronds in an updraft gasifier. Proceedings of the 4th International AIP Conference, Meeting of Advances in Thermofluids, (IMAT' 11), Volume 1440, pp: 972-980, Malaka, Malaysia.

2. Guangul, F. M. and Sulaiman, S. A. and Moni, M. N. Z. and Atnaw, Samson Mekbib and Konda, R. E. (2012) Investigation of the Hygroscopic Property of Oil Palm Fronds for Gasification Process. In: 3rd International Conference on Production, Energy and Reliability, 12-14 June 2012, Kuala Lumpur, Malaysia.

3. Konda, R. E. and Sulaiman, S. A. and Ariwahjoedi, B. Syngas production from gasification of oil palm fronds with an updraft gasifier. Journal of Applied Science, 12 (24). ISSN 1812-5654, DOI: 10.3923/jas.2012, pp: 2555-2562.

4. Guangul, F. M. and Sulaiman, S. A. and Moni, M. N. Z. and Atnaw, Samson Mekbib and Konda, R. E. (2013), Determination of the Equilibrium Moisture Content of Oil Palm Fronds Feedstock for Gasification Process. Asian Journal of Scientific Research, 6 (2). ISSN 19921454, DOI: 10.3923/ajsr.2013, pp. 360-366.

5. Ramzy E. Konda, Sulaiman, S. A. Bambang Ariwahjoedi, Prediction of Heating Values of Oil Palm Fronds from Ultimate Analysis. J. Applied Science, 13 (3). ISSN 1812-5654 DOI: 10.3923/jas.2013, pp: 491-496.

6. Shaharin A. Sulaiman, Nor Hazwani Mat Razali, Ramzy E. Konda, Samson M. Atnaw and Mohd Nazmi Z. Moni. On Diversification of Feedstocks in Gasification of Oil Palm Fronds. In: 2nd International Conference on Mechanical Engineering Research (ICMER2013), 1-3 July 2013, Pahang, Malaysia.

APPENDIX A

EXPERIMENTAL DATA FOR OPF CHARACTERIZATION

Table A.1 Experimental results of drying OPF

Time (h)	Tip part		Middle part		Root part	
	Average weight loss (g)	Residual weight (%)	Average weight loss (g)	Residual weight (%)	Average weight loss (g)	Residual weight (%)
0	18.72	100	17.38	100	17.76	100
1	14.46	78.6	13.38	77.0	12.85	72.3
2	11.27	63.9	11.12	64.0	10.6	59.7
3	10.49	56.0	9.57	55.0	8.84	53.7
4	9.13	48.8	8.37	48.1	7.52	42.2
5	7.99	42.7	7.41	42.6	6.5	36.6
6	7.08	37.8	6.65	38.3	5.88	33.1
7	6.47	34.5	6.08	35.0	5.53	31.1
8	6.12	32.7	5.71	32.8	5.35	30.1
9	5.97	31.9	5.48	31.5	5.21	29.4
10	5.93	31.7	5.38	31.0	5.13	28.9
11	5.91	31.6	5.34	30.7	5.07	28.6
12	5.90	31.5	5.33	30.6	5.05	28.5
13	5.90	31.5	5.32	30.6	5.04	28.4
14	5.90	31.5	5.32	30.6	5.03	28.3
15	5.90	31.5	5.31	3.06	5.03	28.3
24	5.87	31.4	5.28	30.4	5.00	28.1

Table A.2 Experimental result of OPF proximate analysis

Sample No.	Proximate analysis (dry basis %)			
	MC	VM	FC	Ash
A	8.422	69.039	18.219	4.320
B	8.179	70.008	19.006	2.807
C	8.612	69.529	19.016	2.843
D	9.889	67.666	19.592	2.853
Average	8.776	69.061	18.958	3.026

Table A.3 Experimental result of OPF ultimate analysis and heating value

Sample No.	Ultimate analysis (dry basis %)					HHV
	C	H	N	S	O	
1	40.050	4.810	0.601	0.060	54.379	15.052
2	41.170	3.954	0.585	0.026	54.311	15.252
3	41.270	3.860	0.585	0.031	54.254	15.283
4	41.340	3.401	0.731	0.004	52.524	15.364
5	40.390	4.195	0.755	0.031	54.129	15.366
6	40.760	3.516	0.501	0.036	55.187	15.379
7	40.790	3.448	0.875	0.034	52.673	15.390
8	40.900	3.696	0.798	0.027	53.579	15.463
9	41.070	3.885	0.626	0.044	54.375	15.490
10	41.070	4.639	0.736	0.055	53.500	15.504
11	41.770	3.810	0.765	0.059	53.596	15.599
12	41.830	4.228	0.636	0.100	52.706	15.613
13	41.250	3.608	0.636	0.048	54.458	15.681
14	41.830	4.584	0.674	0.118	52.794	15.861
15	41.720	4.657	0.649	0.037	52.937	15.943
16	41.100	3.935	0.507	0.010	54.448	15.951
17	41.360	3.884	0.610	0.026	54.120	16.034
18	41.740	4.007	0.587	0.027	53.639	16.216
19	41.890	3.989	0.590	0.016	53.515	16.449
20	41.540	3.790	0.600	0.062	54.008	16.484
21	42.310	4.148	0.481	0.036	53.025	16.497
22	42.400	4.092	0.557	0.024	52.927	16.574
23	42.300	4.774	0.788	0.085	52.053	16.975
24	42.290	4.920	0.739	0.022	52.029	17.106
25	42.810	4.911	0.561	0.020	51.698	17.290
26	43.680	5.268	0.609	0.137	50.306	18.081
27	43.850	4.985	0.690	0.010	50.465	18.099
28	43.570	4.786	0.641	0.042	50.961	18.190
29	43.630	4.958	0.641	0.045	50.763	18.207
30	44.180	5.066	0.559	0.056	50.139	18.283

Table A.4 Temperature range and weight loss of OPF under nitrogen atmosphere

TG curve	Stage 2 (Active pyrolysis)		Stage 3 (Passive pyrolysis)		Remaining Weight (%)
Heating rate (^{o}C/min)	Temperature range (^{o}C)	Weight loss (%)	Temperature range (^{o}C)	Weight loss (%)	
20	251.73-392.2	58.99	392.2-860	12.33	21.15
30	254.12-398.68	59.43	398.68-860	11.57	20.63
40	262.98-407.18	58.26	407.18-860	11.31	21.03

Remaining weight is char and ash residue

Table A.5 Temperature range and weight loss of OPF under oxygen atmosphere

TG curve	Stage 2 (holocellulose degradation)		Stage 3 (Lignin degradation)		Stage 3 Char oxidation		Remaining Weight (%)
Heating rate (^{o}C/min)	Temperature range (^{o}C)	Weight loss (%)	Temperature range (^{o}C)	Weight loss (%)	Temperature range (^{o}C)	Weight loss (%)	
20	260.9-381.6	51.08	381.6-467.1	12.08	467.1-542.9	24.13	3.73
30	264.6-381.1	52.63	383.1-454	8.86	454-530.5	23.97	3.80
40	279.4-386.9	54.42	386.9-457.8	7.95	457.8-556.5	30.74	5.95

Remaining weight is ash residue

Table A.6 Temperature range and weight loss of different size of OPF under oxygen atmospherte at heating rate of 30oC/min

TG curve	Stage 2 (holocellulose degradation)		Stage 3 (Lignin degradation)		Stage 3 Char oxidation		Remaining Weight (%)
Particle size (mm)	Temperature range (^{o}C)	Weight loss (%)	Temperature range (^{o}C)	Weight loss (%)	Temperature range (^{o}C)	Weight loss (%)	
<0.212	261.1-378.6	51.8	378.6-485.4	12.99	485.4-540.4	22.03	7.07
212-325	273.6-390.9	50	390.9-486	11.68	486-562.1	23	3.86
0.6-1.18	282.7-392.8	48.77	392.8-484.7	10.75	484.7-548.3	22.33	3.62
>1.18	262-388.7	49.72	388.7-487.2	9.71	487.2-580	0.98	5.75

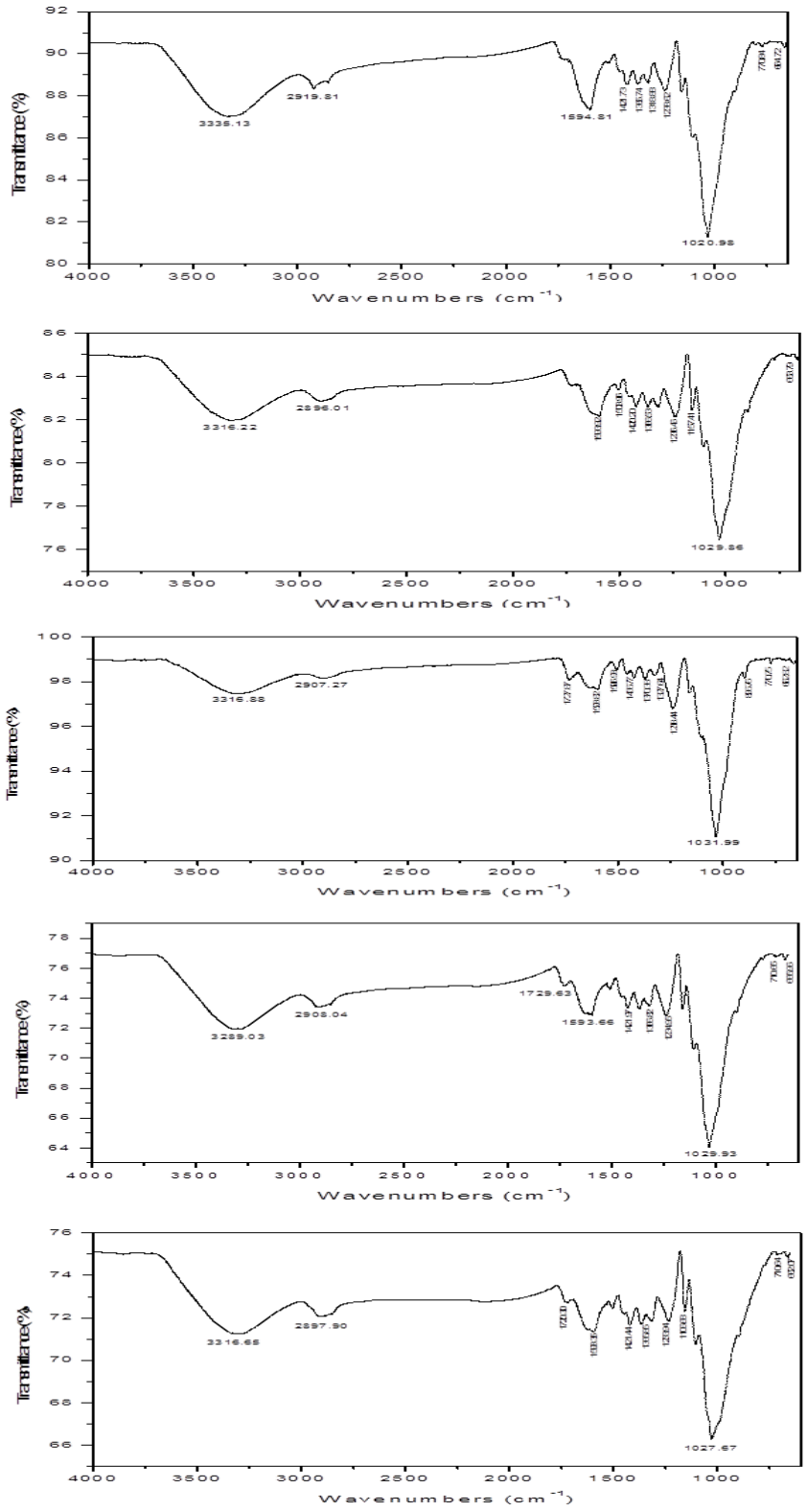

Figure A.1 Experimental result of FT-IR spectra of OPF samples

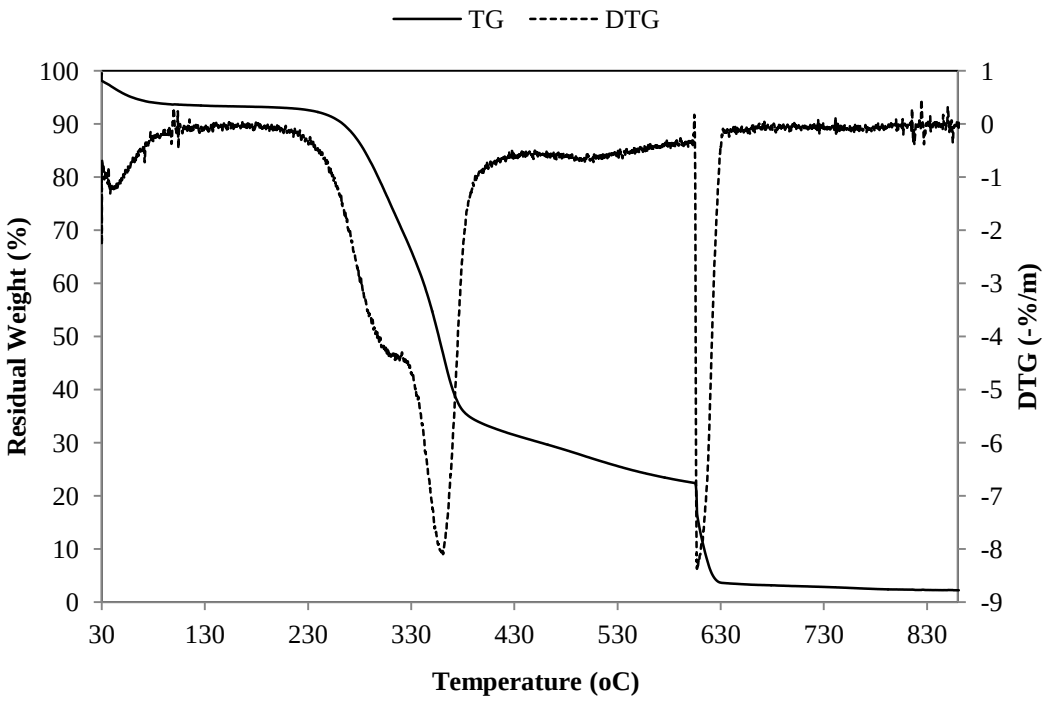

Figure A.2 Experimental result of OPF proximate analysis (sample A)

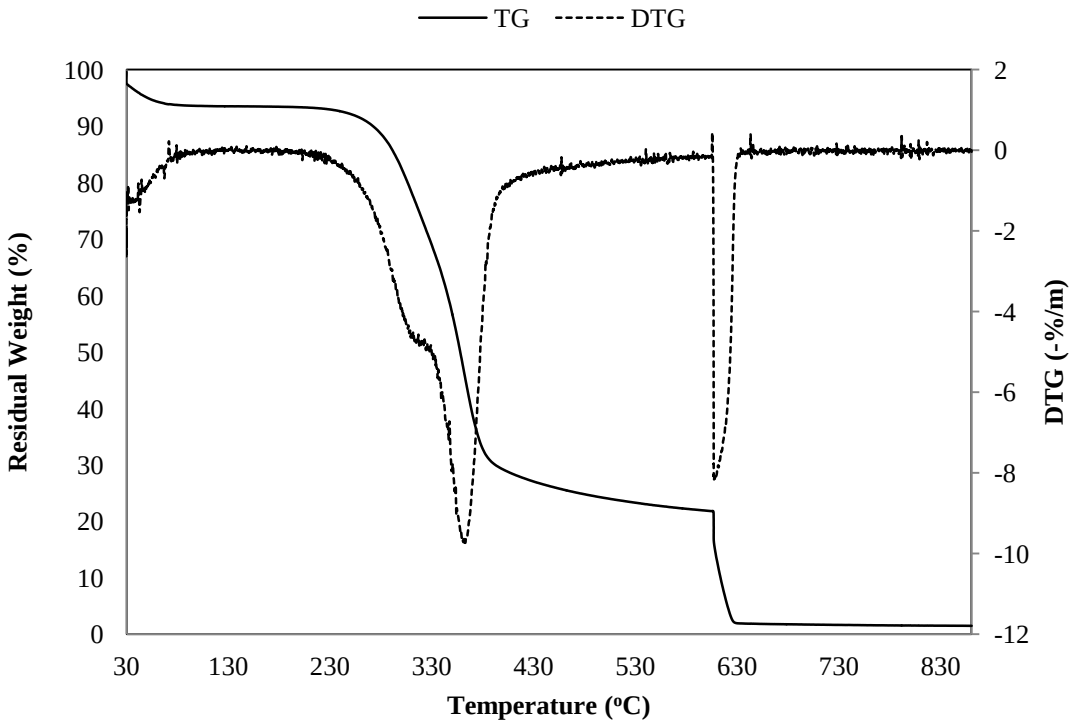

Figure A.3 Experimental result of OPF proximate analysis (sample B)

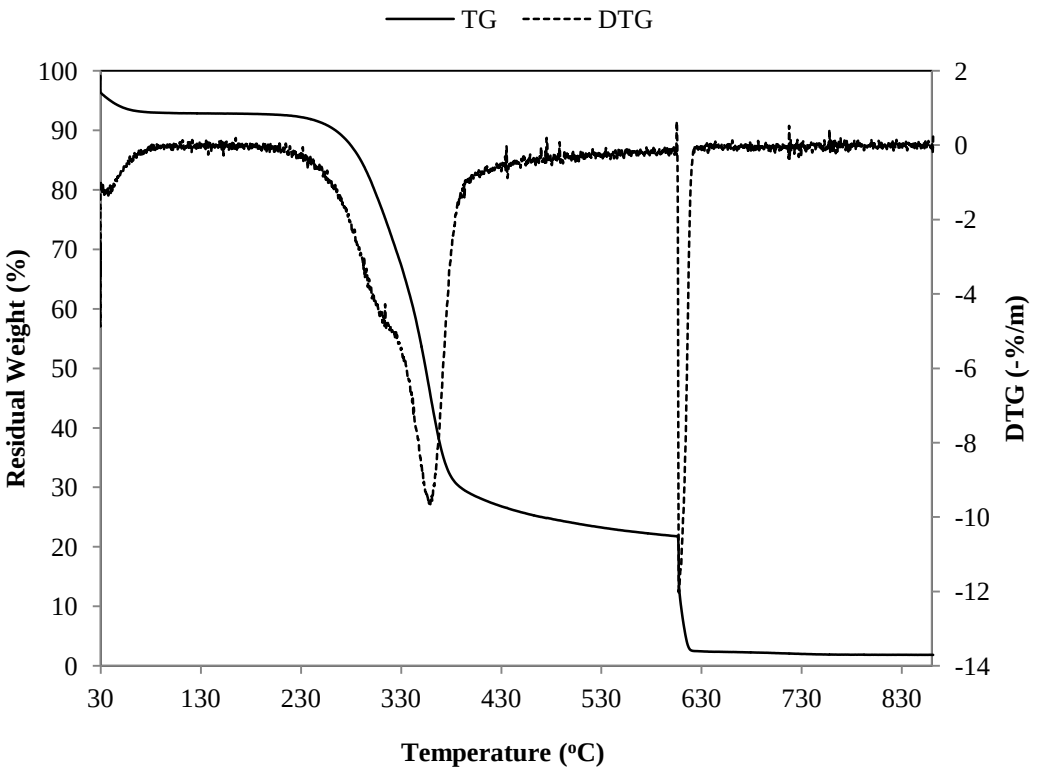

Figure A.4 Experimental result of OPF proximate analysis (sample C)

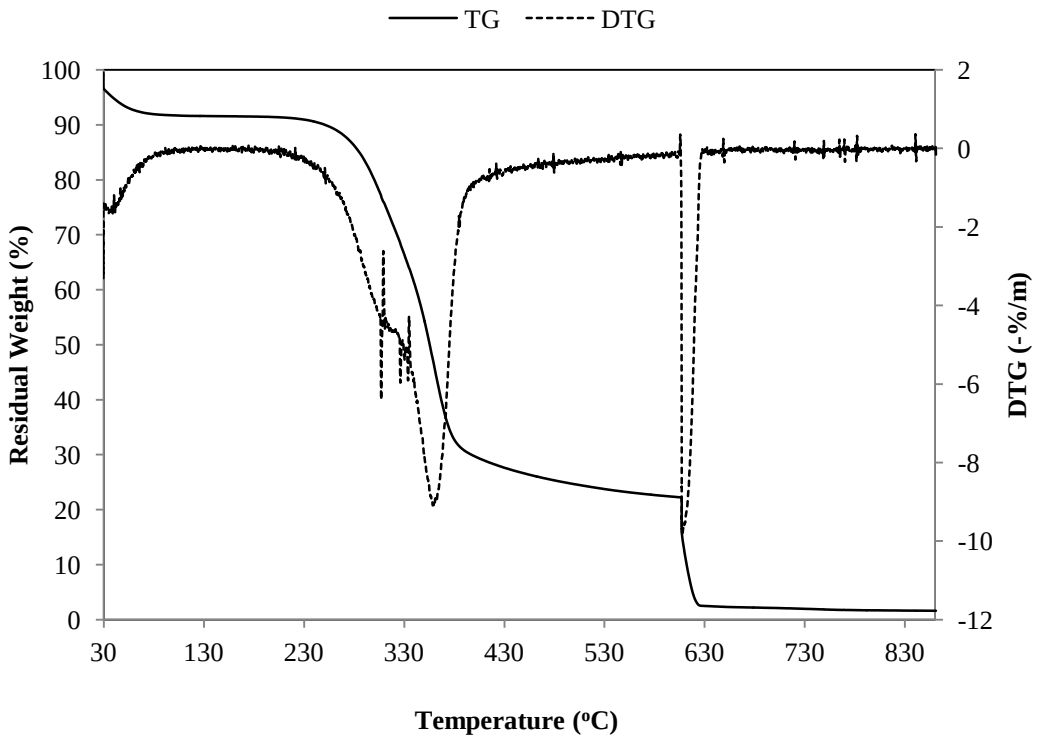

Figure A.5 Experimental result of OPF proximate analysis (sample D)

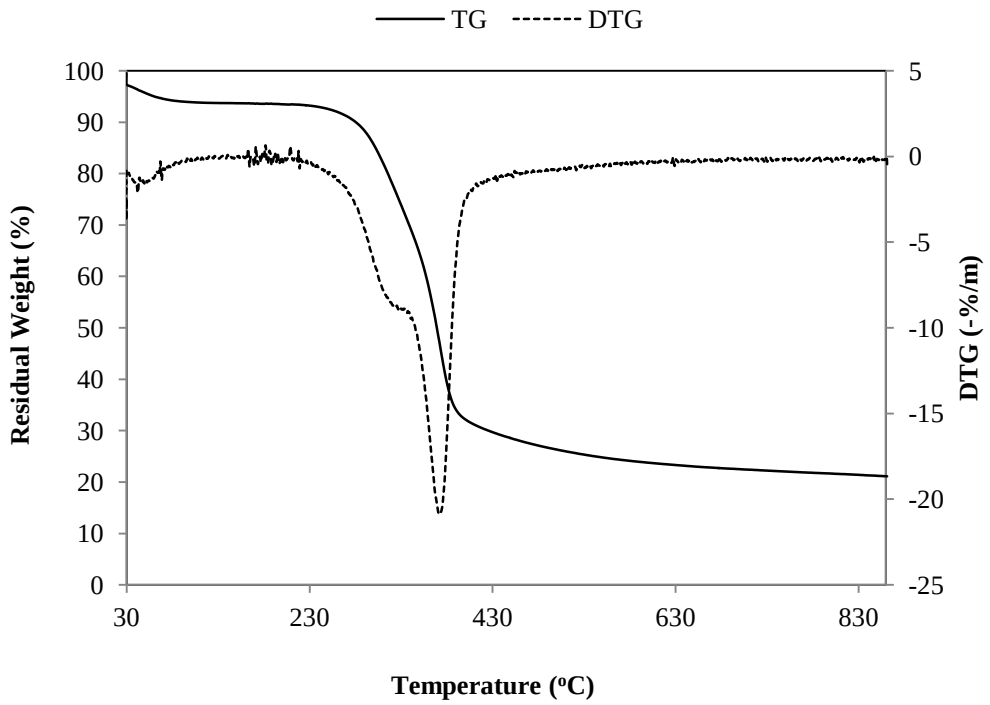

Figure A.6 Experimental result of TGA under N_2 atmosphere at heating rate of 20°C/min

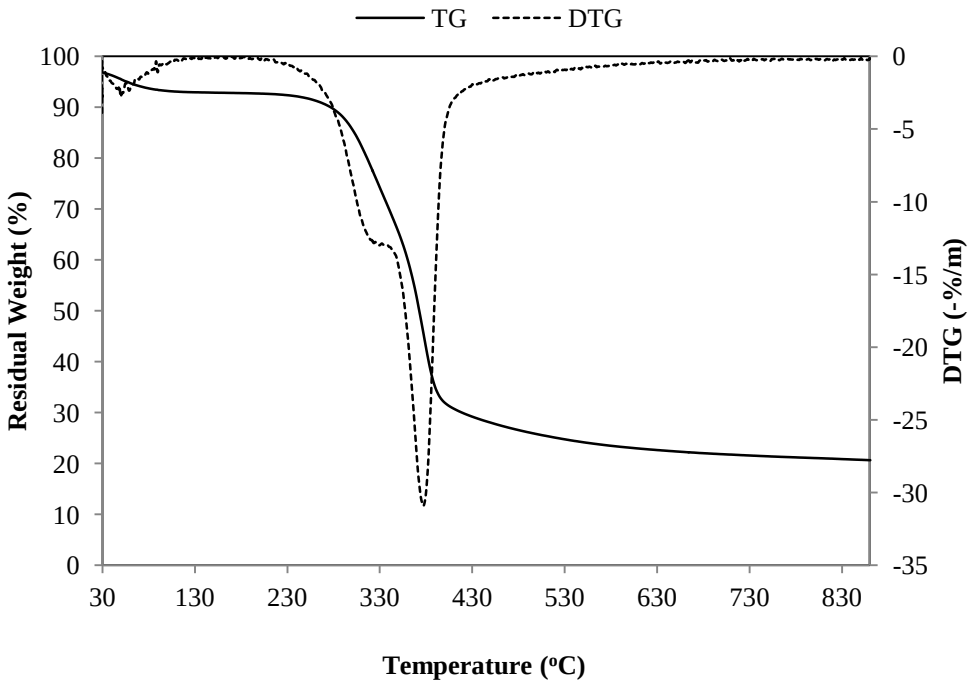

Figure A.7 Experimental result of TGA under N_2 atmosphere at heating rate of 30°C/min

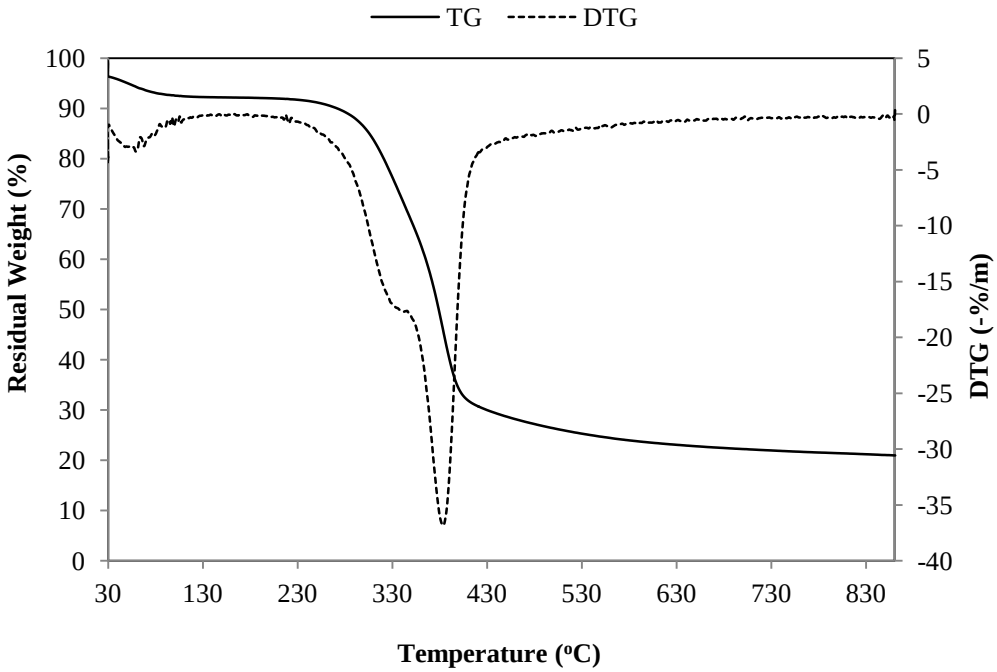

Figure A.8 Experimental result of TGA under N_2 atmosphere at heating rate of 40°C/min

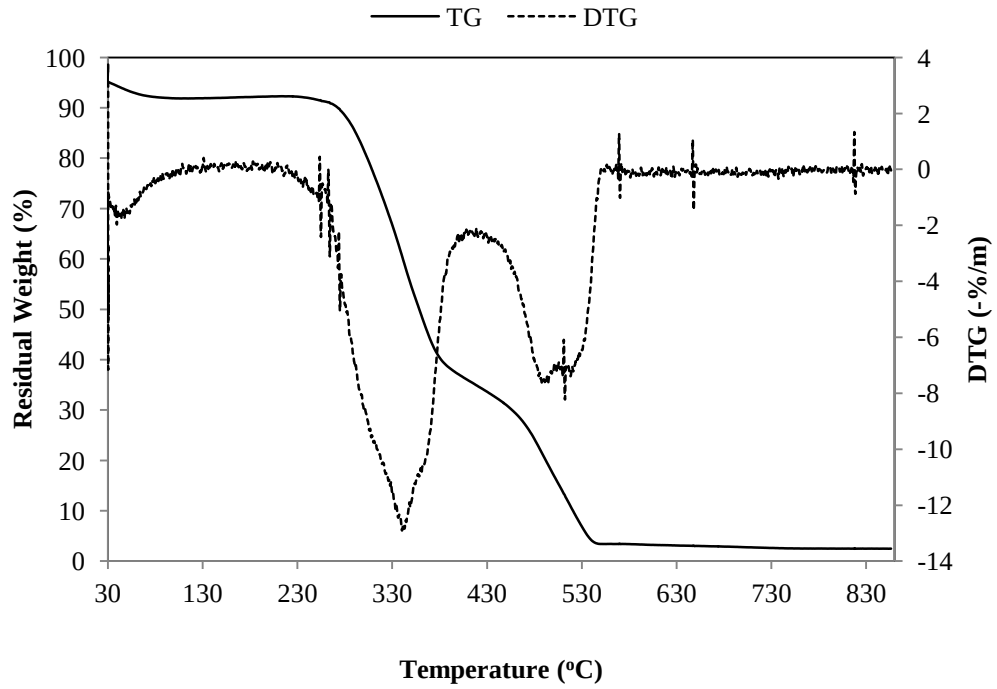

Figure A.9 Experimental result of TGA under O_2 atmosphere at heating rate of 20°C/min

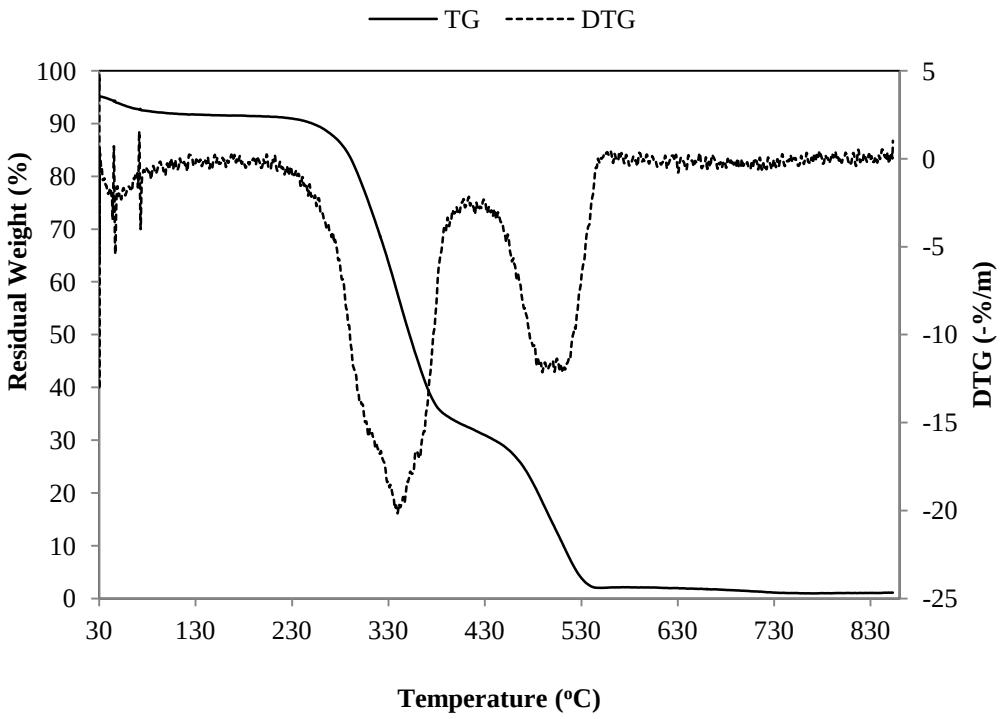

Figure A.10 Experimental result of TGA under O_2 atmosphere at heating rate of 30°C/min

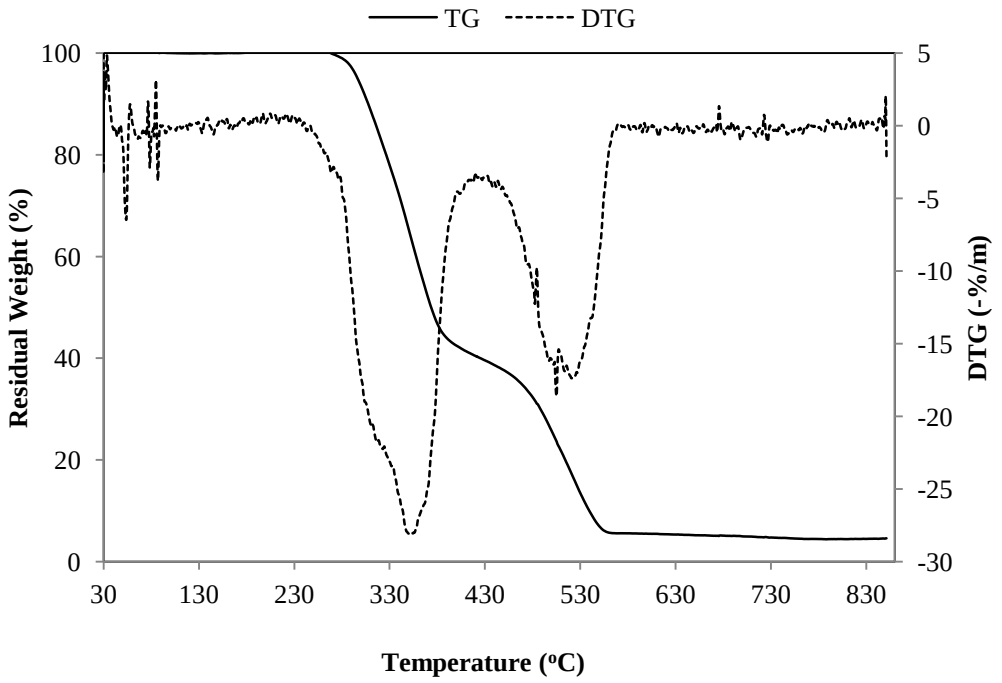

Figure A.11 Experimental result of TGA under O_2 atmosphere at heating rate of 40°C/min

APPENDIX B

EXPERIMENTAL DATA FOR OPF GASIFICATION

Table B.1 Experimental result of an average gas product composition as a function of equivalence ratio

Measured parameters.	Equivalence ratio				
	0.18	0.22	0.29	0.35	0.40
CO (vol. %)	17.73	21.09	23.10	20.20	14.17
CO_2 (vol. %)	13.97	12.27	10.63	10.70	18.87
CH_4 (vol. %)	1.36	1.47	1.20	0.91	0.29
H_2 (vol. %)	5.50	6.54	6.66	5.79	2.33
N_2 (vol. %)	61.44	58.63	58.41	62.40	64.34
Combustible gas (CO, H_2 and CH_4)	24.59	29.10	30.96	26.90	16.79
Syngas (CO+H_2)	23.23	27.63	29.76	25.99	16.50
Condensate and tar (gm)	28.35	19.10	13.61	12.62	9.84
Ash and char (gm)	2087	1382	678	552	833

Table B.2 Experimental result of an average gas product composition as a function of OPF moisture content

Measured parameters.	Moisture content (%)				
	0	15	30	40	60
CO (vol. %)	26.04	22.04	19.11	15.37	9.57
CO_2 (vol. %)	9.30	9.54	10.74	13.10	12.50
CH_4 (vol. %)	1.11	1.04	0.94	1.10	0.92
H_2 (vol. %)	6.22	6.48	6.23	6.42	4.38
N_2 (vol. %)	57.57	59.90	62.98	64.01	72.63
Combustible gas (CO, H_2 and CH_4)	33.37	30.56	26.28	22.89	14.87
Syngas (CO+H_2)	32.26	28.52	25.34	21.79	13.95
Condensate and tar (ml)	93	210	290	430	760
Ash and char (g)	485	532	574	629	1138

Table B.3 Experimental result of an average gas product composition as a function of OPF particle size

Measured parameters.	Particle size (mm)				
	<5	13-25	38-50	64-90	>250
CO (vol. %)	21.10	26.43	22.78	18.87	12.35
CO_2 (vol. %)	11.57	7.68	8.07	13.25	13.10
CH_4 (vol. %)	1.20	1.08	0.76	1.33	0.67
H_2 (vol. %)	5.98	5.90	5.35	5.37	3.75
N_2 (vol. %)	60.16	58.90	62.74	61.18	70.17
Combustible gas (CO, H_2 and CH_4)	28.28	33.41	29.19	29.89	16.77
Syngas ($CO+H_2$)	27.08	32.33	28.13	24.24	16.10
Condensate and tar (ml)	137	118	274	212	123
Ash and char (g)	745	825	990	700	1250

Table B.4 Experimental result of an average gas product composition as a function of primary air position

Measured parameters.	Primary air position				
	Case 1	Case 2	Case 3	Case 4	Case 5
CO (vol. %)	22.61	18.48	19.57	24.73	20.54
CO_2 (vol. %)	9.51	12.75	13.13	9.05	13.69
CH_4 (vol. %)	1.20	2.33	2.96	1.17	2.32
H_2 (vol. %)	6.48	7.61	8.02	7.26	8.19
N_2 (vol. %)	59.2	58.83	56.32	58.55	55.27
Combustible gas (CO, H_2 and CH_4)	30.56	30.78	31.72	33.12	32.66
Condensate and tar (gm)	240	195	205	197	210
Ash and char (g)	532	2138	2651	1014	2256

Case 1: below the grate, Case 2: through the grate, Case 3: above the grate, Case 4: 50% below and 50% through the grate, Case 5: 50% below and 50% above the grate

Table B.5 Experimental result of an average gas product composition as a function of secondary air position

Measured parameters.	Secondary air position			
	Case A	Case B	Case C	Case D
CO (vol. %)	22.61	23.47	24.70	23.29
CO_2 (vol. %)	9.51	8.91	8.33	8.97
CH_4 (vol. %)	1.24	1.79	1.72	1.27
H_2 (vol. %)	6.48	7.32	7.91	6.25
N_2 (vol. %)	59.2	58.62	55.37	59.64
Combustible gas (CO, H_2 and CH_4)	30.56	32.47	34.30	31.69
Condensate and tar (ml)	240	179	180	600
Ash and char (g)	532	695	1105	1324

Case A: without secondary air, Case B: injection the secondary air through the combustion zone, Case C: injection the secondary air through the reduction zone, Case D: injection the secondary air through the pyrolysis zone

Table B.6 Experimental result of an average gas product composition as a function of secondary to primary air ration (Reduction zone)

Measured parameters.	Secondary to primary air ratio (%)			
	17	27	40	56
CO (vol. %)	24.70	24.41	18.97	16.11
CO_2 (vol. %)	8.33	9.26	11.86	9.01
CH_4 (vol. %)	1.72	1.54	1.49	1.06
H_2 (vol. %)	7.91	6.93	5.59	4.65
N_2 (vol. %)	55.37	57.63	62.09	69.17
Combustible gas (CO, H_2 and CH_4)	34.30	32.11	26.06	21.82
Condensate and tar (ml)	180	420	370	520
Ash and char (g)	1105	1374	1500	1981

Table B.7 Experimental result of an average gas product composition as a function of secondary to primary air ration (Combustion zone)

Measured parameters.	Secondary to primary air ratio (%)			
	17	27	56	100
CO (vol. %)	23.47	22.37	20.84	20.54
CO_2 (vol. %)	8.91	9.92	13.34	13.96
CH_4 (vol. %)	1.79	2.12	2.60	2.32
H_2 (vol. %)	7.32	7.42	8.15	8.19
N_2 (vol. %)	58.62	58.18	55.07	53.36
Combustible gas (CO, H_2 and CH_4)	32.47	31.92	31.59	32.66
Condensate and tar (ml)	179	420	500	210
Ash and char (gm)	695	1643	1812	2256

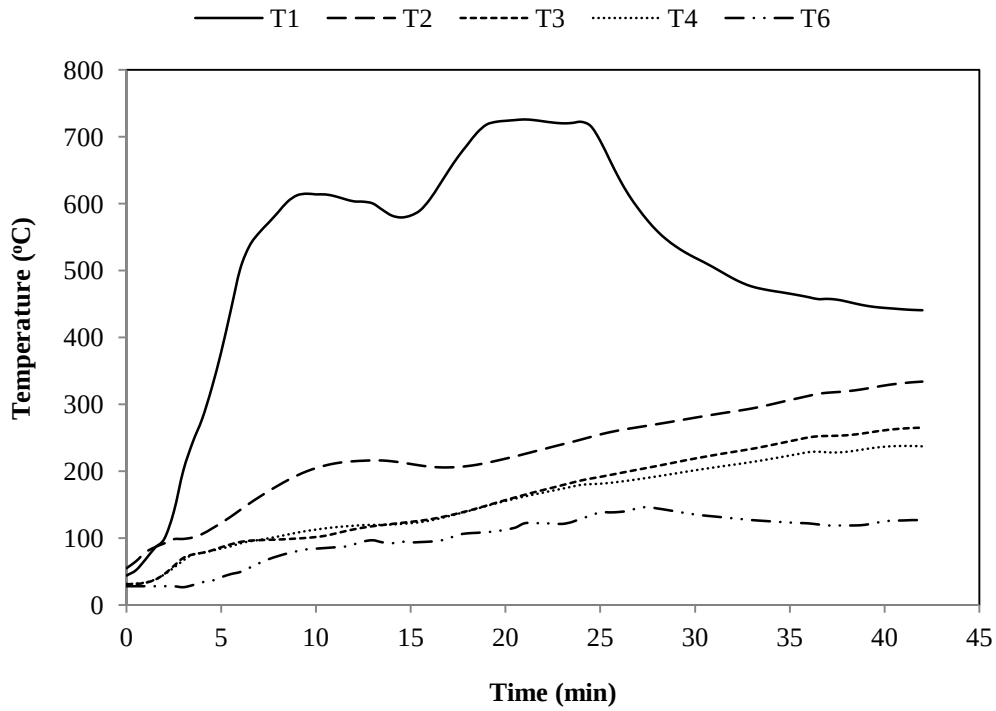

Figure B.1 Temperature profile during gasification of OPF (0% moisture content)

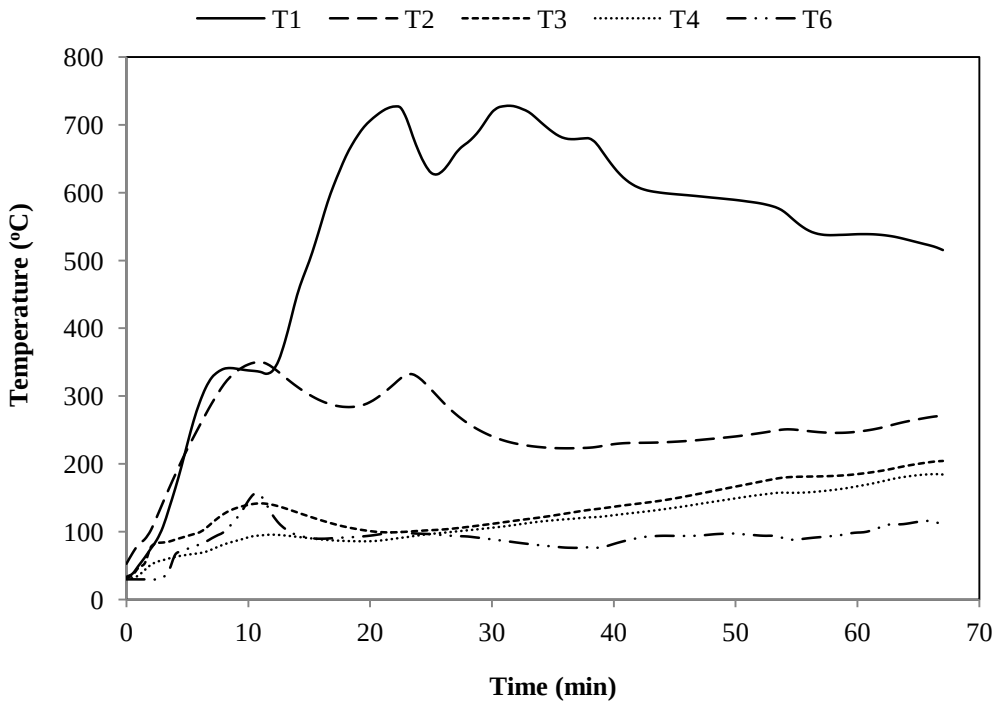

Figure B.2 Temperature profile during gasification of OPF (15% moisture content)

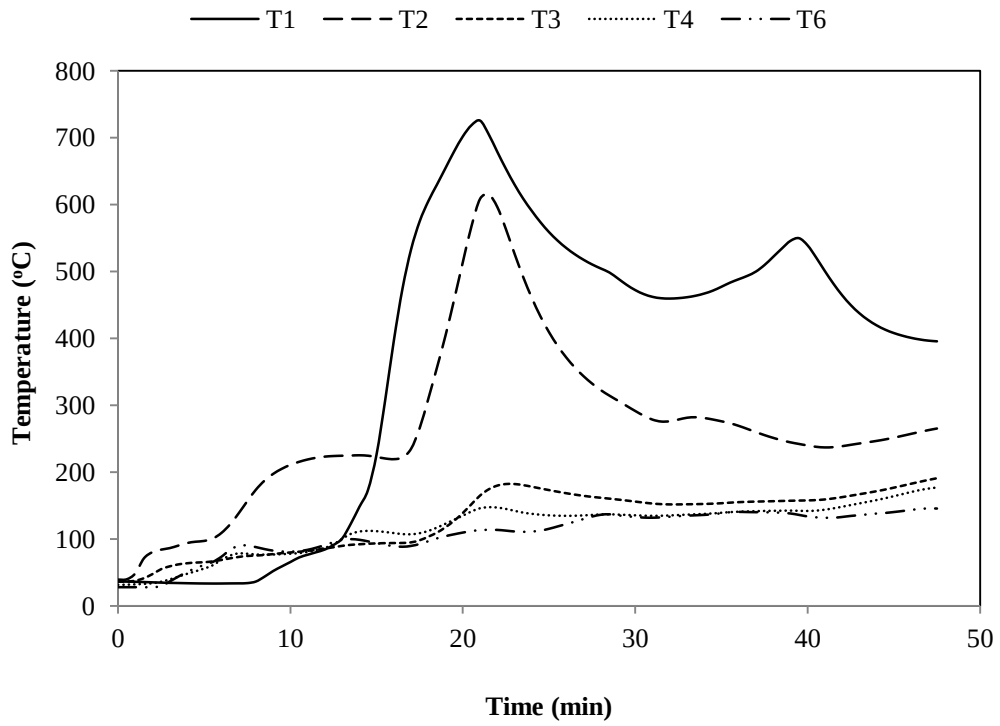

Figure B.3 Temperature profile during gasification of OPF (30% moisture content)

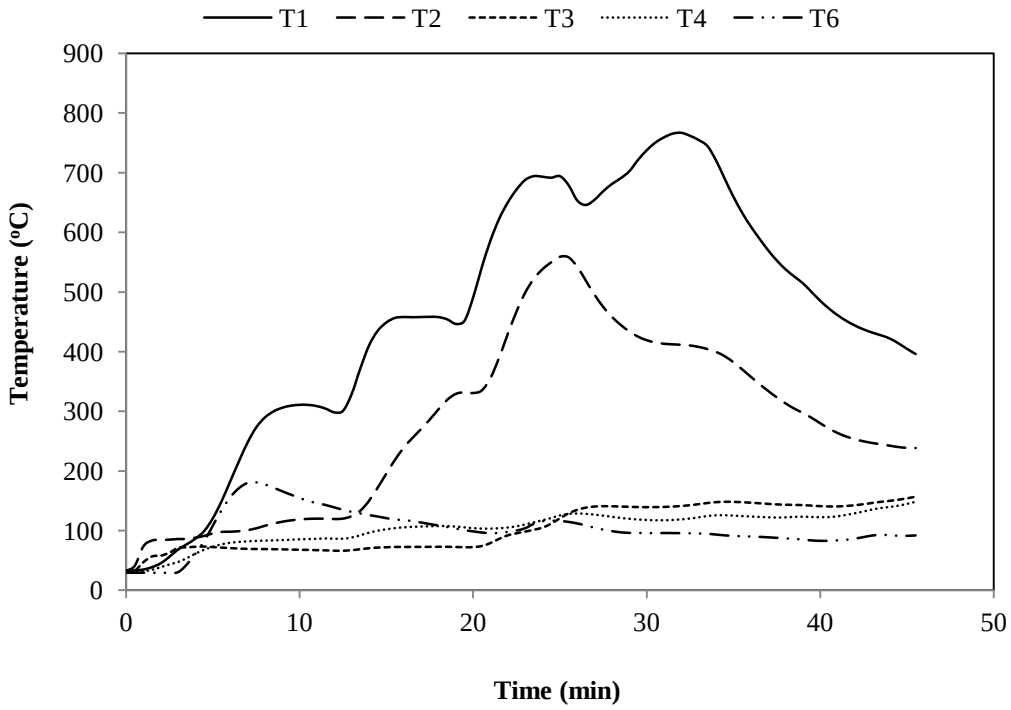

Figure B.4 Temperature profile during gasification of OPF (40% moisture content)

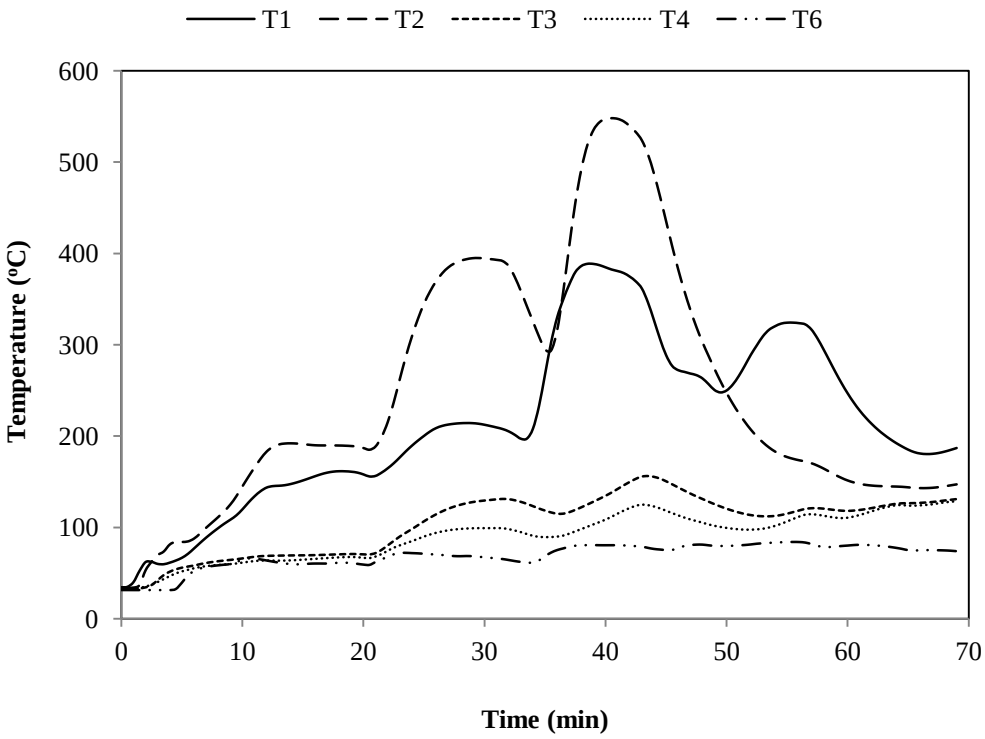

Figure B.5 Temperature profile during gasification of OPF (60% moisture content)

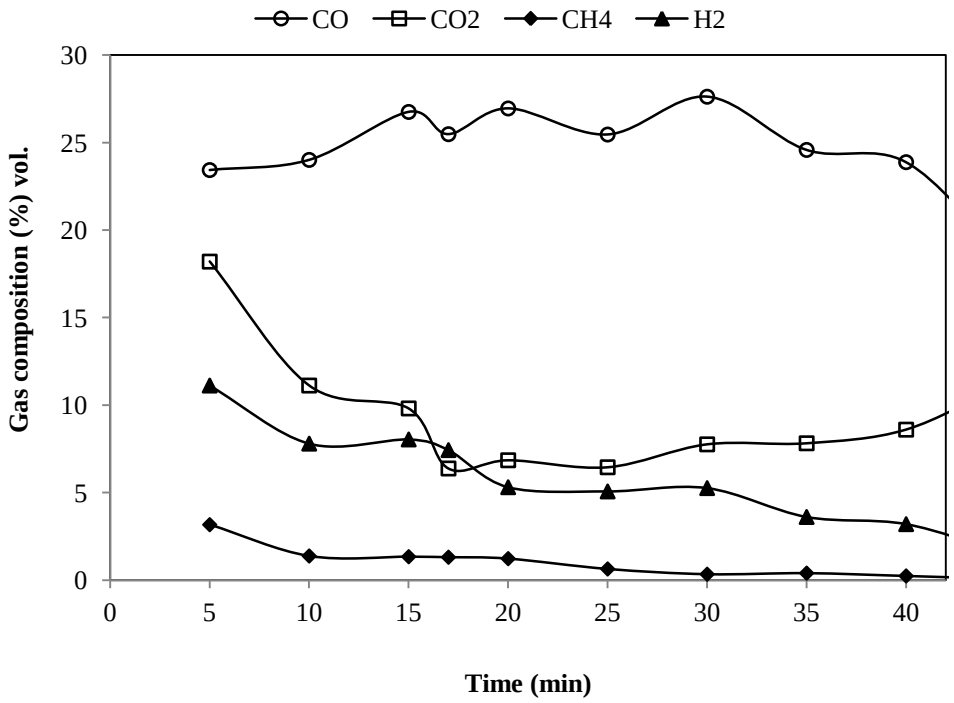

Figure B.6 Variation of syngas composition with time (0% moisture content)

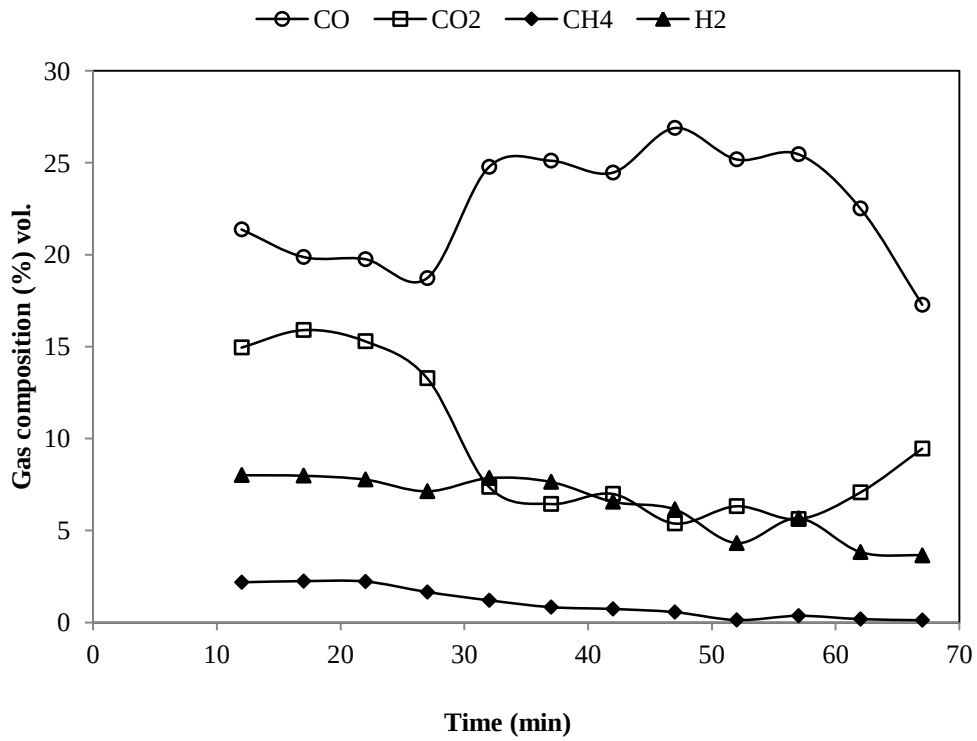

Figure B.7 Variation of syngas composition with time (15% moisture content)

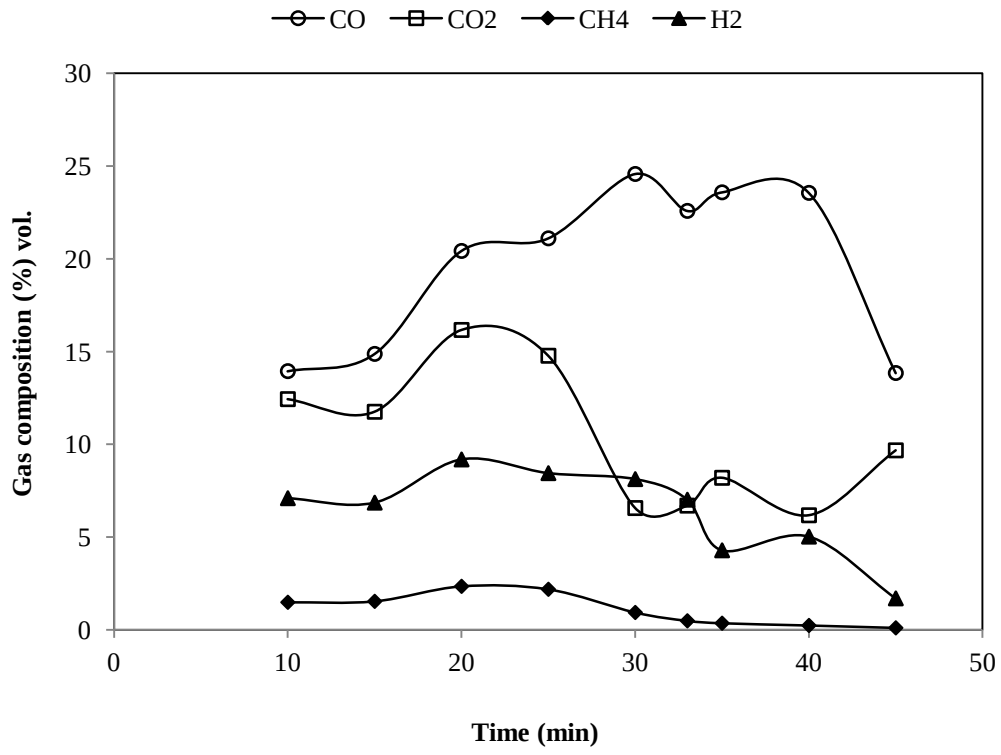

Figure B.8 Variation of syngas composition with time (30% moisture content)

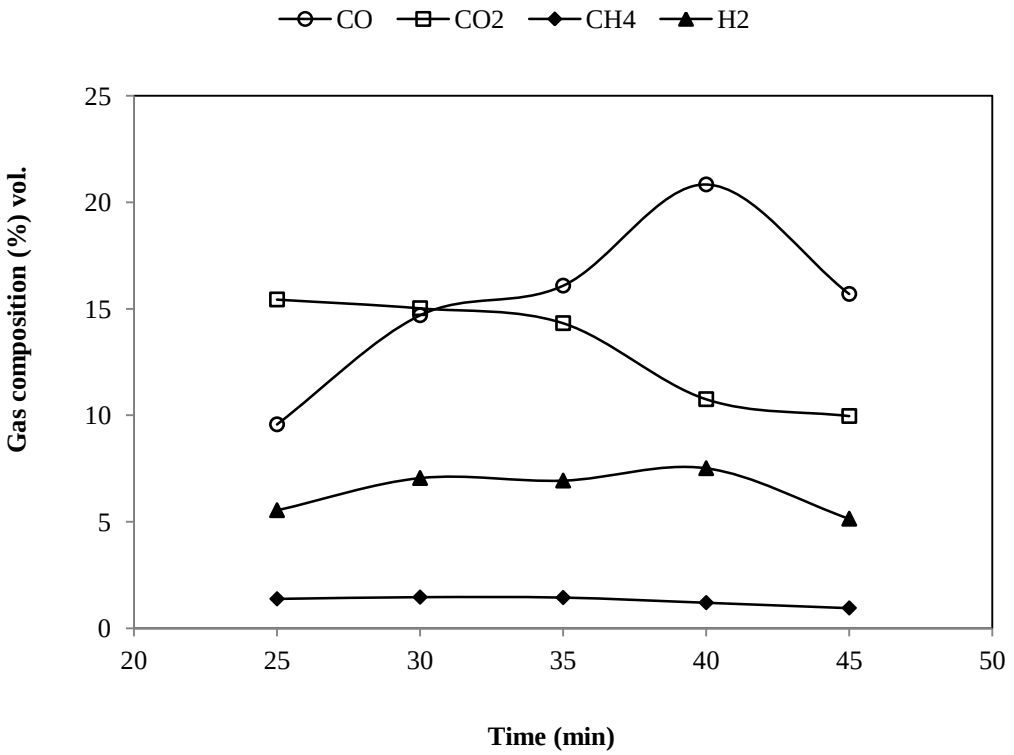

Figure B.9 Variation of syngas composition with time (40% moisture content)

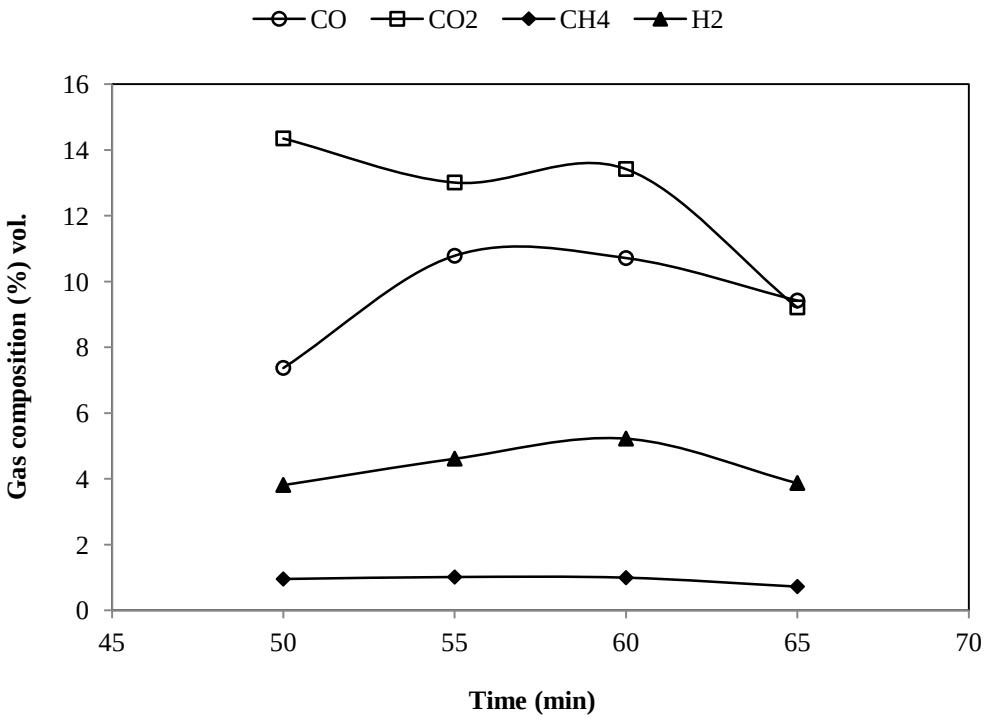

Figure B.10 Variation of syngas composition with time (60% moisture content)

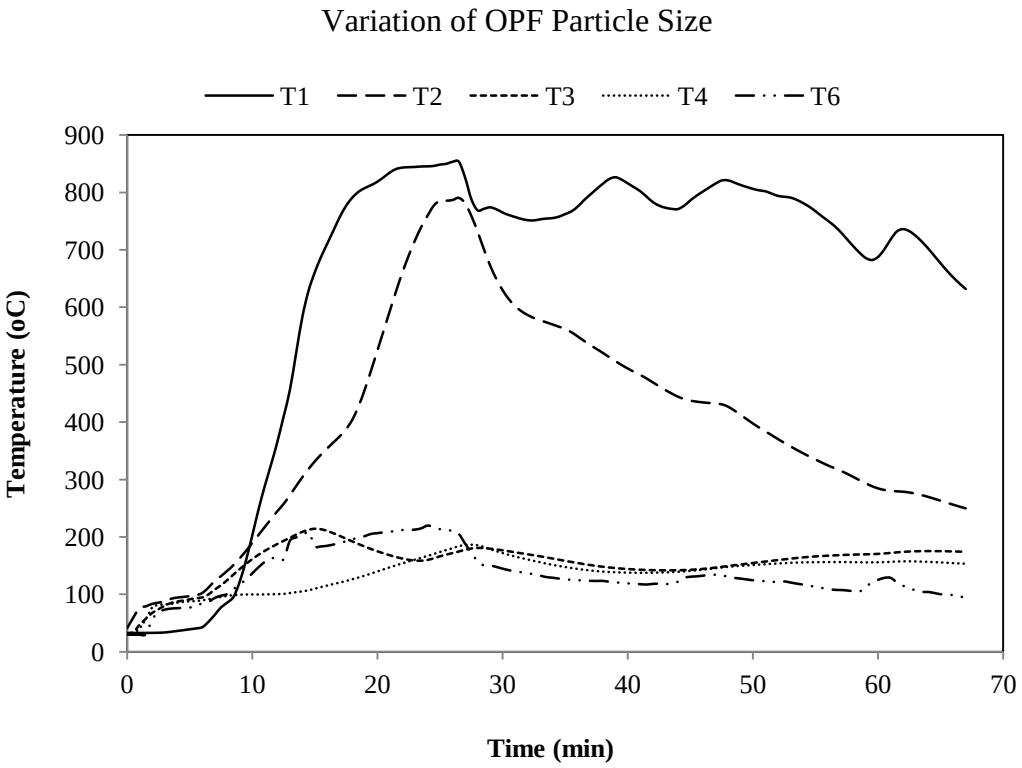

Figure B.11 Temperature profile during gasification of OPF (size: less than 5 mm)

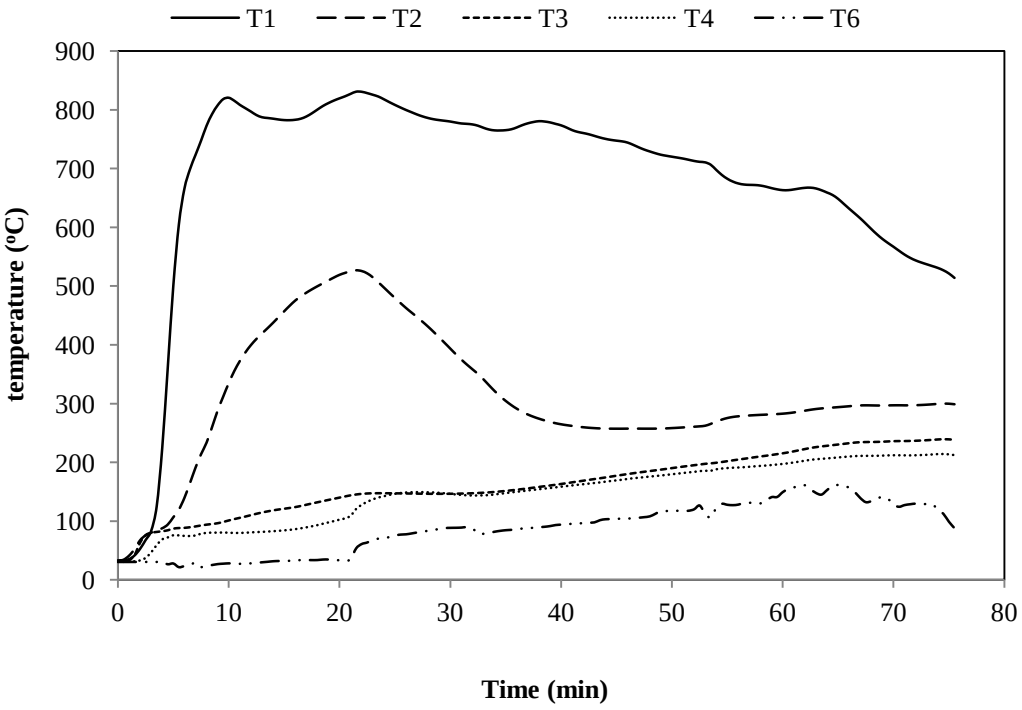

Figure B.12 Temperature profile during gasification of OPF (size: 13-25 mm)

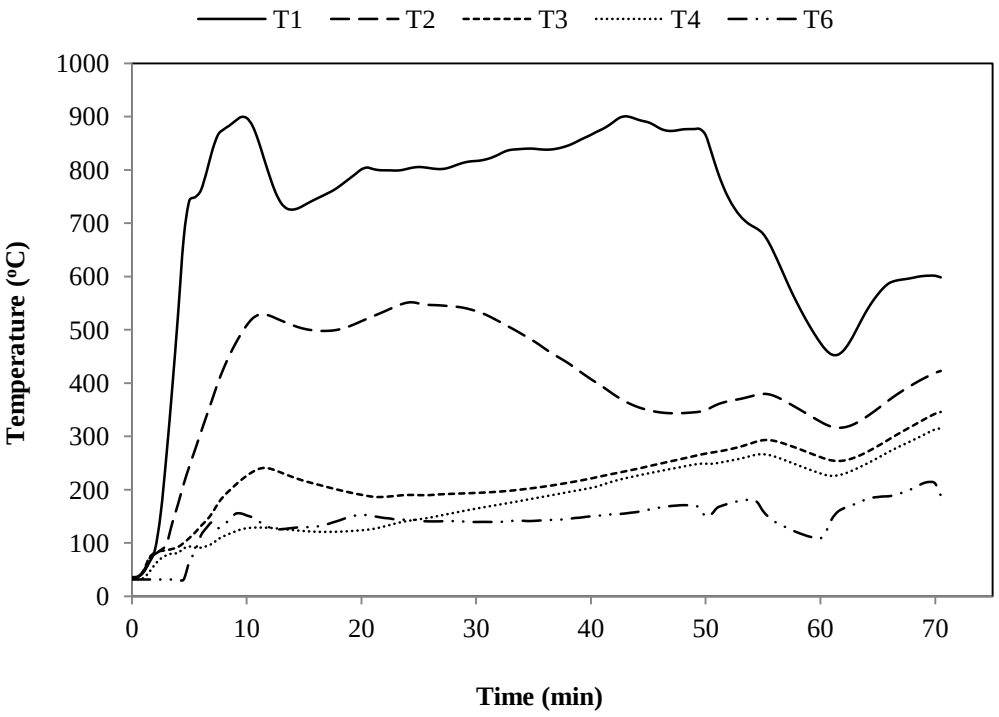

Figure B.13 Temperature profile during gasification of OPF (size: 38-51 mm)

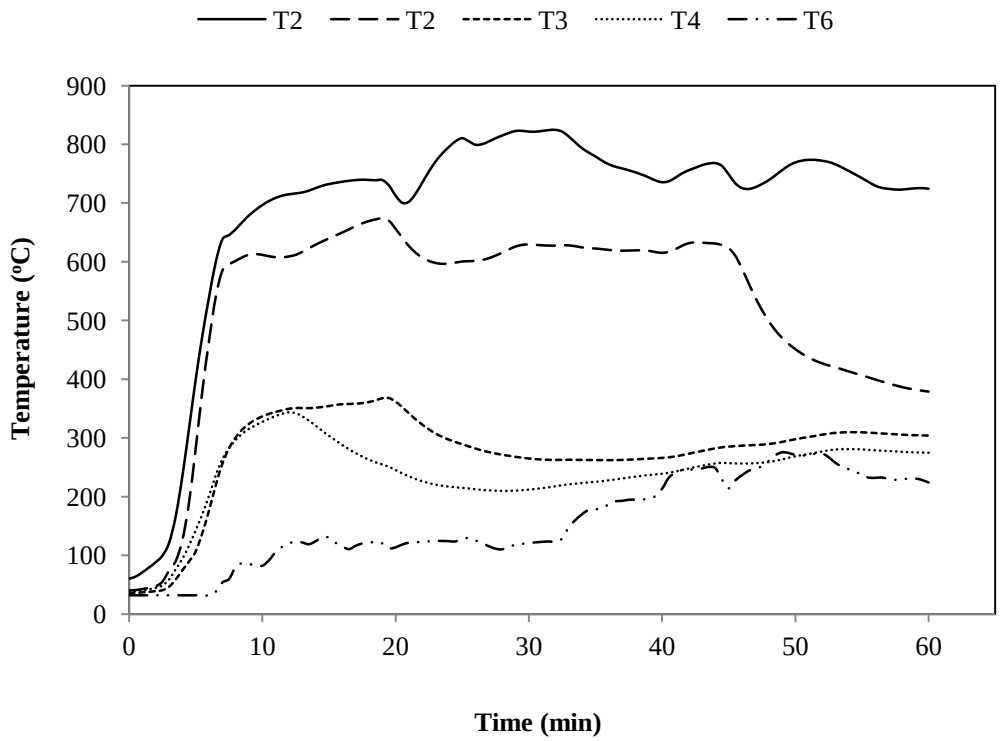

Figure B.14 Temperature profile during gasification of OPF (size: 64-90 mm)

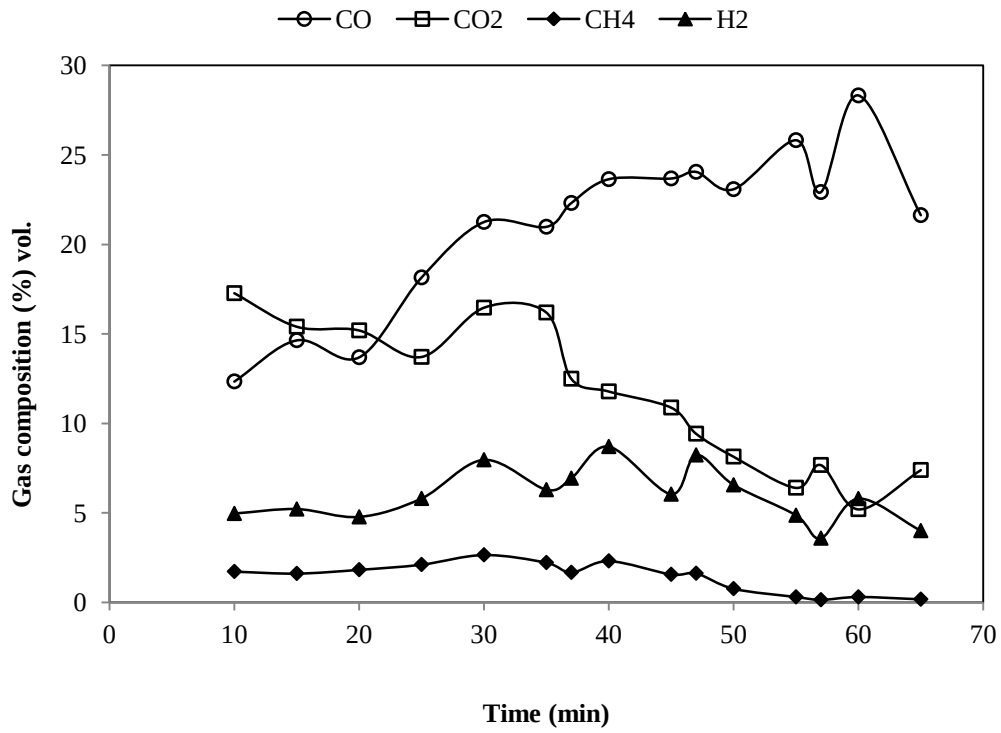

Figure B.16 Variation of syngas composition with time (size: less than 5 mm)

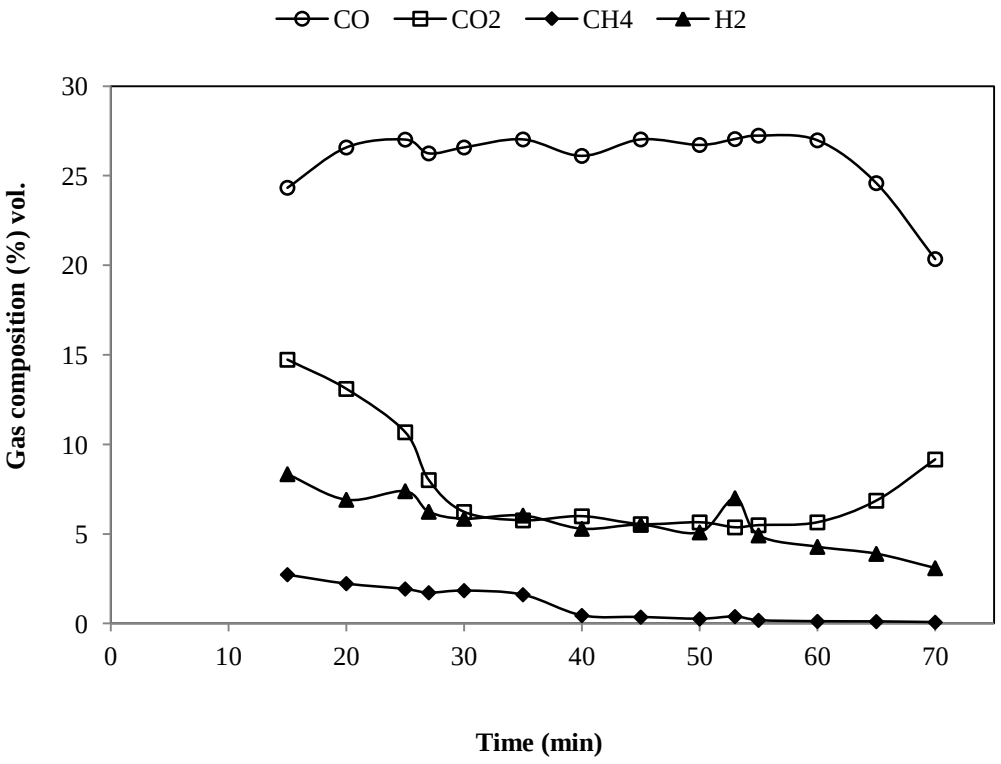

Figure B.17 Variation of syngas composition with time (size13-25 mm)

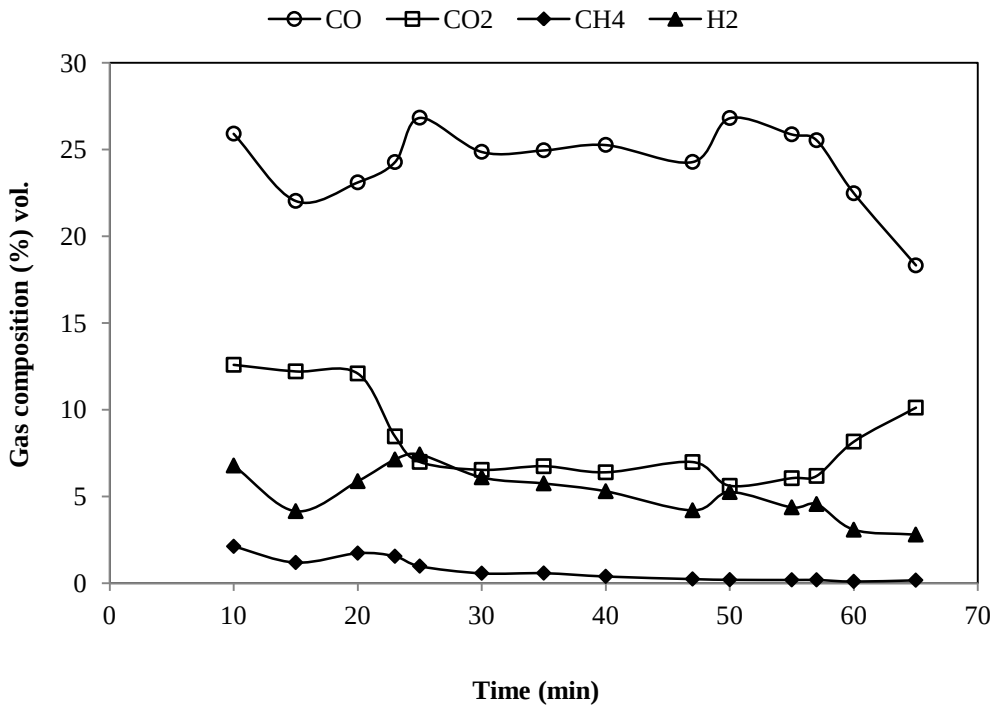

Figure B.18 Variation of syngas composition with time (size: 38-51 mm)

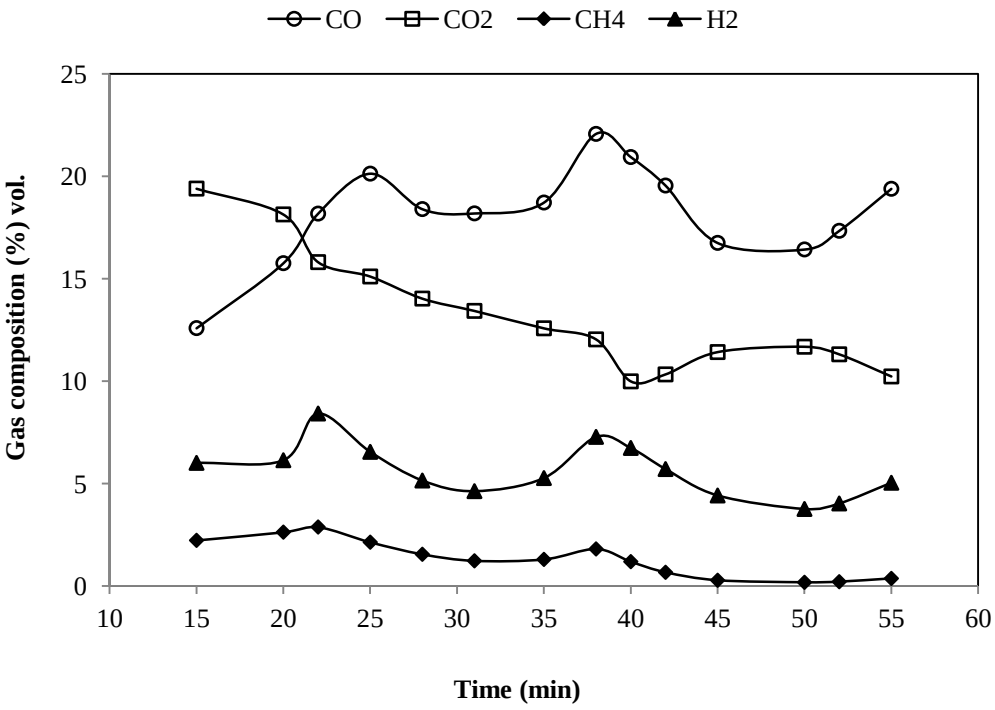

Figure B.19 Variation of syngas composition with time (size: 64-90 inch)

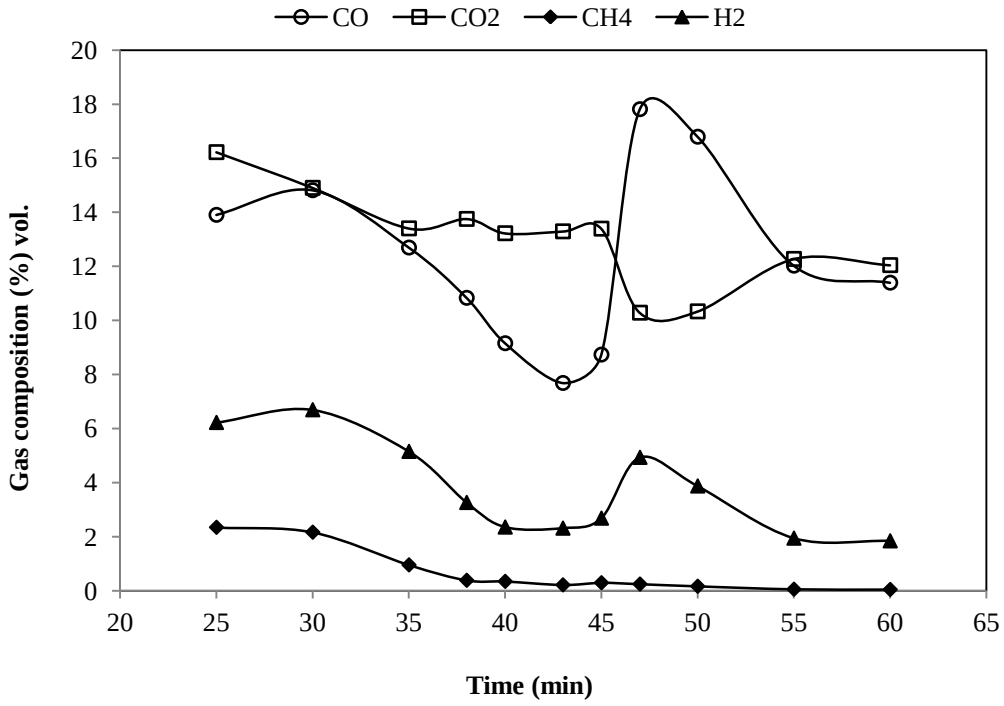

Figure B.20 Variation of syngas composition with time (size: larger than 250 mm)

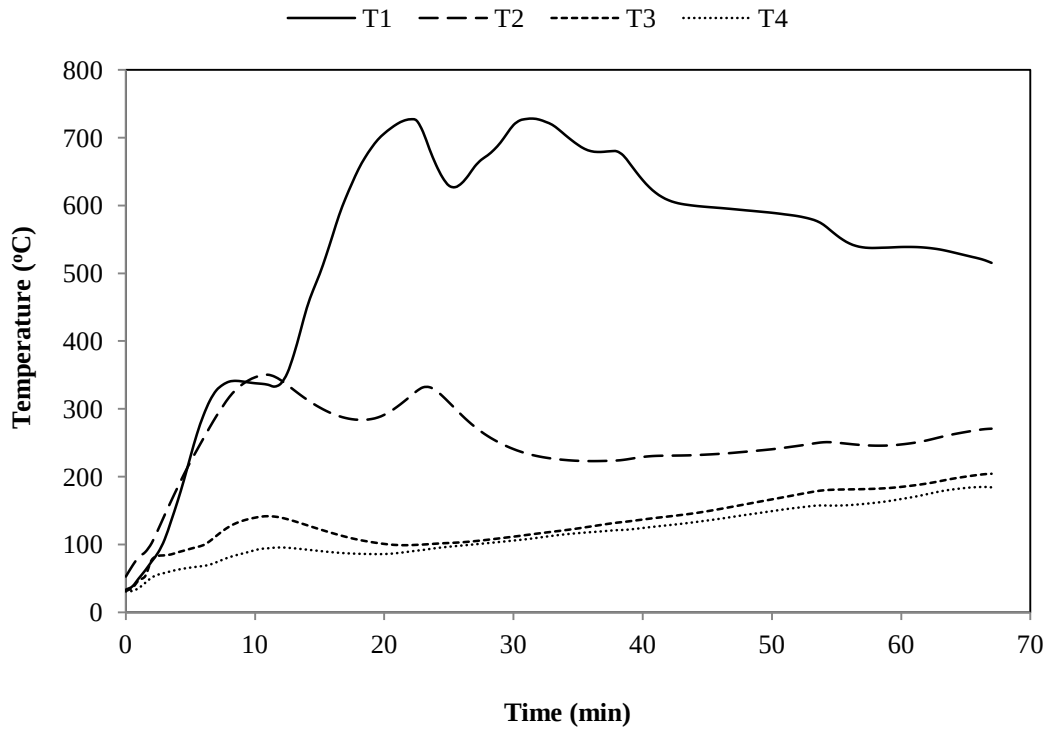

Figure B.21 Temperature profile during gasification of OPF (below the grate)

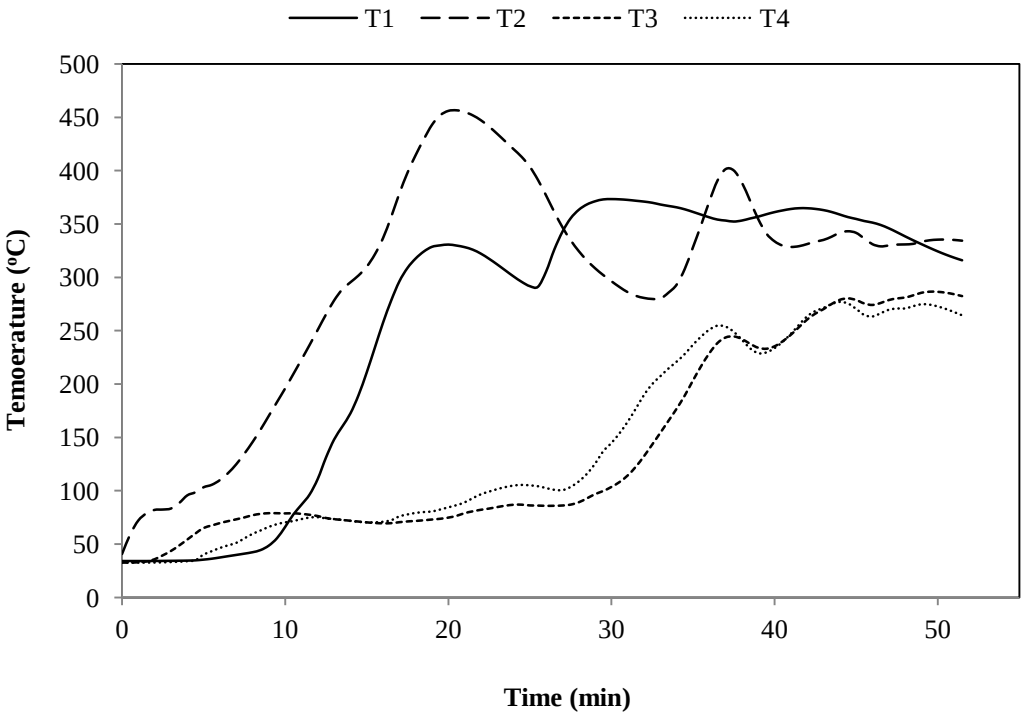

Figure B.22 Temperature profile during gasification of OPF (through the grate)

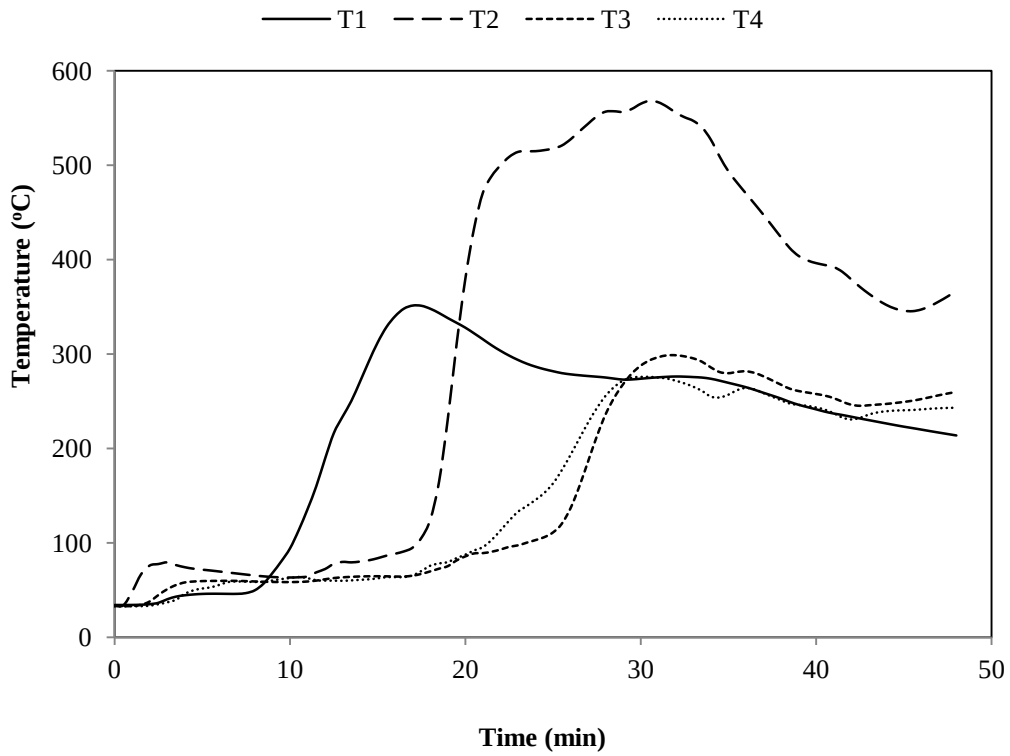

Figure B.23 Temperature profile during gasification of OPF (above the grate)

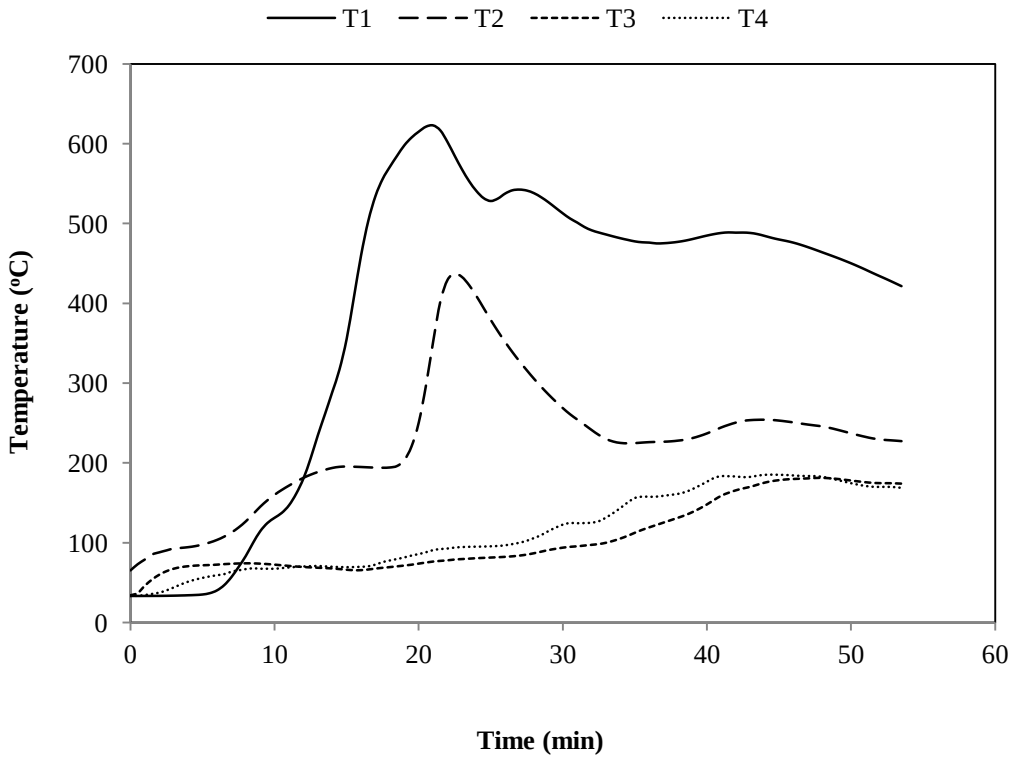

Figure B.24 Temperature profile during gasification of OPF (below-through the grate)

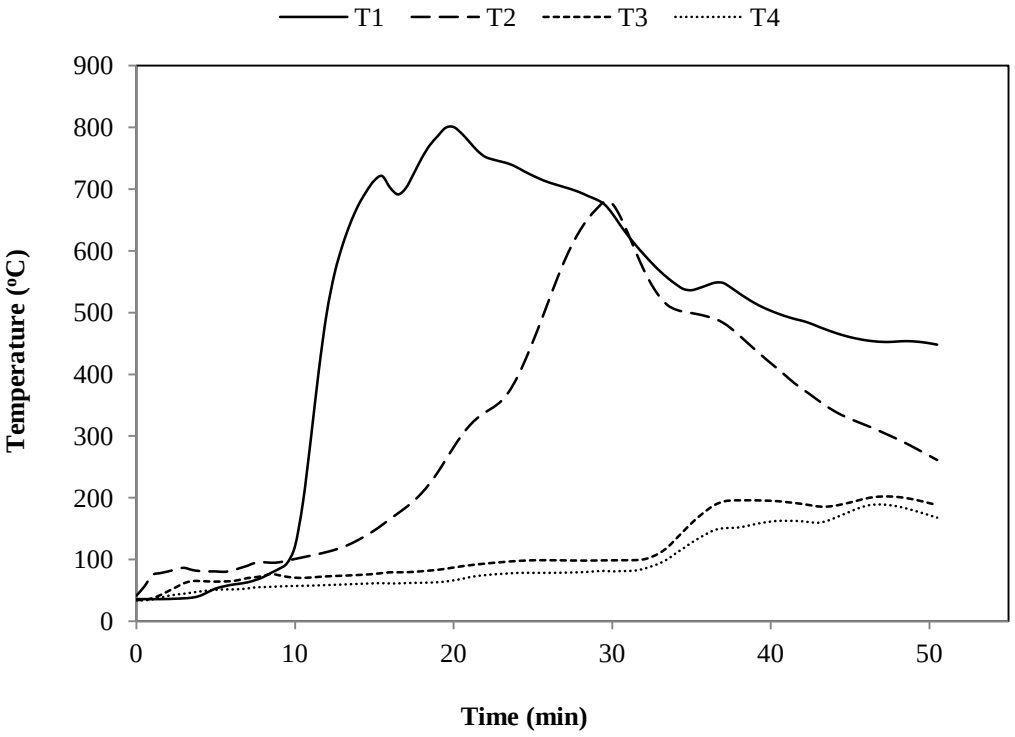

Figure B.25 Temperature profile during gasification of OPF (below-above the grate)

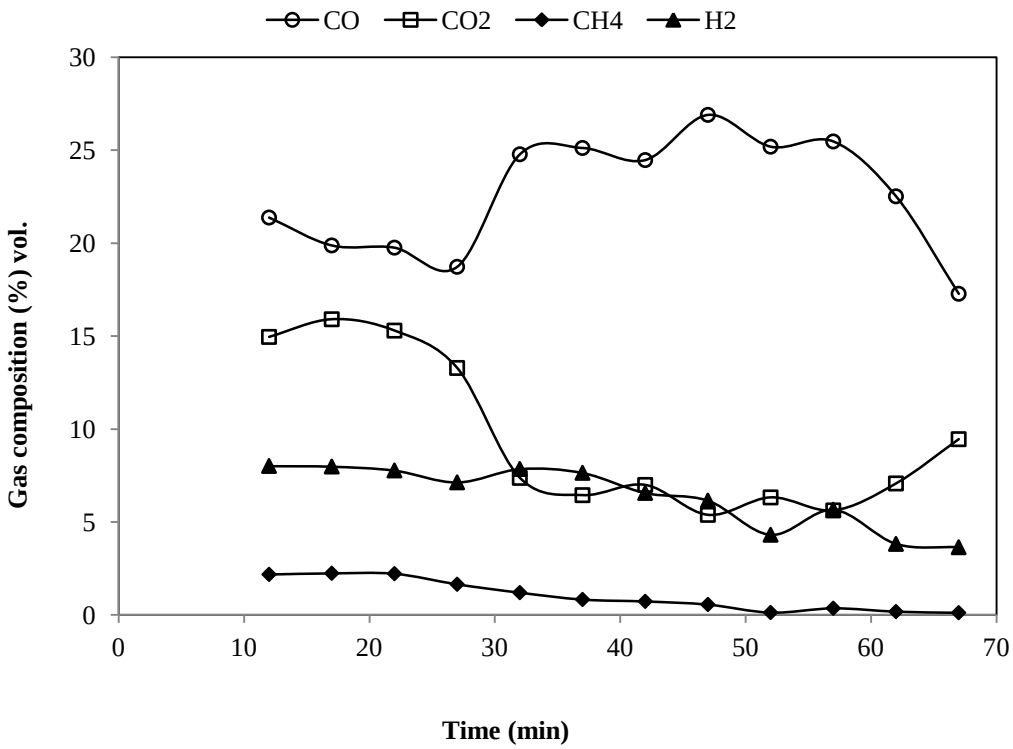

Figure B.26 Variation of syngas composition with time (below the grate)

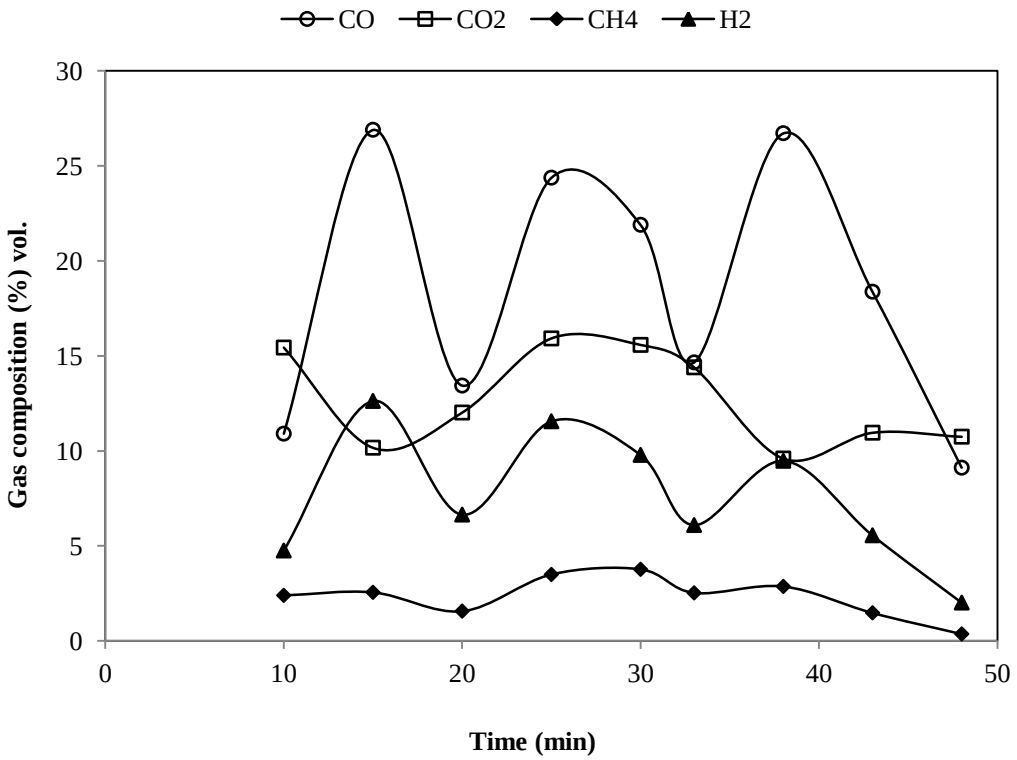

Figure B.27 Variation of syngas composition with time (through the grate)

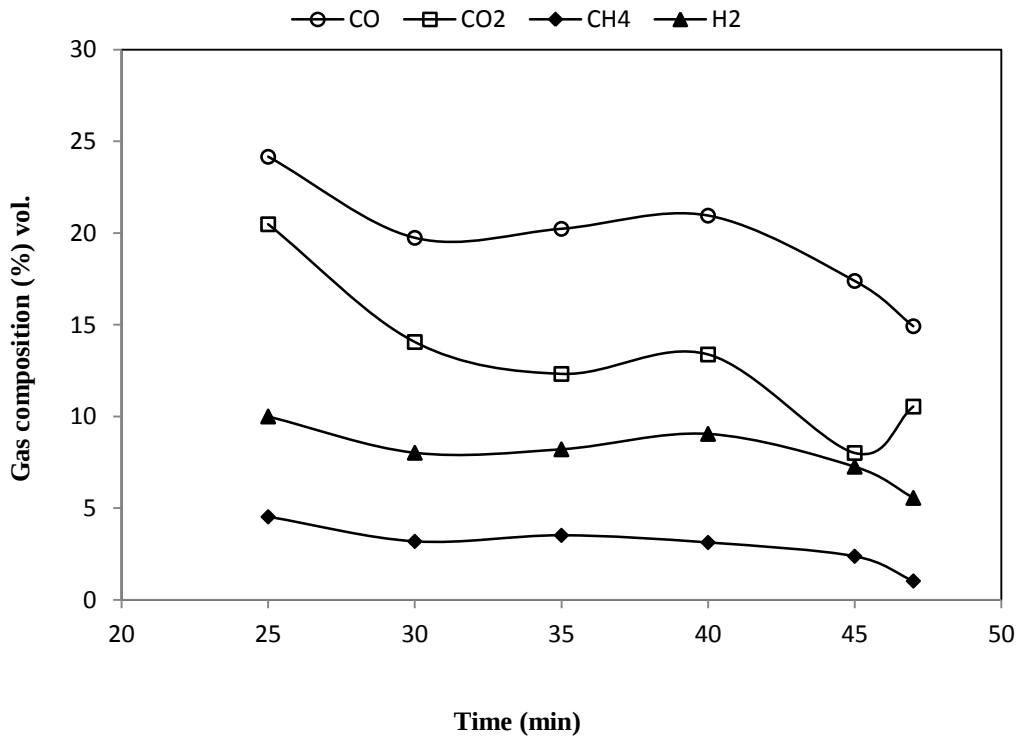

Figure B.28 Variation of syngas composition with time (above the grate)

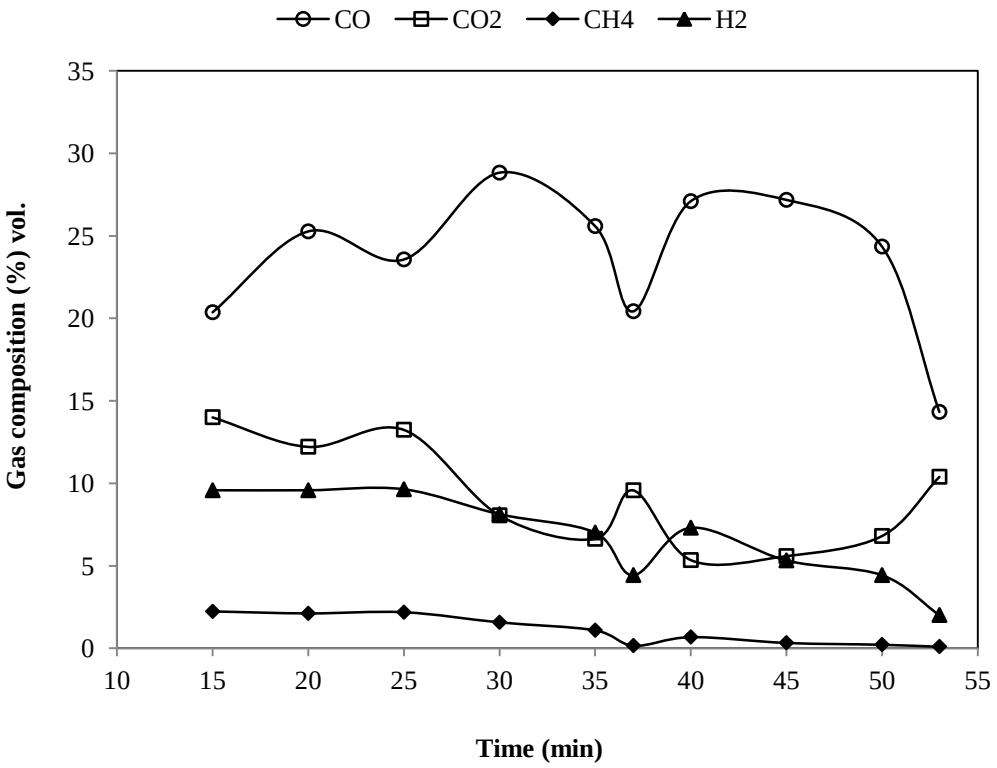

Figure B.29 Variation of syngas composition with time (below-through the grate)

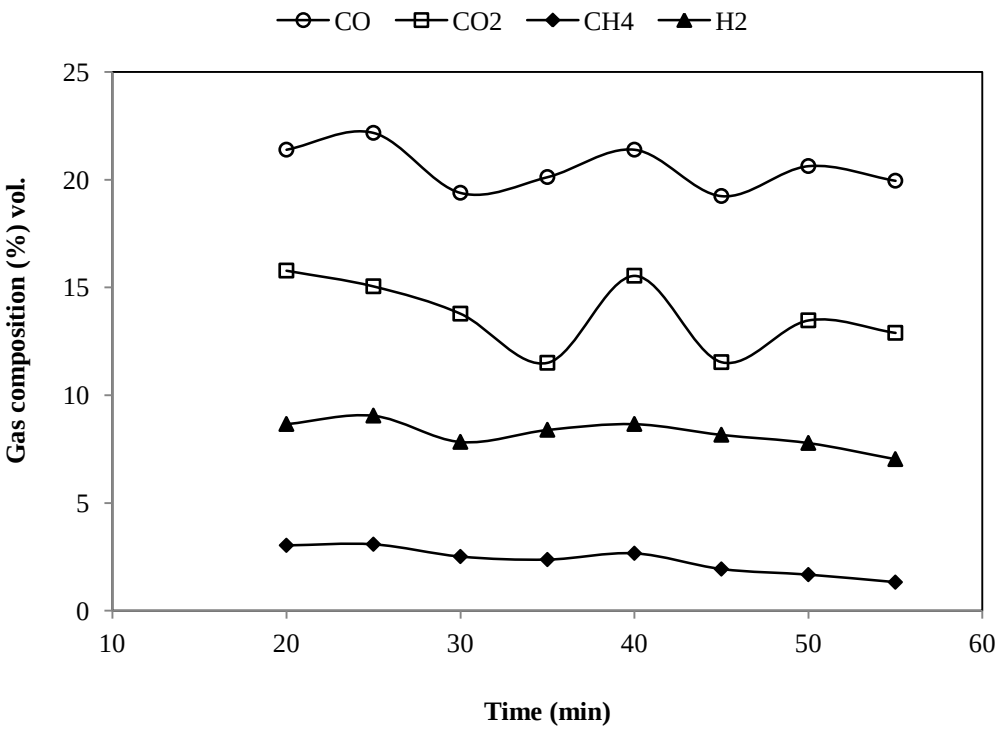

Figure B.30 Variation of syngas composition with time (below-above the grate)

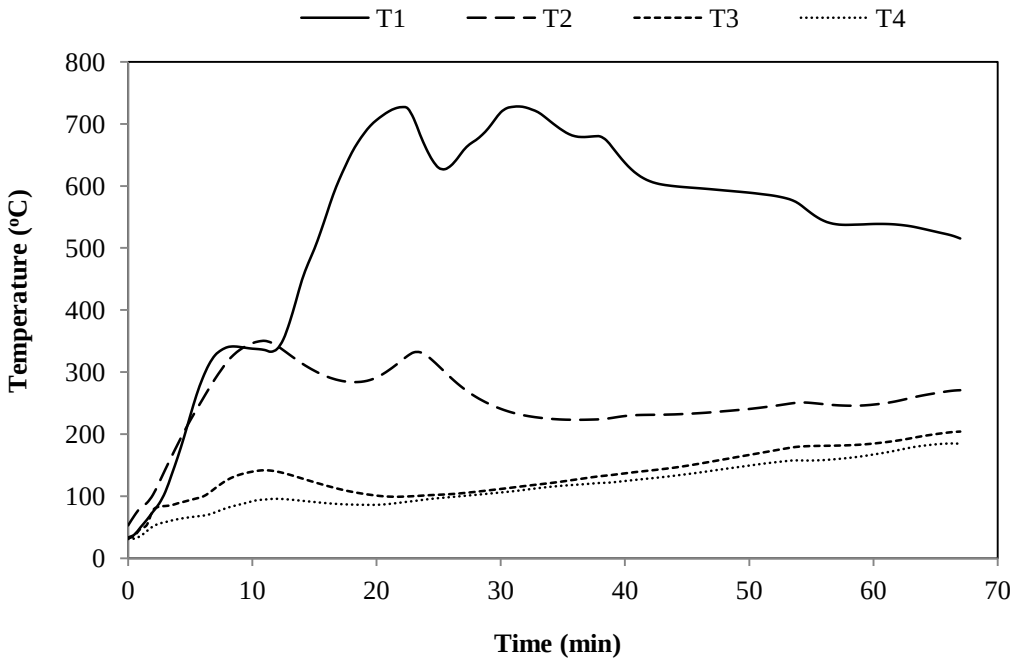

Figure B.31 Temperature profile during gasification of OPF in case of no secondary air

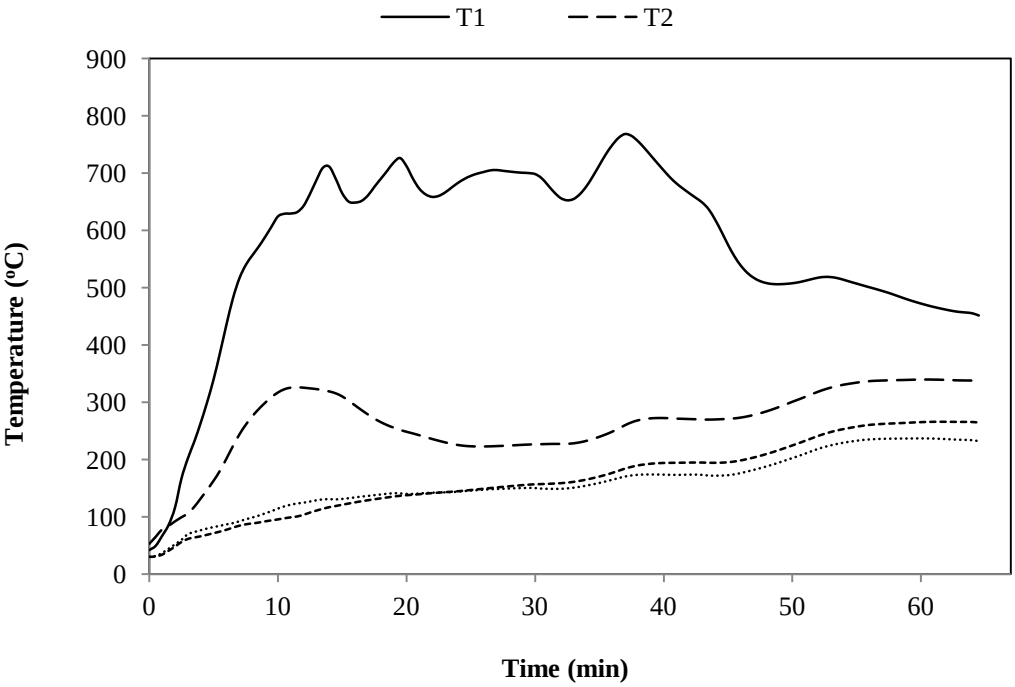

Figure B.32 Temperature profile during gasification of OPF in case of injecting secondary air through combustion zone

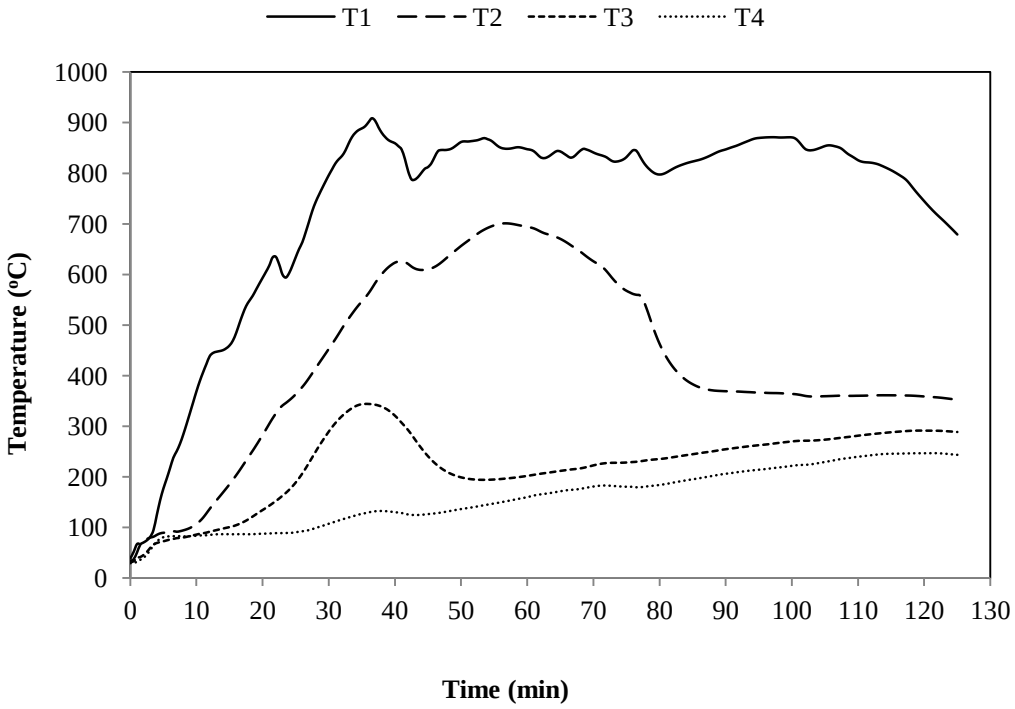

Figure B.33 Temperature profile during gasification of OPF in case of injecting secondary air through reduction zone

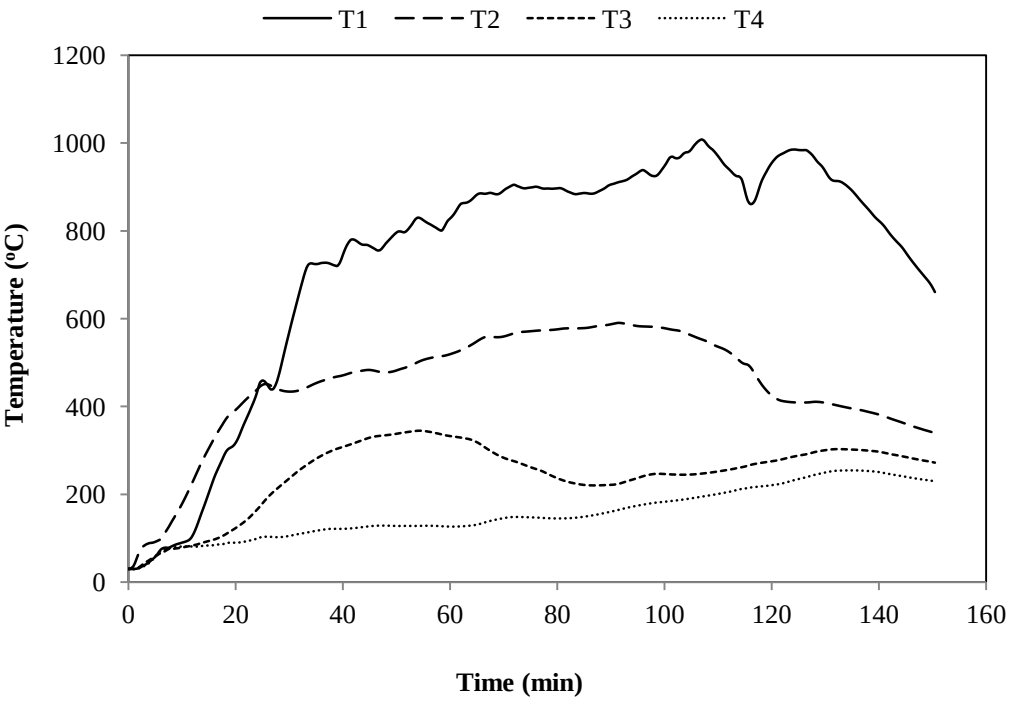

Figure B.34 Temperature profile during gasification of OPF in case of injecting secondary air through pyrolysis zone

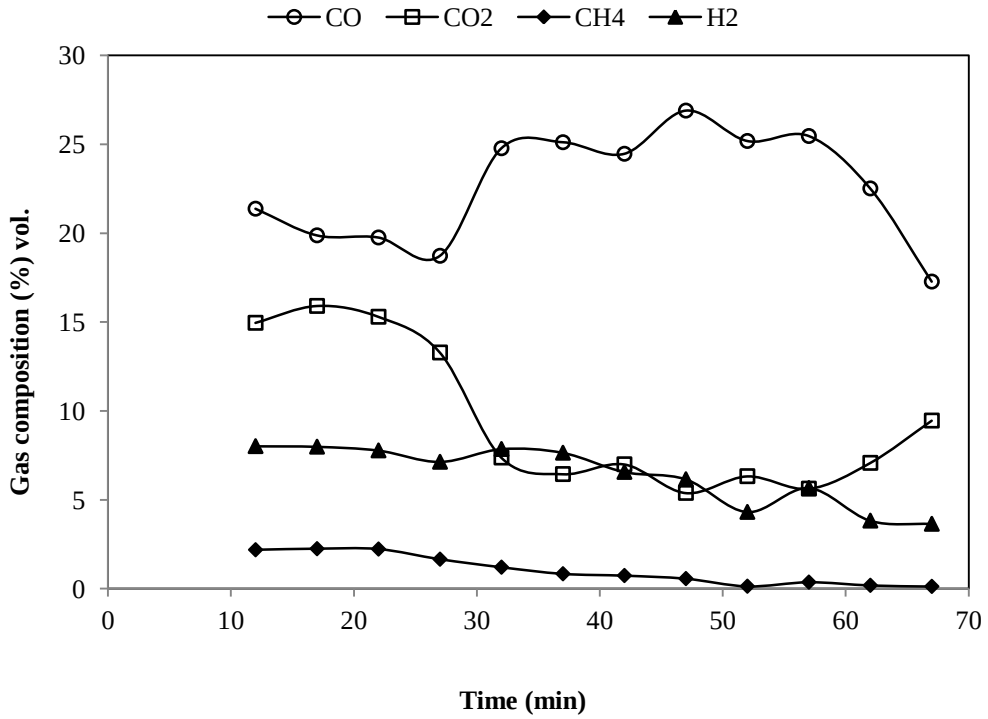

Figure B.35 Variation of syngas composition with time in case of no secondary air

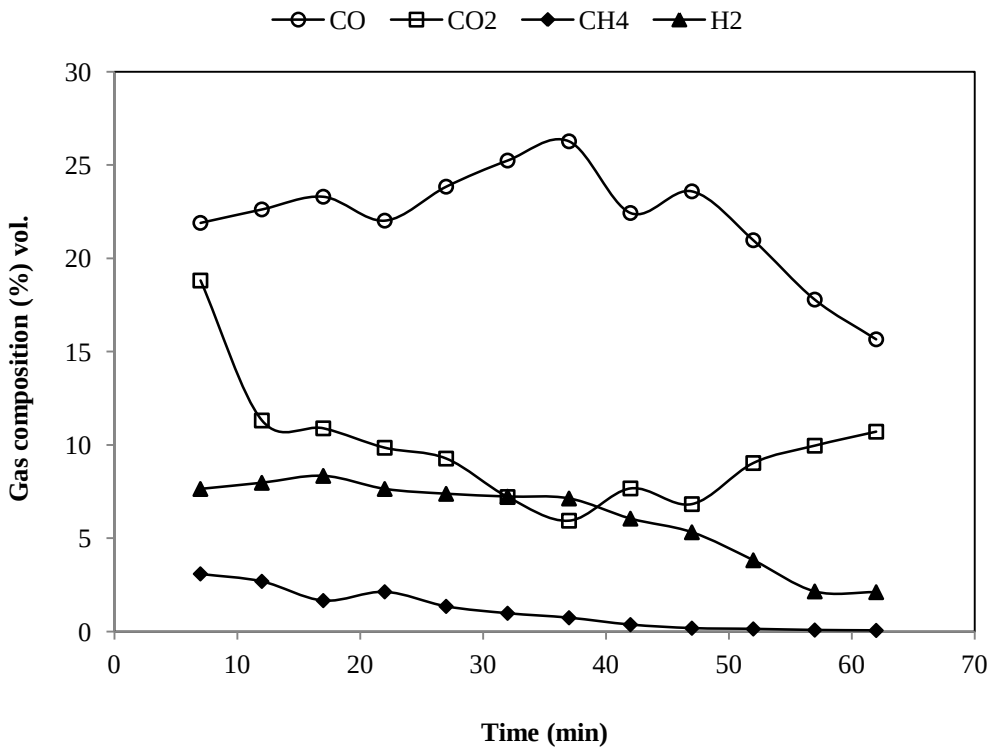

Figure B.36 Variation of syngas composition with time in case of injecting secondary air through combustion zone

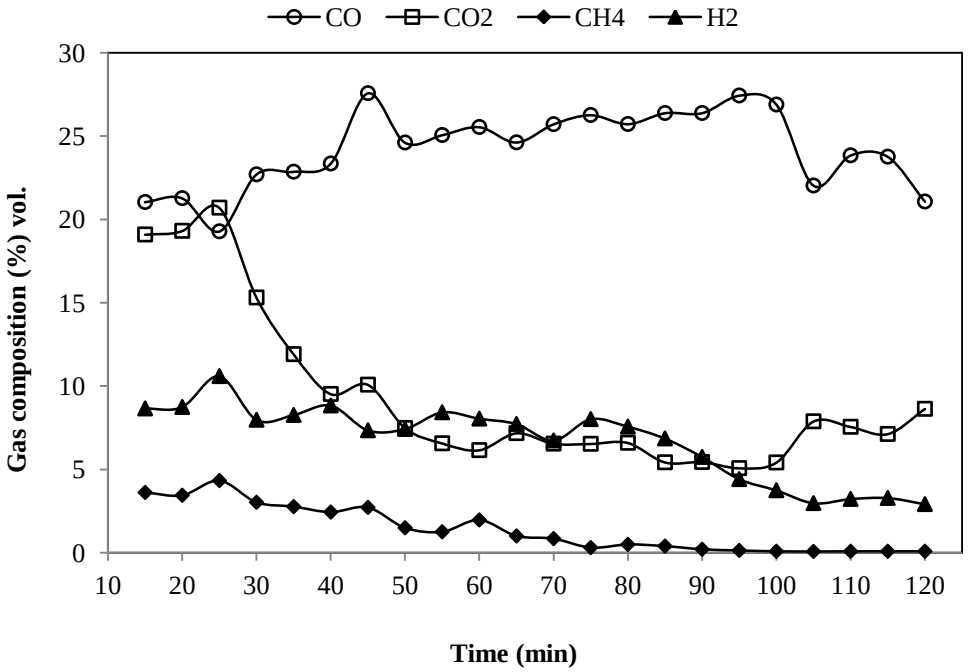

Figure B.37 Variation of syngas composition with time in case of injecting secondary air through reduction zone

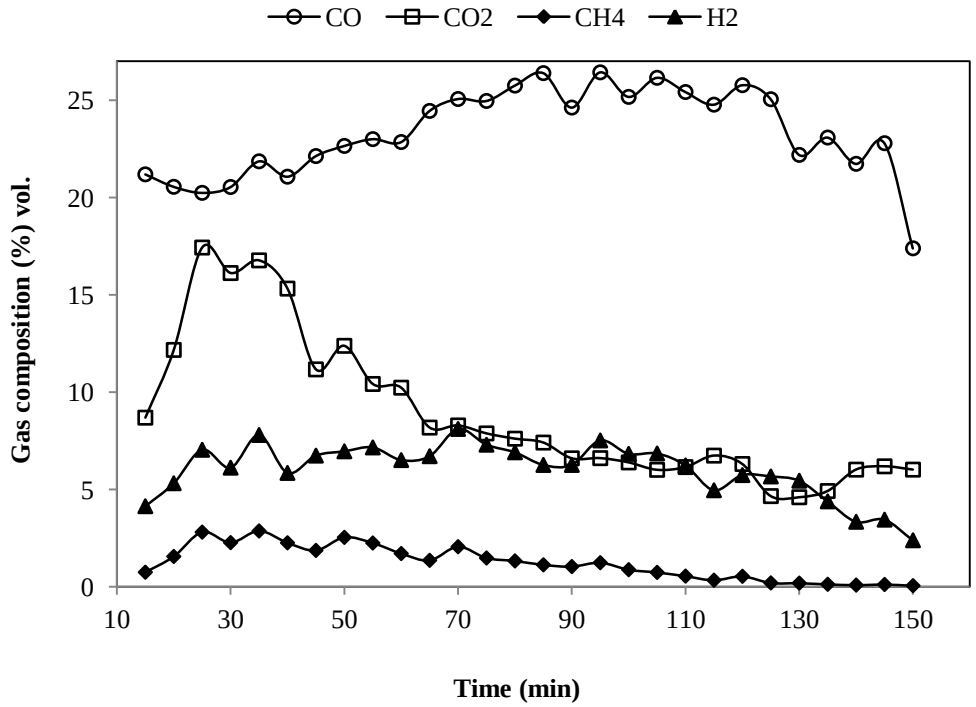

Figure B.38 Variation of syngas composition with time in case of injecting secondary air through pyrolysis zone

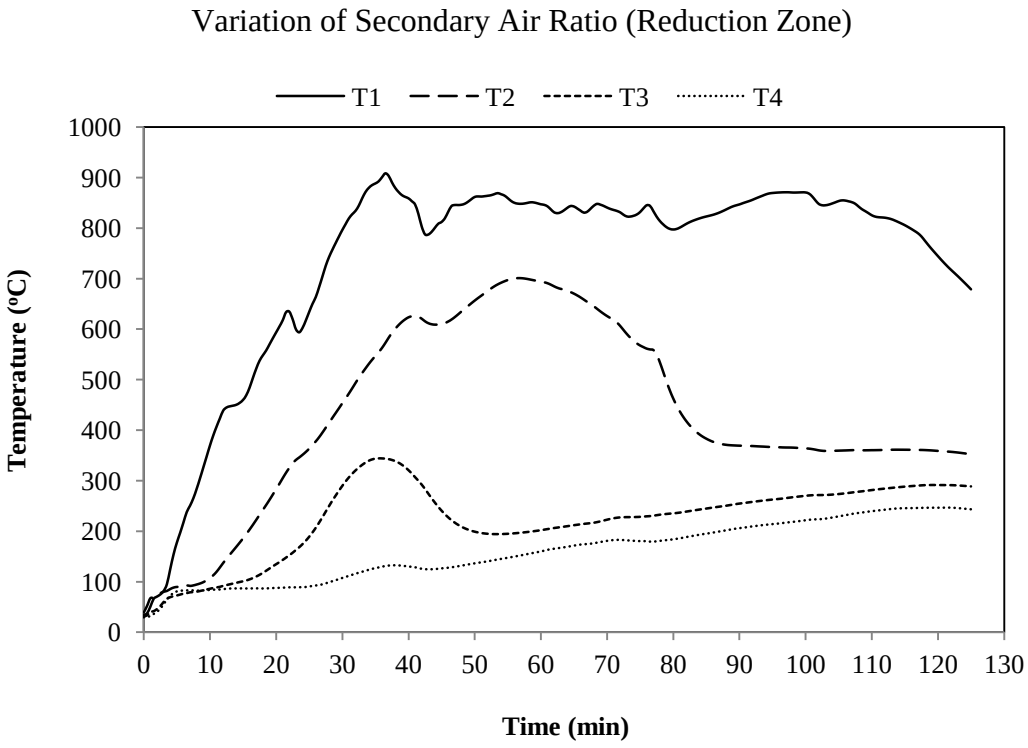

Figure B.39 Temperature profile during gasification of OPF in case of injecting secondary air through reduction zone at ratio of 0.17

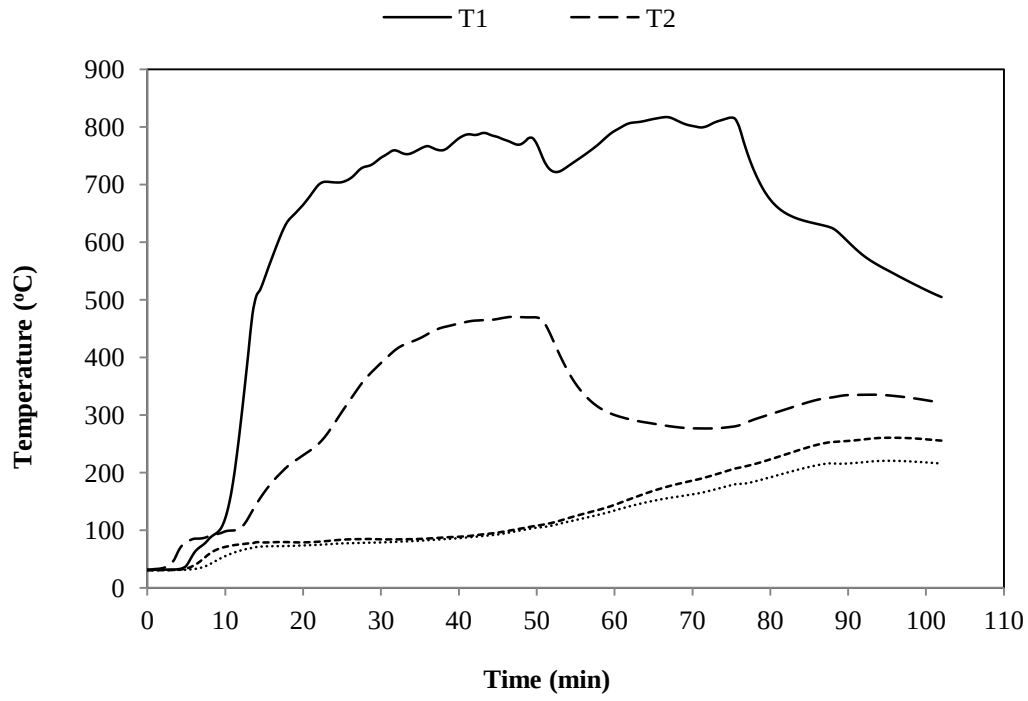

Figure B.40 Temperature profile during gasification of OPF in case of injecting secondary air through reduction zone at ratio of 0.27

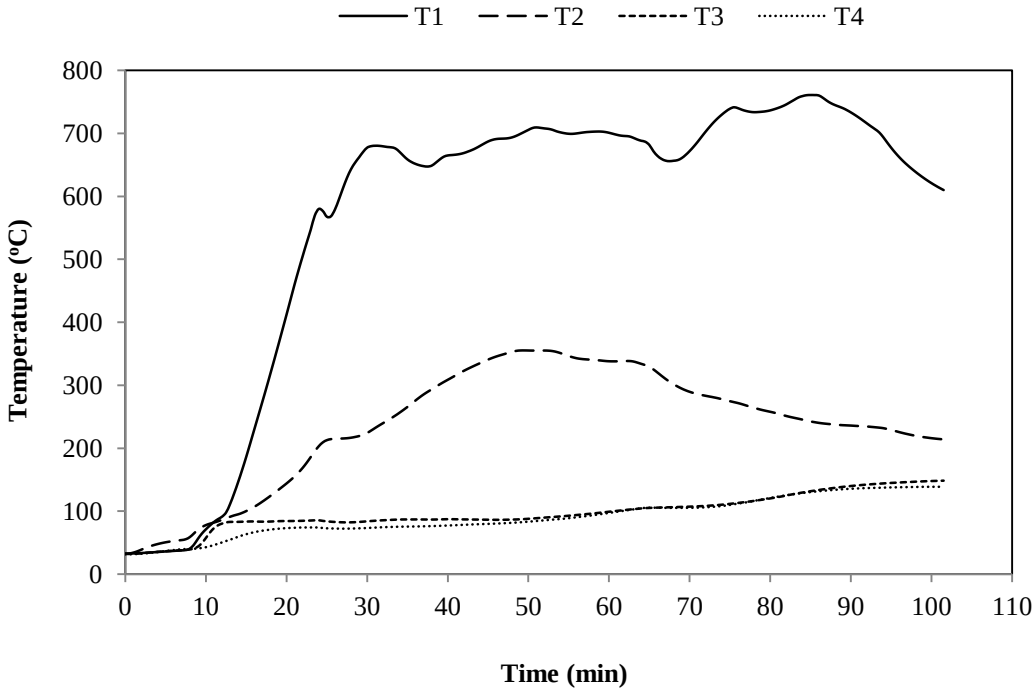

Figure B.41 Temperature profile during gasification of OPF in case of injecting secondary air through reduction zone at ratio of 0.4

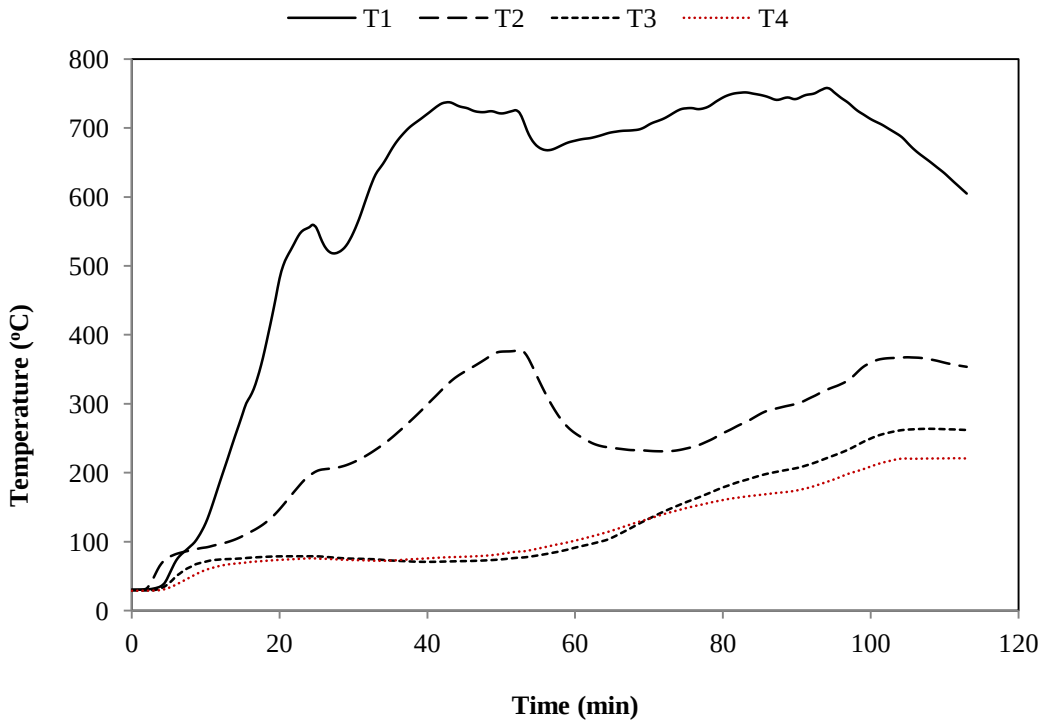

Figure B.42 Temperature profile during gasification of OPF in case of injecting secondary air through reduction zone at a ratio of 0.56

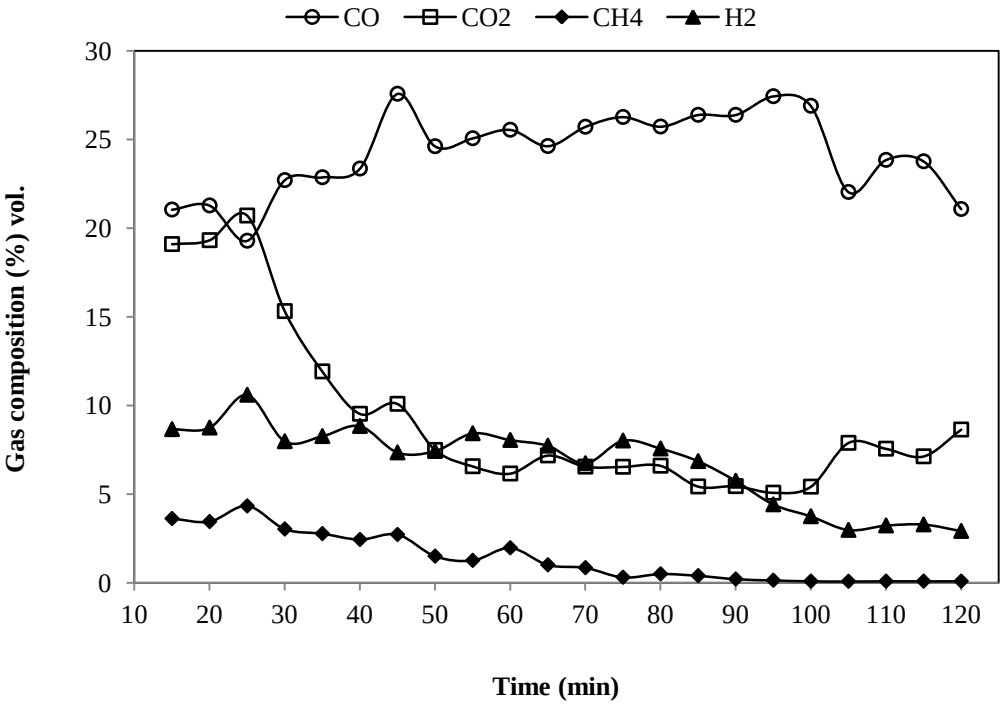

Figure B.43 Variation of syngas composition with time in case of injecting secondary air through reduction zone at a ratio of 0.17

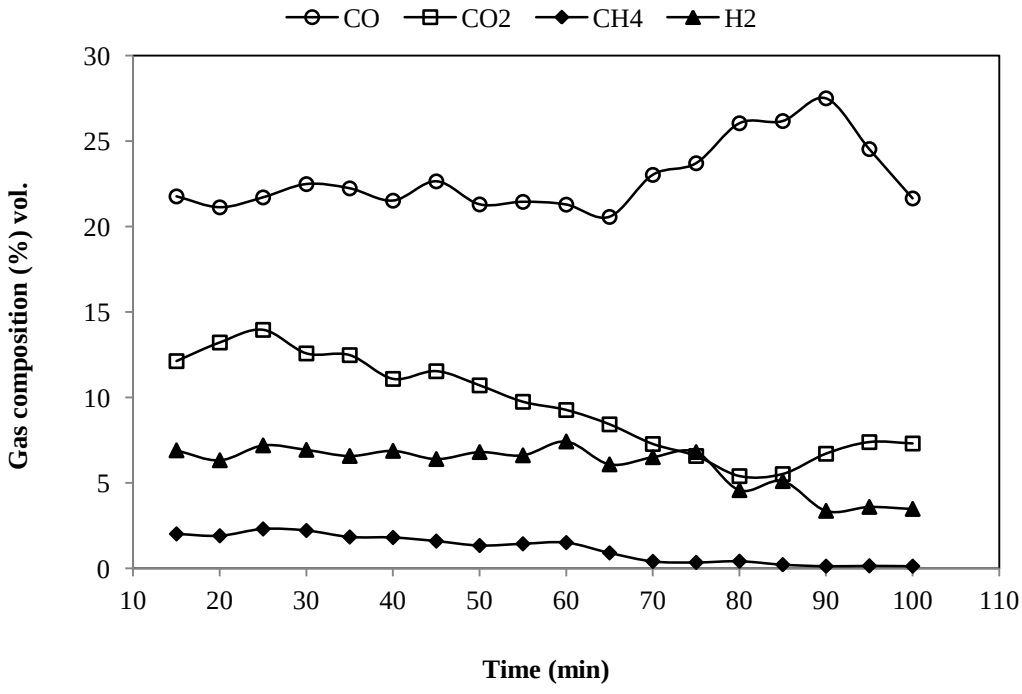

Figure B.44 Variation of syngas composition with time in case of injecting secondary air through reduction zone at a ratio of 0.27

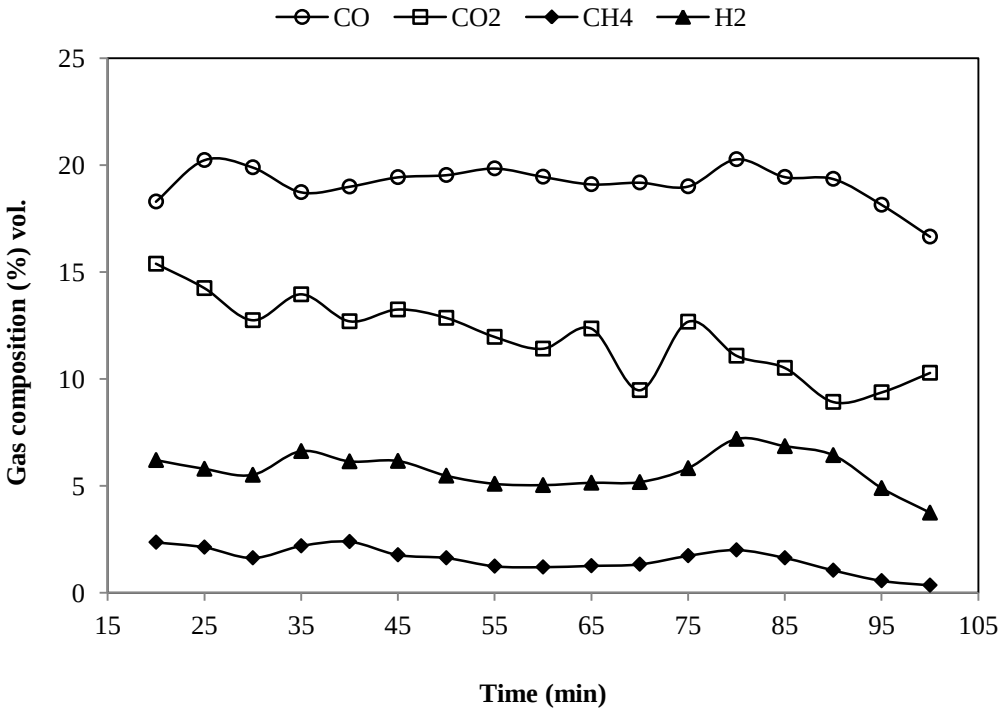

Figure B.45 Variation of syngas composition with time in case of injecting secondary air through reduction zone at a ratio of 0.4

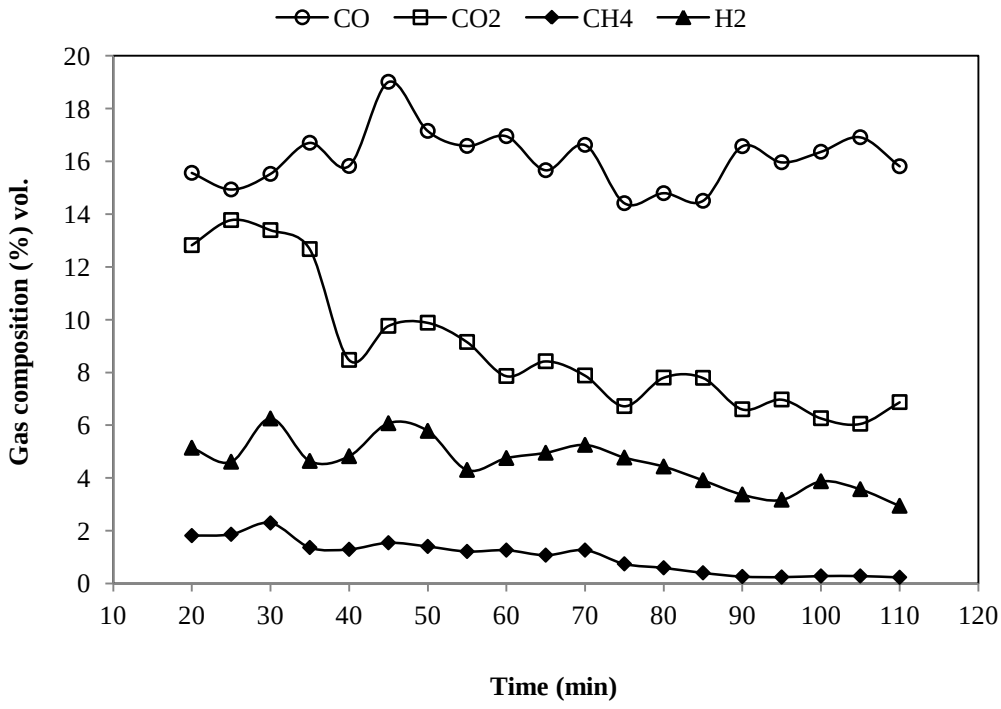

Figure B.46 Variation of syngas composition with time in case of injecting secondary air through reduction zone at a ratio of 0.56

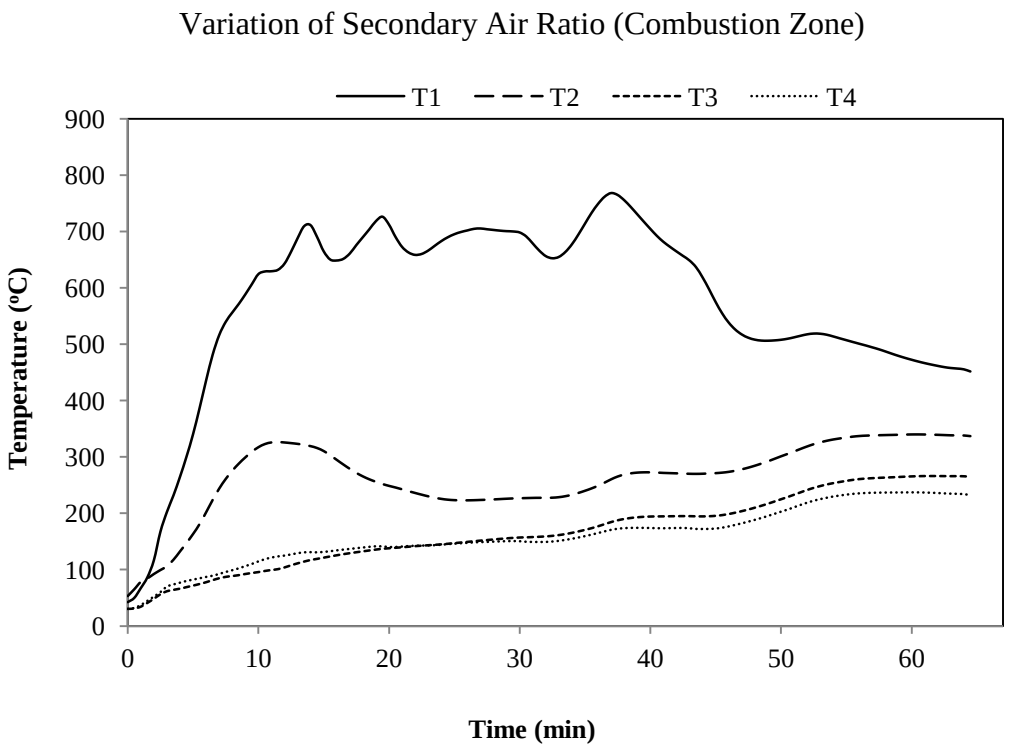

Figure B.47 Temperature profile during gasification of OPF in case of injecting secondary air through combustion zone at a ratio of 0.17

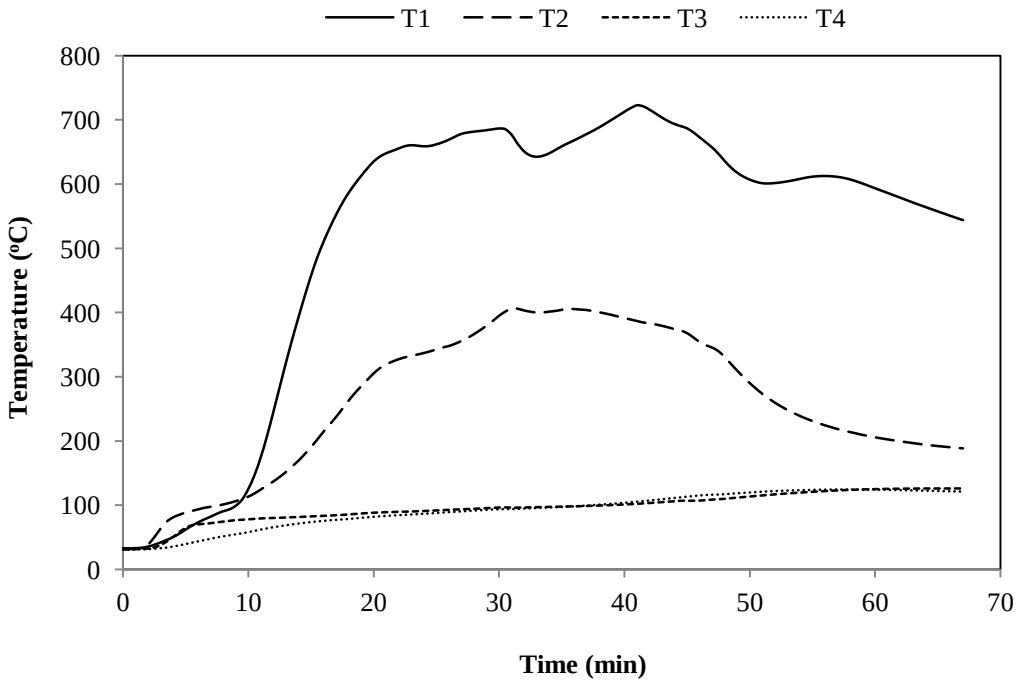

Figure B.48 Temperature profile during gasification of OPF in case of injecting secondary air through combustion zone at a ratio of 0.27

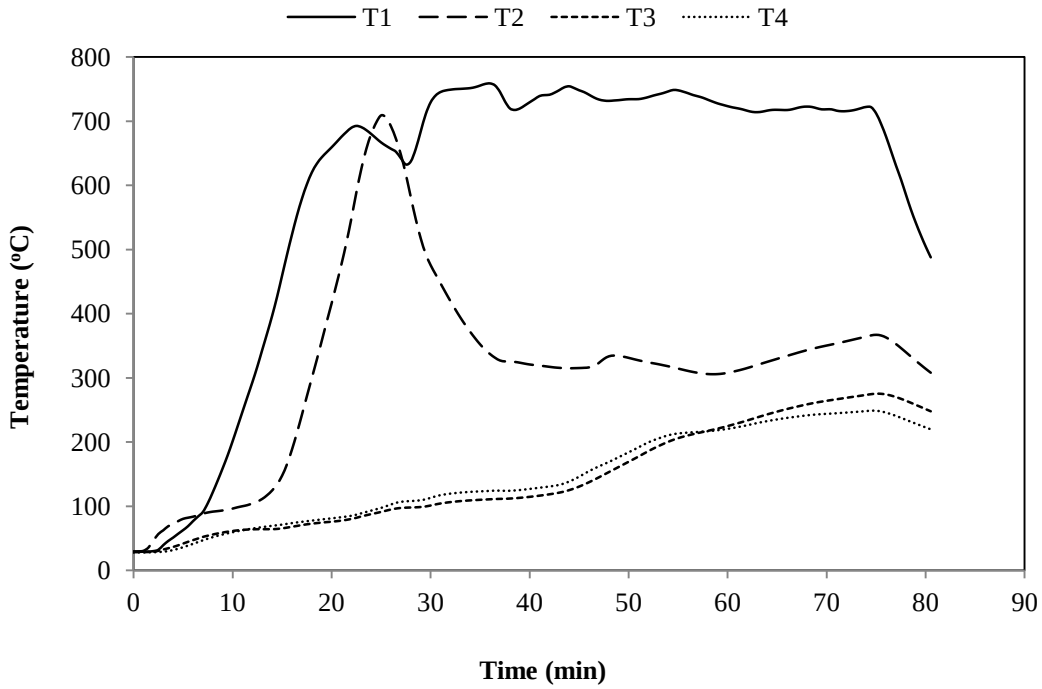

Figure B.49 Temperature profile during gasification of OPF in case of injecting secondary air through combustion zone at a ratio of 0.56

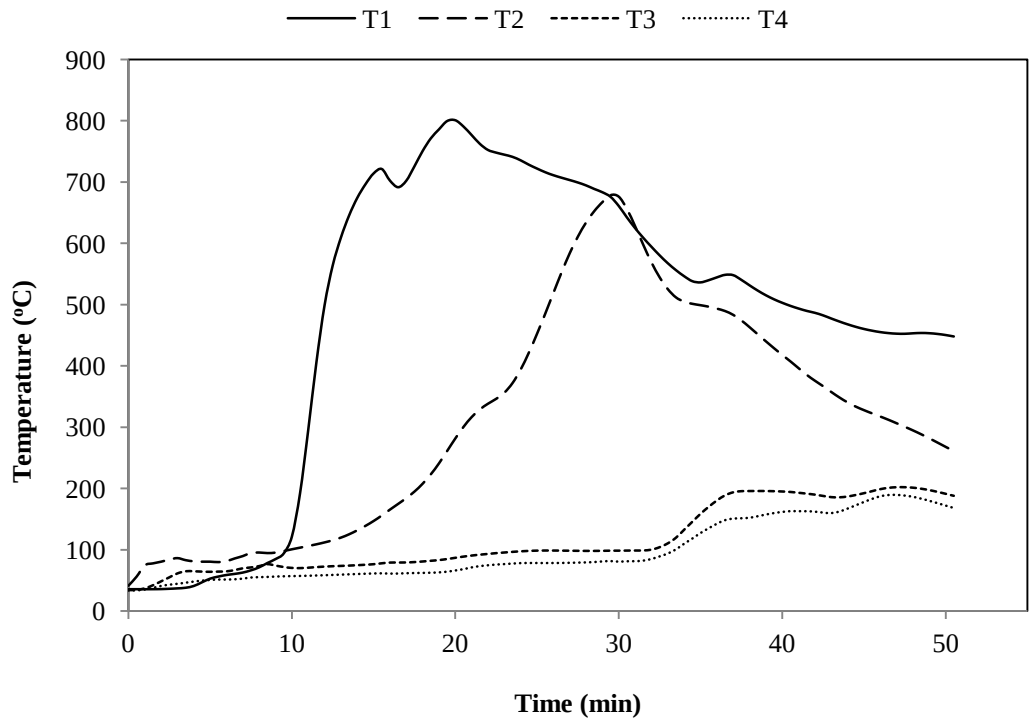

Figure B.50 Temperature profile during gasification of OPF in case of injecting secondary air through combustion zone at a ratio of 1.0

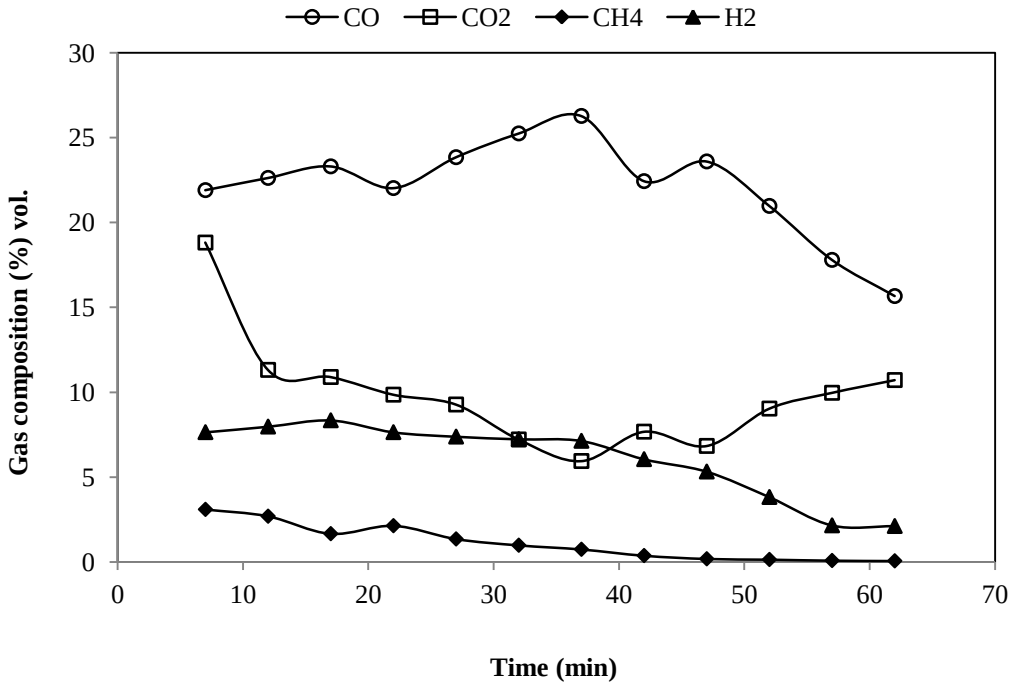

Figure B.51 Variation of syngas composition with time in case of injecting secondary air through combustion zone at a ratio of 0.17

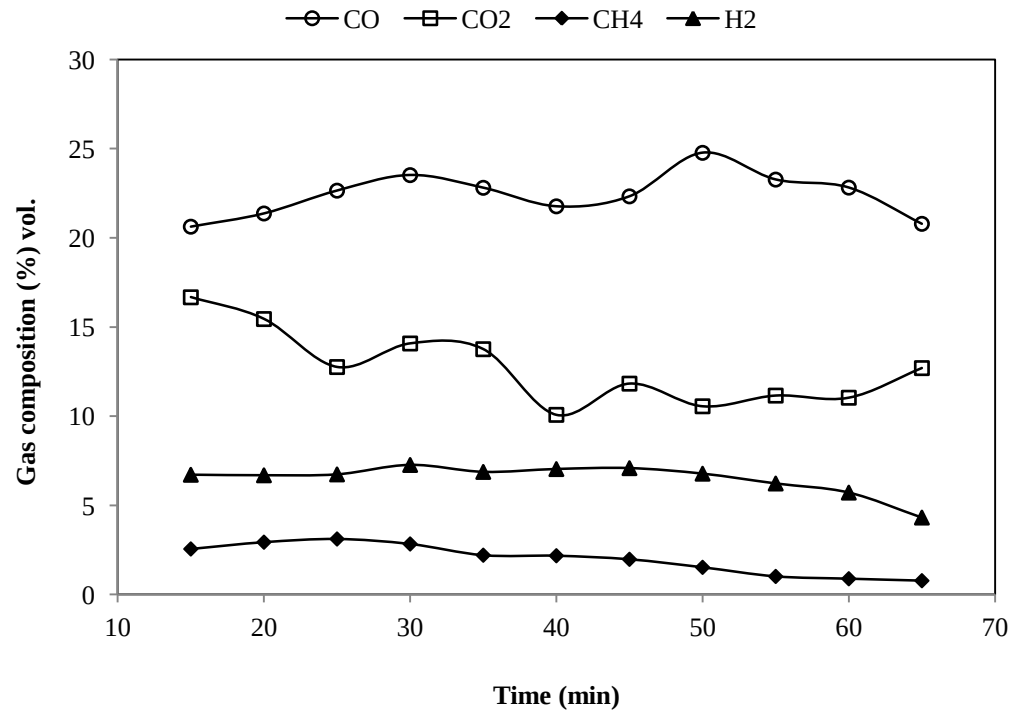

Figure B.52 Variation of syngas composition with time in case of injecting secondary air through combustion zone at a ratio of 0.27

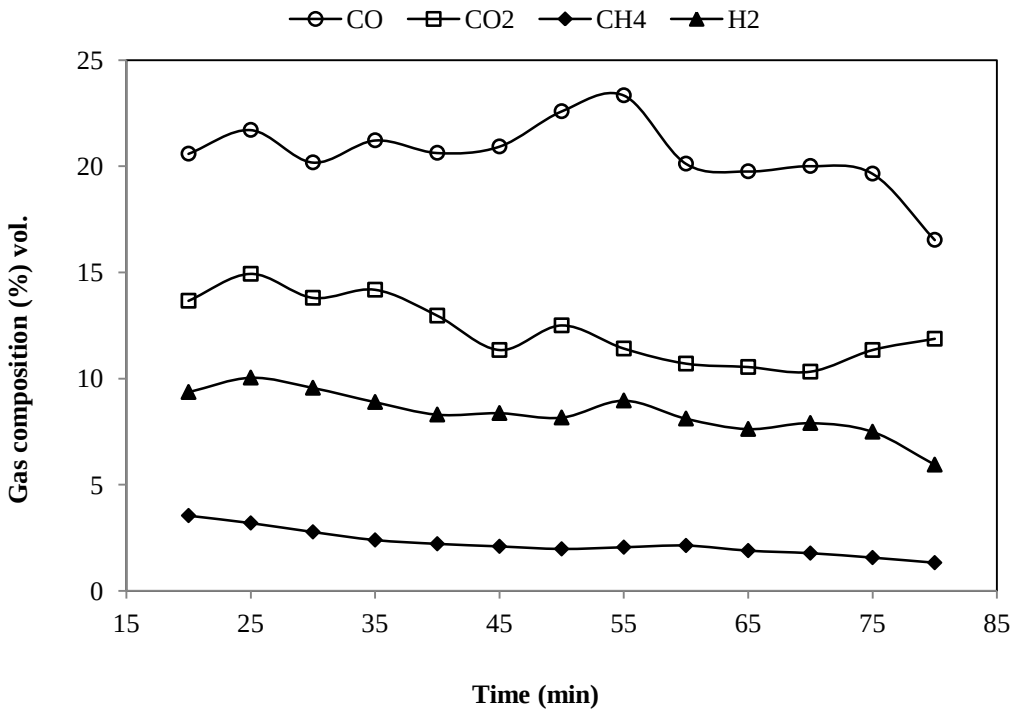

Figure B.53 Variation of syngas composition with time in case of injecting secondary air through combustion zone at a ratio of 0.56

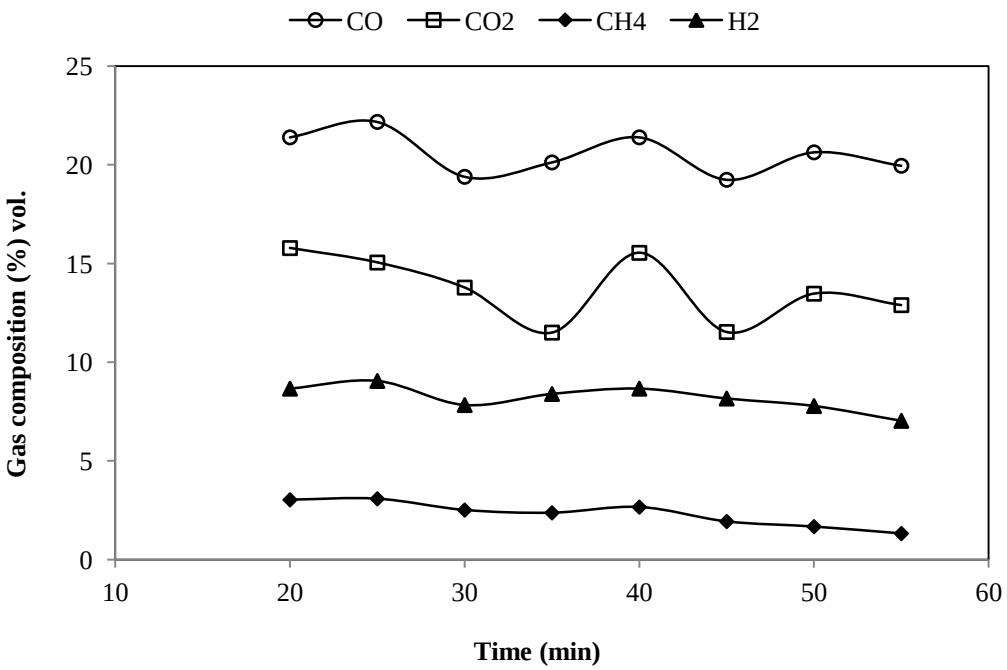

Figure B.54 Variation of syngas composition with time in case of injecting secondary air through combustion zone at a ratio of 1.0

APPENDIX C

MASS BALANCE

Table C.1 Summary of overall mass balance

	Mass input (kg/h)			Mass output (kg/h)				
No.	OPF	Air	Total	Gas	Char-ash	Condensate	Total	Closure (%)
1	14.14	15.84	30.25	21.49	1.88	0.43	28.80	80.0
2	12.31	17.23	29.23	23.69	1.07	0.28	23.73	84.8
3	11.43	20.16	32.45	28.27	0.48	0.22	31.30	89.3
4	11.85	23.04	38.89	31.73	0.61	0.20	32.34	92.7
5	12.31	25.92	38.23	29.36	0.64	0.85	30.85	81.0
6	10.58	20.16	30.74	27.93	0.49	0.10	28.52	92.8
7	9.56	20.16	29.72	26.62	0.46	0.21	27.29	91.8
8	9.00	20.16	29.16	25.27	0.57	0.29	26.13	90.0
9	8.70	20.16	28.86	27.55	0.55	0.37	28.48	98.6
10	8.33	20.16	28.49	26.28	0.80	0.63	27.71	97.3
11	12.83	20.16	32.99	26.55	0.71	0.14	27.39	83.1
12	10.82	20.16	30.98	27.34	0.64	0.10	28.08	90.6
13	10.60	20.16	30.76	26.64	0.75	0.21	27.60	91.0
14	10.29	20.16	30.45	26.10	0.64	0.21	26.95	88.5
15	9.23	20.16	30.09	23.18	1.25	0.12	24.55	81.6
16	9.23	20.16	29.39	26.25	0.41	0.21	26.87	91.4
17	10.81	20.16	30.97	27.24	1.93	0.20	29.37	94.8
18	11.65	20.16	31.81	28.24	2.57	0.20	31.01	97.5
19	10.00	20.16	30.16	27.72	0.85	0.21	28.77	95.4
20	9.84	20.16	30.00	27.81	1.85	0.21	29.87	101.6
21	9.23	20.16	29.39	26.25	0.41	0.22	26.87	91.4
22	10.00	20.16	30.16	27.12	0.58	0.15	27.85	92.4
23	8.72	20.16	28.88	24.86	0.64	0.17	25.67	89.0
24	8.18	20.16	28.34	22.34	0.60	0.60	23.87	84.2
25	8.62	20.16	28.88	24.86	0.64	0.17	25.67	89.0
26	8.20	20.16	28.78	22.03	0.79	0.42	23.24	81.0
27	7.81	20.16	28.36	22.10	0.72	0.68	23.51	82.9

Table C.1 (continue) Summary of overall mass balance

	Mass input (kg/h)			Mass output (kg/h)				
No.	OPF	Air	Total	Gas	Char-ash	Condensate	Total	Closure (%)
28	7.81	20.16	27.97	20.00	1.03	0.62	21.55	77.0
29	10.0	20.16	30.16	27.12	0.58	0.15	27.85	92.4
30	9.84	20.16	30.00	27.40	1.35	0.34	29.09	97.0
31	9.92	20.16	30.08	27.93	1.40	0.41	29.74	98.9
32	9.84	20.16	30.00	29.29	1.81	0.17	31.26	1.04